

**PETROGENESIS OF THE MAWAT
OPHIOLITE COMPLEX AND THE
ASSOCIATED CHROMITITE,
KURDISTAN REGION, NE IRAQ**

A Thesis

*Submitted to the College of Science, University of Sulaimani
in Partial Fulfillment of the Requirements for the Degree of
the Doctor of Philosophy in Geology*

By

Tola Ahmed Mirza

M. Sc. In Geology, Baghdad University, 1997

Supervised By

Dr. Sabah Ahmed Ismail
Assistant Professor

March 2008 A.D.

Nawroz 2708 KU

We, the examining committee, hereby certify that we have read this thesis and examined the student in its contents and whatever relevant to it and that in our opinion it is adequate to be accepted for the Degree of Doctor of Philosophy in geology /Ore geology.

Signature:

Name: Dr. Mazin Y. Tamer Agha Hassan

Scientific title: Professor

Professor

Address: University of Salahddin

Date: / / 2008

(Chairman)

Signature:

Name: Dr. Mohammad E. Al

Scientific title: Assistant.

Address: University of Baghdad

Date: / / 2008

(Member)

Signature:

Name: Dr. Ayten Hadi. Ali

Scientific title: Assistant. Professor

Address: University of Baghdad

Date: / / 2008

(Member)

Signature:

Name: Dr. Rafaa Zair. Jassim

Scientific title: Consultant.

Address:

Date: / / 2008

(Member)

Signature:

Name: Dr. Hikmat S. Aljalel

Scientific title: Assistant. Professor

Professor

Address: University of Salahddin

Date: / / 2008

(Member)

Signature:

Name: Dr. Sabah A. Isamil

Scientific title: Assistant.

Address: University of Kirkuk

Date: / / 2008

(Member and supervisor)

Approved by the Council of the College of Science

Signature:

Name: Dr. Prekhan M. Jaf

Scientific title: Assistant. Professor

Date: / / 2008

Supervisor Certification

I certify that this thesis entitled (Petrogenesis of the Mawat Ophiolite Complex and the associated chromitite, Kurdistan Region, NE Iraq) was prepared under my supervision at the University of Sulaimani in a Partial Fulfillment of the Requirements for the Degree of Doctor of Philosophy in Geology.

Signature:

Name: Dr. Sabah Ahmed Ismail

Scientific title: Assistant Professor

Address: College of Science/ Kirkuk

Department of Applied Geology

Date: / / 2008

In view of the available recommendations, I forward this thesis for debate by the examining committee.

Signature :

Name : Dr. Kamal Haji Karim

Title: Assistant professor

Address: University of Sulaimani

College of Science

Department of Geology

Date: / / 2008

ACKNOWLEDGMENTS

Thanks to God for giving me health and brains to achieve this thesis. The presidency of Sulaimani University, College of Science and Department of Geology deserve my appreciation for giving me this opportunity to get the degree of Doctorate of Philosophy.

The author expresses her sincere appreciation to Dr. Sabah A. Ismail for his kind supervision, numerous discussions and continuous support during this study.

I also thank Professor Ahmed H. Ahmed at Helwan University for his constructive comments which helped me in completing this thesis. I wish to express my thanks to Dr. Khaldoon Al-Bassam for encouraging me to choose this specialty.

Miss Dian and her group at GeoAnalytical Laboratory, School of Earth and Environmental Sciences Department, Washington State University are thanked for XRF, ICP-MS, and microprobe analyses. I am very grateful to the staff of the Genalysis Laboratory Services Pty Ltd, Western Australia for their help in PGE and trace element analyses.

I would also like to thank Miss Kazi Hassan Saleh who has made the language evaluation for this thesis.

My husband Ibrahim, grateful acknowledged for all of his assistance I will never forget his kindness and his sentiment during this study. My special thanks go to my father for his moral support that has got me to this point. I would like to express my appreciation to my father- in- law, Mr. Muhamad Jaza Muhyaldin for his encouragement during this study.

I am also grateful to all my sisters and brothers, especially Mr. Twana Ahmed Mirza for his supports and kindness. At the end of this research I would like to express my grateful thanks to all those who have supported me to achieve this thesis.

ABSTRACT

The Mawat ophiolite complex is one of the major Cretaceous ophiolite complexes in northeastern Iraq and is situated at about 30 Km north east of Sulaimani. It represents part of the Iraqi Zagros Thrust Zone (IZTZ) which is an integral part of Alpine-Himalayan Orogenic belt. This complex consists of ultrabasic, basic, volcanic and sub volcanic rocks. The present study describes petrographical and chemical feature of the ultrabasic, chromitite and gabbro rocks in main six traverses in order to understand the genesis of these rocks.

The major outcrop of the ultrabasic bodies is located in the eastern part of the complex with a minor occurrence in the south and south western part. The Mawat ultrabasic rocks characterized by harzburgite affinity with very minor occurrence of lherzolite. Nine pods of chromitite are distinguished in 2 Km north of Kuradawi village. The pods were enveloped by dunite and hosted by harzburgite and they are irregular to lens-like in shape ranging from 0.5-12m in length and (30cm -2m) in width. All types of rock in the studied area are affected by various degrees of metamorphism. The present study shows that the ultrabasic rocks plot in the field of low amphibolite facies and the chromitite rocks plot in the field of green schist facies. The results of XRF analysis for ultrabasic rocks reveal that these rocks are characterized by enrichment in large ion lithophile element (LILE) and depletion in high field strength elements (HFSE). The negative Nb anomaly and describe spider diagrams reveal a supra-subduction zone (SSZ). The chondrite normalized REE pattern of dunite and harzburgite of MOC are characterized by a U-shape, with slight depletion in middle REE (MREE) (Eu-Dy) relative to light REE(LREE), (La-Sm) and heavy REE (HREE), (Ho-Lu) which are attributed to the absence of hornblende and presence of olivine and orthopyroxene in dunite and harzburgite. While Lherzolite shows enrichment of MREE and HREE relative to LREE due to the presence of clinopyroxene and orthopyroxene and olivine.

The pyroxenite rocks show clear cross-cutting relationship with peridotite and gabbro rocks and are classified as low alumina pyroxenite which include two types of clinopyroxenite and olivine webstrite pyroxenite. The chondrite-normalized REE pattern of pyroxenite rocks show variable REE distribution

enrichment of LREE and MREE relative to HREE and in other samples show LREE depletion, with positive Eu-anomaly. These two patterns are typical of pyroxenite in ophiolitic complex. The origin of pyroxenite rocks of MOC is interpreted to be a result of segregation and transport of boninitic melt in SSZ.

The basic rocks of MOC have comparable compositions; enriched in FeO relative to Na₂O, K₂O and MgO, hence, it is classified as tholeiitic. The overall chondrite normalized REE patterns of gabbroic rocks is akin to flat lying REE patterns. Such flat lying patterns resemble the rocks formed in island arc tholeiitic (IAT) and subduction-related setting. The clinopyroxene chemistry of the gabbroic rocks also supports the assertion that gabbroic rocks of MOC are related to island arc and boninitic rocks which have a linkage with SSZ.

The chromitite rocks vary in texture, and degree of alteration and exhibit as high Cr chromian spinel. The Cr#_s of chromian spinel ranges from 0.7-0.8 average 0.73 in dunite, quite similar in the high-Cr chromitite (0.74), whereas it ranges between 0.56-0.84 the average (0.671) in harzburgite. Platinum group elements (PGEs) and Au were determined for the first time using Ni fire assay (NIS/MS) from podiform chromitite and associated dunite and harzburgite. Chondrite normalized PGE patterns are variably fractionated showing conventional IPGE over PPGE enrichment. According to the PGE content, in the chromitite rocks of MOC two groups were distinguished: (1) the PGE-rich chromitite which have approximately 1094 ppb as total PGE, being highly enriched in IPGE and depleted in PPGE and related to the deeper section. (2) The PGE-poor chromitite which PGE content < 750 ppb and also enriched in IPGE with depletion in PPGE which are generated in Moho transition zone (MTZ). The high Cr#_s and low TiO₂ character of chromian spinel in ultrabasic and chromitite rocks of the studied area leads the conclusion that the formation of MOC may have been linked with some high-Mg, high Cr-suprasubduction zone magma such as high Mg andesite, boninite or high Mg-tholeiite where partial melting is quite high in the approximating of paleo-ridge.

The comparisons between Cr#_s in ultrabasic and chromitite rocks of studied area with other ophiolites elsewhere show that they are regionally similar to those of Cretaceous especially those of New Caledonia, and locally similar to

Bulfat igneous complex and Qalander location A. This is attributed to the fact that ultrabasic rocks of MOC are related to depleted mantle rocks and closely resemble with alpine-type peridotites probably produced from medium spreading center and having genetic linkage with fore-arc setting of suprasubduction zone. The estimated temperatures of formation of chromitite rocks are 1336 C° and 1313 C°, 1307 C° and 1358 C° in dunite harzburgite and Lherzolite respectively. The variation of estimated temperatures was related to subsolidus re-equilibration between spinel and olivine during post-magmatic process.

List of Contents

Subject	Page No.
Acknowledgments	I
Abstract	II
List of contents	V
List of Tables	VIII
List of Figures	IX
List of Appendices	XV
Chapter One: Introduction	1
1.1 Preface	1
1.2 Geographic location	3
1.3 Sampling	4
1.4 Previous studies	8
1.5 Aim of the study	13
1.6 Geology of the studied area	14
1.6.1 The Ultrabasic Rocks	15
1.6.2 The basic rocks	15
1.6.3 The volcanic rocks	16
1.6.4 The minor intrusions	17
1.7 Tectonic setting	17
1.8 Analytical technique	19
1.8.1 Microscopic study	19
1.8.2 XRF and ICP-MS analysis	20
1.8.3 Microprobe analysis	21
1.8-4 Platinum group analysis	22
Chapter Two: Ultrabasic Rocks	23
2.1 Introduction	23
2.2 Petrography of ultrabasic	24
2.2.1 Dunite	24
2.2.2 Harzburgite	25
2.2.3 Lherzolite	28

2.2.4 Pyroxenite	28
2.2.5 Chromitite	29
2.2.6 Alteration of ultrabasic rocks	30
2.3 Geochemistry of ultrabasic rocks	35
2.3.1 Geochemistry of major elements	35
2.3.2 Geochemistry of trace elements	38
2.4 Geochemistry of rare earth elements (REE)	43
2.5 Spider diagrams of ultrabasic rocks in MOC	49
2.6 Mineral chemistry	52
2.6.1 Olivine composition	52
2.6.2 Pyroxene composition	53
2.6.3 Alteration minerals	58
2.6.4 Accessory chromite composition	58
2.7 Accessory chromite alteration.	62
Chapter Three: Chromitite rocks	67
3.1 Introduction	67
3.2 The major ore types	68
3.2.1 Massive chromitite ore	68
3.2.2 Brecciate chromitite ore	68
3.2.3 Disseminated chromitite ore	69
3.3 Mineral inclusion in chromian spinel	69
3.4 Accessory Chromite	70
3.5 Mineral chemistry	75
3.5.1 Spinel composition	75
3.5.2 Chemistry of matrix	83
3.5.3 Chemistry of inclusions	84
3.6 Chromite alteration	86
3.7 Platinum group elements in chromitite rocks of MOC	91
3.8 Geochemistry of PGE and Au	92
3.9 Comparison of PGE distribution	97

3.10 Distribution and fractionation of PGE in chromitite rocks of MOC	98
3.11 Distribution and fractionation of PGEs in dunite and harzburgite of MOC	99
3.12 Base metal	100
Chapter Four. The Basic Rocks	103
4.1 Petrography of gabbroic rocks	103
4.1.1 Banded gabbro	103
4.1.2 Coarse gabbro	107
4.1.3 Sheared gabbro	108
4.2 Geochemistry of gabbroic rocks	112
4.2.1 Behavior of Major and trace elements in gabbroic rocks	112
4.2.2 REE geochemistry and trace elements of the gabbroic rocks in MOC	126
4.3 Mineral chemistry	129
Chapter Five: Genesis of Ultrabasic and Chromitite Rocks	134
5.1 Geothermometry	134
5.2 Oxygen fugacity of chromian spinel in MOC chromitite	136
5.3 Partial melting	137
5.4 Comparison of chromite from MOC with chromite elsewhere	141
5.5 Origin of podiform chromitites	145
Chapter Six: Tectonic Setting of MOC	148
6-1 Introduction	148
6-2 Tectonic setting indication from the ultrabasic rocks of MOC	148
6.3 Tectonic implications from chromitite rocks	153
6.4 Tectonic implication from gabbroic rocks	157
Chapter Seven	160
7.1 Conclusions	160
7.2 Recommendations	163
References	164
Appendices	

List of Tables

Tables	Page No.
Table 1-1 Coordination and localities of studied samples along the main selected traverses with main rock types	7
Table 2-1 Modal volume % of mineral composition in dunite of MOC	26
Table 2-2 Modal volume % of mineral composition in harzburgite rocks of MOC.	27
Table 2-3 Modal volume % of mineral composition in lherzolite rocks of MOC	27
Table 2-4 Modal volume % of mineral composition in pyroxenite rocks of MOC	27
Table 2-5 Representative XRF bulk rock analysis of dunite (9), harzburgite (15), lherzolite (9), and pyroxenite (10) in Mawat Ophiolite Complex, n= number of analyzed sample	37
Table 2-6 Representative ICP-MS bulk rock analysis of dunite (3) harzburgite (10), lherzolite (6), and Pyroxenite (8) rocks in Mawat Ophiolite Complex (n= number of analyzed samples)	45
Table 2-7 Representative microprobe analysis of dunite (3 *), harzburgite (5*) lherzolite (4 *), and pyroxenite (6 *). [Cr#: Cr/(Cr+Al), Mg#: Mg/(Mg+Fe ²⁺), Fe ²⁺ #: Fe ²⁺ / (Fe ²⁺ +Mg), Fe ³⁺ #: Fe ³⁺ / (Fe ³⁺ +Al+Cr) atomic ratio]	54
Table 3-1 Modal volume % of chromitite rocks in MOC.	71
Table 3-2 Microprobe analysis of chromian spinel in chromitite rocks. Cr#: Cr/(Cr+Al), Mg#: Mg/(Mg+Fe ²⁺), Fe ³⁺ #: Fe ³⁺ / (Fe ³⁺ +Al+Cr) atomic ratio (Number of O = 4)	78
Table 3-3 Microprobe analysis of matrix minerals from chromitite rocks of Mawat Ophiolite Complex. [Mg#: Mg/(Mg+Fe ²⁺), Fe ²⁺ #: Fe ²⁺ / (Fe ²⁺ +Mg) atomic ratio]	79
Table 3-4 Microprobe analysis of mineral inclusions in chromitite rocks of Mawat Ophiolite [Mg#: Mg/(Mg+Fe ²⁺), Fe ²⁺ #: Fe ²⁺ / (Fe ²⁺ +Mg) atomic ratio.	80
Table 3-5 Whole-rock platinum-group element contents (ppb) of representative samples from MOC	94
Table 3-6 Chemical compositions of base metals (BM) in chromitite rocks from the MOC.	94
Table 4-1 Modal % of minerals composition of gabbroic rocks in MOC	106
Table 4-2 The results of XRF analysis of gabbroic rocks in Mawat ophiolite complex	115
Table 4-3 The results of REE analysis (ICP-MS) of gabbroic rocks in MOC	114
Table 4-4 Microprobe analyses for mineral composition of different types of gabbroic rocks in MOC. Mg#: Mg/(Mg+Fe ²⁺), Fe ²⁺ #: Fe ²⁺ / (Fe ²⁺ +Mg) atomic ratio	131
Table 5-1 Calculated temperatures of formation for studied samples according to (Roeder 1979)	135

List of Figures

Figures	Page No.
Fig. 1-1 A: Ophiolite succession and seismic layers of oceanic crust; B: Histogram of formation ages of Ophiolites in the world; C: Ophiolite belt in the world (Akira ISHIWATARI, 2003)	2
Fig. 1- 2 Location and topographic map of the studied area showing the studied traverses and distributions of samples	5
Fig. 1-3 Geological map of Mawat-Chwarta area, Kurdistan Region, NE Iraq (Al-Mehaidi, 1974 modified by Mirza and Ismail, 2007)	6
Fig. 2-1 Classification and nomenclature of ultrabasic rocks in MOC (Diagram from Best, 2001 and Bose, 1997)	26
Fig. 2-2 Outcrop of dunite characterized by spheroid weathering.	31
Fig. 2-3 Olivine and pyroxene with accessory chromian spinel in dunite, (A: under PPL, B: XP)	31
Fig. 2-4 Porphyroclastic to cataclastic texture in dunite and serpentinization along olivine cracks, (A: under PPL, B: XP)	31
Fig. 2-5 Pyroxenite dykes in the harzburgite rocks	31
Fig. 2-6 Kinked clinopyroxene in harzburgite (under XP)	32
Fig. 2-7 Radiated aggregate of orthopyroxene and serpentinized olivine in harzburgite, (A: under PPL, B: XP)	32
Fig. 2-8 Alteration of pyroxene in harzburgite to talc and tremolite.(Under A: PPL, B: XP)	32
Fig. 2-9 Vermicular chromite grain with olivine and pyroxene in harzburgite rocks of MOC, (A: under PPL, B: XP)	33
Fig. 2-10 Serpentinization of olivine and formation of secondary magnetite in lherzolite. (Under A: PPL, B: XP)	33
Fig. 2-11 Coarse crystal of clinopyroxene contains small patches of amphibole (Under A: PPL, B: XP)	33
Fig. 2-12 Pyroxenite dykes cutting the gabbro rocks in MOC.	34
Fig. 2-13 Coarse clinopyroxene and orthopyroxene in a matrix of granulated olivine in pyroxenite. (Under A: PPL, B: XP)	34
Fig. 2-14 Mesh textured pseudomorphs after olivine and relict chromian spinel in serpentinite ultrabasic rocks of MOC contain small inclusion of olivine (A: PPL under PPL, B: XP)	34
Fig. 2-15 Plots of major oxides versus MgO in whole ultrabasic -rock (dunite, harzburgite, lherzolite, and pyroxenite)	40
Fig.2-16 Plots of trace elements versus MgO in whole ultrabasic rocks of MOC (dunite, harzburgite, lherzolite, and pyroxenite)	41
Fig. 2-17 Variation diagrams of Ni and V versus MgO in MOC ultrabasics. Discriminative fields of Harzburgite (Har), Lherzolite (Lhr), Dunite (Dun) and Pyroxenite (Pyr) from Pfeiefer, (1990)	42
Fig. 2-18 Chondrite-normalized REE patterns of dunite in MOC	47
Fig. 2-19 Chondrite-normalized REE patterns of harzburgite in MOC	47
Fig. 2-20 Chondrite-normalized REE patterns of lherzolite in MOC	48

Fig. 2-21 Chondrite-normalized REE patterns of pyroxenite in MOC	48
Fig. 2-22 Chondrite - normalized trace element patterns (spider diagram) of the dunite in MOC	50
Fig. 2-23 Chondrite - normalized trace element patterns (spider diagram) of the harzburgite in MOC	50
Fig. 2-24 Chondrite - normalized trace element patterns (spider diagram) of the lherzolite in MOC	51
Fig. 2-25 Chondrite - normalized trace element patterns (spider diagram) of the pyroxenite in MOC	51
Fig.2-26 Relationships between the Fo content of olivine and the Cr/(Cr+Al) atomic ratio (Cr#) of chromian spinel in peridotites rocks from the MOC. OSMA olivine spinel mantle array from Arai (1994a)	56
Fig.2-27 Pyroxene compositions in the system CaSiO ₃ -MgSiO ₃ -FeSiO ₃ , general compositional field are from Klein et al. (1993)	57
Fig.2-28 Al ₂ O ₃ – Mg # relationship of clinopyroxene in peridotite and pyroxenite rocks in MOC	57
Fig. 2-29 Classification of amphiboles in studied samples (after Leak et al 1997).	60
Fig.2-30 SiO ₂ - Al ₂ O ₃ - MgO triangle, show the field of serpentine mineral group (Wickes and Plant, 1979)	60
Fig.2-31 Plots of Cr# versus Mg# for chrome spinel in chromitite, dunite, harzburgite and lherzolite. The Alpine-type field is from Irvan (1967). The high-Al, high Cr, and high Fe field from Mei-Fu (1992)	61
Fig.2-32 Cr-Al-Fe ⁺³ atomic ratio of chromian spinel in ultrabasic rocks of MOC.	61
Fig. 2-33 MgO vs. FeO relationship of chromian spinel in ultrabasic rocks in MOC	62
Fig.2-34 Microprobe traverses across an altered accessory chromite in dunite from MOC.	64
Fig. 2-35 Microprobe traverses across an altered accessory chromite in harzburgite from MOC	65
Fig. 2-36 The plots of Fe ⁺³ -Cr-Al of studied samples and solves curve for different metamorphic Cr-spinel phases (Purvis et al., 1972; Evans & Frost, 1975; Suita & Strider, 1996).	66
Fig. 2-37 The relationship of MgO-Cr ₂ O ₃ of the chromite from the peridotite of MOC	66
Fig. 3-1 Chromitite pod envelopes with dunite in north of Kuradawi village	72
Fig. 3-2 A: Vein type and B: densely disseminated chromite in Ser Shiw valley	72
Fig.3-3 Anhedral crystals of chromite showing pull-a part texture and most of chromite grains exhibit thin rims of ferritchromite; the white interstitial represents the matrix. (A: under PPL. B: under XP)	72
Fig. 3-4 The Amphibole matrix between the chromite grains in massive ore type (Under XP)	73
Fig.3-5 Light grey subhedral chromite crystal in massive chromite ore contains secondary mineral phases (under PPL)	73

Fig. 3-6 Silicate mineral inclusions in chromite grain (A: under PPL, B, XP, 100X)	73
Fig. 3-7 Brecciated chromitite rocks, the chromite grain transected by many cracks. (A: under PPL, B: XP)	73
Fig. 3-8 Light grey brecciated chromite grain under reflected light microscope (PPL)	74
Fig. 3-9 Disseminated subhedral to anhedral chromite crystal in a matrix of olivine in north of Kuradawi village (A: under PPL, B: XP)	74
Fig. 3-10 Euhedral chromite inclusions in dunite envelopes the chromitite rocks. (A: under PPL, B: XP)	74
Fig. 3-11 The relationship between Mg# vs. Cr# in chromian spinel of chromitite rocks in MOC.	81
Fig.3-12 Variation of Cr ₂ O ₃ vs. Al ₂ O ₃ of chrome spinel in the Mawat podiform chromitite. Compositional field of podiform & stratiform chromitite (Bonavia et al., 1993)	81
Fig. 3-13 Variation of TiO ₂ Wt % vs. Cr ₂ O ₃ of chromitite from MOC the boundary between stratiform and podiform (Bonavia et al. 1993)	81
Fig. 3-14 Cr-Al-Fe ⁺³ atomic ratio of chromian spinel in chromitite rocks of MOC	82
Fig.3-15 Cr ₂ O ₃ -Al ₂ O ₃ -Fe ₂ O ₃ diagram for podiform chromitite rocks in MOC (Steven, 1944)	82
Fig. 3-16 C# versus TiO ₂ content for chromite in MOC chromitite and their hosting dunite and harzburgite. Boninitic and MORB fields were defined by Arai (1992)	83
Fig. 3-17 Chemical composition of matrix and inclusion chlorite in MOC chromitite, (a: Fe vs. Si b: Si vs. Fe/Fe+Mg c; Si vs. Cr.), (Hey 1954)	85
Fig. 3-18 SiO ₂ - Al ₂ O ₃ - MgO triangle, shows the field of serpentine mineral group (Wickes and Plant, 1979)	85
Fig. 3-19 Variation of major oxide from core to rim across grain in massive chromitite rocks (Sample W19)	88
Fig. 3-20 Variation of major oxide from core to rim across grain in disseminated chromitite rocks (sample W29)	89
Fig. 3-21 The plots of Fe ⁺³ -Cr-Al of chromitite samples and fields for different metamorphic C-spinel phases (after Purvis et al., 1972, Evans & Frost, 1975, Suita and Strider, 1996)	90
Fig.3-22 Variation of major oxide from core to rim across grain in brecciated chromitite rocks (sample W30)	90
Fig. 3-23 Chondrite-normalized PGE content for podiform of chromitite from MOC.	95
Fig. 3-24 Chondrite-normalized PGE patterns of dunite and harzburgite of the MOC	95
Fig.3-25 PGE content versus Pd / Ir ratio diagram for podiform chromitite from MOC.	96
Fig. 3-26 Triangular diagram (Harris and Cabri, 1991) illustrating compositions of Platinum group minerals of MOC chromitites.	96

Fig. 3-27 (A and B) Chondrite-normalized PPGE / IPGE diagrams versus Σ PGE for the MOC chromitite and related ultrabasic rocks, A -the upper inset plot shows trends and fields for important types of chromite deposits (CH: chondrite, UM: upper mantle) B - plottes of studied samples on this diagram which is following ophiolitic trend.	101
Fig. 3-28 Plots of Pt/Pt* ($Pt_N / (Rh_N * Pd_N)$) versus Pd/Ir for the MOC chromitite shows that partial melting process which has influence on PGE concentration in chromitite rocks. Fractionation and partial melting trends from (Garuti et al. 1997b)	102
Fig. 4-1 Classification and nomenclature of gabbroic rocks in MOC (Diagram from Bose, 1997)	107
Fig. 4-2 Green to greenish grey banded gabbro in Ser Shiw valley	109
Fig. 4-3 Completely crushed plagioclase revealed that transformed to a cloudy mesh of fine aggregate of epidote under the effect of tectonic. (A: under PPL, B: XP).	109
Fig. 4-4 Slightly affected plagioclase and amphibole by crushing, (A: under PPL, 4X, B: under XP)	109
Fig. 4-5 Porphyroclastic texture in banded gabbro (A: under PPL, B: under XP)	109
Fig. 4-6 Polysynthetic twining in plagioclase (under XP)	110
Fig. 4-7 Subhedral hornblende crystal in banded gabbro (A: under PPL, B: under XP)	110
Fig.4-8 Acicular crystal of actinolite resulted from the alteration of clinopyroxene. (A: under PPL, B: XP)	110
Fig. 4-9 Granulated plagioclase, apatite and quartz in banded gabbro near the shear zone. (A: under PPL, 4X, B: under XP)	110
Fig. 4-10 Coarse clinopyroxene crystal contains small patches of amphibole. (A: under PPL, 10X, B: under XP)	111
Fig. 4-11 Sheared gabbro between Amadin and Mirawa village traversed by small veins	111
Fig. 4-12 Sheared gabbro with fine grain of plagioclase, amphibole and accessory minerals quartz and magnetite. (A: under PPL, B: under XP, 40X)	111
Fig.4-13 Jenson (1976) plots of gabbroic rocks in MOC showing its tholeiitic character.	117
Fig. 4-14 YTC diagrams (Davies et al., 1979 in Shamim Khan, et al. 2005) for gabbroic rocks of MOC indicating their tholeiitic affinity	117
Fig. 4-15 Zr- P ₂ O ₅ suggesting the tholeiitic affinity of gabbroic rocks of MOC.	117
Fig 4-16 A : Total alkali versus silica (Irvan and Baragar, 1971). B : AFM (Irvan and Baragar, 1971) C : K ₂ O versus silica (Le Maitre et al., 1989) diagrams of the gabbroic rock samples from MOC	118
Fig. 4-17 The plots of MgO vs major oxides of gabbro rocks in MOC [Fig.4-17c, and f the trends are from (Boztng et al. 1998)]	119
Fig.4-18 The plots of MgO vs. trace elements of gabbro rocks in MOC	120
Fig.4-19 Zr versus major elements plots for basic rocks of MOC	122

Fig. 4-20 Zr versus trace elements plots for basic rocks in MOC	123
Fig. 4-21 Some selected geochemical diagrams representing fractional crystallization process in the MOC gabbroic rocks (the trends and fields are from Wilson (1989).	124
Fig. 4-22 Zr vs. rare earth elements plots in the MOC basic rocks	125
Fig. 4-23 Chondrite-normalized REE patterns of gabbroic rocks in MOC	128
Fig. 4-24 Chondrite-normalized spider diagrams of gabbroic rocks in MOC	128
Fig. 4-25 Composition variation of plagioclase in gabbroic rocks of MOC	132
Fig. 4-26 Pyroxene compositions in the system Wo-En-Fs general compositional field are from Beccaluva, et al (1989).	132
Fig. 4-27 Cr ₂ O ₃ -Al ₂ O ₃ -Fe ₂ O ₃ diagram opaque minerals in MOC. (Steven, 1944)	133
Fig. 5-1 Plots of $\Delta \log fO_2$ vs. $Fe^{3+}/\sum Fe$ of chromite in chromitite, dunite, and harzburgite of MOC. showing the range of FMQ buffer (Parkinson & Richard, 1999)	137
Fig. 5-2 Al ₂ O ₃ Wt % in orthopyroxene (a) and clinopyroxene (b) versus Cr# in spinel diagrams for Mawat peridotites. Abyssal and fore-arc peridotite fields for orthopyroxene compositions from Bonatti and Michael (1989) and Parkinson et al. (2003), Abyssal and fore-arc peridotites field compositions from Usyal et al., (2007)	139
Fig. 5-3 Cr# vs. Mg# Compositional variation of Cr# versus TiO ₂ of chrome spinel from the peridotite of MOC. Abyssal peridotite field is from Dick and Bullen (1984) and Arai (1994a), fore-arc peridotite is from Ishii, et al. (1992), Parkinson and Pearce (1998) and boninite field is (from Van der Laan et al., 1992) and Sobolv and Danyushevsky (1994)	140
Fig. 5-4 V vs. Yb abundance (Pearce et al. 2000) for whole rock data shown with fractional melting trends for the oxygen fugacities of FMQ-1, FMQ, and FMQ+1 imply that the primary composition of peridotite samples suite from Mawat are similar to fertile MORB mantle (FMM) and modified by interacting hydrous melt generated in a suprasubduction environment as a result of the increasing degree of partial melting	140
Fig.5-5 Comparison of Cr# of spinel in chromitite and associated dunite and peridotite of Proterozoic and Phanerozoic ophiolites (Arai, 1997). Note that the Cr# of spinel in chromitite and dunite is quite similar, while it is not correlated with that of enclosing peridotite	143
Fig. 5-6 Comparison of Cr# of chromian spinel in chromitite and ultrabasic rocks of MOC with other localities in Iraq. Source data from (Ismail et al., 2007, Hamasalh, 2004, Buda, 1988, and Al-Chalabi, 2004 and the present study)	144

Fig. 5-7 Schematic illustration of genesis of podiform chromitite (a) oxidized hydrous melt generated by melting of hydrous mantle was supplied to harzburgite. (b) Close-up of the reaction zone (square in a). The reaction between harzburgite and the melt caused decomposition of orthopyroxene (OPX) and give rise to dunite. The reaction produced the high-Cr spinel in dunite and the secondary melt rich in SiO ₂ . The mixing with primary melt may have promoted spinel crystallization. Phase diagrams from Tamura and Arai, (2005)	147
Fig.6-1 Tectonic discrimination diagram (Pearce, 1985) showing the plots of ultrabasic rocks from MOC in the field supra subduction zone, (SSZ)	151
Fig. 6-2 Diagram showing ranges of Cr# of spinels in peridotites from different tectonic settings (Lee, 1999). The heavy-line part represents the majority of data plots. The ranges of Cr# in peridotites and chromitite rocks of MOC are indicated	151
Fig. 6-3 Comparative Cr# vs. Mg# plot chromian spinel of chromitites ultrabasic and pyroxenite of MOC and those in peridotites from (1) Mariana Trench (fore-arc basin; Ohara and Ishii, 1998), (2) Vela Basin and Mariana Trough (back-arc basins; Ohara et al., 1996 and 2002)	153
Fig. 6-4 Compositional variation of Cr# versus TiO ₂ of chrome spinel from the peridotite of MOC. Abyssal peridotite field is from Dick and Bullen (1984) and Arai, (1994a), fore-arc peridotite is from Ishii et al., (1992), Parkinson and Pearce (1998) and boninite field is from Van der Laan et al., (1992) and Sobolv and Danyushevsky (1994)	152
Fig.6-5 Relation between TiO ₂ vs. Al ₂ O ₃ of chromite in the studied area (SSB; Suprasubduction zone; LIP, large igneous province; MORB, mid ocean ridge basalt; OIB, ocean island basalt (Kamentsky et al. 2001)	153
Fig.6-6 Relation between Fo olivine and Cr# of spinel in chromitite rocks of MOC follow the spinel mantle array and plots in the field of relatively primitive arc magmas (basalt and high-Mg andesite). The field of OSMA, and primitive arc magma Arai, 1987, = the region of mantle peridotites)	156
Fig.6-7 Relationship between (Fe ⁺³ / (Fe ⁺³ +Al+Cr) atomic ratio and TiO ₂ Wt%. of chromitite rocks in MOC. The discrimination boundaries of spinel compositions of MORB, Arc magma and intraplate magma are (Arai, 1992a)	156
Fig. 6-8 TH-Hf-Ta tectonic discrimination diagrams (Wood, 1980) of rocks from MOC gabbroic rocks, N-MORB: is normal mid-ocean basalt, E-MORB: is enriched mid- ocean ridge basalt, WPB: within plate basalt	158
Fig.6-9 Cr-Y variation of gabbroic rocks from the MOC (the discrimination fields Pearce, 1980). IAT, Island arc tholeiitic, MORB, mid oceanic ridge basalt, WPB, within = plate basalt, SSZ, supra subduction zone.	158
Fig. 6-10 Co-variation diagrams of studied pyroxene indicating their tectonic settings.	159

List of Appendices

- Appendix 1: WSU XRF precision, limit of determination (2-sigma)
- Appendix 2: Detection limits of REE and trace elements using ICP-MS.
- Appendix 3: The results of XRF analyses of Dunite rocks in MOC
- Appendix 4: The results of XRF analyses of harzburgite rocks in MOC
- Appendix 5: The results of XRF analyses of lherzolite rocks in MOC.
- Appendix 6: The results of XRF analyses of pyroxenite rocks in MOC.
- Appendix 7: The results of REE analyses (ICP-MS) for dunite rocks in MOC and the chondrite REE values from O'Neill and Palme, (1998).
- Appendix 8: The results of REE analyses (ICP-MS) for harzburgite rocks in MOC.
- Appendix 9: The results of REE analyses (ICP-MS) of lherzolite in MOC.
- Appendix 10: The results of REE analyses (ICP-MS) of pyroxenite in MOC.
- Appendix 11: The results of microprobe analyses of mineral composition in dunite of MOC
- Appendix 12: The results of microprobe analyses of mineral composition of harzburgite in MOC
- Appendix 13: The results of microprobe analyses of mineral composition in lherzolite of MOC.
- Appendix 14: The results of microprobe analyses for mineral composition in pyroxenite rocks of MOC.

Chapter One

Introduction

1.1 Preface

Alpine-type ophiolite is a columnar section of igneous rock composed of upper basalt member, middle gabbro member and lower peridotite member (Fig1-1 A) and it is interpreted to be thrust sheet of ancient oceanic lithosphere which has been obducted over the continental crust in the course of orogeny.

It may have formed either at divergent plate boundaries which is mid-oceanic ridges (MOR) or convergent plate boundaries which is supra-subduction zones (SSZ). These types are identified by chemical composition of the rocks and minerals in comparison with those from various tectonic settings on the earth at present. The term ophiolite means snake stone in Greek, basalt and gabbro are commonly altered to patchy green rocks, and peridotite is mostly changed into black, greasy serpentinite. Ophiolite was first described in the Alps in the 20th century, and was later discovered from almost every orogenic belt on the earth. It occurs as a nappe (intact thrust sheet) or as a melange (tectonic mixture of fragments). In collisional orogenic belts, ophiolites generally lie on older continental basement. In circum-Pacific orogenic belts, however, ophiolites generally lie on younger accretionary complexes (Ishiwatari, 2003).

Petrological characteristics of ophiolites are very useful as indicators of tectonic and magmatic processes of lithosphere formation and accretion. The mantle peridotite samples dredged from the mid-ocean ridges are mostly lherzolite, while those dredged from the supra subduction zones (trench walls) are mostly harzburgite. Reported formation ages of ophiolites show three distinct peaks at about 750, 450, 150 Ma, respectively (Fig.1-1 B). These are called ophiolite pulses. Each pulse corresponds to the period of worldwide magmatic event as represented by voluminous granite intrusions. Production rate of oceanic crust was distinctly high during the 80 and 120 Ma interval of Cretaceous time, as evidenced by wide area of the ocean floor formed in this interval (Fig. 1-1 B).

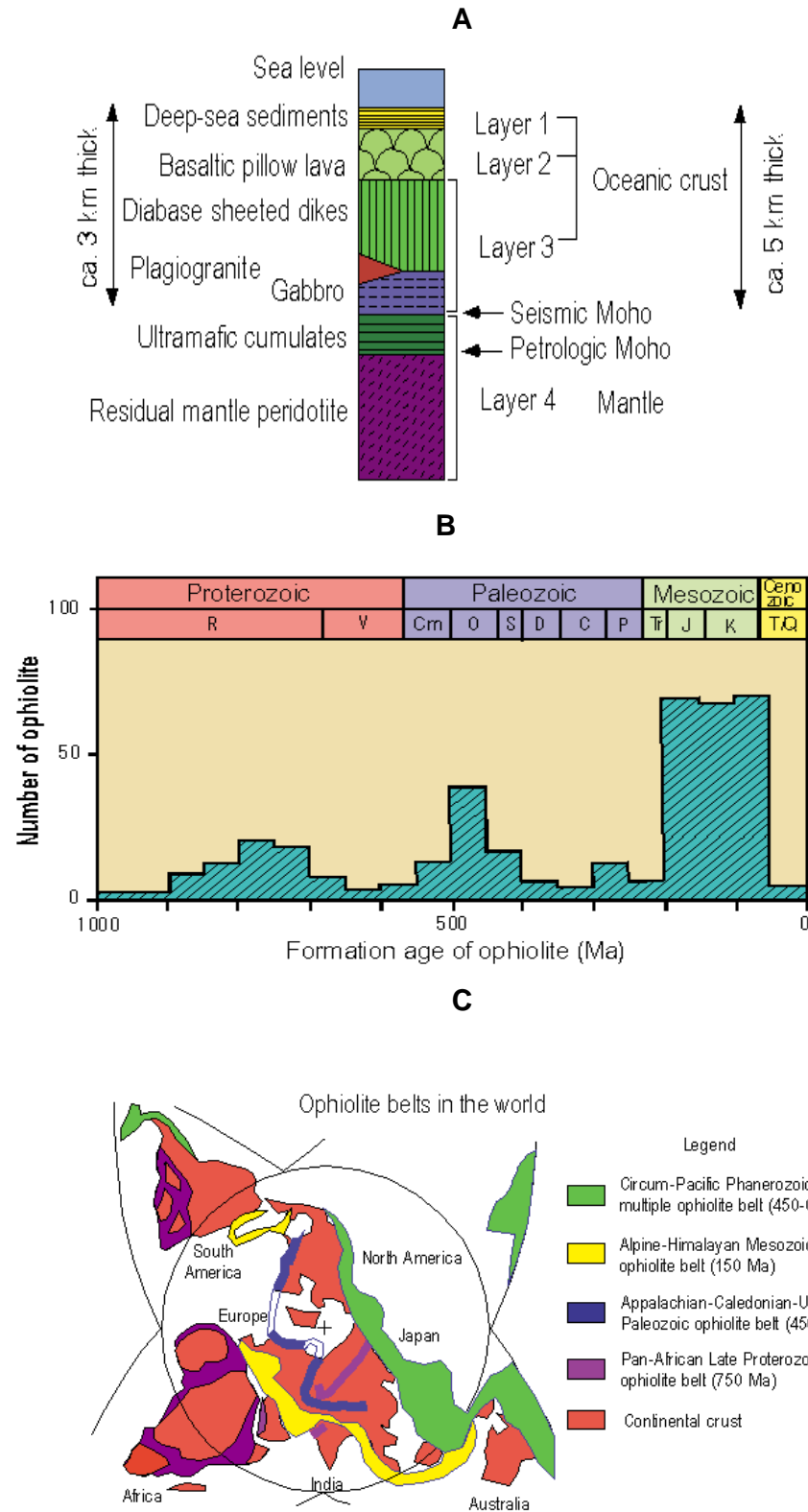


Fig.1-1 **A:** Ophiolite succession and seismic layers of oceanic crust; **B:** Histogram of formation ages of Ophiolites in the world; **C:** Ophiolite belt in the world (Akira Ishiwatari, 2003)

Ophiolites issued by each pulse tend to form a particular ophiolite belt. Late Proterozoic (ca. 750 Ma) ophiolites are distributed in Pan-African orogenic belt, early Paleozoic (ca. 450 Ma) ophiolites appear in the Appalachian-Caledonian-Uralian belt, and Mesozoic (ca. 150 Ma) ophiolites dominate the Alpine-Himalayan belt (Fig.1-1 C).

The Mawat Ophiolite Complex (MOC) is one of the best exposed oceanic lithosphere located 30km of Sulaimani which is a part of Iraqi Zagros Thrust Zone (IZTZ). There are few studies dealing with petrogenesis of ultrabasic and basic rocks of MOC such as (Aqrawi, 1990, Zekaria, 1992, and Aswad, et al., 1993). Their interpretations about the petrogenesis of these rock types and tectonic setting are controversial. For this reason different rock types namely ultrabasic, basic and chromitite rocks have been selected in the studied area located in MOC. In order to explain the petrogenesis and tectonic settings of MOC the study focused on chromite composition in these rocks types as a good indicator for petrogenesis and tectonic settings. The study also focused on the distribution and concentration of platinum group elements in chromitite rocks of MOC, for the first time, which are considered as one the target for petrogenetic and tectonic interpretations to approve the genesis of the MOC.

1-2 Geographic Location

The area under study is located 30km. northeastern of Sulaimani and about 5km north of Chwarta-Iraqi Kurdistan Region. The area of investigation lies between longitude (45° 28.00' E-45° 36.00' E), and latitude (35° 48.00' N - 35° 52.00' N) (Fig. 1-2). It comes under the survey map scale (1: 125000). The Mawat Igneous Complex represents elevated area which is triangular in outline and represents a rugged topography and complicated structures consisting of high mountain peaks and irregular steep valleys; it covers about 250 square kilometers. It is bordered by Lesser Zab River (Iranian Borders) from the north and by topographically low region composed of sedimentary rocks from east, south and west.

The Mawat Ophiolite Complex (MOC) represents part of the Iraqi Zagros thrust zone which is a member of the Alpine Himalayan orogenic belt of Cretaceous age (Buda & Al –Hashimi, 1977). It trends NE-SW in the northeastern part of Iraq, and covers an area of about 250 square kilometers (Fig.1-3). The stratified igneous complex of MOC consists (from bottom to top) of a thick sequence about >2000m of serpentinized ultrabasic rocks (dunite, harzburgite, and lherzolite), pyroxenite and chromitite. Tectonically overlain by amphibolized gabbro, metagabbro and green schist which are associated with intermediate and acidic minor intrusions. The major outcrop of ultrabasic is in the eastern part of the complex. However small occurrences of these ultrabasic are also present in the western and southern part. Gabbroic rocks are the main rock types present in the Mawat Ophiolite Complex, and seem to form the majority of the complex. The gabbroic rocks in the northern and southern parts are overlain tectonically by metavolcanic rocks (spilitic basalt, metabasalt, metadiabase, green schist and amphibolites). Basic and ultrabasic masses are associated with intermediate and acidic minor intrusions.

1-3 Sampling

193 samples were collected from main six traverses along most igneous bodies which cover the greater part of the exposed complex rocks. The traverses are nominated in Figure 1-2. Coordination and number of samples from these traverses are listed in Table 1-1.

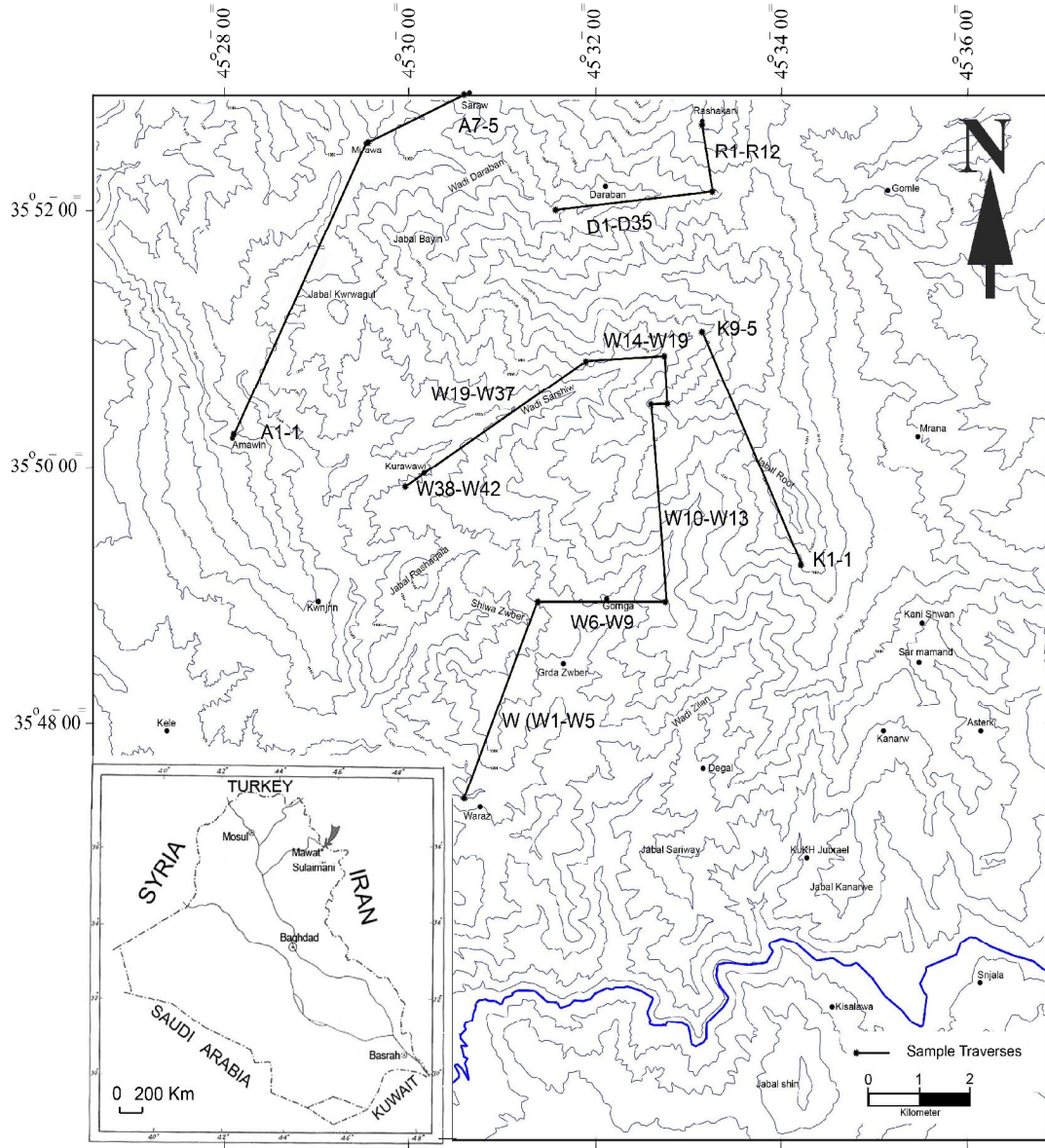


Fig. 1- 2 Location and topographic map of the studied area showing the studied traverses and distributions of samples.

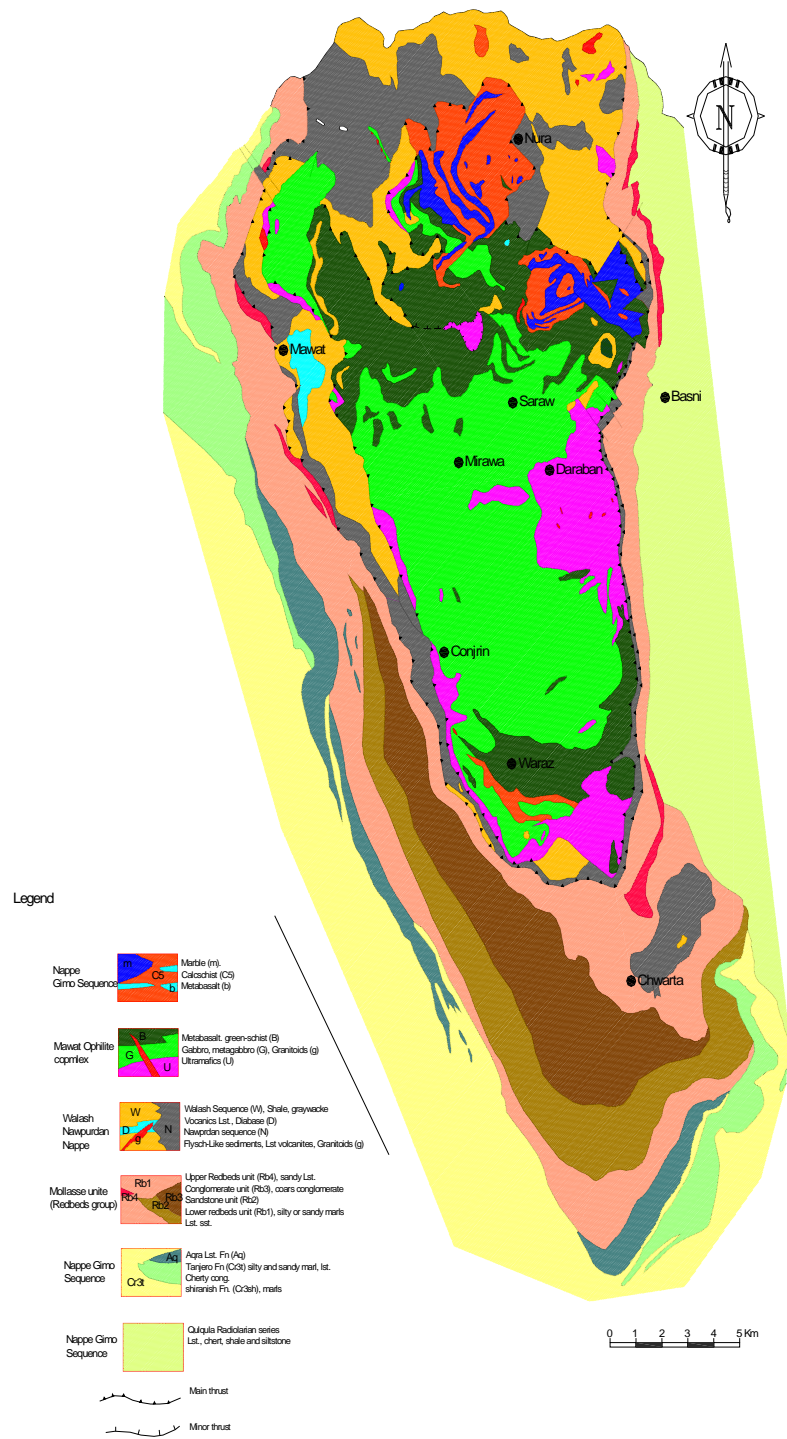


Fig. 1-3 Geological map of Mawat-Chwarta area, Kurdistan Region, NE Iraq (Al-Mehaidi, 1974)

Table 1-1 Coordination and localities of studied samples along the main selected raverses with main rock types.

Traverse	Selected locations	Symbol	Coordination	Number of collected samples	Main rock types
1	Rash Kani-Daraban 1	R	35° 52.710' N 45° 33.155' E To 35° 52.08' N 45° 31.493' E	35 samples	Serpentinized ultrabasic rocks and coarse gabbro
	Daraban1-Daraban2	D	35° 52.08' N 45° 31.493' E To 35° 52.13' N 45° 33.157' E	47 samples	Peridotites , pyroxenite With little abundant of gabbro, amphibolites rocks
2	Amaden-Merawa	A	35° 50.19' N 45° 28.10' E To 35° 52.59' N 45° 29.54' E	8 samples	Gabbro with minor acidic intrusions
	Merawa-Saraw	A	35° 52.59' N 45° 29.54' E To 35° 53.44' N 45° 30.67' E	5 samples	Gabbroic rocks
3	Waraz	W	35° 47.31' N 45° 30.656' E	5 samples including W1 to W5 from the banded gabbro	Banded gabbro ,volcanic basic igneous rocks and intermediate igneous rocks(The samples from banded gabbro)
	Goranga	W	35° 48.982' N 45° 31.423' E	3 samples (W6-W9)	Banded gabbro and intermediate igneous rocks. samples from banded gabbro
	Kanakarash	W	35° 48.982' N 45° 31.423' E	4 samples (W9-13)	Banded gabbro Meta gabbro and serpentinite
	Top of Ser Shiw valley-1	W	35° 50.501' N 45° 32.657' E	6 samples (W14-W19)	Dunite, peridotite, pyroxenite and serpentinite
4	Ser Shiw valley- 2	W	35° 50.56' N 45° 32.710' E	19 samples (W19-W37)	Chromitite rocks envelops with dunite and separated by harzburgite
	Ser Shiw valley- 3	W	35° 50.842' N 45° 32.774' E		
5	Kuradawi -1	W	35° 50.889' N 45° 31.931' E	5 samples (W38-W42)	Banded gabbro
	Kuradawi-2	W	35° 49.94' N 45° 30.2' E		
6	Shakha Root	K	35° 49.242' N 45° 34.079' E	56 samples including K1-1 to K9-5	Peridotite, pyroxenite with banded and coarse gabbro
	Top of Ser-Shiw valley	K	35° 51.042' N 45° 33.066' E		Peridotites with pyroxenite dyke

1.4 Previous Studies

Horn and Lees (1943) introduced the Nappe zone occurrence for Iraqi Zagrose unit which they subdivided into three structural sub-units namely the Igneous Nappe, the Metamorphic Nappe and Radiolarian Zone.

Lehner (1954) draw the first geological map of Mawat and north part of Chwarta using scale 1:100000.

Bolton (1957), modified the Lehner (1954) map and mapped the Qandil, Bulfat, and Mawat range (scale 1: 100,000). According to the mainly field studies and other available data he concluded that this zone is composed of three major structural units from top to bottom, Qandil metamorphic series, Walsh volcano sedimentary sequence and the Naopurdan shally series.

Bolton (1958) concluded that the Mawat mass with its igneous rocks, is allochthonous and indicate that the Mawat mass consists of two thrust sheets as a Nappe. The lower sheet consists of sedimentary sequence of grey clastic interbedded with massive nummulitic limestone. These clastics were correlated with the Naopurdan series (Eocene- Oligocene). The upper sheet is formed by complex sequence of regionally metamorphosed red shale's and limestones, metamorphosed basic volcanic and intrusive bodies. He correlated this sheet with Walsh volcanic series of Eocene age. These Nappes overly a heterogeneous ground of sedimentary rocks ranging in age from Middle Cretaceous to Pliocene.

Smirnov and Nelidov (1962) investigated the northeastern thrust zone for metallic occurrences; their findings were not different to the finding of Bolton apart from their belief that the Mawat igneous Complex was intruded in situ.

Al- Etabi (1972) studied the petrography of basic-ultrabasic igneous rocks and metamorphic rocks part of Mawat complex. The basic rocks represented by gabbro which is sub-divided to amphibolites gabbro, fine gabbro, pyroxene gabbro and meta gabbro. He also sub-divided the ultrabasic rocks in to dunite, peridotite, and pyroxenite.

Akif et al. (1972) forwarded the preliminary report on geology and mineralization of Sershiw ultrabasic body and they divided the ultrabasic

rocks in this area into dunite, chromite dunite, pyroxene peridotite, pyroxenite and hornblende.

Jassim (1972, 1973) investigated the central sector of the Mawat Complex and recognized numerous magmatic events and he gave special attention to petrographic description and textural modification of the ultrabasic and basic rocks in the area. He concluded that the gabbros show igneous layering related to crystal settling and that the modifications in the mineralogy occurred partly while the gabbros were in the semi-solid state and partly during thrusting process.

Mashek and Etabi (1973) studied the petrology of igneous and metamorphic rocks of Mawat Complex, they recorded that the relation between basic and ultrabasic rocks is not always distinct. Also he concluded that pyroxenite is younger than gabbroic rock and ultrabasic rocks.

Al – Mehaidi (1975) suggested that the Mawat Igneous Complex represents an Ophiolitic sequence and consists from bottom to top of ultrabasic, gabbro and diabases.

Al- Hassan (1975) studied the petrology of both Mawat and Penjwin Igneous Complexes, and found similarities in texture, mineralogy and chemistry of igneous masses of both and concluded that these complexes had similar genesis and had suffered similar post- magmatic history.

Al-Hashimi and Al-Mehaidi (1975) studied the Ni, Cu, and Cr dispersion in Mawat Ophiolite Complex, and concluded that the differences in Cr and Ni content in the heavy fraction correspond to primary petrological difference between described rock types and Cu had low primary contents in the different rocks and relatively high contents along fractures and sheared zone, associated with small acidic intrusions cutting both gabbro and basaltic rocks.

Jassim and Al-Hassan (1977) made a petrographic comparison between Mawat and Penjwin Igneous Complexes. They showed that the two complexes are similar in most respect and suffered probably similar magmatic and post-magmatic history. They found that the gabbros and

ultrabasic rocks were uralitized and serpentinized respectively, probably during semi-solid emplacement of the bodies, and these processes were closely followed by marginal emplacement of the minor intrusions and dynamic metamorphism during transportation by thrusting of allocthonous masses. They also showed that cryptic variations occur in the gabbro away from the outer contact with the ultrabasic rocks.

Buda and Al-Hashimi (1977) studied the petrology and geochemistry of Mawat Igneous Complex and they showed that it consists of succession of rocks peridotite (lherzolite, dunite), podiform and schlieren type chromites, banded Gabbro, pyroxene Gabbro, meta basalt, spilite, keratophyre with minor intrusion of acidic magmatite (albite granite). They conclude that this association is typical of Alpine type orogenic belt.

Aswad, and Ojha, (1984) studied the petrology and geochemistry of coarse-grained altered sub volcanic, hypabyassal rocks (spilitized diabase) in southern part of Mawat Ophiolite Complex between Waraze and Kanaro villages. Petrographically, they distinguished that these rocks consist of coarse grained albite, hornblende- actinolite and the latter makes 40-50% of total volume of the rocks which show uralitization. From the distribution of immobile elements (Zr, Y, Cr, and Ni) they concluded the tectonic environment which is inferred to be ocean-floor basaltic type.

Buday and Jassim (1987) classified the Chwarta- Mawat area within Walsh-Pinjween sub zone. Also they gave some petrographic description and geochemical analysis of the igneous rocks in MOC.

Aswad and Elias (1988) studied the petrogenesis, geochemistry and metamorphism of sub volcanic rocks of the Mawat Ophiolite Complex. By using the (K^{40} , Ar^{40}) isotopic analysis they indicated that the age of the metamorphism is Albine-Cenomanian. They also described the metamorphic conditions by low-pressure and medium temperature with steep geothermal gradient of $140C^{\circ}/ Km$.

Al- Saadi (1990) studied the volcanic rocks of the thrust zone in Shalair valley, Mawat, and Bulfat. Geochemically he concluded that the volcanic

rocks of Mawat are mostly basic rocks subjected to alteration processes in spite of preservation of some original textures and structures and grossly similar to greenschist facies. They contain high concentrations of Cr, Co, and a medium amount of V. He concluded that the rocks of Mawat are characterized by their ophiolitic origin with tholeiitic affinity.

Aqrabi (1990) studied the ultrabasic and gabbro in an area around Shakha Root mountain of Mawat Ophiolite Complex. His study revealed that the ultrabasic rocks tectonite is composed from bottom to top of lherzolite, harzburgite and dunite. These rocks are characterized by tectonic fabric. From the geochemical study he suggested that the tectonite represent refractory residual of the upper mantle subjected to different degrees of partial melting. The gabbroic rocks display textural feature which result from recrystallization, tectonic deformation, alteration and metamorphism processes and the source of primary magma of gabbroic rocks is not related to the underlying tectonite.

Zekaria (1992) studied the petrology and geochemistry of southern part of Mawat Ophiolite Complex and indicated that the peridotite tectonite is composed of (lherzolite, harzburgite, and dunite) from bottom to top. The basic rocks composed of banded and isotropic gabbro, diabase and basalt, from the geochemical evidence illustrated that the tectonite represents depleted upper mantle origin which are subjected to different degrees of partial melting at mantle condition. They suggested that these rocks plot in the fields of ocean – floor basalt and low- tholeiites.

Al-Samman et al. (1996) studied the geochemical variation in volcanic rocks (metabasalt) at Waraz area of Mawat Ophiolite Complex, and he concluded that the chemical variation in metabasalt is due to two main processes: secondary alteration processes and primary magmatic processes. He also indicated that submarine weathering was limited, extend within volcanic rocks and their effects have been submerged by the later low grade hydrous regional metamorphism. Based on the immobile elements in

Waraz samples he showed that the majority of rocks are basic in composition with minimal differentiation and are tholeiitic in character.

Aswad (1999) discussed the tectonic evolution of the region of Northeastern Iraq in view of two Ophiolite Complex, namely Mawat and Penjwin. He concluded that the Mawat Penjwin region is the product of arc-continent collision, and the tectonic perturbations resulting from the intra-ocean convergence produce IAT and CAB magma of Walsh. His study revealed that the culminating oceanization episode that produced Mawat – Penjwin Ophiolite was of the Albian-Cenomanian age and recommended that the time span of ocean crust formation was 97-118 Ma.

Aqrawi (2000) studied the serpentinite rocks from Mawat, Penjween, Galala and Rayat and their utilization for ceramic industry. From his study indicate that the uses of these materials are suitable in the formation of cordierite ceramics (i.e. electrical, ceramics, cordierite refractories).

Numan, N.M.S., 2000. Studied the Major Cretaceous tectonic events in Iraq and he concluded that the major geodynamic inversion took place in the Cretaceous in Iraq from extensional tectonism of Triassic and Jurassic into compressional tectonism throughout the Cretaceous and Tertiary.

Mohammed (2004) studied the petrology and geochemistry of Penjwin and Mawat serpentinites rocks and he concluded that the Mawat serpentinite rocks represents isolated body of fore-arc formed by hydration of mantle wedge rocks along subduction at depth 15-30 Km and serpentinized by water derived from the down-going oceanic crust through a series of dehydration reaction and emplacement into Walsh volcanic series diapirically.

Karim (2005) considered the Mawat – Chwarta area as a graben formed by subsidence attributed to the normal faulting.

Jassim and Goff (2006) considered the MOC as more complete than the Penjwin complex and do not contain a complete ophiolite sequence. They described that the MOC to consist of about 600-1000m of basalt (Mawat Group) intruded by a plutonic complex of ultrabasic, pyroxenite, layered and coarse gabbro, diorites, dolerite dykes and late stage plagiogranite

differentiates overlain by roof unit of 600m of interbedded marble and basalt (Gimo Group).

Koyi (2006) studied the petrochemistry, petrogenesis, and isotope dating of Walash volcanic rocks of Mawat- Chwarta area (Waraz, Kanaro) indicated that the Walash volcanic rocks affected by lower amphibolites facies during ocean-floor metamorphism. He also revealed that the majority of these rocks are basic in composition with differential to andesite sub alkaline (tholeiite and calc alkaline) affinities. He related these rocks to island arc tholeiite and calc alkaline basalt and these rocks belong to (M.Eocene- U- Eocene) age.

Farjo (2006) studied the geochemistry and petrogenesis of the volcanic rocks of Mawat Ophiolite Complex. From the geochemical evidence he indicated that the Mawat Ophiolite was formed in the early stages of intraoceanic young supra – subduction zone at palaeo- ridge axis. He also indicated that these volcanic rocks have originated from the same mantle source dominated by harzburgite and dunite. He considered the Gimo sequence as a part of the Ophiolite and not covered the Ophiolite.

Mirza and Ismail (2007) studied the minor acidic intrusions in the area between Amaden and Mirawa (shear zone) of MOC and they concluded that these minor acidic intrusions were trondhjemite in compositions and their origin is related to the result of partial melting of hydrated basaltic / gabbroic rocks.

1.5 Aim of the study

The main aims of this study were:

1. Detailed study of the mantle rocks of MOC including detailed petrological and chemical characteristics of ultrabasic (dunite, harzburgite, lherzolite pyroxenite, chromitite) and gabbroic rocks and to compare them with other ophiolites. Also to conclude the genesis and tectonic setting of the area based on chemical composition of these rocks types.
2. To study the chromite ore deposits within Zagros Thrust Zone and to give mineralogical composition and geochemical aspects. To clarify the genesis of the formation of chromites ores in the area also to make a comparison of

chromitite rocks of MOC with other chromite occurrences in ZTZ as well as to comparing them with regional chromitite rocks of the world.

3. Study of distribution and concentration of platinum group elements (PGEs) within ultrabasic.

4. Determination the geothermometry of the formations with determining the degree of partial melting of the rocks.

1.6 Geology of the studied area:

The Mawat Ophiolite Complex is situated 30 Km north east of Sulaimani city. It represents part of the Iraqi Zagros thrust zone .The Complex extends for 25 Km striking NE- SW parallel to thrust zone with a width of 7-12 km, thus it covers an area of about 250 square Km (Fig. 1-3). It is bounded by Lesser Zab River from the north and is totally surrounded by sedimentary sequence from the east, south and west except for the northern part of the contacts which are tectonic (Al-Hassan,1975). The Mawat Ophiolite Complex consists of two thrust sheets as Nappes (Al-Mehiaidi, 1975). The lower sheet consists of sedimentary sequences of grey clastic interbedded with massive nummulitic limestone. These clastic were correlated with Naopurdan Formation (Eocene-Oligocene).The upper sheet is a complex sequence of regionally metamorphosed red shale's, limestone, and metamorphosed basic volcanic and intrusive bodies. This sheet is correlated with Walash Volcanic Series (Eocene age). The Naopurdan and Walash sheets generally overlie some flysch sediment of Upper Cretaceous age (Shiranish, Aqra, and Tanjero) Formations and superimposed by the Mawat Nappe which is an Ophiolite and depositionally overlapped by Gimo sequence. Both the Mawat Ophiolite and Gimo sequence underwent mostly low grade regional metamorphism prior to Nappe movement (Al-Mehiaidi, 1975; Al-Hassan, 1975).The major rocks types in Mawat Ophiolite Complex are basic and ultrabasic rocks, with small bodies of acidic and intermediate minor intrusions dyke in the western part of the Complex. These major rock types from bottom to top are as follows:

1.6.1 The Ultrabasic Rocks

The ultrabasic rocks are composed of serpentized dunite, harzburgite, lherzolite, chromitite and pyroxenite. It ranges from few meters to about 15 square kilometers (Fig. 1-3) thickness overlying tectonically the Walsh-Naopurdan Nappe rocks (Al-Mehiadi, 1975). The major part of ultrabasic exists in Daraban, Ser-Shiw, and Shakha Root areas, however, minor bodies are found in southeastern and north western part (Al-Etabi, 1972, Akif et.al. 1972, Jassim and Al-Hassan, 1977 and Aqrawi, 1990). The ultrabasic rocks consist mainly of harzburgite and dunite with minor abundances of lherzolite, pyroxenite and chromitite. These rocks are affected by various degrees of serpentinizations at the bottom (Jassim, 1972).

The pyroxenites are intermingled with the dunite, harzburgite tectonite, and seem to cut through the banded gabbro at the same time. Pegmatite pyroxenite is also common as patches with the coarse gabbro body; they are formed mostly of olivine webstrite and clinopyroxenite (Buday, 1987). The chromitite bodies are exposed at about 2 km north of Kuradawi village as occurs as massive podiform and as disseminated and accessory type in Ser-Shiw - Shakha Root area which are associated with dunite and harzburgite.

The chromitite bodies are enclosed in dunite envelope and the host rock is harzburgite. In Daraban and Ser-Shiw area the ultrabasic rocks are bordered by gabbro from the northwest and south whereas from the east it interbedded with nummulitic limestone beds which are correlated with Naopurdan Formation. This contact dips at angle of 20° to 40° toward the west and its taken to be as tectonic contact (Jassim and Al-Hassan, 1977).

1.6.2 The basic rocks

The basic rocks occupy the central part of the ophiolite, they covers an area of about 170 square kilometers. This type of basic rocks consists of amphibolized gabbro, pyroxene gabbro, metagabbro, green schist and albite amphibolites (Jassim, 1972) and (Al-Mehiadi, 1975). The gabbroic rocks are classified by (Al-Etabi, 1972) into amphibolite gabbro, fine grained gabbro with

diabase texture, pyroxene gabbro, and meta gabbro. While the present study and (Jassim and Al-Hassan 1977) classified gabbroic rocks in MOC into:

Banded gabbro

It covers an area about 170 square kilometers, mostly forming the western and northern parts of the complex (Buday, 1987). This body has intrusive contact with green schist in the west, southwest and south. This contact has been obscured by minor intrusions in the western part. To the east the banded gabbro has sharp contact with the coarse pyroxenite gabbro (Jassim, 1973). The banded gabbro are greenish to grayish green color, uniform in mineralogy and texture; it composed of plagioclase, various types of amphibole, chlorite and magnetite. The banded gabbro was classified by Jassim (1972) into three types which are: rhythmic banding, injection banding and alteration banding.

Coarse gabbro

The coarse gabbro has been identified as a separate intrusion by Jassim, (1972) and characterized by very coarse grain > 1 cm with abundance of pyroxene grain. It is spotted-dark green to greenish grey in color, white spot of plagioclase are characteristic throughout. The coarse gabbro occupies about 4 square kilometers on the high ground of Rasha-Kani village and bordered by banded gabbro from the north, west, and south, and by ultrabasic mass of Daraban from the east.

1.6.3 The volcanic rocks

The volcanic rocks mainly exposed in northern and southern part of the Mawat Ophiolite Complex and are about 400m thick. Al- Mehaidi, (1975) distinguished these types of meta volcanic member which are spilitic basalt, meta basalt, and some meta pyroclastic. The basaltic rocks are mostly amygdaloidal and show pillow structure in some places. The meta diabase occupies the transition zone from gabbro to basalt. Buda and Al-Hasshimi (1977) provide an excellent material for studying the spilitic problem related to ophiolite and they reported the presence of these types of extrusive rocks, metabasalt, spilite, and keratophyres. While according to (Aswad and Ojha,

1984) the volcanic rocks of Mawat Ophiolite complex are classified into two groups. The first group is fine grained rocks with volcanic texture such as amygdaloidal, varietic, and pillow structures are occasionally associated with meta pyroclastic metamorphosed to green schist to epidote amphibolite facies. The second group represented by coarse grained altered subvolcanic hypabyssal and gabbroic rocks not confined to volcanic texture but rather show ophitic, subophitic, intersertal and porphyroblastic texture. The upper volcanic rocks from MOC and the volcanic part of Gimo sequence were studied by Farjo, (2006). He concluded that the MOC was formed in the early stage of intraoceanic young supra-subduction zone (SSZ) at palaeo-ridge axis or close to it which lead to contemporaneous eruptions in a fore-arc setting of island arc tholeiitic basalt and boninites.

1.6.4 The minor intrusions

The banded gabbro is severely traversed by shear zones especially in western parts of Merawa (Jassim, 1972; 1973; Jassim and Al-Hassan, 1977; and Mirza and Ismail, 2007). These zones slightly arcuate in form and roughly north- south in orientation and extend for few hundreds of meters in width. The minor intrusions that are especially abundant in the sheared gabbro are classified by Jassim, (1972) into three main types, which are coarse diorite with disseminated pyrite and chalcopyrite, very fine grained quartz diorite (the predominantly type), and aplite granite. Mirza and Ismail, (2007) revealed that the minor intrusions in the area between Amaden and Mirawa villages (the sheared area) are of trondhjemite in composition. These rocks are distinctively enriched in large ions lithophile element LILE compared to high field strength elements HFSE. This feature is commonly apparent in volcanic arc granite.

The origin of plagiogranite in MOC explained as a result of partial melting of hydrated basaltic / gabbroic rocks.

1.7 Tectonic setting

The Zagros suture zone was formed within the Neo-Tethys. They were thrust over Arabian Plate during two distinct phases of obduction and collision, during the Late Cretaceous and Mio-Pliocene. There are many

tectonic subdivisions of Iraqi Zagros Thrust Zone (IZTZ), one of the famous classifications is made by Bolton (1958) he classified the IZTZ into three structural units forming a parautochthonous unit of Tertiary or sometimes Cretaceous age. He distinguished the outer and structurally lowest unit as Naopurdan Series, which is composed of flysch-like sediment. The middle unit, the Walash Series is a volcano-sedimentary sequence of rocks, and the inner and structurally highest unit is the Qandil series. Budy and Jassim, (1987) divide this zone into three tectonic subdivisions as follows:

I-External Zone

- a- Balambo - Tanjero subzone.
- b- Northern- (Ora) Thrust Zone.

II- Central Zone

- a- Qulqula-Khwakurk subzone
- b- Penjwin-Walash subzone

III- The internal Shalair Zone

According to this classification the MOC is located in Penjwin-Walash subzone in central zone of geosynclinals unit. Numan (1997) modified (Dunnington, 1958, Bolton, 1958, and Buday & Jassim 1987) classifications of Iraqi territories in a view of plate tectonic motions and nominated the IZTZ by Subductional tectonic facies of the Iraqi Thrust. Jassim and Goff (2006) identified three tectonic zones within Iraqi Zagros Thrust Zone (IZTZ) comprise from SW:

- 1-The Qulqula-Khwakurk Zone with deformed radiolarites carbonate turbidities and volcanic, and an upper thrust sheet of Triassic platform carbonates.
- 2-The Penjwin-Walash Zone with upper thrust sheets of metamorphosed volcanic, carbonate and pelitic rocks, and lower thrust sheets of non-metamorphosed Paleogene arc volcanic and fore-arc flysch.
- 3-The Shalair Zone comprising thrust sheets of meta-pelitic and meta carbonate of Mesozoic age, Upper Cretaceous arc-volcanic of Late Cretaceous age and metamorphosed Paleozoic rocks of Sanandaje-Sirjan

Zone.

According to this classification the studied area is also located within the Penjwin-Walash Zone. The Mawat Ophiolite Complex (MOC) is situated in north east of Iraq and the complex is part of the Iraqi Zagros Thrust Zone (IZTZ) which in turn is a member of Alpine-Himalayan Orogenic belt of Mesozoic Tethyan oceanic plate, (Buda and Al-Hashimi 1977). The Zagros fold –thrust belt extends for about 2000 Km and developed in an epicontinental, synorogenic proforeland basin, whose evolution has been intimately related to tectonic and structural events of associated Zagros Orogen. The Zagros Orogen is interpreted by Alavi (2004) and Jassim and Goff (2006) as the product of major sequential geotectonic events (1) subduction of Neo-Tethyan oceanic plate beneath the Iranian lithospheric plates during Early to Late Cretaceous time (2) obduction of Neo-Tethyan oceanic slivers (ophiolites) over the Afro-Arabian passive continental margin in Late Cretaceous (Turonian to Campanian) time and (3) collision of Afro-Arabian continental lithosphere with Iranian plate that started in Late Cretaceous. Falcon (1969 and 1974) and (Hessami et al. 2001) divided the Zagros Orogenic into three zones (the thrust zone, the Zagros imbricated zone and the Zagros fold thrust belt). While (Alavi, 2004) divided the Zagros Orogeny into three parallel belts (Urmich –Dokhtar magmatic assemblage, the Zagros imbricated zone (the Sanandaje-Sirjan zone as redefined by Alavi, (1994), after (Stocklin, 1968a, 1977) and Zagros fold thrust belt). The MOC is a part of Zagros imbricated zone which is a zone of thrust faults that have transported numerous slices of metamorphosed and non-metamorphosed Phanerozoic stratigraphic units of Afro-Arabian passive continental margin, as well as its obducted ophiolites, from the collision suture zone on the northeast toward the interior parts of the Arabian cratons to the south west.

1.8 Analytical technique

1.8.1 Microscopic study

Many analytical techniques have been used in the present study beginning with petrographic study using polarized microscope. Modal volume % of

minerals determined by point counting (model E Swift) involving 300 points covering the whole area of a thin section. Some uncertainty is expected because of the small size and alteration of grains. The reflected light microscope type (Meiji) was used for studying the chromite ore.

1.8.2 XRF and ICP-MS analysis

Major and trace elements analyses were taken from X-ray-fluorescence (XRF) analyses carried out on glass fusion beads and powder pellets, respectively, on a Thermo-ARL Advant'XP+ X-ray fluorescence spectrometer (XRF) at GeoAnalytical laboratory, School of Earth and Environmental Sciences, Washington State University. The concentrations of 27 elements in unknown samples are measured by comparing the X-ray intensity for each element with the intensity for two beads each of eight USGS standard samples (PCC-1, BCR-1, DNC-1, W-2, AGV-1, GSP-1, G-2 and STM-1), using the values recommended by Govindaraju, 1994) and two beads of pure vein quartz used as blanks for all elements except Si. A rhodium (Rh) target is run at 50 KV/ 50mA with full vacuum and 25 mm mask for all elements. Precision and limits of determination (2-sigma) of XRF as in (Appendix, 1).

Rare earth elements (REE), and Ba, Th, Nb, Y, Hf, Ta, U, Pb, Rb, Cs, Sr, Sc, and Zr were determined by Hewlett Packard (Agilent) HP 4500 inductively coupled plasma-mass spectrometry (ICP-MS) at the Washington State University, power is 1300 watt under the condition MO^+/M^+ (the proportion of metal ions forming oxides) is minimized. The instrument is run in multi-element mode averaging 10 repeats of 0.5 sec/element for a total integrated count time of 5 sec/elements. Samples were first ground in an iron bowl in a shatterbox swing mill. Two grams of this rock powder is then mixed with an equal amount of lithium tetraborate ($Li_2B_4O_7$) flux, placed into a carbon crucible and fused in a 1000 °C muffle furnace for 30 minutes. The resulting fusion bead is briefly ground again in the chatterbox and 250 mg of this powder is dissolved on a hotplate at 110 °C to dryness, followed by additional evaporation with 2 ml

HClO₄ at 165 °C to convert insoluble fluorides to soluble perchlorates. 2 ml HNO₃, 8 drops of H₂O₂, 3 drops of Hf and internal standard of In, Re, and Ru

are added to the sample which is then diluted up to 60 ml final volume (1:240 final dilution). This combined fusion/dissolution procedure ensures the complete dissolution of zircon and other refractory phases such as garnet, while removing silica and boron as matrix elements by volatilizing them as gaseous fluorides. The detection limits for REE and Ba, Th, Nb, Y, Hf, Ta, U, Pb, Rb, Cs, Sr, Sc, and Zr by using ICP-MS as in (Appendix, 2).

1.8.3 Microprobe analysis

Selective mineral analyses were analyzed by (CAMECA, COMEBAX) dispersive electron probe X-ray microanalyser at Washington State University. Ferrous and ferric iron content of chromian spinel was calculated assuming spinel stoichiometry. Minerals were analyzed on polished thin sections for major and minor elements with a four tunable wavelength dispersive spectrometry microprobe (CAMECA, COMEBAX) at the Washington State University. The operating conditions were 20 KeV accelerating voltage, 13 nA beam current and beam diameters was 5 micron. The counting time was 10 second for (Na, Al, Si, and Fe) ka., 15 seconds for (Mg, Mn, Ni) ka., and 25 seconds for (Ca, Ti, Cr) ka., on the peak of the characteristic X-ray for each element. Calibrations were performed using natural and synthetic standard; albite #4 for Na ka., orthoclase MAD-10 for Al, and K ka., serpentine for Mn ka., diopside #1 for (Mg, Si Ca) ka., olivine #1 for Ni ka., fayallite, Rock port for Fe ka. Selected analytic results are the average of one points and detection limits ranged from 0.012 wt % for Ca ka. to 0.013 wt % for Ti ka. to 0.027 wt % for Al ka to 0.029 wt % for Mg ka to 0.048 wt % for Na ka. Raw intensities for each element were corrected using ZAF method. Six samples of polished thin sections from pyroxenite were analyzed at Cooperation Research Center Kanazawa University with a wave length dispersive microprobe (JEOL Superprob JXA-8800). Raw intensities for each element were corrected using ZAF method. Various natural and synthetic minerals used as standard.

Operating condition was 15 KV for accelerating voltage, 20nA for beam current, and 3 μ m for beam diameter on MgO (periclase). The counting time was 20 s on the peak of characteristic X-ray for each element. Analytical error

is < 0.5 wt % and < 0.1 wt % for major and minor element oxides respectively. Mg#, Cr# and Fe³⁺ #are Mg / (Mg+Fe²⁺) and Cr / (Cr+Al), and Fe³⁺ / (Fe³⁺+Al+Cr) atomic ratios respectively.

1.8.4 Platinum group analysis

Eight samples from eleven pods of Mawat chromitite rocks, and three samples from the host rocks were analyzed for all PGE, Au and other elements (Cu, Fe, Ni, Pb, Zn, Ag, As, Co, Cr, S) using inductively coupled plasma mass spectrometry after fire assay nickel sulfide NIS/Ms collection for PGE and Au and (At/OES stands for AT/OES Multi-acid digest including Hydrofluoric, Nitric, Perchloric and Hydrochloric acids in Teflon Tubes, analysed by Inductively Coupled Plasma Optical (Atomic Emission Spectrometry ICP-AES) for trace elements, at Genalysis Laboratory Services Pty Ltd, western Australia. The samples were dried at 120 degrees Celsius for 4 hours on receipt to satisfy Australian quarantine requirements. Following drying, the samples were crushed to around -10 mm particle size before being fine pulverized in a chrome-steel ring mill to a nominal 85% passing 75 micron particle size. Following preparation about 12 to 13 grams of each sample was catch weighed and assayed using a Nickel Sulphide fire assay collection formulated for the total recovery of all of the Platinum elements. The resulting nickel button is pulverized and a portion digested for analysis by ICP-MS. The type of standard used was American High-Purity or Plasma Chem Corp 1000 mg/l stock solutions for calibration reference materials on the mass spectrometry.

The detection limits are 2 ppb for Os, Ir, Ru, Pt and Pd, 1ppb for Rh and 5 ppb for Au. The detection limits of base metal in chromitite rocks are 1 ppm for Ag, Co, Cu, Ni, and Zn, 5 ppm for As, Pb, 10 ppm for S and 0.01 % for Fe.

Chapter Two Ultrabasic Rocks

2.1 Introduction

The ultrabasic bodies of MOC are comprised mainly of peridotite, dunite, serpentinite, chromitite and pyroxenite. The major outcrops of these rocks are in the eastern part of MOC, namely Daraban village-Ser Shiw valley and Shakha Root area covering an area about 15 square kilometers. However minor bodies are found in the southeast and northwestern parts of the MOC (Al-Etabi, 1972; Akif et.al. 1972 Jassim, 1972 and 1973; Masek and Al- Etabi, 1973). The harzburgite is always dominant over dunite, while the lherzolite represents subordinate amount of ultrabasic rocks of MOC. Lenticular concentrations of massive, podiform to disseminated chromites occur in both dunite and the harzburgite. The chromitite is closely associated with dunite: a chromite pod is enclosed by dunite envelope and the pods are separated by harzburgite.

The dunite are ball shape, light green to pale brown on weathered surface that break into olive-green to dark green characterized by the absence of layering and present of spheroid weathering, fine to medium grain size composed mainly of olivine and disseminate crystals of chromium spinel. Dunites are affected by variable degrees of serpentinization. Harzburgite and lherzolite are characterized by presence of layering having dark green to dark brown color and containing coarse crystals of pyroxene. They are cross cut by dykes of pyroxenite. The pyroxenite dykes were more associated with harzburgite and to a lesser extent with lherzolite. The pyroxenite dykes which are cross cutting the harzburgite in the extreme north of Shakha Root area are about 10-15 cm in width and extend for more than 5 m. They are fine grained, pale brown to greenish grey in color. The pyroxenite are also found as small lenses and dykes cross cutting the gabbro rocks, characterized by coarse grained dark green color. All pyroxenite rocks of Mawat are affected by variable degrees of alteration to talc and asbestos.

Four traverses covering approximately all ultrabasic body were selected in the present study. These traverses are given in (Fig. 1-6) and (Table 1-1).

-Rasha Kani – Daraban traverse.

-Daraban 1-Daraban 2 traverse.

-Kuradawi – Ser-Shiw traverse

- Shakha Root traverse.

152 ultrabasic samples are collected from these traverses. Detailed petrographic study of these samples are examined by using polarized microscope and modal volume % of minerals was determined by point counting (model E swift) involving 300 points covering the whole area of a thin section the results in (Tables 2-1, 2-2, 2-3, and 2-4)

The classification adopted for the ultrabasic rocks of MOC are based on Streckeisen, 1973) modified by Bose, (1997), and Best, (2001) (Fig. 2-1).

2.2 Petrography of ultrabasic

2.2.1 Dunite

Dunite is abundant in MOC and forms mostly the outer zone of the ultrabasic sequence. This rock is characterized by spheroidal shape (Fig. 2-2). The dunite mass is pale brown on weathered surface that break into olive – green and dark green rock. Dunite rocks have homogenous lithologic characteristic consisting of olivine as main constituent, accessory chromian spinel and traces of orthopyroxene in some specimen (Fig. 2-3). Based on microprobe analysis olivine minerals from fresh dunite are forsterite olivine (Fo. ₈₉₋₉₂). The modal % of olivine are more than 90 % (Table 2-1) and are variable in size ranging from 0.02 to 2.6 mm show undulatory extinction, kink bands. Coleman (1977) related this phenomenon to very diffuse grain boundaries. The dunite has xenomorphic granular texture cataclastic, porphyroclastic to mylonitic texture (Fig. 2-4) which exhibits tectonic fabric. The dunites are affected by variable degree of serpentinization and exhibit typical mesh structure along fracture and grain outlines. The orthopyroxene and clinopyroxene are present in small quantities 0-4 %. The pyroxenes are affected by various degrees of alteration to tremolite.

The main accessory mineral in dunite is represented by chromian spinel and its content varies from 1 to 5 % and. Chromian spinel is frequently euhedral to subhedral and has an opaque rim and fresh red core, ranging in size from 0.05 to 1mm.

2.2.2 Harzburgite

Harzburgite is the most abundant ultrabasic rocks type in MOC. The field appearance of harzburgite is massive body containing dykes of pyroxenite (Fig. 2-5). The constituent minerals are olivine (0.03-1.5mm across). Olivine ranges between 72-87modal volume% (Table 2-2) and the olivine, orthopyroxene and clinopyroxene are commonly deformed (Fig. 2-6).

Clinopyroxene is frequent and closely associated with orthopyroxene even if it occurs as discrete grain. Orthopyroxene is sometimes relatively coarse but characteristically forms radial aggregates (Fig. 2-7). The harzburgite body are suffered from various degrees of serpentizations. Olivine replaced by serpentine, orthopyroxene replaced by talc and clinopyroxene replaced by tremolite (Fig.2-8). The chromian spinel is vermicular to subhedral (0.5mm to 1.5 mm), all of the above minerals occur as coarse to medium subhedral to anhedral grains producing granular interlocking fabric with protoclastic texture.

Chromian spinel is brown to reddish brown under the plane polarized microscope. Arai, (1997) related this color of chromian spinel to high Cr # content. The rims are sometimes opaque due to replacement by ferric chromites Chromian spinel (modal abundance ≤ 3 %) in harzburgite are frequently vermicular and intergrowth with orthopyroxene and/or clinopyroxene (Fig. 2-9) whereas in dunite has more than 3 volume %.The olivine in harzburgite is characterized by the same optical properties of olivine in dunite but the grain size is smaller.

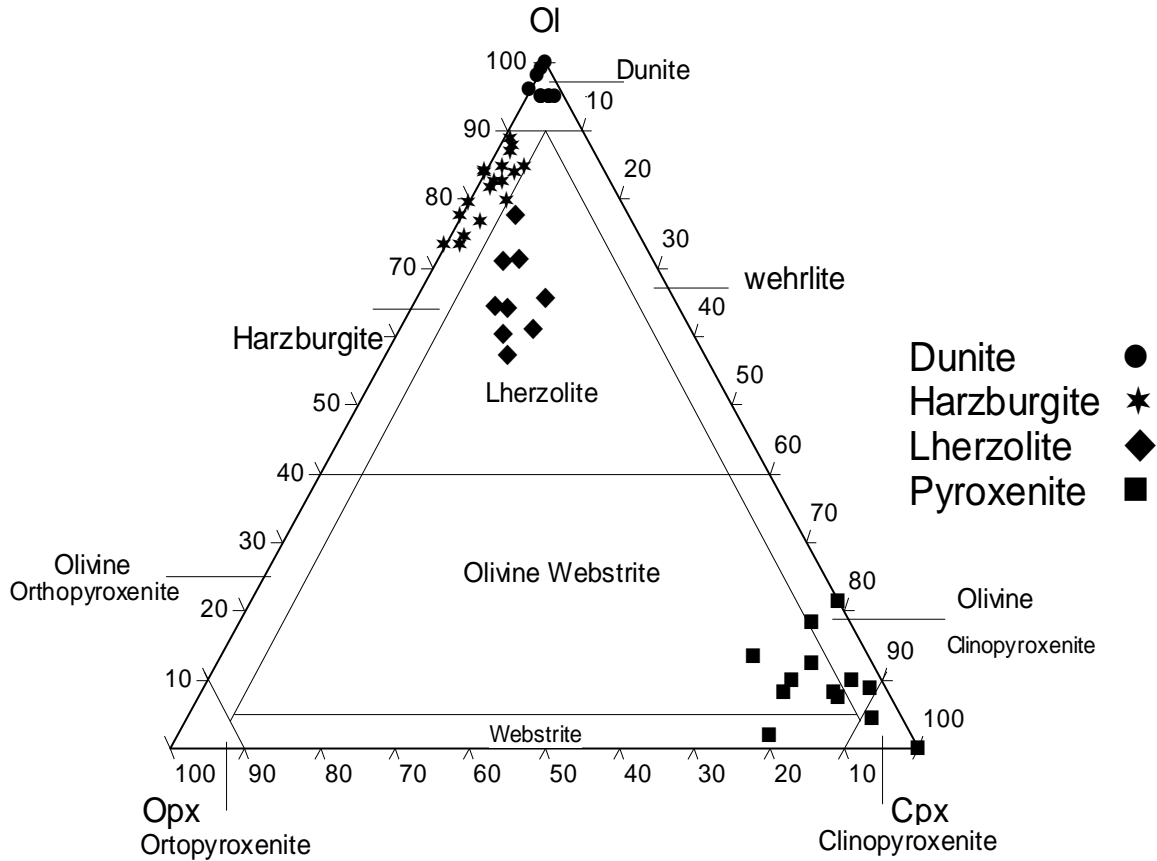


Fig. 2-1 Classification and nomenclature of ultrabasic rocks in MOC (Diagram From Streckeisen, 1973) modified by Best, (2001) and Bose (1997).

Table 2-1 Modal volume % of mineral composition in dunite of MOC.

S.No.	Olivine	Orthopyroxene	Clinopyroxene	Chromite
R10-1	97	2	0	1
R10-2	94	1	4	1
W15	93	2	3	2
W17	93	4	0	3
W20	92	3	2	3
W21	94	1	0	5
W23	96	0	0	4
W37	93	3	2	2
W38	93	2	3	2

Table 2-2 Modal volume % of mineral composition in harzburgite rocks of MOC.

S.No.	Olivine	Orthopyroxene	Clinopyroxene	Chromite
R6	78	20	0	2
R7	84	13	2	1
R8	80	14	3	3
W12	81	15	2	2
W14	83	16	0	1
W16	84	10	5	1
W19	81	16	2	1
W34	86	10	2	2
W35	79	15	5	1
W36	83	12	4	1
D23	87	11	2	0
D24	87	10	1	2
D34	72	24	2	2
K7-5	76	20	3	1
K9-2	72	26	0	2
K9-4	77	22	0	1
A1-2	84	16	0	0
A1-5	73	23	2	2

Table 2-3 Modal volume % of mineral composition in lherzolite rocks of MOC.

S.No.	Olivine	Orthopyroxene	Clinopyroxene	Chromite
K3-1	65	17	17	1
K4-1	77	15	7	1
K4-2	59	25	14	2
K4-5	56	26	16	2
K5-1	64	23	13	0
K5-2	70	20	9	1
K7-6	61	21	18	0
D32	71	18	11	0
D33	63	24	11	2

Table 2-4 Modal volume % of mineral composition in pyroxenite rocks of MOC.

S.NO.	Olivine	Orthopyroxene	Clinopyroxene	plagioclase	Chromite
R12	0	0	88	9	3
D15	8	2	81	5	4
D35	18	5	75	0	2
W13	21	0	77	0	2
K2-1	4	4	87	0	5
K2-2	8	7	83	0	2
K3-2	7	7	82	4	0
K4-3	10	4	86	0	0
K4-4	12	8	78	0	2
k6-2	10	12	78	0	0
K9-1	2	19	79	0	0
K9-5	13	15	70	0	2
A12-4	8	14	77	0	1

2.2.3 Lherzolite

Lherzolite is restricted in occurrence and its exposures are at the extreme north of Shakha Root; Ser-Shiw valley and Daraban villages. The main constituents of the rock are forsterite rich olivine which range between 59-77 % (Table 2-3) with orthopyroxene and clinopyroxene. Olivine crystals have rounded shape and range between 0.5 mm to 1.2 mm in diameter. The crystals are fractured and serpentinized along fractures. Olivine serpentinization has apparently caused the formation of secondary magnetite (Fig. 2-10). According to Buda and Al-Hashimi (1977) magnetite is formed as a result of olivine serpentinizations. Recent study (Wang et al. 2005) shows that the formation of magnetite is attributed to the alteration of orthopyroxene.

Orthopyroxene and clinopyroxene occur as large crystals and they are more than 0.2mm in diameter subhedral to euhedral crystals and set in a matrix of olivine and pyroxene. The modal % of orthopyroxene ranges from 15% to 26 % and clinopyroxene from 7 % to 18 % respectively (Table2-3). Some of clinopyroxene grains have small patches of altered pyroxene to amphibole either to say it had been uralitized. (Fig. 2-11), other clinopyroxene grains are partially altered to amphibole, (Jassim and Al-Hassan, 1977 and Zekaria, 1992) related this alteration to uralitisation. The main accessory minerals in lherzolite of the studied samples are represented by chromite which is occurring as small subhedral crystals with modal volume percent less than 3 %. They are subhedral to anhedral, dark reddish brown to black in color.

2.2.4 Pyroxenite

Pyroxenite are of a pale brown to greenish color in outcrop, medium- to coarse grained rocks occurring as a narrow belt at the contact of the dunite-harzburgite mass and as small dykes cutting across the harzburgite and gabbro (Fig. 2-5 and Fig. 2-12). Pyroxenite in MOC occurs as few isolated bosses within gabbro.

Pyroxenite dykes cutting the gabbro have a thickness ranging from 10-15 cm and show coarse granular texture. The coarse crystalline pyroxenite includes

webstrite and clinopyroxenite. They are made up of clinopyroxene and orthopyroxene with subordinate amount of olivine, plagioclase and chromite the modal % abundance as in (Table 2-4). Pyroxene crystals range in size from 1.5 to 4 mm in diameter and are anhedral to subhedrals in outline. Based on microscope study and determination of extinction axial angle $2V$ (ranges from 54° - 59°) show that the main clinopyroxene are diopside in compositions, which is compatible with (Jassim and Al-Hassan 1977). Clinopyroxenes are commonly coarser than orthopyroxene, although some of the clinopyroxene grains are characterized by the presence of small exsolution lamellae of orthopyroxene. The clinopyroxene of the studied samples appears under the microscope as pale green to colorless. While the orthopyroxene were colorless to pale light green. The microprobe analyses of orthopyroxene indicate that they are enstatite to bronzite in composition.

Pyroxenite has magmatic allotrimorphic, texture this texture defined by (Kopylova et al., 1999) as anhedral pyroxenes or by subhedral orthopyroxene and anhedral clinopyroxene. Olivine forms anhedral small grains along pyroxene margins and irregular crystals poikilitically enclosed by clinopyroxene (Fig. 2-13), in some studied thin sections pyroxene is partially altered to amphibole and talc. Table 2-4 summarizes the modal volume % of these minerals. Variably sericitized plagioclase (< 5%) is intergranular to clinopyroxene and amphibole. Plagioclase is mainly bytownite (An_{70-80}) and this indicates likely magmatic in origin.

Opaque minerals in the pyroxenite rocks represent by chromian spinel (0-5 volume %), are disseminated with an anhedral grain.

2.2.5 Chromitite

The chromitite rocks of MOC occur as podiform and disseminated chromitite in NE of Kuradawi village and Shakha Root area. Nine pods of chromitite are found in NE of Kuradawi village. They are bluish grey in appearance, fine- to medium-grain size and enveloped by dunite and each pod separated by harzburgite. Chromitite rocks are composed of subhedral to anhedral chromian

spinel grain the matrix is chlorite and serpentine. Details are given in the chapter three.

2.2.6 Alteration of ultrabasic rocks

Alteration of ultrabasic rocks is a widespread phenomenon in all studied samples. Along the main tectonic zones the rocks are completely altered and behave as a lubricant for advancing tectonic movement. The olivine altered to serpentine and orthopyroxene altered to talc, while clinopyroxene altered to tremolite and chlorite depending on Al and Ca content of different type of pyroxenes.

The ultrabasic rocks of MOC have been moderately and strongly affected by alteration as described previously. The alteration of the Mawat ultrabasic rocks are of two distinct types based on mineralogical association. The first and less common is low-temperature serpentinization in which olivine is altered to mesh-textured serpentine, orthopyroxene is altered to basitite. The second type is most common, it has higher temperature alteration in which olivine is replaced by serpentine and orthopyroxene by tremolite and talc, and also reaction rims from around many of the chrome spinels can be observed (Fig.2-14).

The petrographic study and the results of microprobe analyses of Mawat serpentine show they are colorless to yellowish under polarized light and consist mainly of chrysotile-lizardite serpentine.



Fig. 2-2 Outcrop of dunite characterized by spheroid weathering.

A

B

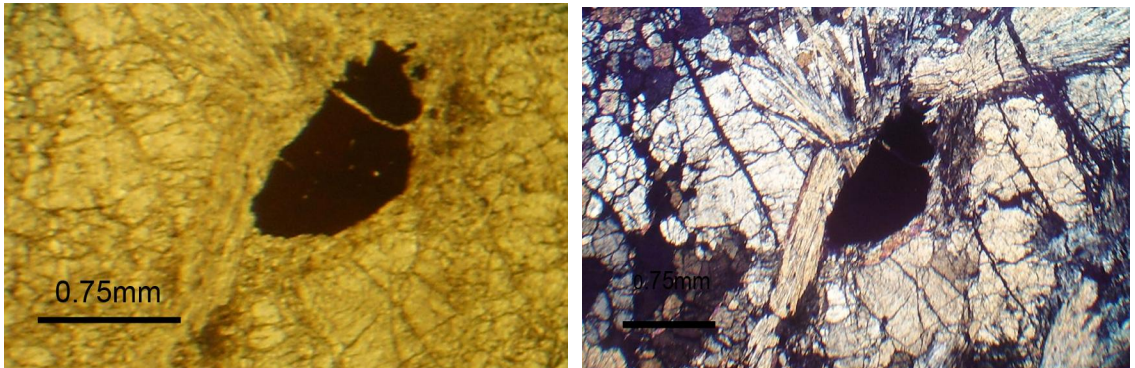


Fig. 2-3 Olivine and pyroxene with accessory chromian spinel in dunite, (A: under PPL, B: XP).

A

B

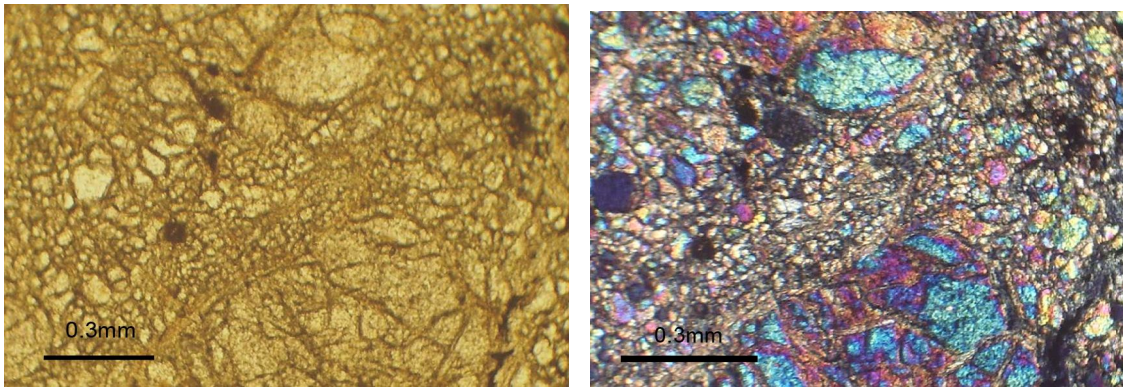


Fig. 2-4 Porphyroclastic to cataclastic texture in dunite and serpentinization along olivine cracks, (A: under PPL, B: XP).



Fig. 2-5 Pyroxenite dykes in the harzburgite rocks.

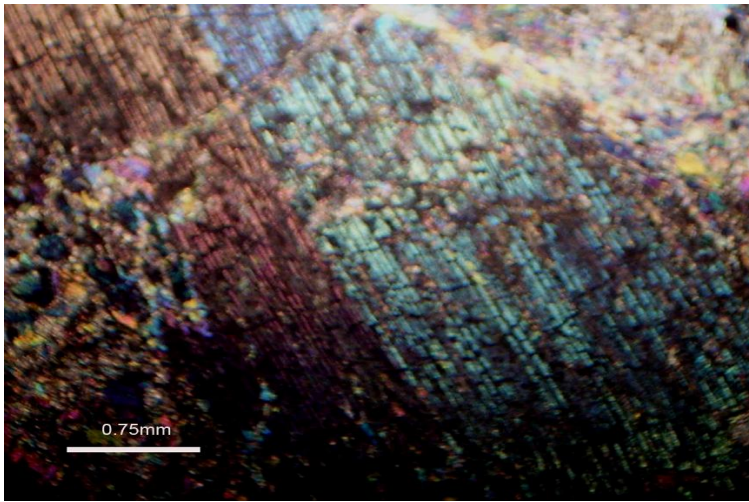


Fig. 2-6 Kinked clinopyroxene in harzburgite (under XP)

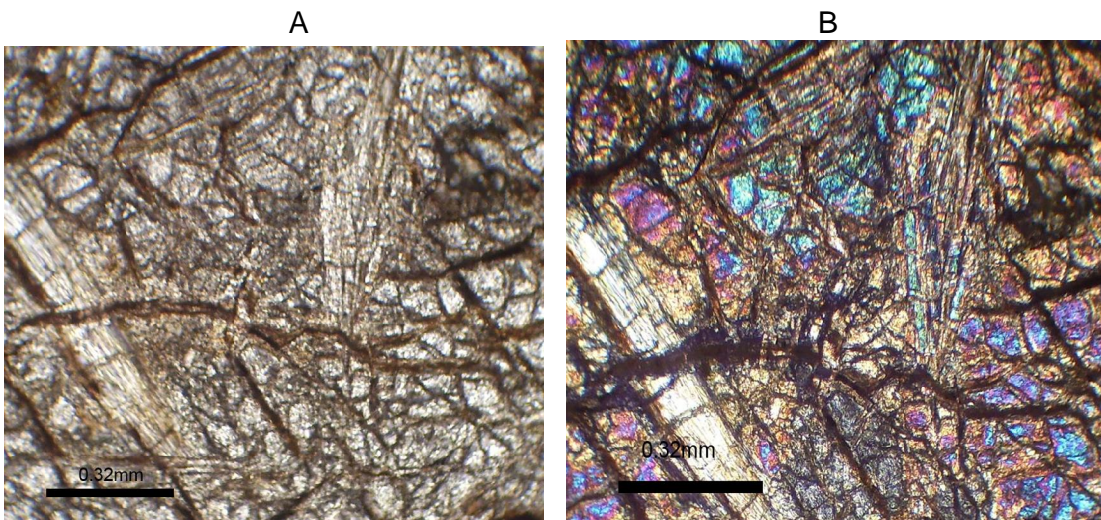


Fig. 2-7 Radiated aggregate of orthopyroxene and serpentinized olivine in harzburgite, (A: under PPL, B: XP).

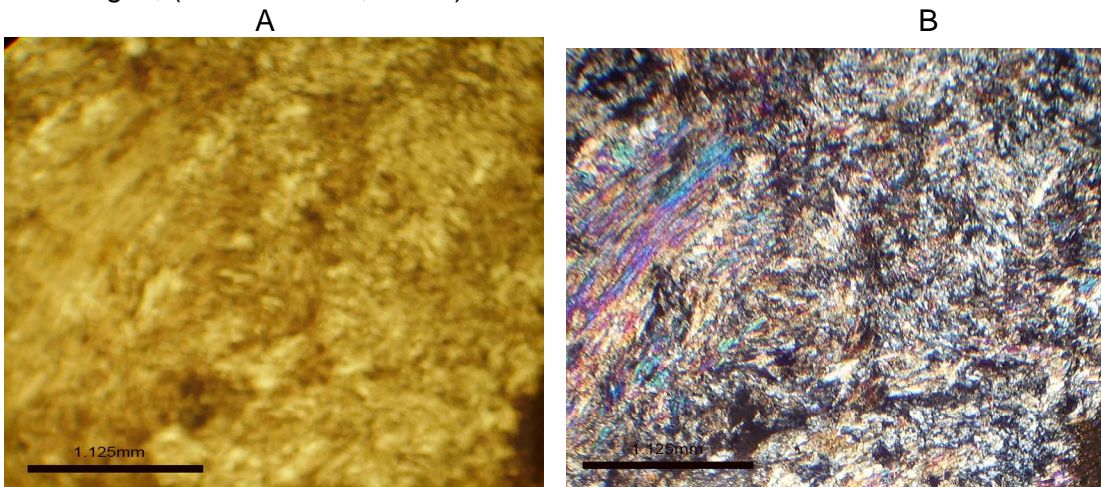


Fig. 2-8 Alteration of pyroxene in harzburgite to talc and tremolite. (Under A: PPL, B: XP)

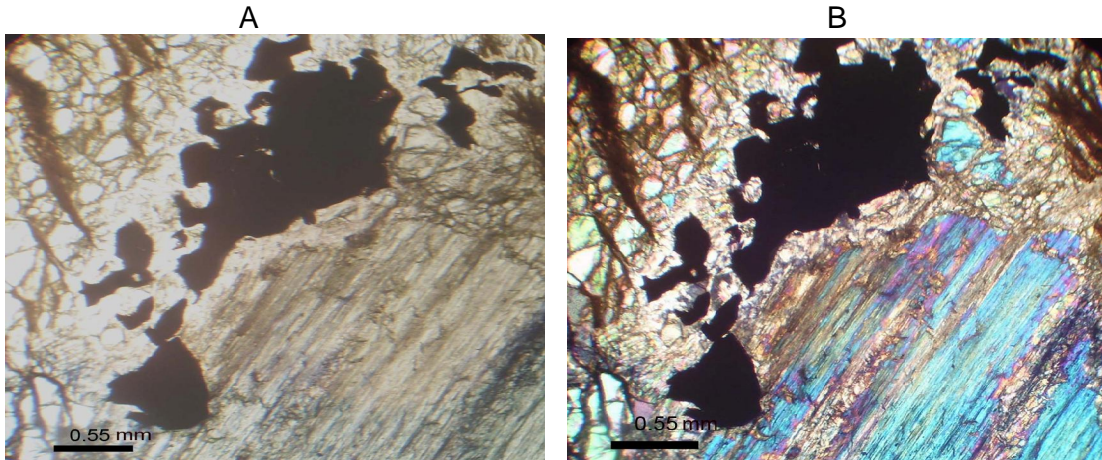


Fig. 2-9 Vermicular chromite grain with olivine and pyroxene in harzburgite rocks of MOC, A: under PPL, B: XP).

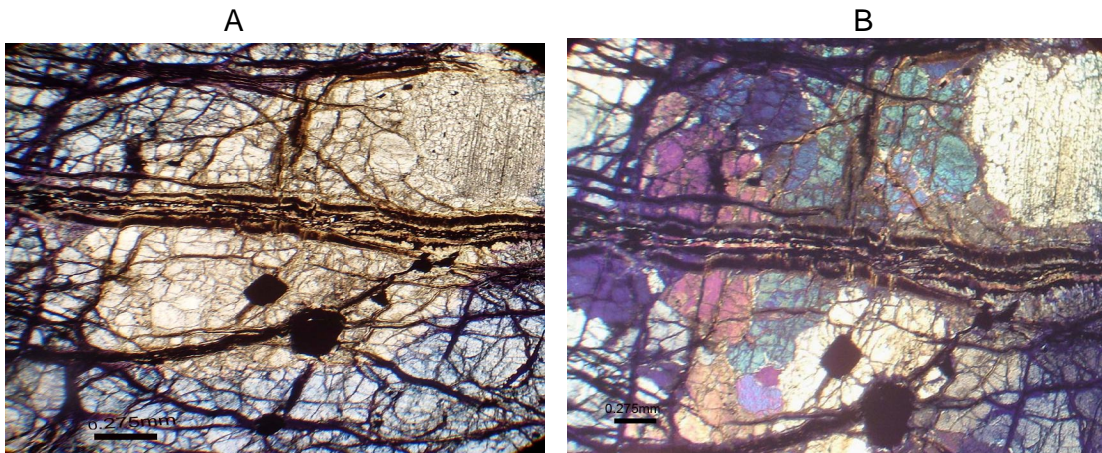


Fig. 2-10 Serpentinization of olivine and formation of secondary magnetite in lherzolite. Under A: PPL, B: XP).

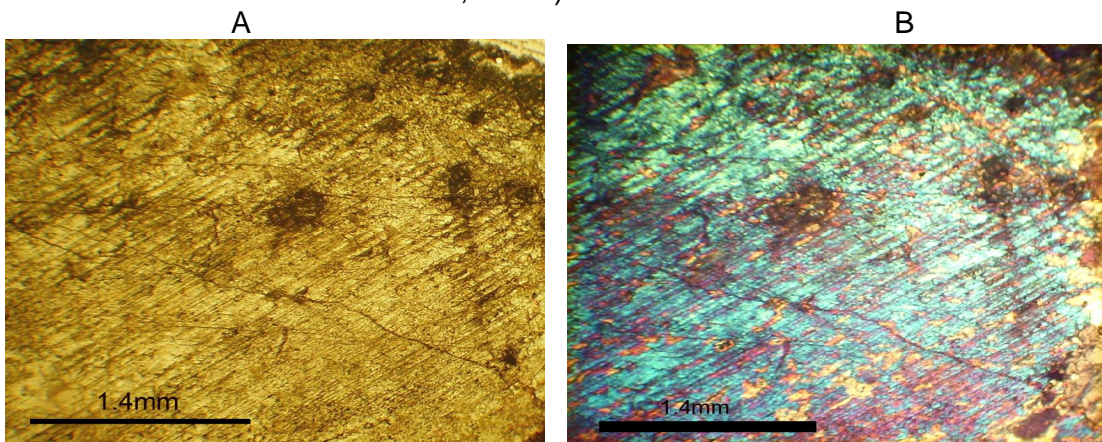


Fig. 2-11 Coarse crystal of clinopyroxene contains small patches of secondary tremolite (Under A: PPL, B: XP).



Fig. 2-12 Pyroxenite dykes cutting the gabbro rocks in MOC.

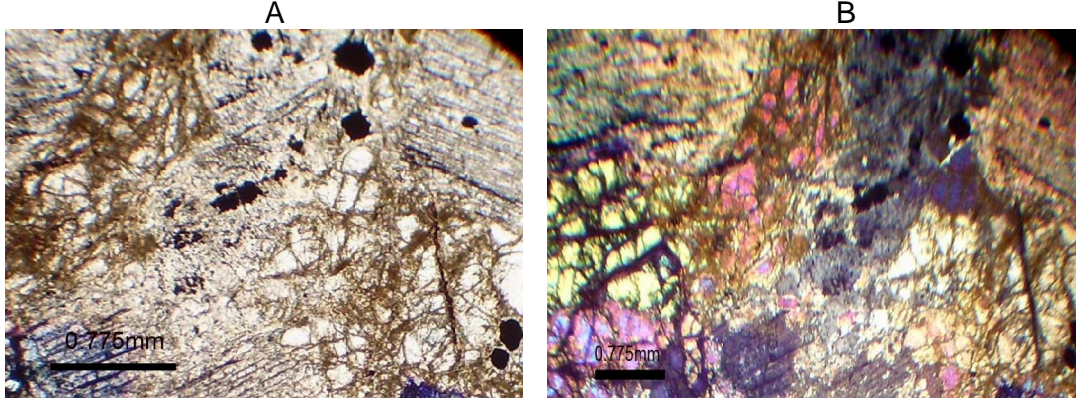


Fig. 2-13 Coarse clinopyroxene and orthopyroxene in a matrix of granulated olivine in pyroxenite. (Under A: PPL, B: XP).

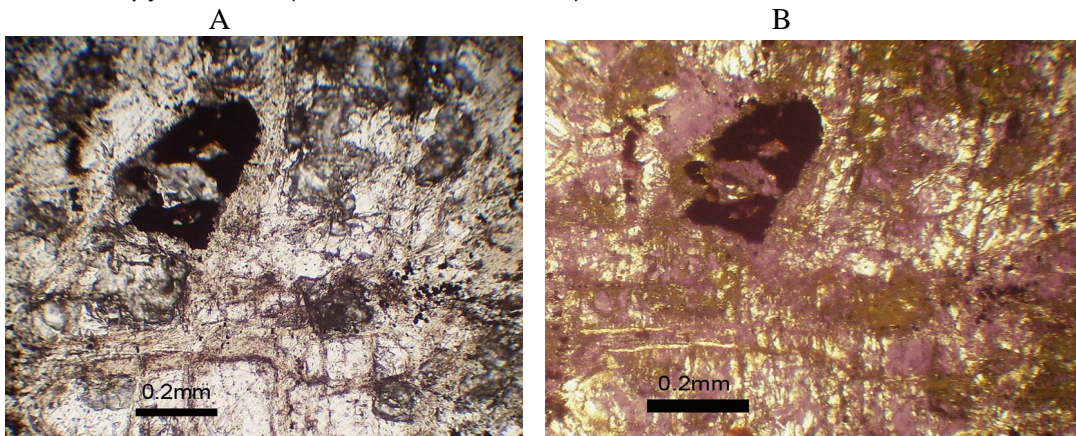


Fig. 2-14 Mesh textured pseudomorphs after olivine and relict chromian spinel in serpentinite ultrabasic rocks of MOC contain small inclusion of olivine (A: PPL under PPL, B: XP).

2.3 Geochemistry of ultrabasic rocks

Major and trace elements analyses were taken from X-ray fluoresces (XRF) analyses carried out on glass fusion beads and powdered pellets. Nine samples of dunite and 15, 9, 10 samples from harzburgite, lherzolite and pyroxenite respectively were analyzed. Representative XRF analyses of ultrabasic rocks were listed in (Table 2-5) and the detail tables of analysis in (Appendix 3, 4, 5, 6). Three samples of dunite and 10, 6, and 8 samples from harzburgite, lherzolite and pyroxenite respectively were analyzed for the rare earth element (REE) and Ba, Th, Nb, Y, Hf, Ta, U, Pb, Rb, Cs, Sr, Sc, and Zr content. Representative ICP-MS analyses of ultrabasic rocks were tabulated in (Table 2-6) and the detail tables of analyses are listed in (Appendix 7, 8, 9, 10). The REE and trace elements were normalized using the chondrite-normalizing values published by O'Neill and Palme, (1998) (Appendix 7).

2.3.1 Geochemistry of Major elements

The geochemistry of Mawat ultrabasic rocks are characterized by content of MgO in the range of 22.26-45.6 wt % and SiO₂ from (35.47 -50.91 wt %) the abundances of FeO range from (4 to 12.01 wt %). Cr content range between 15562-2068 ppm, Ni range from 3002 to 498 ppm. Average bulk rock magnesium numbers $100 * \text{MgO} / \text{MgO} + \text{FeO}$, are generally $\geq 84, 82, 73,$ and 74 in dunite, harzburgite, lherzolite, and pyroxenite respectively (Tables 2-5) (Appendix 3, 4, 5, 6). The comparatively high contents of Cr and Ni are the diagnostic of MOC ultrabasic rocks.

The major and trace element variation diagrams with MgO wt % were used as a fractionation index (Fig. 2-15) and (Fig. 2-16). As illustrated in (Fig. 2-15) the variations observed in ultrabasic rocks as well as pyroxenite rocks of MOC.

The whole data set show negative correlation between MgO with SiO₂, Al₂O₃, CaO, and TiO₂. The inverse correlation between MgO with SiO₂, Al₂O₃, CaO, and TiO₂ are related to the proportion of olivine, orthopyroxene, clinopyroxene and spinel. Coleman, (1977) and Katzir et al., (1999) attributed this inverse correlation to depletion process caused by partial melt extraction.

Orthopyroxene, clinopyroxene and spinel are the only minerals containing Al₂O₃, in the studied samples the mean of Al₂O₃ content in dunite, harzburgite

and lherzolite are (0.318, 0.591, 1.462 % Al_2O_3) respectively. These values are close to the mean values of Al_2O_3 found by (Coleman, 1977) which are 0.35%, 0.89, 1.6. Peridotite with high MgO content have in general the lowest concentrations of Al_2O_3 , CaO, TiO_2 and incompatible elements that preferentially partition into the liquid phase during partial melting (Palme. and O'Neil, 2004) and /or due to the nature of source rocks.

Alteration (serpentinization) processes are also responsible for element deviations, particularly the strong depletion of calcium, and sodium relative to MgO as well as variation of SiO_2 and Al_2O_3 with MgO and slightly increase with FeO, because all samples are ultrabasic rocks where there is enrichment in ferromagnesian minerals and depletion in silica and other elements, or either to say the slightly positive correlation between FeO-MgO (Fig. 2-15d) indicates the invariable partition of Mg and Fe within olivine, orthopyroxene and clinopyroxene. Some of deviation from covariation trends in (Fig. 2-15) may be accounted by mineralogical heterogeneities. The heterogeneous distribution of pyroxene and spinel affect their chemical composition. This is especially true for pyroxenite , lherzolite, harzburgite and dunite where the pyroxenite and lherzolite are more enriched in clinopyroxene (more Al_2O_3 , CaO, Na_2O content), while the harzburgite and dunite are more enriched in refractory minerals such as olivine, orthopyroxene and spinel. Other deviations such as slightly positive trend of MgO with FeO are ascribed to textural mineralogical evidence for refertalization or modal metasomatism and are therefore ascribed to melt-rock interaction (Bodinier and Godard, 2004). It can be concluded that the FeO contents are independent of MgO in all ultrabasic rocks and the change of MgO/FeO ratio reflects mainly the change in the composition of coexisting olivine and orthopyroxene.

Chemical analysis of the collected samples showed that an average (Na_2O 0.08 %) and (K_2O 0.0035 %) in dunite, 0.083 % Na_2O 0.0035 % K_2O in harzburgite, and in lherzolite was 0.087% Na_2O 0.0011 % K_2O . These values are in agreements with the values that are found by (Aqrawi, 1990). He recorded (0.01 % Na_2O , and % K_2O) in dunite and (0.033 Na_2O , 0.01%, K_2O %), (0.103 % Na_2O , 0.037% K_2O %) in harzburgite and lherzolite respectively. The negative correlation between Na_2O , K_2O and MgO and trace amount of alkali is probably contained within the pyroxene.

Table 2-5 Representative XRF bulk rock analysis of dunite (9), harzburgite (15), lherzolite (9), and pyroxenite (10) in Mawat Ophiolite Complex, n= number of analyzed sample.

Rock type Sample No.	Dunite (n=9)		Harzburgite (n=15)		Lherzolite (n=9)		Pyroxenite (n=10)	
	W21	W23	R6	W19	K3-1	K4-2	R12	D15
SiO ₂	39.27	39.62	38.87	41.34	43.59	41.6	49.03	50.02
TiO ₂	0.008	0.005	0.007	0.007	0.060	0.029	0.03	0.04
Al ₂ O ₃	0.28	0.12	0.1	0.57	1.03	1.5	2.04	2.09
FeO*	7.97	7.71	8.31	6.89	11.34	11.78	4.41	6.35
MnO	0.125	0.123	0.124	0.111	0.204	0.188	0.181	0.105
MgO	44.99	45.32	38	43.22	31.84	35.87	26.86	25.07
CaO	2.30	2.06	0.09	1.58	7.98	3.46	14.17	10.89
Na ₂ O	0.08	0.08	0.06	0.08	0.11	0.1	0.33	0.54
K ₂ O	0.00	0.00	0	0	0.00	0	0.022	0.02
P ₂ O ₅	0.003	0.002	0.007	0.009	0.004	0.011	0.006	0.007
LOI (%)	4.43	4.12	13.64	5.38	2.76	4.55	2.55	3.74
Sum	99.46	99.16	99.21	99.19	98.92	99.09	99.63	98.87
100*MgO/MgO+FeO	84.95	85.45	82.05	86.25	73.73	75.27	85.89	85.21
Traces(ppm)								
Ni	2575	2750	2986	2576	1019	1516	687	2119
Cr	3053	1636	3600	2068	2694	4127	2115	2191
Sc	6	5	4	8	33	20	16	19
V	20	15	17	24	112	79	51	61
Ba	4	5	7	7	7	7	3	1
Rb	1	0	0	0	0	0	0	0
Sr	64	70	2	37	2	3	2	25
Zr	2	1	3	5	2	3	2	5
Y	0	1	1	1	2	2	3	6
Nb	0.0	0.0	0	0	0.0	0.1	0.4	0.3
Ga	1	0	1	3	2	1	2	4
Cu	4	6	3	6	14	4	72	110
Zn	30	22	53	38	64	57	30	26
Pb	0	0	1	1	0	0	1	2
La	0	4	3	3	1	0	1	5
Ce	1	0	0	0	0	0	1	5
Th	0	0	0	0	0	0	1	0
Nd	6	2	1	0	0	1	1	5
sum tr.	5765.843	4516.348	6682	4777	3950.925	5820.1	2988.4	4634.3

* Total iron content

In MOC the average TiO_2 in dunite, harzburgite, lherzolite, and pyroxenite are 0.0075 %, 0.0089 %, 0.026, and 0.072 % respectively. The relatively low TiO_2 content is the characteristic of Alpine type ophiolites (Al-Hassan, 1982), and (Arai, 1992). As in Fig.2-15b the negative trend of TiO_2 -MgO, with a strongly depleted TiO_2 content is observed. This relation ascribed to primary mantle process in upper mantle, prior to tectonic emplacement of peridotites, and the degree of partial melting of asthenospheric mantle (Frey et al., 1985, Bodinier, 1988, McDonough and Frey, 1989).

2.3.2 Geochemistry of trace elements

The average Ni content of dunite in MOC is 0.281% and 0.239 % in harzburgite, the lherzolite and pyroxenite also appear to have 0.189 %, 0.0775% average Ni content. These values are compatible with the values of NiO in peridotite given by Coleman (1977) in which the NiO average in dunite is 0.31% (Ni, 0.24 %), in harzburgite NiO, 0.38 %, (Ni, 0.29%) while in lherzolite the NiO is 0.31% (Ni, is 0.18%).

The compatible element (Ni) increases with increasing MgO content (Fig. 2-16a). Thus the trend has been interpreted as the concentration of Ni is mainly with olivine and to lesser extent in the orthopyroxene. Using the discriminant fields of dunite, harzburgite, lherzolite and pyroxenite (Fig. 2-17a) from Pfeifer (1990), show that peridotite of MOC straddle both the harzburgite and lherzolite fields. The positive and negative correlation of Ni and V, respectively, with MgO in the ultrabasic rocks of MOC are consistent with melt extraction.

The same concluded by Palme and O'Neill, (2004) and related the trend of increasing Ni and decreasing in V content, with MgO in ultrabasic rocks to various degree of melt extraction following the least-depleted peridotite (lherzolite) i.e. lowest in Ni should be the closest in composition to the primitive mantle.

The Cr content in dunite ranges between 1.556 wt % to 0.1636 wt %, in harzburgite ranges from 0.360 % to 0.207 %, in lherzolite the Cr content ranges between (0.423-0.232 %), and in pyroxenite ranges from 0.347 % to

0.212 %, (Appendix 3, 4, 5, and 6). The Cr in dunite and harzburgite is mainly a function of modal amount of chromite and orthopyroxene.

The negative trends of Sc-MgO, V-MgO, Ga-MgO in ultrabasic rocks of MOC (Fig. 2-16 c, d, k) are expected because these elements are mildly incompatible during melting, therefore preferred to concentrate in the melt rather than in minerals, this explains the negative relationship with MgO, (Engler et al., 2002 and Ahmad Hassan, personal communications, 2007). Niu (2004) suggests that Sc, V, and Ga are more or less immobile or unaffected by serpentinization and seafloor weathering; therefore it follows such a trend.

The apparent scatter of Cu, Zn (Fig. 2-16, L, m) may suggest formation of minor phases whose distribution is heterogeneous on scale of small size. Niu et al. (2002 a, and 2003) suggest that these minor phases as chromite (Cr, Zn, Fe) sulphides (Cu, Ni, Fe), native metal/alloys (Ni, Co, Fe) are probably the responsible phases. Coleman (1977) and (Engler, 2002) suggested that the low concentration of Cu in ophiolite rocks may be related to the primary magma low in Cu or possible postigneous removal of Cu as a result of hydrothermal alteration. As noted, all ultrabasic rocks of MOC are affected by alterations (Serpentinizations) hence depletion in Cu content is more related to hydrothermal effect.

The ultrabasic rocks of MOC are characterized by low Zr, and Y, ≤ 6 ppm (Table 2-5) (Appendix, 3, 4, 5, and 6), the Zr-MgO, and Y-MgO show negative trends (Fig 2-16 i and h). Y, and Zr, are incompatible high-field strength elements (HFS), which means it is preferred to be concentrated in the melt rather than in minerals. This means the early formed minerals in basic magma (like olivine and pyroxenes) will be depleted in Y and Zr.

Among the lithophile trace elements, the highly incompatible elements (HIE), (Rb, Ba, Nb, and Th) are strongly dispersed on the magnesium covariation diagrams. The scattering trends of Ba, Nb, Zr, Th, and Ga (Fig. 2-16 e, j, h, n, and k) are attributed to their incompatibility during mantle melting.

Rb has a large ionic radius and the only element able to replace the Rb is K^{+1} (ionic radius 1.33 \AA). The ultrabasic rocks in MOC are very low in K_2O content.

Hence we expect also low Rb content and they do not show any relationship with MgO content (Fig. 2-16 f). The Rb also are mobile during the alteration; therefore the low values of Rb are due to leaching from the rocks by circulating fluids (Al-Samman et al., 1996).

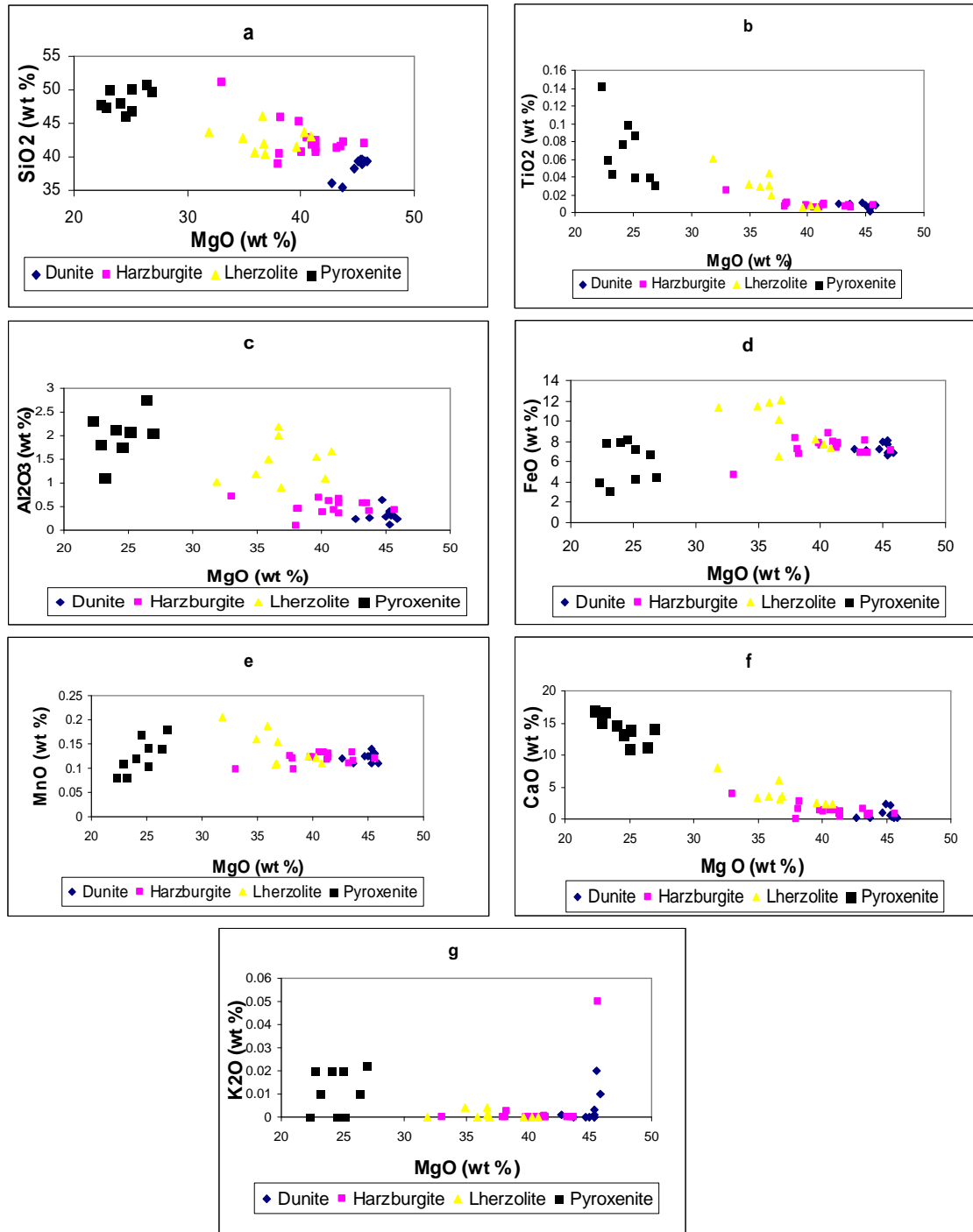


Fig. 2-15 Plots of major oxides versus MgO in whole ultrabasic -rock (dunite, harzburgite, lherzolite, and pyroxenite).

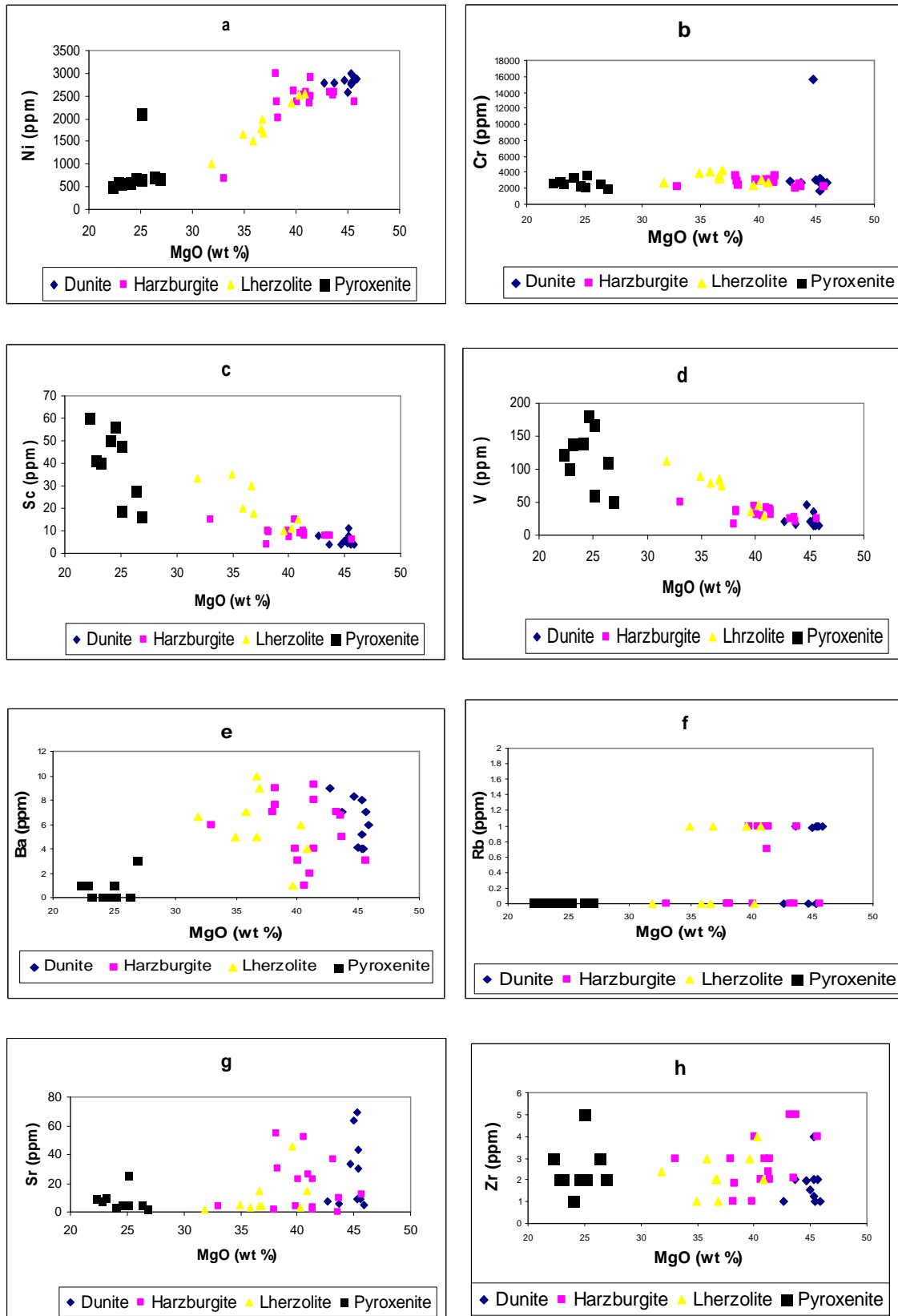


Fig. 2-16 Plots of trace elements versus MgO in whole ultrabasic rocks of MOC (dunite, harzburgite, lherzolite, and pyroxenite).

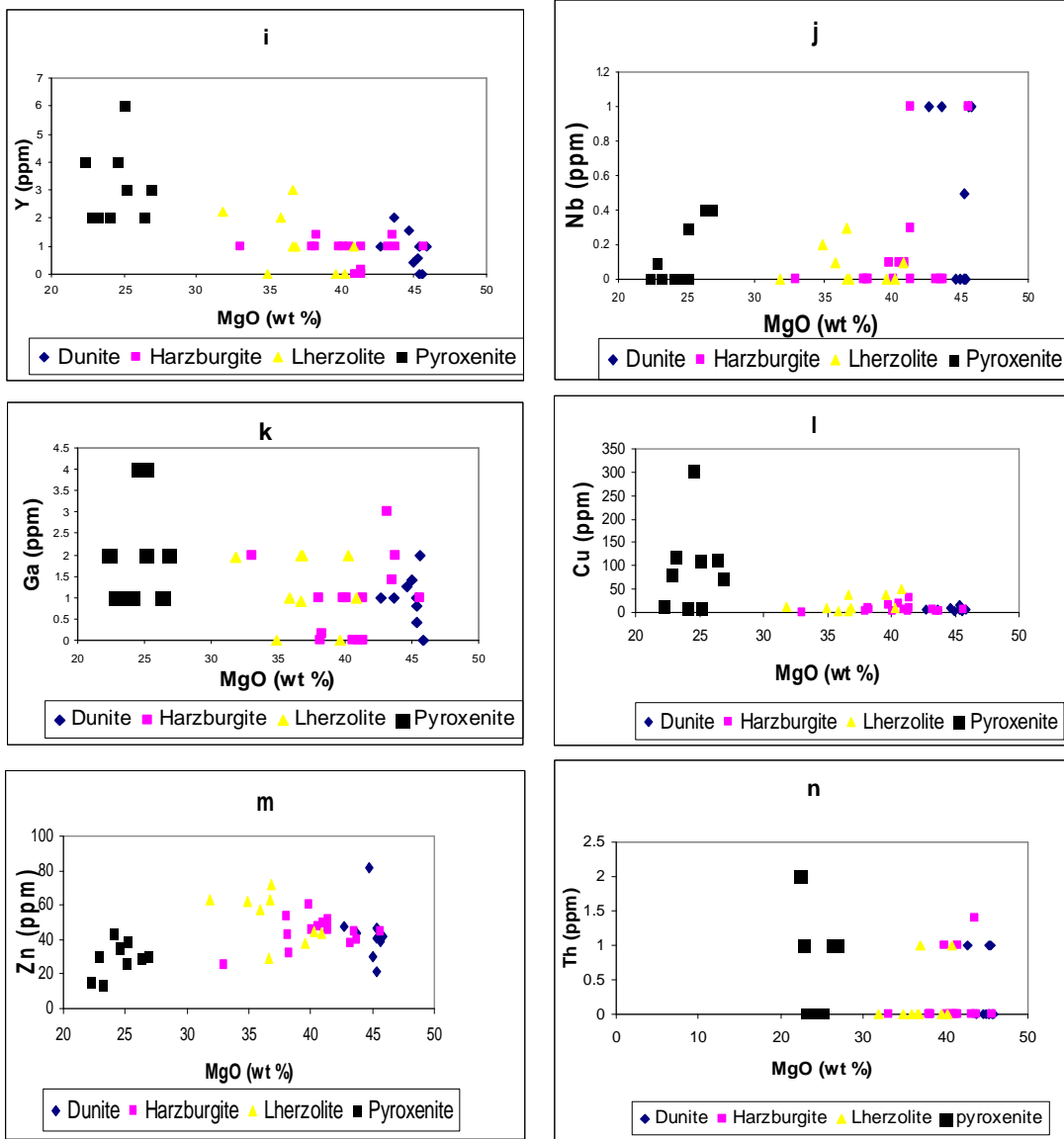


Fig. 2-16 Continued.

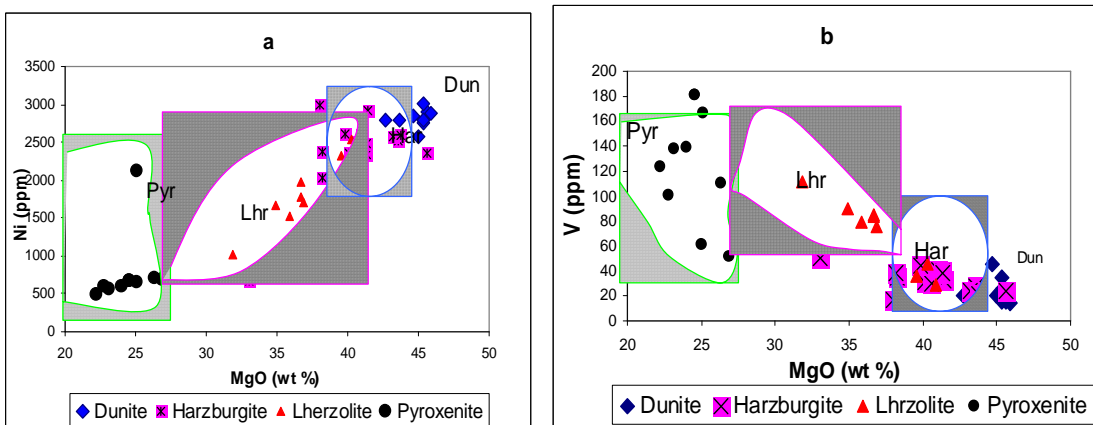


Fig. 2-17 Variation diagrams of Ni and V versus MgO in MOC ultrabasics. Discriminative fields of Harzburgite (Har), Lherzolite (Lhr), Dunite (Dun) and Pyroxenite (Pyr) from Pfeifer,(1990)

2.4 Geochemistry of rare earth elements (REE)

The REE are relatively immobile during low grade metamorphism, weathering and hydrothermal alteration. So the REE patterns are largely controlled by the chemistry of the source rocks. The representative REE analysis for ultrabasic rocks in MOC are listed in (Table 2-6) and the details of samples analyzed are in Appendix 7, 8, 9, 10. The chondrite-normalized REE patterns for ultrabasic rocks from MOC are presented in Figs. 2- 18, 2-19, 2-20 and 2-21 using normalizing values published by O'Neill and Palme, (1998).

The dunite and harzburgite defined a pronounced slightly U shaped depletion in middle REE (Eu-Dy) relative to light REE (La-Sm) and heavy REE (Ho-Lu). The LREE values are between 0.066 to 0.792 times chondrite in dunite and from 0.066 to 0.875 in harzburgite. The depletion of MREE relative to LREE and HREE may be attributed to the absence of hornblende and the presence of olivine and pyroxenes (Niu, 2004) and/or to the nature of the source rocks. The chondrite-normalized REE patterns of lherzolite characterized by U-shape patterns and the fluctuation in the trend of the patterns may be related to the alteration effect. The LREE values of lherzolite are between 0.066 to 0.733 and HREE are between 0.08 to 1.32. The relative enrichment of middle and heavy REE relative to LREE in lherzolite is due to the presence of clinopyroxene.

A characteristic of most of these samples is a distinctly positive Eu anomaly. Europium exists as Eu^{+2} and Eu^{+3} , and Eu^{+2} readily substituted for Ca^{+2} in plagioclase (Berger et al., 2001). Peridotites have very low Eu concentrations (Parkinson et al. 1992). The LREEs depletion and Eu enrichment indicate plagioclase crystallization in open system or secondary effect due to serpentinizations processes (Bodiner and Godard, 2004 and Engler et al., 2002). Because the dunite, harzburgite and lherzolite samples of studied area do not contain abundant modal plagioclase, therefore the positive Eu anomaly may be related to the hydrothermal effect and the decomposition of pyroxene is likely to occur and be replaced by sheet silicate, Eu^{+2} can be substituted for

Ca⁺² by breakdown of clinopyroxene, the result is enrichments of Eu. (Parkison et al., 1992).

In general the chondrite –normalized REE patterns of MOC ultrabasic rocks generate the slightly U shaped pattern. These rocks are characterized by minimum values for MREE and relative enrichments of both LREE and HREE. LREE/MREE > chondrite; MREE/HREE < chondrite; LREE/HREE~ chondrite.

The U-shaped REE patterns and these ratios are typical of ophiolitic ultrabasic rocks (Coleman, 1977; Tankkut, 1990) which are compatible with the supra-subduction zone (Hamasalh, 2004). Parkinson et al. (1998) and Melcher et al. (2002) claimed that residual ultrabasic rocks from SSZ (fore-arc setting) always exhibit U-shaped chondrite normalized pattern. The pyroxenite rocks which show clear cross-cutting relationship with peridotite, were generally deformed at high temperature, but only partially transported into peridotite foliation. Hence their igneous origin is hardly disputable (Ve'til et al., 1988 in Bodinier and Godard, 2004). The geochemistry of pyroxenite in MOC are characterized by high Mg# (Mg /Mg+Fe) (0.749-0.879) and Al₂O₃ contain less than 2.8 wt % (Table 2-5) and (Appendix 6). Bodinier and Godard (2004) classified pyroxenite due to Al₂O₃ content in to two group low Al₂O₃ (≤ 10 wt %) and high Al₂O₃ (> 10 wt %) pyroxenite. Accordingly the MOC pyroxenites are classified as low Al₂O₃ group. In addition to this the low rare earth elements abundances (Appendix 10) are coupled with large ion lithophile elements (chondrite –normalized) relative to adjacent rare earth elements (Fig. 2-21) and are the characteristic of pyroxenite of MOC.

The chondrite –normalized REE patterns of representative pyroxenite from MOC (Fig. 2-21) shows variable REE distributions. All samples except D15, D35, and R12 are enriched in LREE and MREE relative to HREE with convex-upward REE patterns. While the samples D15, D35, and R12 show slightly LREE depleted pyroxenite dikes, with positive Eu anomaly. According to (Rivalenti et al., 1995) both the two patterns type can be observed in ophiolitic complex. The positive Eu anomalies indicate the presence of plagioclase. The relatively flat HREE patterns are consistent with the presence of significant amount of clinopyroxene (Parkison et al., 1992).

Table 2-6 Representative ICP-MS bulk rock analysis of dunite (3) harzburgite (10), lherzolite (6), and Pyroxenite (8) rocks in Mawat Ophiolite Complex (n= number of analyzed samples)

Rock type Sample No.	Dunite (n=9)		Harzburgite (n=15)		Lherzolite (n=9)		Pyroxenite (n=10)	
	W21	W23	R6	W19	K3-1	K4-2	R12	D15
SiO ₂	39.27	39.62	38.87	41.34	43.59	41.6	49.03	50.02
TiO ₂	0.008	0.005	0.007	0.007	0.060	0.029	0.03	0.04
Al ₂ O ₃	0.28	0.12	0.1	0.57	1.03	1.5	2.04	2.09
FeO*	7.97	7.71	8.31	6.89	11.34	11.78	4.41	6.35
MnO	0.125	0.123	0.124	0.111	0.204	0.188	0.181	0.105
MgO	44.99	45.32	38	43.22	31.84	35.87	26.86	25.07
CaO	2.30	2.06	0.09	1.58	7.98	3.46	14.17	10.89
Na ₂ O	0.08	0.08	0.06	0.08	0.11	0.1	0.33	0.54
K ₂ O	0.00	0.00	0	0	0.00	0	0.022	0.02
P ₂ O ₅	0.003	0.002	0.007	0.009	0.004	0.011	0.006	0.007
LOI (%)	4.43	4.12	13.64	5.38	2.76	4.55	2.55	3.74
Sum	99.46	99.16	99.21	99.19	98.92	98.09	99.63	98.87
100*MgO/MgO+FeO	84.95	85.45	82.05	86.25	73.73	75.27	85.89	85.21
Traces(ppm)								
Ni	2575	2750	2986	2576	1019	1516	687	2119
Cr	3053	1636	3600	2068	2694	4127	2115	2191
Sc	6	5	4	8	33	20	16	19
V	20	15	17	24	112	79	51	61
Ba	4	5	7	7	7	7	3	1
Rb	1	0	0	0	0	0	0	0
Sr	64	70	2	37	2	3	2	25
Zr	2	1	3	5	2	3	2	5
Y	0	1	1	1	2	2	3	6
Nb	0.0	0.0	0	0	0.0	0.1	0.4	0.3
Ga	1	0	1	3	2	1	2	4
Cu	4	6	3	6	14	4	72	110
Zn	30	22	53	38	64	57	30	26
Pb	0	0	1	1	0	0	1	2
La	0	4	3	3	1	0	1	5
Ce	1	0	0	0	0	0	1	5
Th	0	0	0	0	0	0	1	0
Nd	6	2	1	0	0	1	1	5
sum tr.	5765.843	4516.348	6682	4777	3950.925	5820.1	2988.4	4634.3

The petrographical study and modal abundant also indicate the presence of and clinopyroxene in significant amount (Table 2-4). In addition to that the samples D15, D35, and R12 represent pyroxenite rocks from the contact between ultrabasic rocks of Rasha Kani - Daraban traverses with coarse gabbro. Their pattern trends differ from the other samples which are related to Shakha-Root and Ser-Shiw valley and occur as small bosses and dykes cutting the gabbro and peridotites. From this it can be concluded that two different stage magma may be caused the formation of pyroxenite dykes, the first one which is enriched in LREE relative to HREE and caused the formation of pyroxenite rocks with LREE enrichment and the second stage magma which is depleted in LREE and enriched in MREE and HREE, the formation of pyroxenite depleted in LREE. This led to say that these pyroxenite rocks are not continuous dykes that cross-cutting both ultrabasic and gabbro rocks. It may be from two stages of magma generation and from two different sources. The pyroxenite dikes have crystallized from HREE depleted, refractory melts that were possibly formed within the massifs, together with refractory peridotite. Edward and Malpas (1995) ascribed the low alumina pyroxenite dikes which are frequent in the harzburgite sequences to segregation and transport of boninitic melts in a supra-subduction setting. Similarly, the pyroxenite of MOC are low –Alumina and they are enriched in LREE and MREE relative to HREE, also the LREE depleted pyroxenite dykes are observed so these pyroxenite dykes cross-cutting peridotites probably related to segregation and transporting of boninitic melts in a supra-subduction zone.

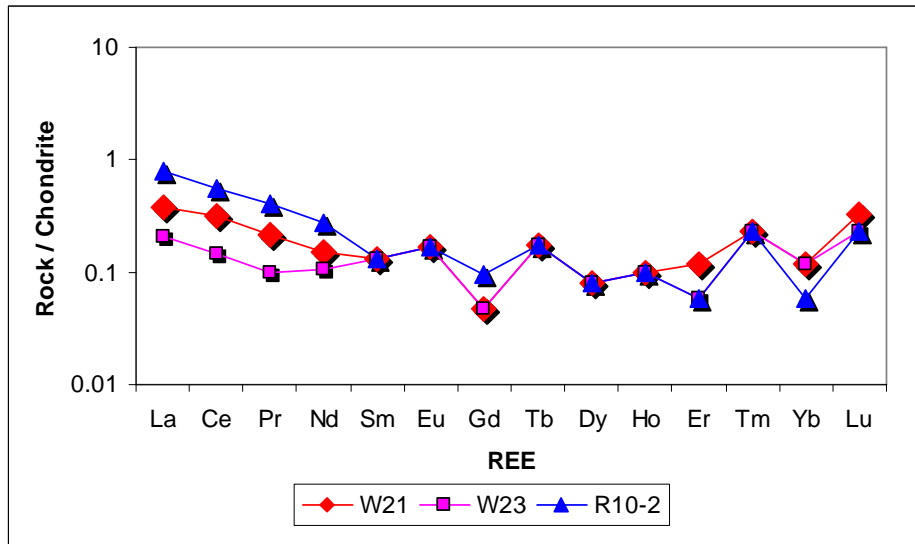


Fig. 2-18 Chondrite-normalized REE patterns of dunite in MOC.

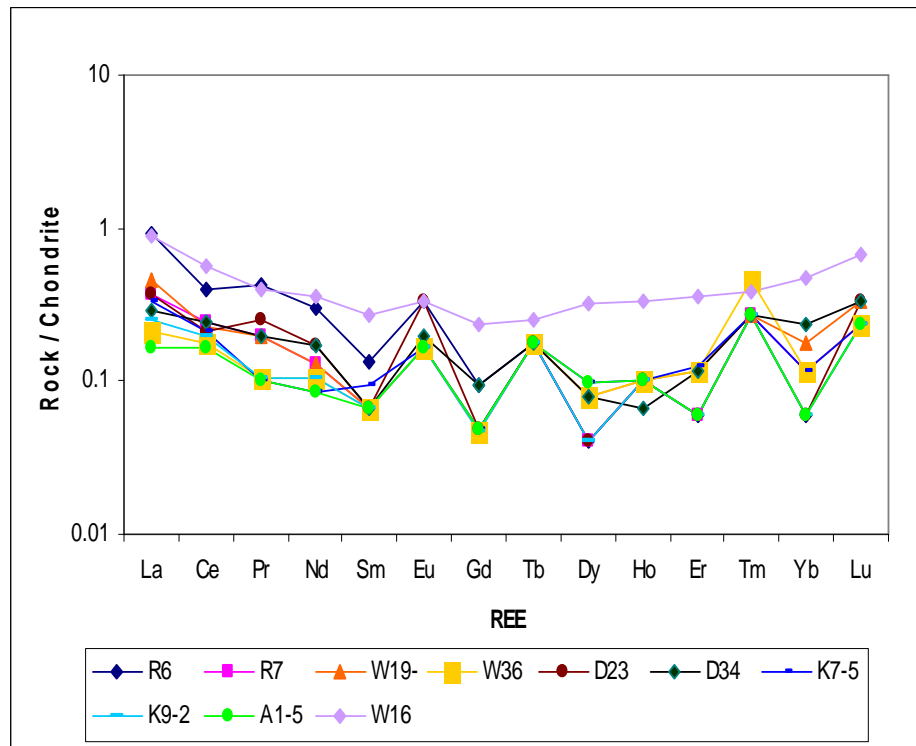


Fig. 2-19 Chondrite-normalized REE patterns of harzburgite in MOC.

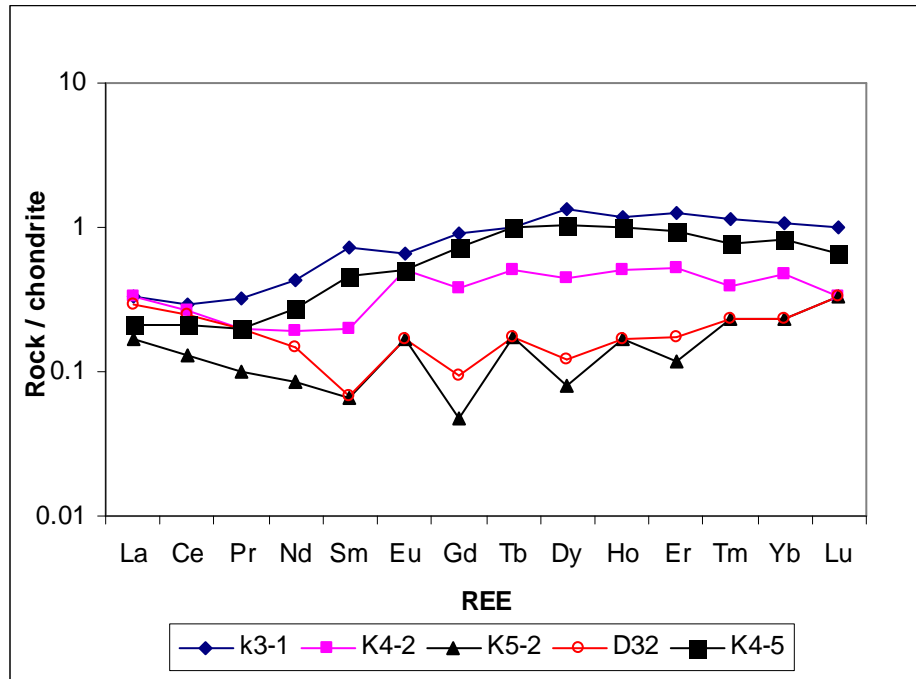


Fig. 2-20 Chondrite-normalized REE patterns of Iherzolite in MOC.

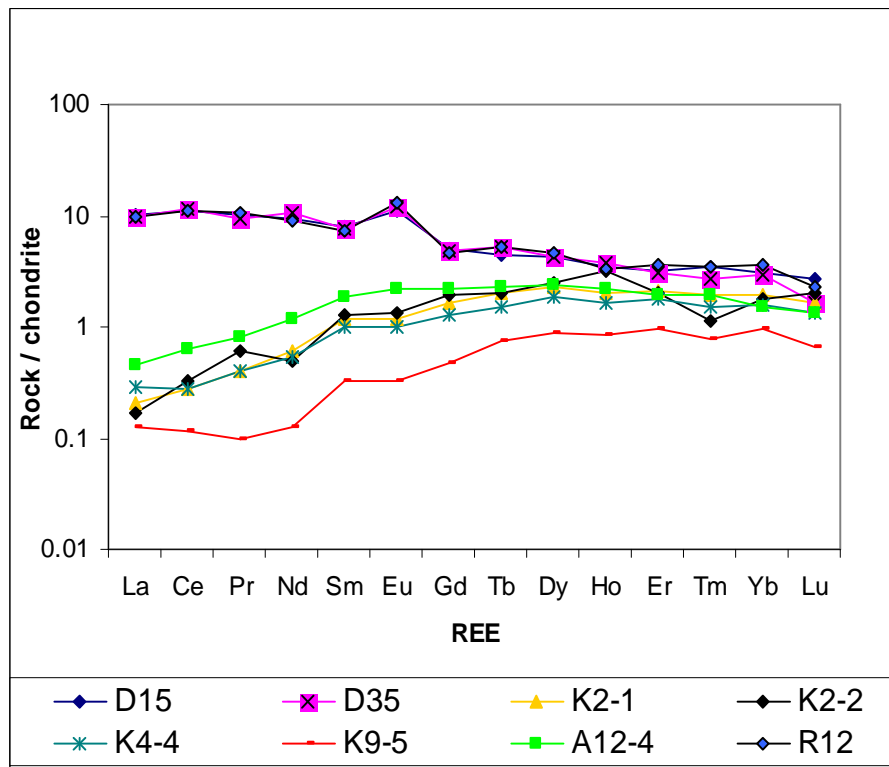


Fig. 2-21 Chondrite-normalized REE patterns of pyroxenite in MOC.

2.5 Spider diagrams of ultrabasic rocks in MOC

Chondrite - normalized spider diagram (Figs. 2-22, 23, 24 and 25), (Table 2-6), and (Appendix 7, 8, 9 and 10) for all ultrabasic rocks in MOC show enrichment in large ion lithophile elements (LILEs) such as (Ba, and Sr) relative to high field strength elements (HFSEs) like (Nb, Y, Zr and Hf).

The highly irregular LILEs abundances are indicative of significant metasomatic alteration (Kim et al., 2003). These elements are usually controlled mainly by fluid phase, which means they can easily be mobile in hot fluids; so the strong positive strontium anomaly in all studied samples may be attributed to the hydrothermal fluids affecting the rocks and leads to serpentinization of ultrabasic rocks. Bodinier and Godard (2004) described the ophiolitic peridotite by more prominent enrichment in alkaline and alkaline-earth elements (Rb, Cs, Sr, and Ba), possibly reflecting a supra subduction zone (SSZ). On the other hand, the HFSEs (the less mobile) are controlled by chemistry of the source and the crystal / melt processes during evolution of the rock. All studied samples display negative Nb and Pb anomalies and generally flat patterns, near or above unity for elements Tb to Lu (Figs. 2-22, 23, 24 and 25). Kim et al. (2003) and Hofman (2004) suggest that the negative Nb, and Pb is indicative to the involvement of mantle source that has been affected by subduction and tectonic environment of supra subduction zone basin (fore-arc setting). Bose (1997) ascribed the negative Nb anomalies in ultrabasic rocks to sequestration of Nb by ilmenite or sphene in the very source during partial melting. However, the negative Nb anomaly has also been attributed to crust contamination by some workers (i.e. Rao et al., 2004). Nb is one of the incompatible elements which are sensitive to the island arc setting; its depletions in studied samples may be indicative to SSZ (fore-arc) environment. Roy, et al. (2004) explained that it is possible due to the subduction of the earlier oceanic (mafic) crust, fluid (\pm silicate melt) was squeezed out from the slab and incorporated into the overlying mantle wedge. As this fluid generally contains H₂O, CO₂ and chloride ions, it will be enriched in moderately strong acids like Rb, Ba, and Sr, whereas they are depleted in very strong acid like Nb.

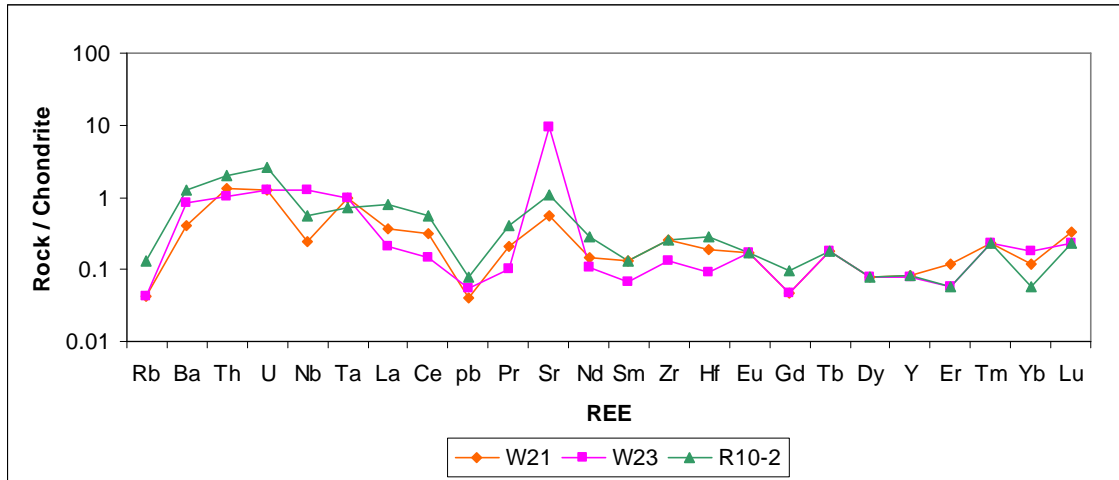


Fig. 2-22 Chondrite - normalized trace element patterns (spider diagram) of the dunite in MOC.

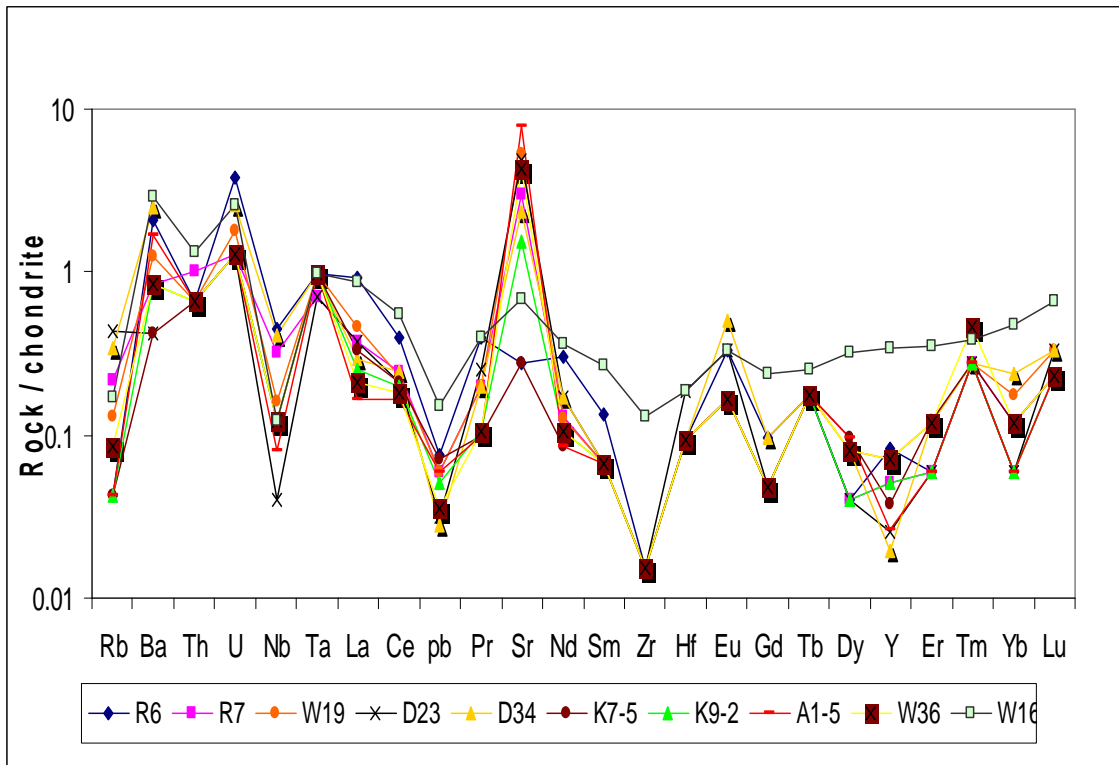


Fig. 2-23 Chondrite - normalized trace element patterns (spider diagram) of the harzburgite in MOC.

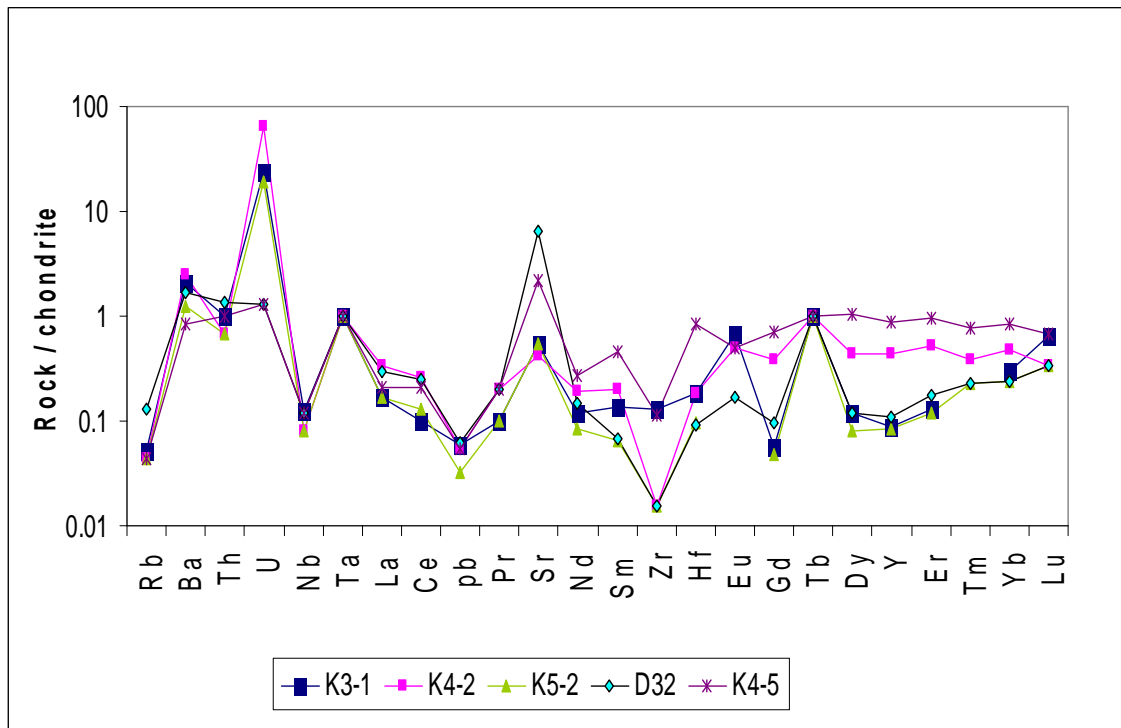


Fig. 2-24 Chondrite - normalized trace element patterns (spider diagram) of the Iherzolite in MOC.

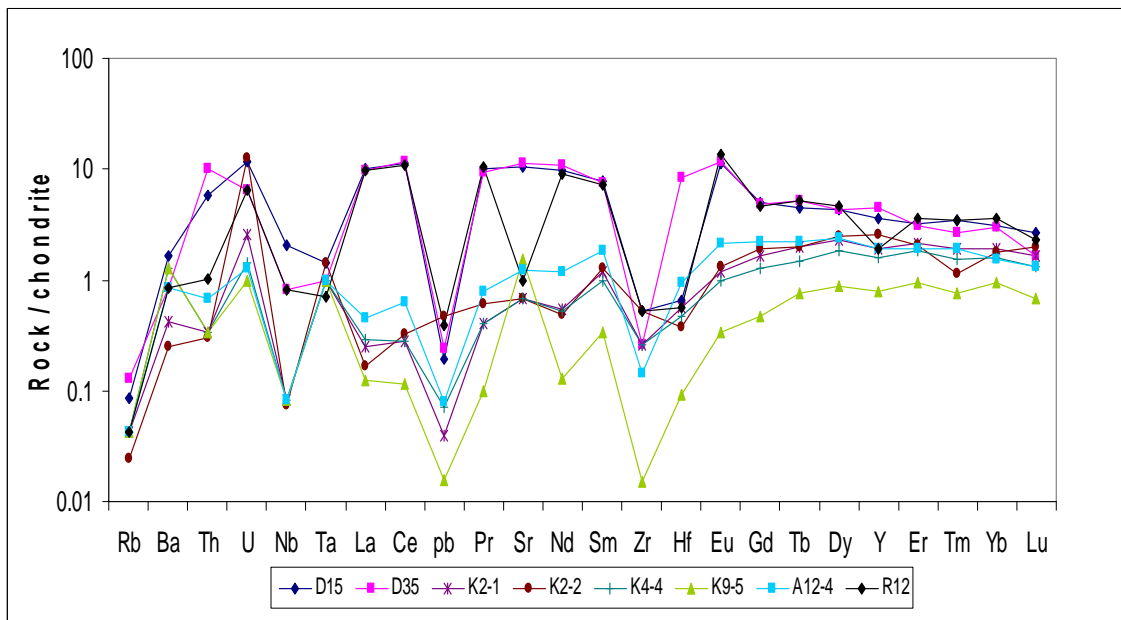


Fig. 2-25 Chondrite - normalized trace element patterns (spider diagram) of the pyroxenite in MOC.

2.6 Mineral chemistry

Selective mineral analyses on 3 samples of dunite, 5 harzburgite, 4 lherzolite were analyzed by (CAMECA, COMEBAX) dispersive electron probe X-ray microanalyser and 6 pyroxenite samples were analyzed by (JEOL Superprob JXA-8800) at Cooperation Research Center Kanazawa University Japan.

Ferrous and ferric iron contents of chromian spinel were calculated assuming spinel stoichiometry. While ferrous and ferric iron contents in pyroxene and amphiboles were calculated according to the procedure proposed by Bohlen and Esson (1979) and (Schumacher 1997 in Leak et al., 1997) respectively. Minerals were analyzed on polished thin sections for major and minor elements. Cr# is the Cr / (Cr+Al) atomic ratio of chromian spinel. Mg# is the Mg / (Mg+Fe_t), $Fe^{2+\#} = Fe^{2+} / (Fe^{2+} + Mg)$, $Fe^{3+\#} = Fe^{3+} / (Fe^{3+} + Cr + Al)$. Atomic ratio for silicate as well as the Mg / (Mg+Fe⁺²) atomic ratio for chromian spinel and olivine, from selected representative analyses are listed in (Tables 2-7). The details of analyses are listed in (Appendix, 11, 12, 13 and 14).

2.6.1 Olivine composition

Olivine and chromian spinel are both residual phases in mantle peridotites and early precipitating phase from primary magmas. The MOC is characterized mainly by forsterite olivine. Mineral chemistry of olivine shows that olivine from dunite are richer in forsterite (Fo. ₉₂₋₉₀) in dunite, (Fo. ₉₂₋₈₉), in harzburgite and (Fo. ₉₀₋₈₄) in lherzolite. They are plotted within olivine –spinel mantle array (OSMA), which is a spinel peridotite restite trend in the term of olivine-spinel compositional relation (Arai 1994a; Fig. 2-26), and characterized by Fo- rich content at a given Cr#. These trends sometimes start within or near the OS mantle array (Fig. 2-26). Dunite is included in the harzburgite range for the olivine-spinel compositional relation. The Cr# of chromian spinel does not show positive correlation with Fo. content of coexisting olivine in peridotites (Fig. 2-26). Harzburgite from MOC, which usually contain very small amounts of clinopyroxene and chromian spinel with an average (Cr # 0.679), belongs to the most refractory tectonic harzburgite (Dick and Bullen, 1984 and Arai, 1994a).

Olivine is the main constituent of peridotite and is a major host for the magnesium, iron, and nickel. The Mg# of olivine reflects the composition of the whole rock, which in turn is related to degree of melt depletion or enrichment in iron. The Mg# of dunite olivine are ranges between 0.895-0.92 and in harzburgite, lherzolite and pyroxenite the ranges 0.893-0.921, 0.836-0.892, 0.81-0.85 respectively, (Table 2-7 and Appendix, 11, 12, 13 and 14). They reflect more iron enrichment nature respectively. Iron rich-olivine are found in lherzolite and pyroxenite where they are interpreted as resulting from physical mixing of iron-rich pyroxenite with normal peridotite, followed by subsequent re-equilibration (Pearson et al., 2004).

2.6.2 Pyroxene composition

The Mg# of orthopyroxene is similar or slightly greater than that of olivine due to relative Fe-Mg partition coefficient (K_D) of ~ 1 ; that is independent of pressure and temperature (Von Seckendorff and O'Neill, 1993). The Mg# of orthopyroxene in dunite ranges between 0.95-0.97; in harzburgite, lherzolite and pyroxenite the ranges are between 0.90-0.92, 0.88-0.9, and 0.83-0.89 respectively (Table 2-7, Appendix 11, 12, 13 and 14). The calcium content is very low in all samples and does not reach 3 Wt%. The Al_2O_3 content of orthopyroxene in dunite, harzburgite and lherzolite varies between 0.164-0.167 Wt %, 0.05-1.63 Wt %, and 0.02-0.78 Wt % respectively. The Al_2O_3 content varies in orthopyroxene, depending on temperature and pressure of equilibration of the samples as well as its bulk composition. Al_2O_3 in pyroxene (regardless of facies) reflects the degree of depletion (Pearson et al., 2004). This is evident in peridotite pyroxene of MOC in which the Al_2O_3 content ranges between 0.02 to 1.63 Wt % (Table 2-7 and Appendix, 11, 12 and 13).

The orthopyroxene of pyroxenite rocks of the studied area are more enriched in Al_2O_3 content 1.69-2.2 Wt % (Appendix 14). The FeO content ranges between 3.5 to 11.16 Wt %, and MgO ranges from 17.23 to 32.42 Wt % and represents by bronzite ($En_{87}Fs_{13}$ and $En_{83}Fs_{17}$) (Fig. 2-27). The Cr_2O_3 content of orthopyroxene is very low in dunite, harzburgite and lherzolite (< 0.04 Wt %); while in pyroxenite orthopyroxene is more enriched (0.36-0.48 Wt %).

Table 2-7 Representative microprobe analyses of dunite (3 *), harzburgite (5*) lherzolite (4*) and pyroxenite (6*). [Cr#: Cr/(Cr+Al), Mg#: Mg/(Mg+Fe²⁺), Fe²⁺#: Fe²⁺ / (Fe²⁺ +Mg), Fe³⁺#: Fe³⁺ / (Fe³⁺ +Al+Cr) atomic ratio].

Rock type S.No.	Dunite			Harzburgite					Lherzolite			Pyroxenite			
	W20- Ol	W20 Amph.	W20 -Sp	R7- Ol	R7- OPX	R7-Amph.	R7 -Serp.	R7 -Sp.	K3-1-Ol	K3-1-CPX	K3-1 Sp.	K2-2 OL	K2-2 CPX	K2-2 OPX	K2-2 Sp.
SiO ₂	38.932	57.163	0.050	40.011	49.981	58.030	42.581	0.003	39.918	53.801	0.077	39.970	53.330	56.450	0.020
Al ₂ O ₃	0.000	0.601	10.821	0.010	0.986	0.162	0.086	11.909	0.022	0.225	24.880	0.000	2.110	1.690	30.920
TiO ₂	0.013	0.066	0.370	0.010	0.010	0.008	42.581	0.062	0.006	0.029	0.302	0.020	0.040	0.010	0.080
FeO	10.179	1.633	36.574	8.589	7.576	6.697	5.576	24.903	15.485	2.503	35.700	14.560	3.090	8.690	29.510
MnO	0.142	0.050	0.507	0.105	0.048	0.199	0.048	0.400	0.182	0.062	0.402	0.250	0.110	0.220	0.410
MgO	48.871	23.603	5.741	50.126	40.016	30.593	40.016	7.924	44.007	17.214	7.347	46.250	17.010	32.420	8.610
CaO	0.016	13.081	0.067	0.004	0.087	0.337	0.087	0.005	0.006	26.154	0.004	0.010	23.350	0.890	0.010
Na ₂ O	0.032	0.062	0.006	0.020	0.023	0.131	0.023	0.029	0.016	0.040	0.012	0.010	0.110	0.000	0.020
K ₂ O	0.006	0.001	0.001	0.001	0.034	0.000	0.034	0.004	0.001	0.000	0.012	0.020	0.020	0.030	0.000
NiO	0.235	0.066	0.094	0.314	0.152	0.089	0.152	0.014	0.122	0.039	0.044	0.230	0.010	0.050	0.080
Cr ₂ O ₃	0.614	0.413	44.948	0.010	0.437	0.058	0.037	54.062	0.002	0.110	31.063	0.030	0.680	0.430	31.270
Totals	99.040	96.736	99.178	99.098	99.350	96.303	88.631	99.316	99.768	100.177	99.843	101.350	99.860	100.880	100.930
O	4.000	23.000	4.000	4.000	6.000	23.000	6.000	4.000	4.000	6.000	4.000	4.000	6.000	6.000	4.000
Si	0.979	7.887	0.002	0.987	1.804	7.928	1.988	0.000	0.988	1.967	0.003	0.990	1.946	1.956	0.001
Al	0.000	0.098	0.411	0.000	0.004	0.026	0.005	0.469	0.001	0.010	0.899	0.000	0.091	0.069	1.109
Ti	0.000	0.007	0.010	0.000	0.000	0.001	0.000	0.002	0.000	0.001	0.007	0.000	0.001	0.000	0.002
Cr	0.000	0.045	1.243	0.000	0.001	0.006	0.001	1.427	0.000	0.003	0.805	0.000	0.020	0.012	0.752
Fe ²⁺	0.214	0.180	0.787	0.177	0.190	0.760	0.218	0.330	0.314	0.080	0.245	0.301	0.090	0.250	0.612
Fe ³⁺	0.000	0.010	0.262	0.000	0.010	0.000	0.000	0.344	0.000	0.000	0.734	0.000	0.000	0.000	0.125
Mn	0.003	0.006	0.015	0.002	0.002	0.023	0.002	0.011	0.004	0.002	0.011	0.005	0.003	0.006	0.011
Mg	1.820	4.855	0.251	1.843	2.387	6.230	2.784	0.359	1.701	0.938	0.310	1.707	0.925	1.674	0.390
Ca	0.000	1.934	0.003	0.000	0.004	0.049	0.004	0.000	0.000	1.025	0.000	0.000	0.913	0.033	0.000
Na	0.002	0.016	0.000	0.001	0.002	0.034	0.002	0.002	0.001	0.003	0.001	0.001	0.007	0.000	0.001
K	0.000	0.000	0.000	0.000	0.002	0.000	0.002	0.000	0.000	0.000	0.001	0.001	0.001	0.001	0.000
Ni	0.005	0.007	0.003	0.006	0.005	0.010	0.006	0.000	0.003	0.001	0.001	0.004	0.000	0.001	0.002
Mg#	0.895	0.964	0.242	0.912	0.926	0.891	0.927	0.521	0.844	0.921	0.560	0.850	0.911	0.870	0.389
Cr#	0.000	0.000	0.751	0.000	0.000	0.000	0.000	0.753	0.000	0.000	0.470	0.000	0.000	0.000	0.404
Fe ²⁺ #	0.105	0.036	0.758	0.088	0.073	0.109	0.073	0.480	0.156	0.079	0.441	0.150	0.089	0.130	0.611
Fe ³⁺ #	0.000	0.065	0.136	0.000	2.068	0.000	0.000	0.150	0.000	0.000	0.301	0.000	0.000	0.000	0.063

Ol: olivine, Amph: Amphibole, Sp: spinel, Serp. Serpentine, CPX: clinopyroxene, OPX: orthopyroxene. * Number of analyzed samples.

This element can be substituted for aluminum and so may vary with temperature and pressure (Nickel, 1986). The Al_2O_3 content in orthopyroxene of pyroxenite are more enriched than those in dunite, harzburgite, and lherzolite; so more substitution of chrome for aluminum and more enrichment of Cr_2O_3 in pyroxenite are observed. The orthopyroxene of dunite, harzburgite and lherzolite represent enstatite and their En and Fs content ranges from $\text{En}_{91}\text{-Fs}_9$ to $\text{En}_{97}\text{Fs}_3$. The orthopyroxene of harzburgite is more affected by serpentinization and alteration process and has been altered to talc. The EPMA results reveal that the talc has composition as $(\text{Mg}_{5.8} \text{Fe}_{0.145} \text{Ca}_{0.003}) (\text{Si}_{7.97}\text{Al}_{0.025}) \text{O}_{10} (\text{OH})_2$ (Appendix 12).

Clinopyroxene is a major host for sodium, calcium, chromium and titanium in mantle xenolith and shows extensive solid solution toward orthopyroxene at high pressure and temperature in the mantle (Koheler, 1990). The Mg# of clinopyroxene in peridotite is slightly greater than that of coexisting olivine due to a K_D greater than 1 (Pearson, 2004). The Mg # of clinopyroxene of MOC peridotite ranges between 0.90-0.96. This variation in Mg# is related to the degree of serpentinization (hydration), the strongly serpentinized has higher Mg# (Appendix 12 and 13). All clinopyroxene is characteristically poor in Na_2O , and rarely exceeds 0.2 Wt % in all studied samples and its plot in the diopsitic field (Fig. 2-27). According to Cr_2O_3 content in clinopyroxene of studied samples it can be represented as chromian diopside. The Al_2O_3 content of lherzolite varies between 0.18-2.81 Wt % and 0.76-1.4 Wt %, 0.77-2.3 Wt % in harzburgite and pyroxenite respectively and is negatively correlated with Mg# (Fig. 2-28). The Cr_2O_3 content ranges from 0.02 to 1.76 Wt % in clinopyroxene of ultrabasic studied samples and (0.19-0.76 Wt %) in pyroxenite (Appendix 12, 13 and 14), the Cr_2O_3 content and Mg# are both compatible components of clinopyroxene in a plutonic rocks of MOC and are almost nearly constant. Dick and Fisher (1984) agreed that clinopyroxene is a measure of the degree of depletion of peridotites. Since dunite in the studied area is almost free of clinopyroxene and the harzburgite contain very small volume % of

clinopyroxene (< 4 %) (Table 2-2), therefore they are assumed to be highly depleted ultrabasic rocks and undergone a high degree of melting.

The pyroxenite rocks commonly have aluminum-rich and low titanium diopside. The pyroxenite rocks in the studied area are mostly olivine webstrite and clinopyroxenite and the extremely refractory nature of mineral phase (olivine, clinopyroxene and chromian spinel) indicates a very high temperature of crystallization for liquid olivine and chromite from high-Mg, low Al_2O_3 parent liquid and suggested that their origin may be hydrous melting of depleted mantle peridotite.

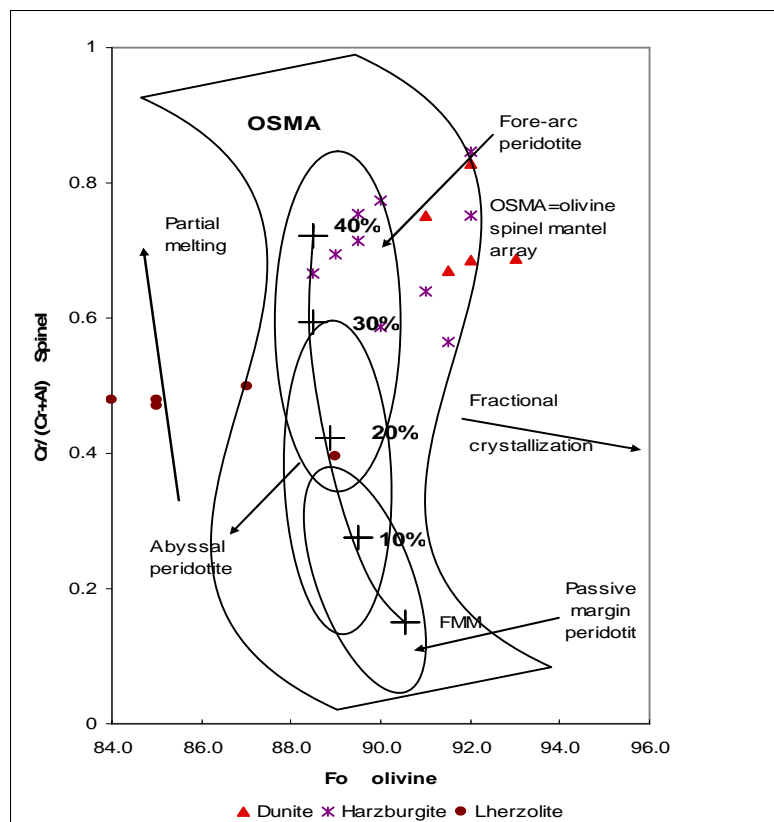


Fig. 2-26 Relationships between the Fo content of olivine and the Cr/(Cr+Al) atomic ratio (Cr#) of chromian spinel in ultrabasic rocks from the MOC. (OSMA), olivine spinel mantle array from Arai, FMM: Fertile MORB Mantle, 10%, 20%, 30%, and 40% represent partial melting % of FMM (1994a)

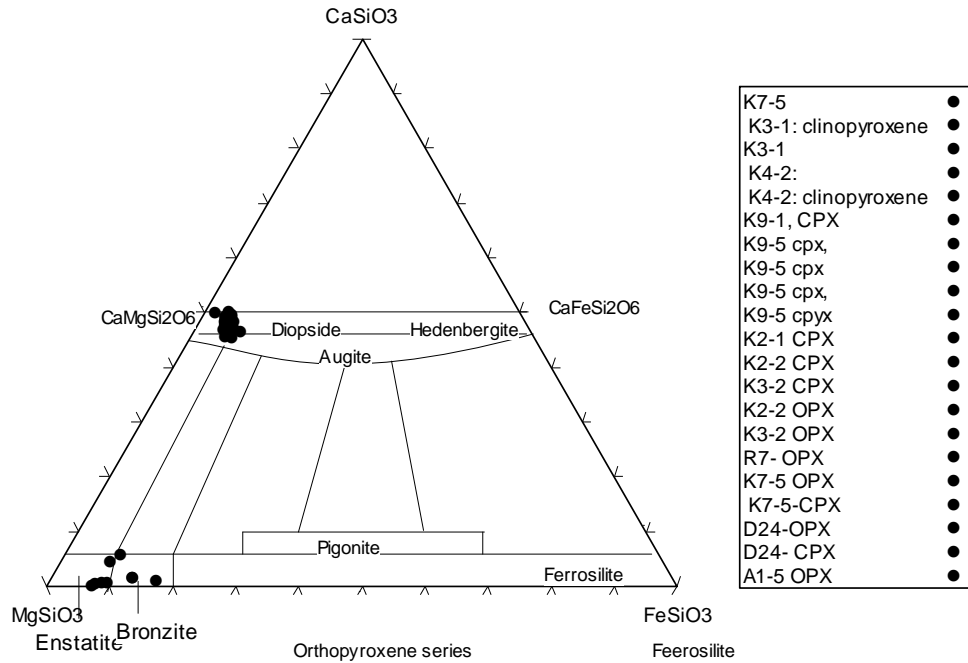


Fig. 2-27 Pyroxene compositions in the system CaSiO₃-MgSiO₃-FeSiO₃ general compositional field are from Klein et al. (1993).

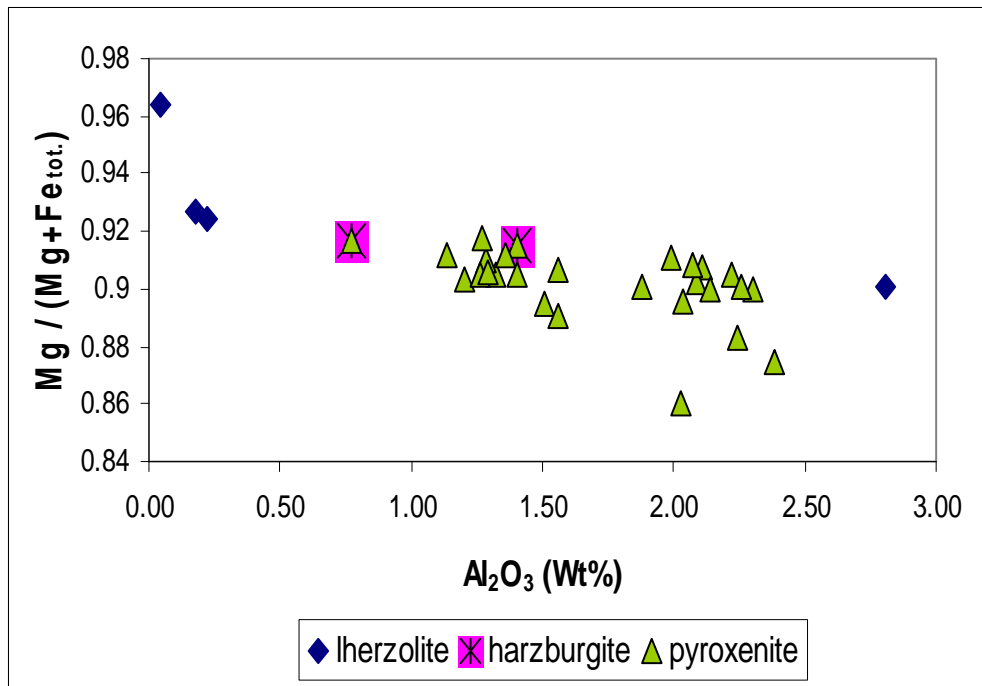


Fig. 2-28 Al₂O₃ – Mg # relationship of clinopyroxene in peridotite and pyroxenite rocks in MOC.

2.6.3 Alteration minerals

Amphibole, serpentine and magnetite are abundant as altered minerals in ultrabasic rocks of MOC. The amphiboles are generally highly magnesian [Mg# ranges from (0.88 to 0.97) and (0.918-0.942)] in peridotites and pyroxenite of studied samples respectively Table 2-7 and Appendix 11, 12, 13, and 14.

Compositional variability of amphibole in ultrabasic and pyroxenite rocks is represented in (Fig. 2-29). The amphiboles in dunite harzburgite and lherzolite are plots in the field of tremolite and for harzburgite represent tremolite and actinolite. The Cr₂O₃ content is below 1 Wt% in all samples and has low TiO₂ content (\leq 0.1 Wt %). Na₂O + K₂O contents of the within- dunite, harzburgite, and lherzolite amphibole are 0.02-0.06 Wt %, 0.01-0.22 Wt % and 0.03-0.4 Wt % respectively and 0.12-0.47Wt % in pyroxenite (Table 2-7), (Appendix 11, 12 and 13). The amphiboles in ultrabasic rocks of MOC are explained as a result of the alteration product of pyroxene.

Serpentine is frequent as altered mineral in harzburgite and lherzolite and as inclusion in chromian spinel in harzburgite. Serpentine in harzburgite has Mg# [Mg/ (Mg+Fe_t) atomic ratio] which ranges from 0.84-0.92, its Cr₂O₃ contents is relatively low below 0.05 Wt %. The Mg# of lherzolite serpentine is more variable with a range between (0.85 to 0.94). Serpentine of dunite, harzburgite, lherzolite are lizardite and chrysotile in composition (Fig. 2-30).

2.6.4 Accessory chromite composition

Chromian spinels from dunite have similar Cr# (0.679-0.851 average 0.733) and lower Mg# (0.182-0.409) than those found in chromitite and plots in the field of high-Cr Alpine type peridotites (Fig. 2-31). The Cr# is only slightly changed or nearly constant in chromitite and dunite rocks of MOC. This may be the earliest precipitating olivine and chrome spinel in primary magmas and are almost identical in chemistry to those of residual if physical conditions are not largely different (Ahmad et al. 2005). Chromian spinel in harzburgite are compositionally distinct from those of chromitite, they are plot in the

field of high- Al, high-Cr and high-Fe, while in chromitite it plots in the field of high-Cr chromian (Fig. 2-31) and (Fig. 2-32).

Chromian spinel in harzburgite has a lower average Cr# 0.679 and has low TiO₂ contents (0.01-0.126 Wt %) compared with those in dunite (Table 2-7), (Appendix 11 and 12). The high-Cr# in dunite and intermediate to high-Cr# in harzburgite with relatively high-Fe⁺³# may be related to iron supplied through cracks to become so called ferritchromite upon alteration.

The Mg# of chromite in chromitite rocks is higher than chromite in associated dunite and harzburgite (Al-Chalabi, 2004 and Ahmad et al., 2005). In the case of spinel in dunite and harzburgite of MOC it has Mg # lower than that of spinel in chromitite; this is related to the presence of serpentine formation around chromite grain in dunite and harzburgite. The formation of serpentine around chromite crystals causes more expense of Mg by serpentine and decrease Mg in spinel.

The differences in severe alteration and serpentinizations may affect spinel in chromitite and peridotite equally. Chromite crystal in harzburgite from all localities of the studied area show a wide range of Cr₂O₃ content (54.06-42.26 Wt %). This is lower than Cr₂O₃ content of chromite from chromitite pods; this corresponds to the modal percent of chromite. The accessory chromites in ultrabasic rocks of MOC also show a systematical enrichment in FeO and depletion in MgO (Fig. 2-33). The MnO content of accessory chromite in dunite, and harzburgite (has a mean value of 0.45, 0.41%) while in lherzolite and pyroxenite (the mean value are 0.35 and 0.37 %) respectively (Appendix 11, 12, 13 and 14). The MnO enrichment is usually associated with alteration.

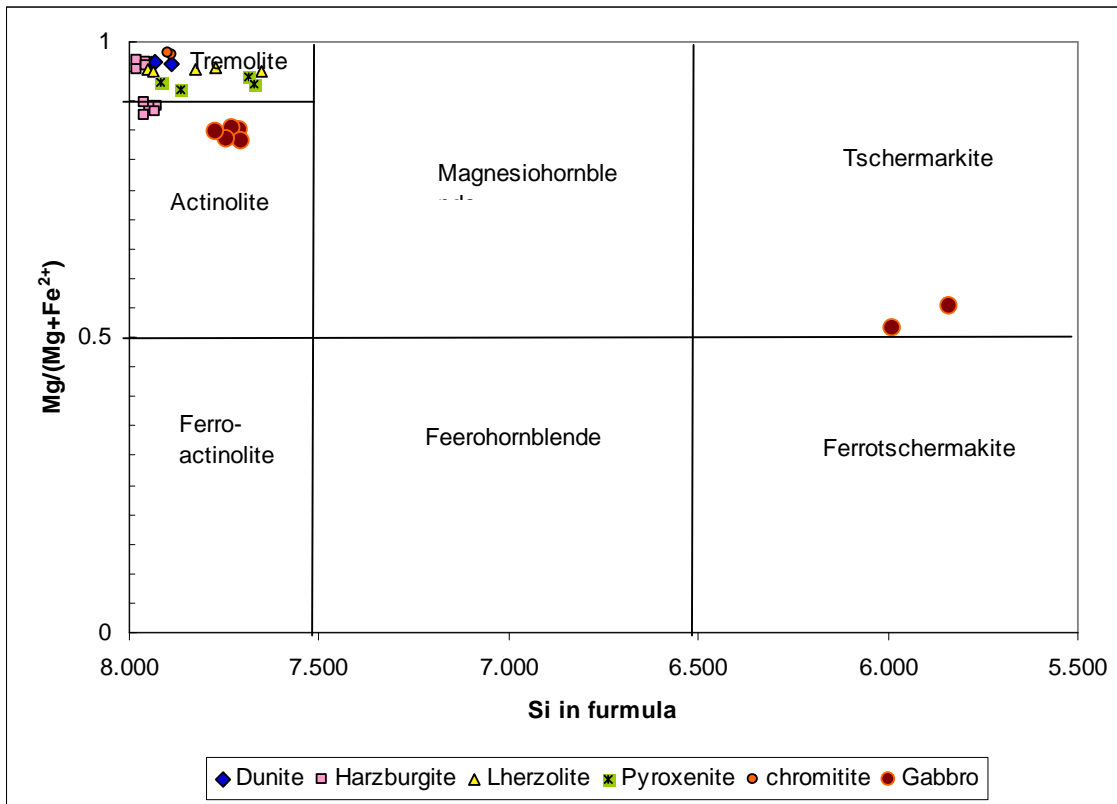


Fig. 2-29 Classification of amphiboles in studied samples (Leak et al., 1997).

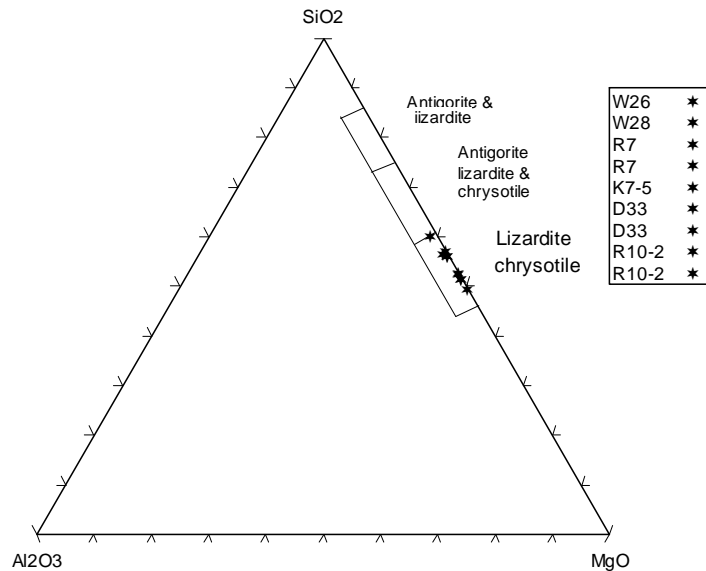


Fig. 2-30 SiO₂ - Al₂O₃- MgO triangle, shows the types of serpentine mineral Group of studied samples (Wickes and Plant, 1979).

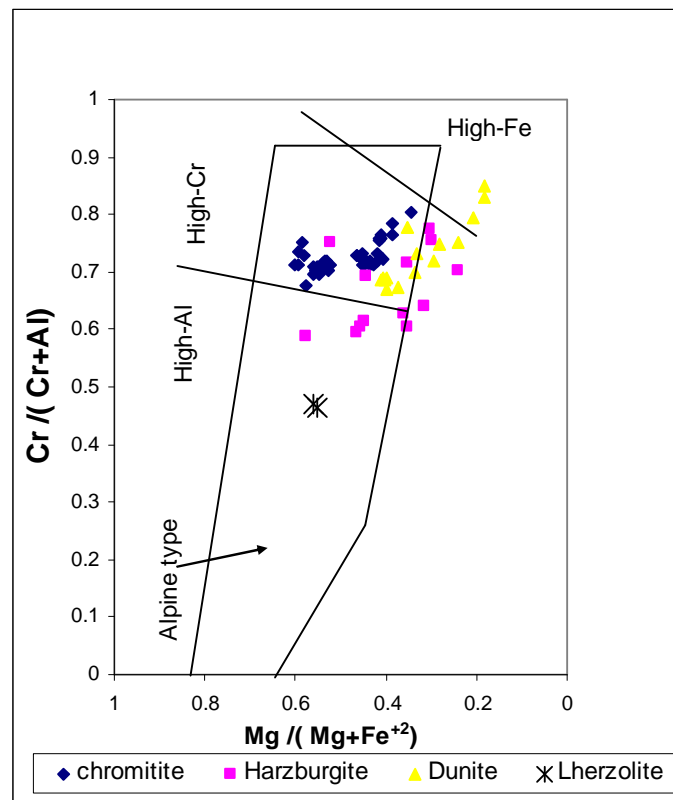


Fig. 2-31 Plots of Cr# versus Mg# for chrome spinel in chromitite, dunite, harzburgite and lherzolite. The Alpine-type field is from Irvan (1967). The high-Al, high Cr, and high Fe field from Mei-Fu (1992).

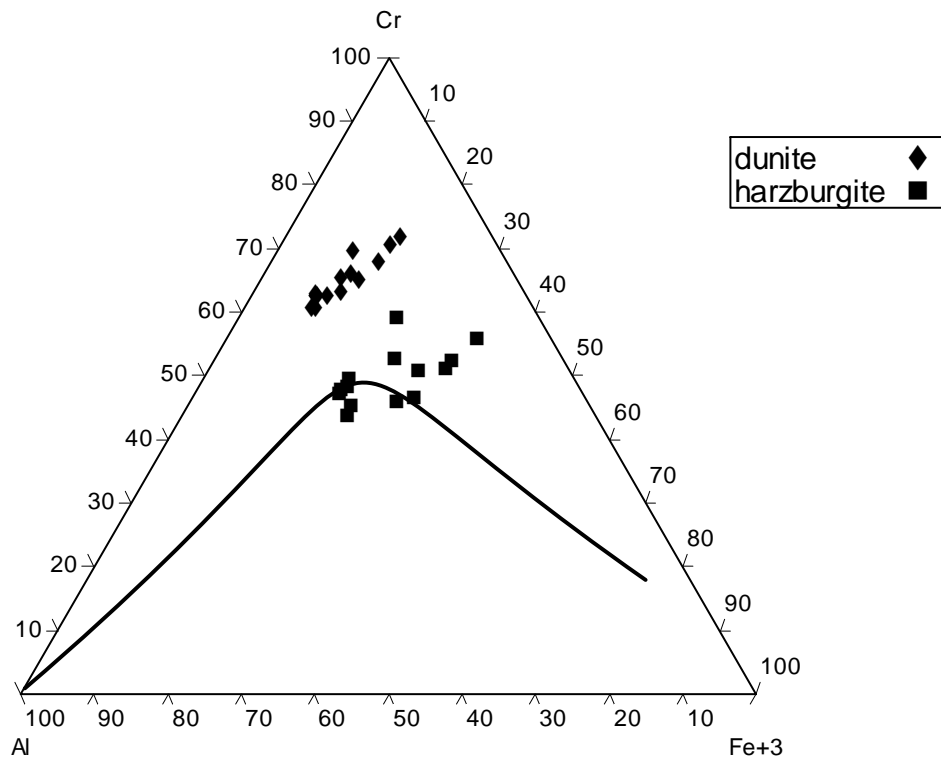


Fig. 2-32 Cr-Al-Fe⁺³ atomic ratio of chromian spinel in ultrabasic rocks of MOC.

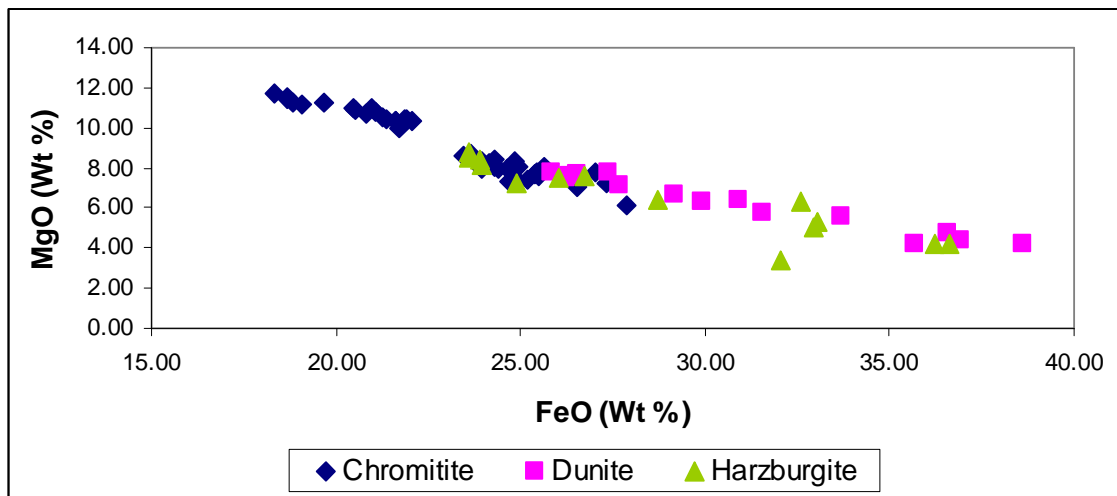


Fig. 2-33 MgO vs FeO relationship of chromian spinel ultrabasic rocks in MOC.

2.7 Accessory chromite alteration

Chromite is common in small quantities in peridotites and its compositions have often been used as petrogenetic indicator. In igneous rocks, the Cr-spinel compositions are sensitive to melt composition, crystallization pressure and degree of melting in the mantle source region (Dick and Bullen 1984 and Kimball, 1990). The compositions of spinels also change with hydrothermal alteration.

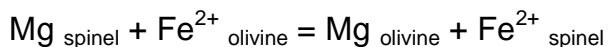
The formation of ferritchromite is highly reflective borders around chromite in ultrabasic rocks of the studied samples; that are enriched in iron but depleted in magnesium and aluminum relative to cores often accompanies serpentinizations. Its origin is unclear although several mechanisms are possible. Ulmer (1974) suggests that the excess Cr and Fe at the rims were derived from the silicates during serpentinizations.

Biliss and Mclean (1975) in Kimball (1990) suggested that the alteration rims were formed during regional metamorphism, initially as magnetite rim during serpentinization and then as ferritchromite as metamorphism increased. Fe^{3+} diffuses from the core, and some of the core is dissolved and then ferritchromite is precipitated as was suggested by Wylie (1987 in Kimball, 1990). Other workers have proposed that the diffusion of Al and Mg out of the spinel during metamorphism results in the formation of chlorite (Shen et al, 1988 and Wang, et al., 2005).

The accessory chromite in ultrabasic rocks of MOC is usually more affected by alteration than those in massive chromitite (Figs. 2-34 and Fig. 2-35). This is attributed to more involvement of subsolidus element redistribution during the metamorphism with silicate phase in the former chromite (Lehmann, 1983).

The EPMA profile in accessory chromite grain from dunite and harzburgite shows two different compositional zones from core to rim: (1) core chromite that retains the primary composition and (2) ferritchromite rim. The accessory chromite shows zoning pattern characterized from core to rim by significant increase in total iron content and Cr_2O_3 and decrease in Mg and Al (Figs. 2-34) and (Fig. 2-35) (Appendix 11, 12 and 13) and plots in the field of lower amphibolite facies (Fig. 2-36). This trend profile is due to modification of the primary chemical composition of core by alteration reaction and the formation of ferritchromite on the rim.

The accessory chromites from MOC have lower Mg# than those of chromite in chromitite rocks. This is due to the presence of serpentine around chromite grain. The altered chromite grain surrounded by magnetite rims and serpentine. The magnetite rims react with the chromite core to produce an Al-poor chromian magnetite mantle around relatively homogeneous chromite core such that the chromite is progressively replaced by chromian magnetite. The re-equilibration would result in much more Fe including Fe^{3+} in the altered chromites, which in turn causes the decrease of both Cr and Al at the same site in the chromite structure (Fig. 2-34 and Fig. 2-35), (Wang et al., 2005). MgO contents of the accessory chromite in ultrabasic rocks of MOC decrease with the decrease of Cr_2O_3 (Fig. 2-37). The decrease of MgO content was also caused by the re-equilibration between the chromite and coexisting silicates (mainly olivine) with falling temperature through the reaction



The change in (Kd) of the exchange reaction forces Mg into olivine and Fe into chromite with falling temperature (Irvan, 1965). Similar reaction between chromite and orthopyroxene has been described by Wang, et al., (2005). The decrease in MgO and increase in FeO_t of the zoned chromite in MOC imply

that the chromite cores apparently continue to equilibrate with surrounding silicate mineral despite the presence of magnetite rims (Barnes, 2000).

Accessory chromites of MOC also show evidence of high-temperature alteration. These spinels are very Fe-rich relative to Mg, and Cr-rich relative to Al (Table 2-7 and Appendix 12 and 13). The ferritchromite could be formed by re-equilibration between secondary magnetite rim and chromite core during serpentinizations (Kimball, 1990).

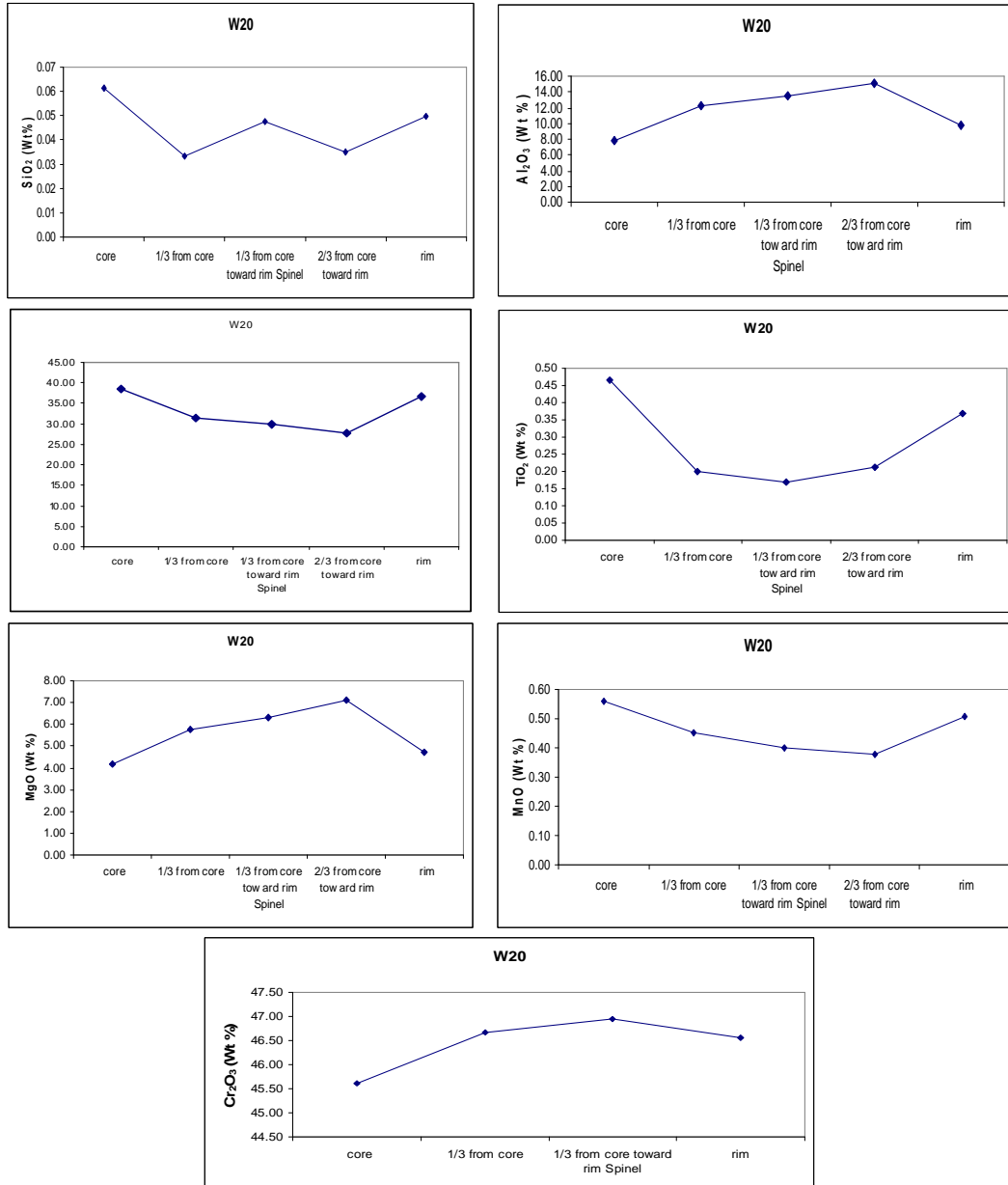


Fig. 2-34 Microprobe traverses across an altered accessory chromite in dunite from MOC.

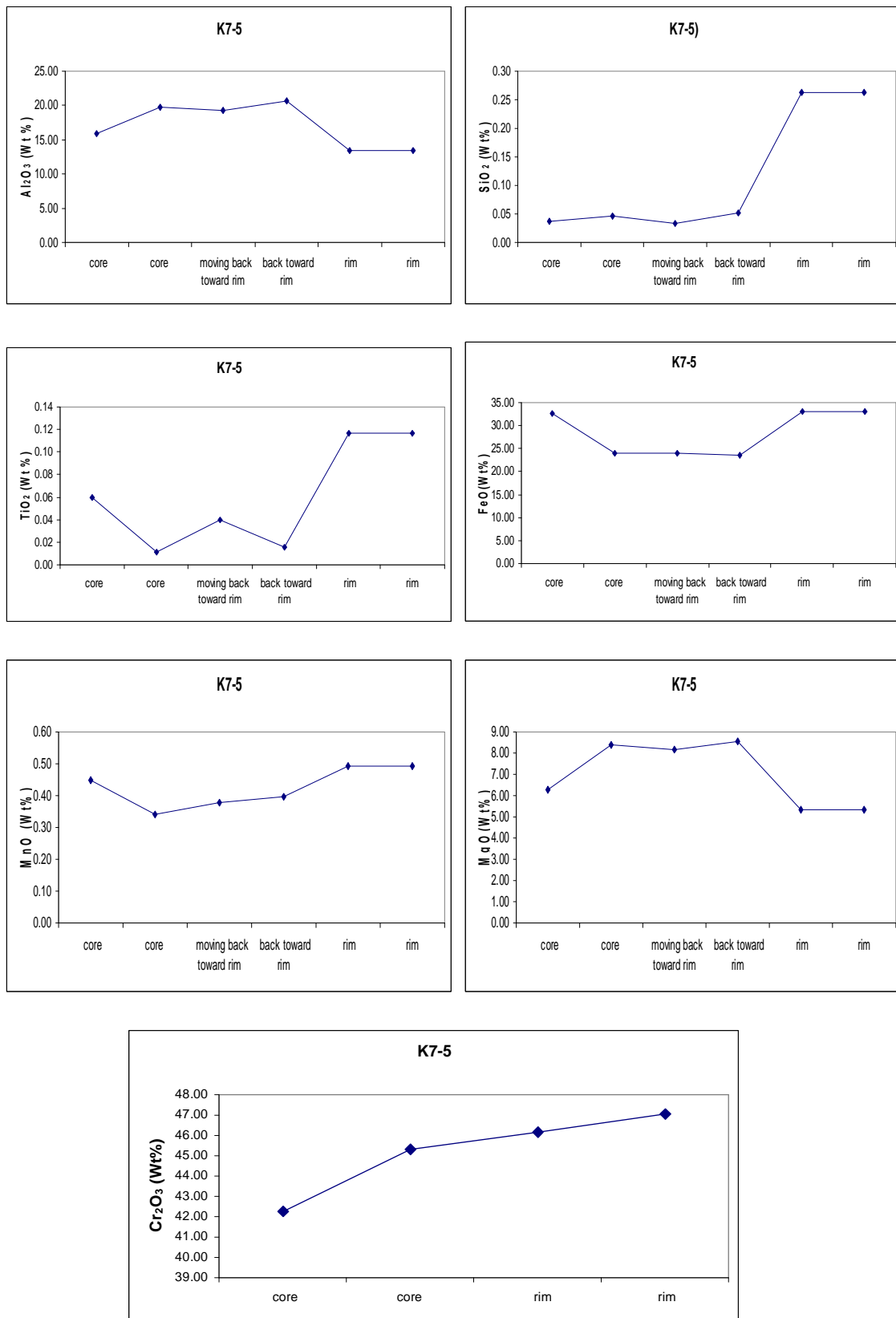


Fig. 2-35 Microprobe traverses across an altered accessory chromite in harzburgite from MOC.

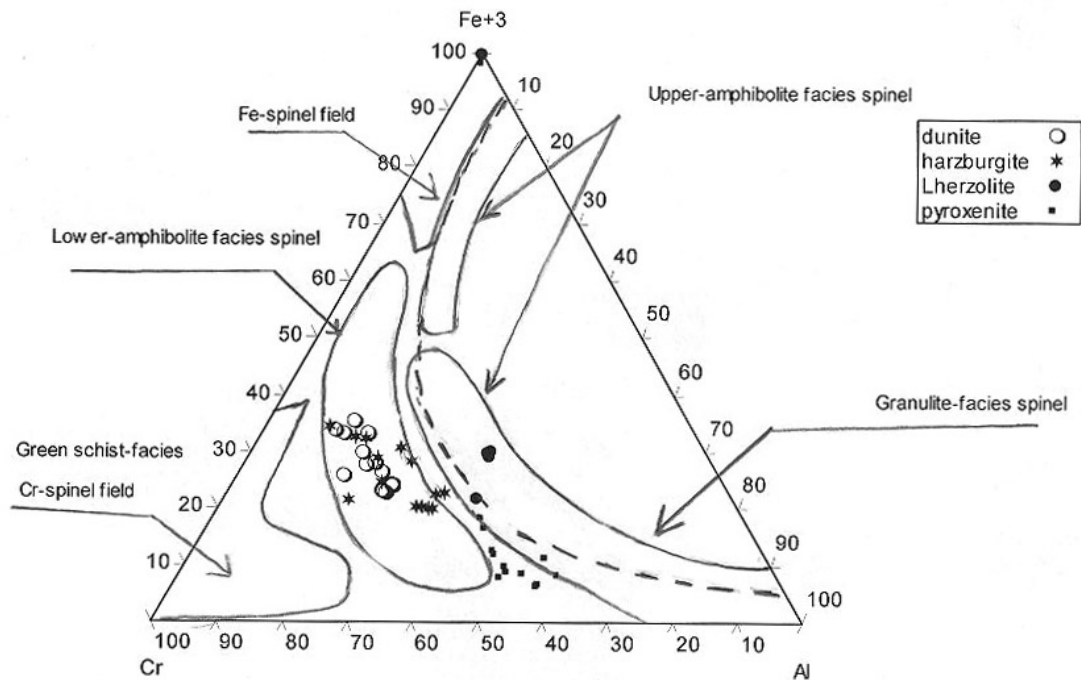


Fig. 2-36 The plots of Fe^{+3} -Cr-Al of studied samples and solves curve for different metamorphic Cr-spinel phases(Purvis et al., 1972; Evans & Frost, 1975; Suita & Strider,1996).

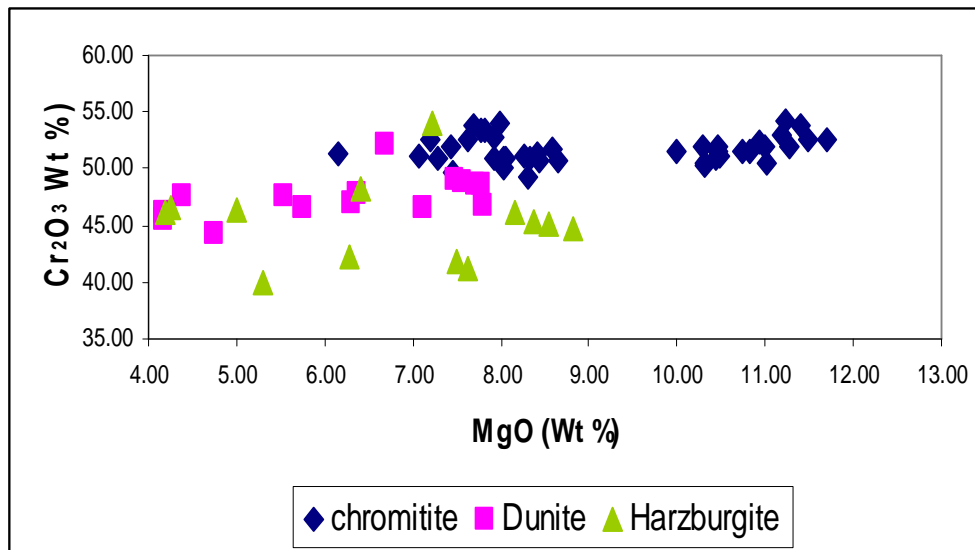


Fig. 2-37 The relationship of MgO-Cr₂O₃ of the chromite from the peridotite of MOC.

Chapter Three Chromitite Rocks

3.1 Introduction

There are very few researches dealing with chromitite rocks from Iraq. These studies are (Masek and Etabi, 1973, Al-Mehaidi, 1974, Al-Hassan, 1975 Buda and Al-Hashimi 1977, Al-Hassan, 1982, Buda, 1988, Al-Chalabi, 2004, Ismail and Al-Chalabi, 2006, Arai, et al., 2006, Ismail, 2007, Ismail et al., 2007 and the present study).

The chromite ore from the studied area was first described by Buda and Al-Hashimi (1977) in Ser Shiw valley as three main types.

1. Massive chromite ore where chromite content is more than 80 %
2. Schlieren type chromite (18 % chromite content).
3. Accessory chromites (approximate 2 % in lherzolite and dunite).

Petrographic study of the chromitite samples are examined by using both polarized transmitted and reflected microscopes. Modal proportions of minerals were determined by point counter (model E swift) involving 300 points covering the whole area of a thin section (Table 3-1).

In the present study the chromitite term used to refer to ultrabasic rocks with more than 20 Volume % of chromian spinel as proposed by Arai (1980) and Miyake, et al. (1997). Detail petrographic, geochemistry and mineral chemistry study of nine pods of chromitites from north of Kuradawi village and numerous smaller chromite rich peridotites are recognized in Ser Shiw valley - Shakha Root area of MOC.

The chromitite pods have lens-shape in a dunite envelope and both rock types are hosted by mantle harzburgite and lherzolite (Fig. 3-1). In the field, the chromitite rocks appear as blush grey, massive (Fig. 3-1) and their dimensions range between (30 cm-2 m) width and (0.5-12 m) length.

Chromitite ore bodies of the MOC belong to the concordant type and the mantle is harzburgite ophiolite type affinity.

Chromitite pods of the MOC have relatively sharp contact with surrounding mantle transition zone dunites which, in turn, enclose lenses from the mantle harzburgite. Chromitite textures are predominantly massive (Fig. 3-1), locally

from dense to thin disseminate (Fig. 3-2 A, B) and appear as banded chromitites, with alternating chromite rich and dunite peridotite-rich present.

Late shearing and faulting obliterating these textures giving rise to cataclastic, pull-apart, and brecciated textures. Many deposits consist of massive and disseminated ore and dunite over a few meter-ranges are frequent. A typical contact shows gradation from fine grained disseminated spinel in the dunite through fine grained and coarse grained chromite ore.

3.2 The major ore types

3.2.1 Massive chromitite ore

Massive ores are composed of 85-75 vol. % chromian spinel (Table 3-1) generally form the central part of the ore bodies. A grain size of chromite range from 0.5mm to more than 3mm interstitial silicate matrix which is mainly composed of secondary chlorite and amphiboles (Figs. 3-3 and 3-4). Massive ores are usually considered as recrystallized ores (Proenza et al., 2001); the gradual contacts to dunite, suggest that coarse grained ore is a primary feature (Melcher et al., 1997).

The massive chromitite are grading locally to disseminated, and shows pull-apart features. These crystals have subhedral to anhedral habit (Fig. 3-3).

Under the reflected microscope they appear as light grey color and they are isotropic with a very thin corroded rim (Fig. 3-5). The chromite grains contain solid inclusions of silicate mineral (Fig. 3-6) and platinum group mineral PGM alloys. Most of chromite grains exhibit thin rims of secondary ferritchromite (Fig.3-3) that may be related to an alteration product of chromite formed during late hydrothermal oxidizing processes probably postdating the main serpentinizations events, the same conclusion was obtained by Proenza et al. (2001) during their study of chromitite ores in Moa-Baracoa ophiolitic massif, eastern Cuba.

3.2.2 Brecciated chromitite ore

Brecciated chromitite ore are composed of 74 - 59 vol. % of chromian spinel (Table 3-1). In this type, chromite, grains are transected by many cracks (Fig.

3-7). These cracks are filled with secondary phase of chlorite, amphiboles and serpentinized olivine. The chromite grain size ranges from (0.5mm – 2.5 mm), the color of chromite under transmitted light is reddish brown and displays a zoning pattern which varies from chromite rich core to ferritchromite rims.

Under the reflected microscope the marginal zones have higher reflectivity due to alteration to ferritchromite (Fig. 3-8). The zonal pattern is attributed to a metamorphic and/ or hydrothermal event which re-equilibrated chromite composition, while the original magmatic composition was preserved in crystal cores only, as supported by similar studies (Al-Hassan, 1982 and Angeli and Vlach, 2004).

With regards to the origin of the matrix of brecciate chromite ores, it appears that this matrix was originally olivine which became altered to serpentine and then to chlorite (Buda and Al-Hashimi, 1977, Buda 1988, Al-Hassan, 1982).

3.2.3 Disseminated chromitite ore

Disseminated chromitite ore either occurs along the margins of massive ore bodies or forms small interdependent ore bodies. These show banded texture defined by alternation of fine grained (less than 2 mm) disseminated chromian spinel and slightly serpentinized olivine (Fig. 3-2 A and B). The disseminated chromitite are more abundant in Ser-Shiw valley and extreme north of Shakha Root while in Daraban area the chromian spinel is seen as accessory type.

The disseminated ore can be formed by ductile deformation. The disseminated chromites crystals are subhedral to anhedral (Fig. 3-9) and contain solid inclusion of silicate minerals mainly olivine and altered clinopyroxene (Fig. 3-10). They are enveloped with dunite and the host rocks are harzburgite, olivine crystals are slightly deformed, kink bands are very frequent and serpentinized along cleavages and cracks. The forsterite content is very high (Fo_{90-92}) in dunite and (Fo_{89-92}) in harzburgite, (Appendix 11 and 12).

3.3 Mineral inclusion in chromian spinel

Silicate mineral inclusions are common in chromian spinel of chromitite, associated dunite envelopes rocks and peridotite host rocks. The silicates have various sizes being less than 1 mm across, with subhedral to anhedral

shape (Fig. 3-6). The constituent mineral inclusions are in order of decreasing abundance; chlorite, serpentine, amphibole, olivine and clinopyroxene.

The variation in inclusion content observed in all of chromitite studied. The brecciated and disseminated chromitite rocks are more enriched in mineral inclusions than associated massive ores.

There are two distinctive types of inclusions the first is (hydrous silicate); mainly chlorite and serpentine inclusions which are anhedral and less than 0.1mm across (Fig. 3-6). The second anhydrous silicate inclusion which is represented by clinopyroxene and olivine mostly with irregular shapes and various sizes. Hydrous silicate inclusions in chromian spinel are absent in the ocean-floor peridotite, whereas they are common in some ophiolites that is usually interpreted as primary one based on textural features (Talkington, et al., 1986; and Auge, 1987 in Arai, 1991). This may in turn lead to a conclusion that the chromite with such hydrous silicate inclusion was formed from some hydrous magma (Auge, 1987 in Arai, 1991) or some hydrothermal fluid at high temperatures (Zohan, et al., 1983 in Arai, 1991). The hydrous silicate inclusions in chromian spinel of chromitite rocks in MOC may be a reaction products between anhydrous peridotite and later impregnated hydrous melt.

The hydrous magma or melt may be most easily available in a supra-subduction zone (Arai, 1991). Chromian spinel is also enriched in clinopyroxene inclusions and olivine in dunite envelopes the chromitite rocks (Fig. 3-10). Chlorite (clinochlorite and peninite) is frequent as inclusions and as interstitial silicate matrix in chromitite rocks of MOC.

3.4 Accessory Chromite

Accessory chromites occur as scattered grains in the serpentized dunite and harzburgite of Daraban, Shakha Root and Ser-Shiw valley. Their volume % abundance shows a range between 1 % to 5% in dunite (Table 2-1) and between 0 to 3% in harzburgite (Table 2-3). Accessory chromite occurs as subhedral to anhedral with grain size range between 0.05- 1mm most of them surrounded by opaque rims under transmitted light (Fig. 2-3) and (Fig. 2-7).

Table 3-1 Modal volume % of mineral compositions of chromitite rocks in MOC.

Mineral S.No.	Chrom.	Olivine	Cinopyroxene	Serpentine.	Chlorite.	Amphibole
Massive						
W19	85	0	0	0	15	0
W25	75	0	0	0	25	0
W28	77	0	0	0	20	3
Brecciated						
W22	70	0	0	0	30	0
W24	70	0	0	0	30	0
W27	73	0	0	2	25	0
W30	74	10	2	4	10	0
W31	59	17	0	9	15	0
W32	74	0	0	12	14	0
W33	67	0	0	3	30	0
Dessiminated						
W26	21	79	0	0	0	0
W29	46	50	1	2	0	1



Fig. 3-1 Chromitite pod envelopes with dunite in north of Kuradawi village.



Fig. 3-2 A: Vein type and B: densely disseminated chromite in Ser Shiw valley.

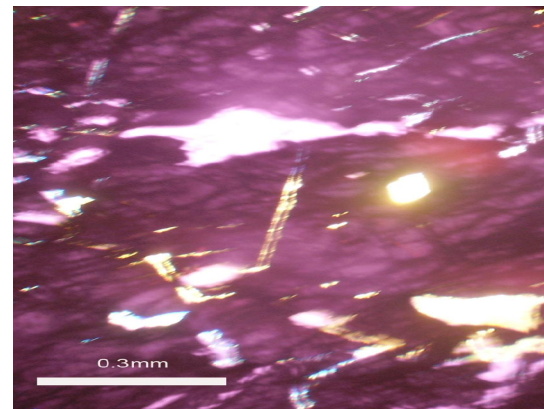
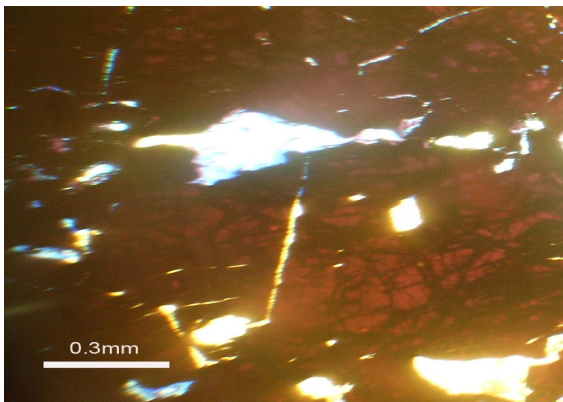


Fig. 3-3 Anhedral crystals of chromite showing pull-a part texture and most of chromite grains exhibit thin rims of ferritchromite, the white interstitial represents the matrix. (A: under PPL. B: under XP).

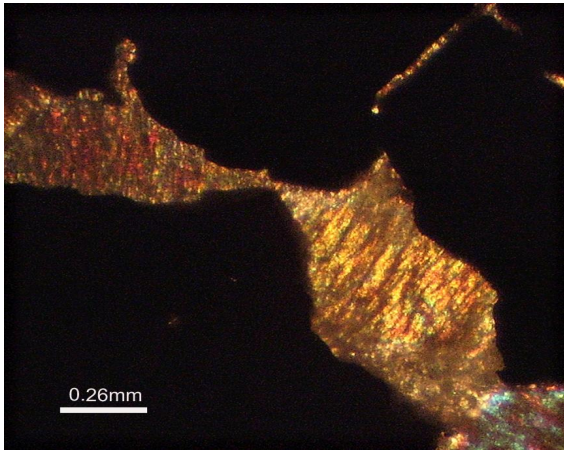


Fig. 3-4 The Amphibole matrix between the chromite grains in massive ore type (under XP)

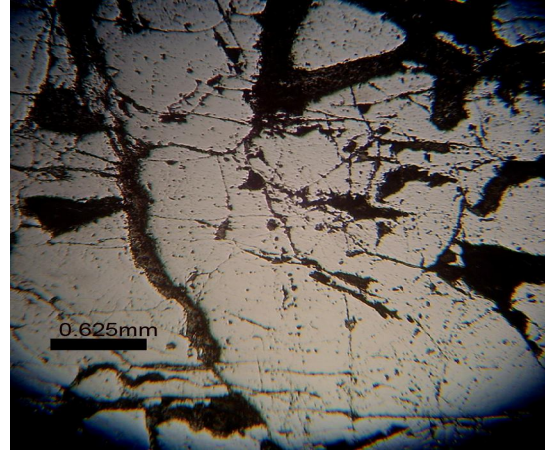
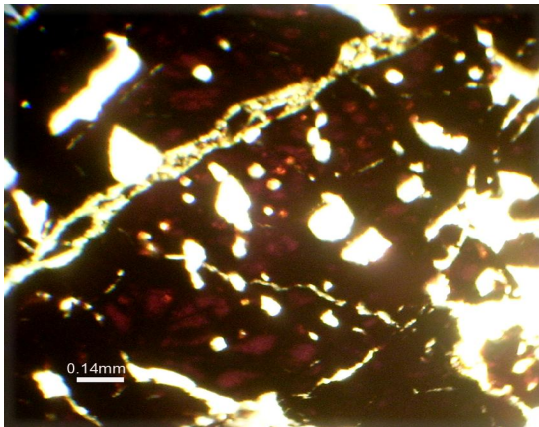


Fig. 3-5 Light grey subhedral chromite crystal in massive chromite ore contains secondary mineral phases (under PPL).

A



B

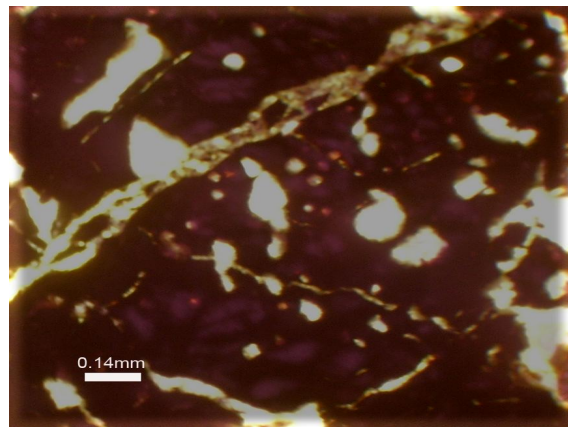
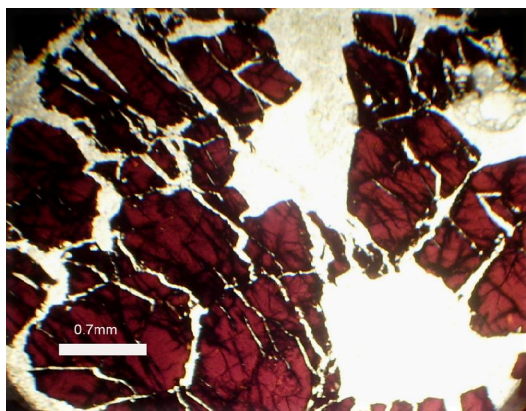


Fig. 3-6 Silicate mineral inclusions in chromite grain (A: under PPL, B, XP, 100X).

A



B

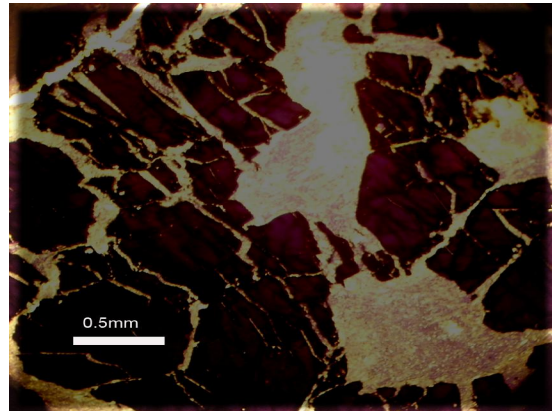


Fig. 3-7 Brecciated chromitite rocks, the chromite grain transected by many cracks. (A: under PPL, B: XP).

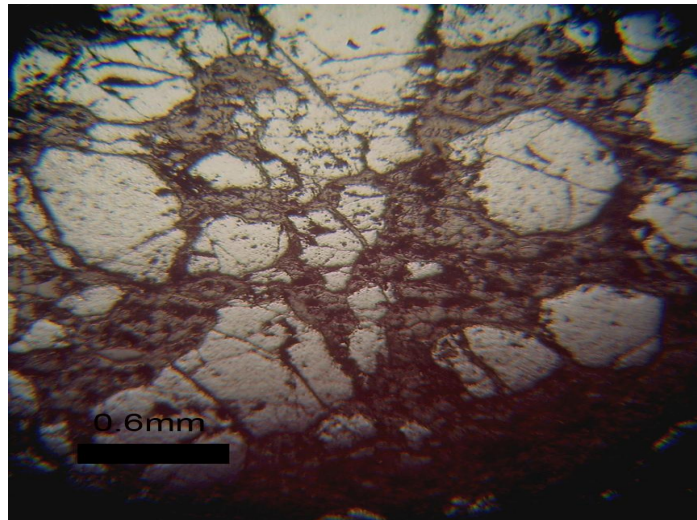


Fig. 3-8 Light grey brecciated chromite grain under reflected light microscope (PPL).

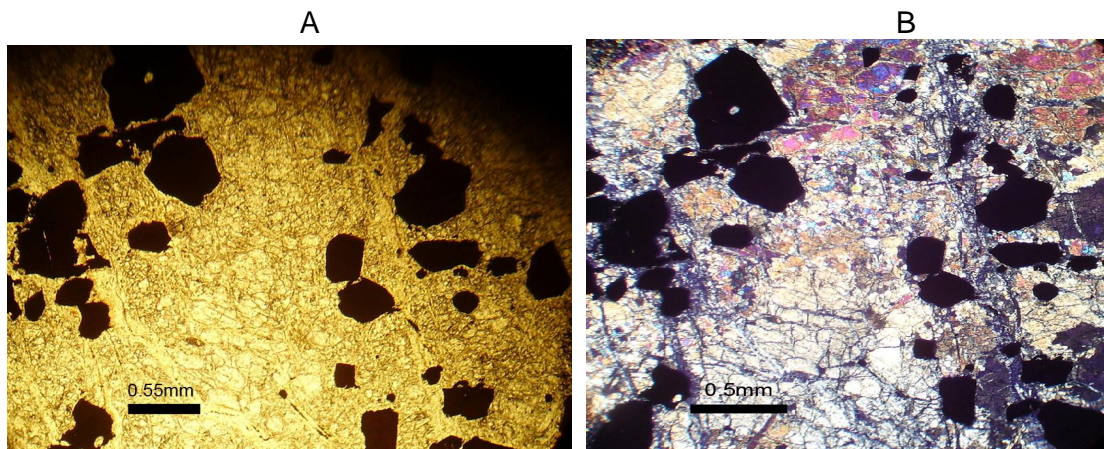


Fig. 3-9 Disseminated subhedral to anhedral chromite crystal in a matrix of olivine in north of Kuradawi village (A: under PPL, B: XP).

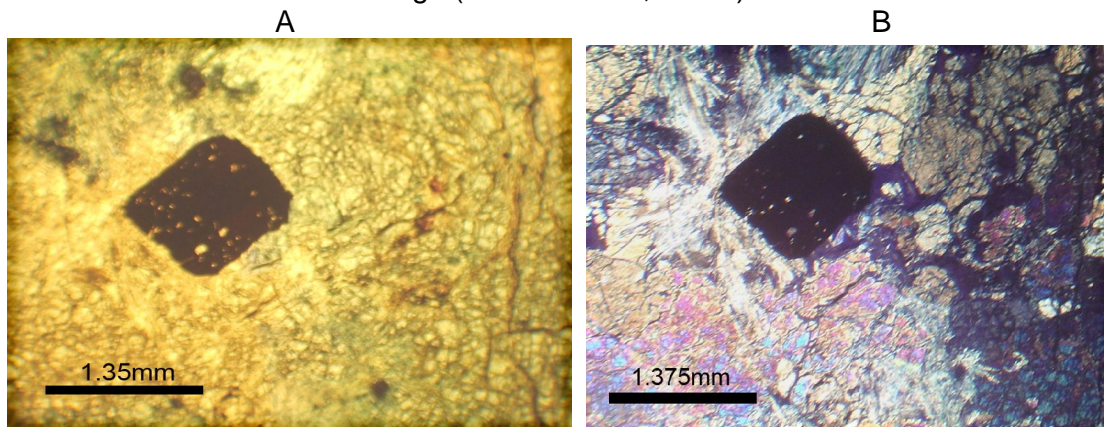


Fig. 3-10 Euhedral chromite crystals in dunite envelopes the chromitite rocks contain inclusion. (A: under PPL, B: XP).

3.5 Mineral chemistry

Selected chromite mineral with matrix and inclusions were analyzed using electron probe micro analysis on different types of the chromitite rocks.

Minerals were analyzed on polished thin sections for major and minor elements with a four tunable wavelength dispersive spectrometry microprobe (CAMECA, COMEBAX). A total of 73 point analyses from 7 thin sections of chromitite rocks were obtained. The results of analyses were listed in (Tables 3-2, 3-3, and 3-4). Mg#, Cr#, and Fe^{+3} # are $Mg / (Mg+Fe^{+2})$, $Cr / (Cr+Al)$ and $Fe^{+3} / (Fe^{+3} +Al+Cr)$ atomic ratios respectively, in analyzed minerals. We assumed all Fe in silicates was ferrous, ferrous and ferric Fe in chromian spinel was calculated from raw analyses assuming spinel stoichiometry.

3.5.1 Spinel composition

Selected microprobe analyses of chromite grains of massive, brecciated and disseminated chromitite rocks are listed in (Table 3-2). There is a little compositional variation from grain to grain and from sample to another sample in the different pod of the same area in the analyzed chromian spinel. Cr_2O_3 content of chromite varies between 49.26 to 54.21 Wt %, 50.17- 54.21 Wt% in massive ore and ranges between 49.57 to 51.98 Wt% in brecciated type while in disseminated type ranges from 50.23 to 53.93 Wt% and classified as aluminum chromite according to (Steven, 1944). The majority of chromitite are uniform Cr# at > 0.7 corresponding to Cr_2O_3 contents ranging between 49.26-54.21 and variety of Mg# from 0.38 to 0.602 (Table 3-2), and displaying negative correlation between the Mg# and Cr# (Fig. 3-11). This relation is possibly the result of the relation proportion of secondary chlorite replacing chromite grain, i.e. difference is related to rim-core analysis. The chromitite in the studied area described as Cr-rich chromite (average Cr# =0.742) and belongs to podiform chromitite of alpine type peridotite (Fig. 2-31). This is in agreement with (Arai, 1992b and Arai & Yurmoto, 1995) who considered the chromitite rocks (Cr# ranges from 0.7 to 0.8) as Cr-rich chromite and belong to podiform chromitite in alpine type peridotite (Fig 3-12). The $Fe^{+3} / (Fe^{+3}+Al+Cr)$

atomic ratios mostly around 0.1 (extremely low corresponding to Fe_2O_3 contents between 5.1 and 7.5 Wt %). The low TiO_2 contents of studied samples (0.1-0.25 Wt %) also indicate its characteristics as podiform chromites (in stratiform chromite TiO_2 content is higher than 0.3 Wt% (Dickey, 1975). This is related to the nature of primary magma which has been generated from depleted source. Ti is strongly partitioned into liquid during partial melting of the upper mantle (Herber, 1982 in Zhou and Ji Bai, 1992). This study indicates that high-Cr chromitites are more depleted in Ti (0.1-0.25 Wt % TiO_2). The low Ti-group spinels have a depleted upper mantle derivation. They are very similar in compositions to spinel in most common ophiolitic peridotites (Dick and Bullen, 1984, Arai 1992b). The plots of TiO_2 vs. Cr_2O_3 (Fig. 3-13) indicate that all samples located in the field are of podiform chromitite.

Nickel content (0.08-0.17 Wt %) of chromitites from the various deposits in ophiolites are similar to those of chromitites in typical podiform chromite deposits (Ahmed, 1984) and to those in Mawat type deposits (0.006-0.099Wt %). The chromitite rocks of the studied area are uniform in spinel chemistry; it is clearly low and uniform in Al_2O_3 and higher Cr_2O_3 , and plots in the field of podiform chromitite (Fig. 3-11), which shows strong negative correlation between Al_2O_3 vs. Cr_2O_3 and this is due to alteration. The uniform Al_2O_3 contents of chromitite from MOC, indicate that the primary magmas from which chromitites crystallized were homogeneous and chromitite were in equilibrium with them. Al_2O_3 abundance depends on melt composition which is a function of pressure, temperature and degree of partial melting (Kamentestky et al., 2001). The chrome spinel is generally very low in Fe^{+3} ratio, all the analyses being located adjacent to the Cr-Al join reflecting the slightly alteration character (Fig. 3-14). The relationship between Al_2O_3 - Cr_2O_3 - Fe_2O_3 (Fig. 3-15) indicates all samples plots in the field of aluminum chromite.

The Mawat chromitite samples have a high Cr# > 0.7 (Table 3-3), which might have crystallized from Cr-rich melt formed by early separation from initial liquid after higher degree of partial melting. Indeed the high Al-rich chromite (Cr# < 0.6), might have formed initial liquid after lower degree of partial melting.

Therefore the high Al-ore forming chromite is richer in Ti than high Cr-chromite (Arai, 1997). Chromites from different tectonic environments have distinctive Cr#, which reflect differences in magma composition (Arai, 1992 and Arai & Yurimoto, 1995). The chromite from Mawat has Cr# > 0.7 and average Cr# = 0.742 (Table 3-2) which are higher than those of MORB (0.2 to 0.54; Allen et al., 1988), lower than those of boninites (0.8 to 0.9; Roeder and Reynolds, 1991) and it is close to ophiolitic podiform chromitite Cr# ranges between 0.6-0.8 (usually 0.7-0.8) (Arai, 1997). The Cr# vs. TiO₂ of the Mawat chromitite composition plots outside the fields defined by boninites and mid-ocean ridge basalt (MORB) (Fig. 3-16). Instead, the compositions fall between these fields and within the compositional range defined by Cr-rich chromite.

The chromian spinel in chromitite rocks from MOC have slightly considerable amount of MnO (Table 3-3). Manganese enrichment in chrome spinel is usually associated with alteration or metasomatism (Ahmad et al., 2001), the studied samples are slightly enriched in MnO which indicate its alteration.

In general we can summarize the crystal chemistry of chromite minerals (based on 4 oxygen number) as $(\text{Fe}^{+2}_{0.49} \text{Mg}_{0.46}) (\text{Cr}_{1.387} \text{Al}_{0.527} \text{Fe}^{+3}_{0.16})_2 \text{O}_4$.

Table 3-3 Microprobe analysis of matrix minerals from chromitite rocks of Mawat Ophiolite Complex. [Mg#: Mg/(Mg+Fe²⁺), Fe²⁺#: Fe²⁺ / (Fe²⁺ +Mg) atomic ratio].

Samples	W19 Chl.	W19 Chl.	W25 Chl.	W29 Chl.	W29 Chl.	W33 Chl.	W33Chl.	W33 Chl.	W33Chl.	W36 Chl.	W28Amph.	W30 Amph.	W26 Ol	W26 Ol	W26 Ol	W29 Ol	W29 Ol	W30 Ol
SiO ₂	36.223	36.101	37.933	36.577	37.963	36.732	38.017	36.451	36.985	38.689	57.797	57.865	41.165	41.140	40.564	40.414	40.430	41.046
Al ₂ O ₃	21.119	20.928	18.526	19.295	16.319	18.526	17.887	19.254	19.569	15.890	0.340	0.767	0.005	0.005	0.024	0.003	0.019	0.011
TiO ₂	0.056	0.037	0.048	0.034	0.018	0.008	0.025	0.039	0.061	0.002	0.054	0.050	0.016	0.008	0.002	0.001	0.010	0.005
FeO	2.244	2.217	1.184	2.864	2.826	2.449	2.023	2.620	2.651	3.456	1.015	0.849	6.937	6.646	6.725	8.522	8.659	4.676
MnO	0.012	0.022	0.015	0.038	0.010	0.016	0.007	0.009	0.009	0.026	0.021	0.009	0.126	0.106	0.124	0.058	0.018	0.111
MgO	37.342	37.541	39.040	38.026	38.796	38.609	38.842	38.268	38.100	38.289	24.449	23.910	51.373	51.732	51.246	50.642	50.570	53.096
CaO	0.020	0.016	0.019	0.016	0.027	0.020	0.024	0.007	0.026	0.009	13.592	13.480	0.006	0.004	0.009	0.001	0.002	0.006
Na ₂ O	0.010	0.060	0.025	0.049	0.043	0.030	0.003	0.052	0.007	0.026	0.064	0.154	0.025	0.012	0.025	0.015	0.001	0.012
K ₂ O	0.081	0.047	0.020	0.021	0.002	0.029	0.032	0.047	0.039	0.016	0.001	0.028	0.001	0.006	0.004	0.001	0.020	0.008
NiO	0.232	0.224	0.362	0.220	0.216	0.182	0.181	0.210	0.168	0.160	0.102	0.121	0.339	0.338	0.310	0.328	0.339	0.486
Cr ₂ O ₃	2.661	2.805	2.828	2.861	3.779	3.430	2.961	3.043	2.401	3.437	0.140	0.282	0.008	0.004	0.034	0.014	0.013	0.141
Prob. Sum	100.000	100.000	100.000	100.000	100.000	100.032	100.000	100.000	100.018	100.000	97.574	97.495	100.000	100.000	99.005	100.000	100.081	99.598
O=	28.000	28.000	28.000	28.000	28.000	28.000	28.000	28.000	28.000	28.000	23.000	23.000	0.994	4.000	4.000	4.000	4.000	4.000
Si	5.864	5.846	6.110	5.943	6.157	5.952	6.141	5.917	5.998	6.284	7.891	7.896	0.000	0.992	0.992	0.984	0.984	0.990
Al	4.018	3.983	3.507	3.685	3.111	3.528	3.396	3.673	3.730	3.034	0.055	0.123	0.000	0.000	0.001	0.000	0.001	0.000
Ti	0.007	0.005	0.006	0.004	0.002	0.001	0.003	0.005	0.007	0.000	0.006	0.005	0.000	0.000	0.000	0.000	0.000	0.000
Cr	0.404	0.426	0.427	0.436	0.575	0.521	0.448	0.463	0.365	0.523	0.015	0.030	0.000	0.000	0.001	0.000	0.000	0.003
Fe	0.303	0.299	0.159	0.388	0.382	0.331	0.272	0.354	0.358	0.468	0.116	0.097	0.140	0.134	0.138	0.173	0.176	0.094
Mn	0.002	0.003	0.002	0.005	0.001	0.002	0.001	0.001	0.001	0.004	0.002	0.001	0.003	0.002	0.003	0.001	0.000	0.002
Mg	9.068	9.119	9.432	9.268	9.438	9.385	9.412	9.318	9.268	9.329	4.976	4.864	1.861	1.872	1.868	1.850	1.847	1.909
Ca	0.003	0.003	0.003	0.003	0.005	0.003	0.004	0.001	0.005	0.002	1.988	1.971	0.000	0.000	0.000	0.000	0.000	0.000
Na	0.003	0.019	0.008	0.015	0.014	0.009	0.001	0.016	0.002	0.008	0.017	0.041	0.001	0.001	0.001	0.001	0.000	0.001
K	0.017	0.010	0.004	0.004	0.000	0.006	0.007	0.010	0.008	0.003	0.000	0.005	0.000	0.000	0.000	0.000	0.001	0.000
Ni	0.030	0.029	0.047	0.029	0.028	0.024	0.023	0.027	0.022	0.021	0.011	0.013	0.007	0.007	0.006	0.006	0.007	0.009
Mg#	0.968	0.968	0.983	0.960	0.961	0.966	0.972	0.963	0.963	0.952	0.977	0.980	0.930	0.933	1.000	0.915	0.913	0.953
Fe ²⁺ #	0.032	0.032	0.017	0.040	0.039	0.034	0.028	0.037	0.037	0.048	0.023	0.020	0.070	0.067	0.000	0.085	0.087	0.047

Chl: chlorite, Amph: amphibole, Ol: olivine.

Table 3-4 Microprobe analysis of mineral inclusions in chromitite rocks of Mawat Ophiolite Complex. [Mg#: Mg / (Mg+Fe²⁺), Fe²⁺#: Fe²⁺ / (Fe²⁺+Mg) atomic ratio.

Samples	W19Chl.	W26 Ser	W28 Ser										
SiO ₂	36.460	37.243	36.599	35.981	37.283	36.362	37.776	37.635	39.638	36.875	38.397	50.634	55.200
Al ₂ O ₃	20.256	18.256	19.149	17.774	19.899	20.066	18.131	17.246	15.199	18.399	17.781	0.116	0.924
TiO ₂	0.042	0.039	0.050	0.027	0.050	0.041	0.034	0.039	0.032	0.033	0.032	0.011	0.023
FeO	2.403	2.405	2.117	1.338	1.546	1.487	1.341	1.743	1.513	3.247	2.075	2.653	4.938
MnO	0.006	0.041	0.015	0.004	0.023	0.013	0.003	0.020	0.070	0.117	0.030	0.076	0.038
MgO	37.993	37.964	37.739	37.672	39.160	37.284	38.736	38.713	40.292	37.557	37.925	45.641	35.727
CaO	0.002	0.001	0.008	0.017	0.025	0.031	0.020	0.087	0.011	0.063	0.071	0.045	0.477
Na ₂ O	0.005	0.003	0.031	0.029	0.059	0.026	0.050	0.111	0.029	0.059	0.009	0.063	0.041
K ₂ O	0.025	0.020	0.006	0.015	0.034	0.019	0.005	0.052	0.028	0.031	0.087	0.027	0.022
NiO	0.241	0.220	0.241	0.347	0.358	0.349	0.332	0.277	0.280	0.233	0.208	0.323	0.982
Cr ₂ O ₃	2.571	3.814	4.063	6.797	1.562	4.374	3.572	4.078	3.069	3.619	3.445	0.411	1.628
Prob. Sum	100.003	100.007	100.017	100.000	100.000	100.052	100.000	100.000	100.161	100.233	100.060	100.000	100.000
O=	28.000	28.000	28.000	28.000	28.000	28.000	28.000	28.000	28.000	28.000	28.000	14.000	14.000
Si	5.909	6.025	5.913	5.788	6.030	5.854	6.084	6.077	6.381	5.985	6.192	2.044	2.218
Al	3.858	3.471	3.636	3.360	3.782	3.797	3.432	3.273	2.875	3.510	3.370	0.006	0.044
Ti	0.005	0.005	0.006	0.003	0.006	0.005	0.004	0.005	0.004	0.004	0.004	0.000	0.001
Cr	0.391	0.578	0.615	1.025	0.237	0.660	0.539	0.617	0.463	0.551	0.521	0.016	0.061
Fe	0.325	0.324	0.285	0.179	0.208	0.200	0.180	0.235	0.203	0.439	0.279	0.089	0.165
Mn	0.001	0.006	0.002	0.001	0.003	0.002	0.000	0.003	0.009	0.016	0.004	0.003	0.001
Mg	9.236	9.212	9.146	9.089	9.500	9.004	9.358	9.377	9.729	9.143	9.174	2.764	2.153
Ca	0.000	0.000	0.001	0.003	0.004	0.005	0.004	0.015	0.002	0.011	0.012	0.002	0.021
Na	0.002	0.001	0.010	0.009	0.018	0.008	0.016	0.035	0.009	0.019	0.003	0.005	0.003
K	0.005	0.004	0.001	0.003	0.007	0.004	0.001	0.011	0.006	0.006	0.018	0.001	0.001
Ni	0.031	0.029	0.031	0.045	0.047	0.045	0.043	0.036	0.036	0.030	0.027	0.010	0.032
Mg#	0.966	0.966	0.970	0.981	0.979	0.978	0.981	0.976	0.976	0.954	0.971	0.969	0.929
Fe ²⁺ #	0.034	0.034	0.030	0.019	0.021	0.022	0.019	0.024	0.024	0.046	0.029	0.031	0.071

Chl: chlorite, Ser. Serpentine.

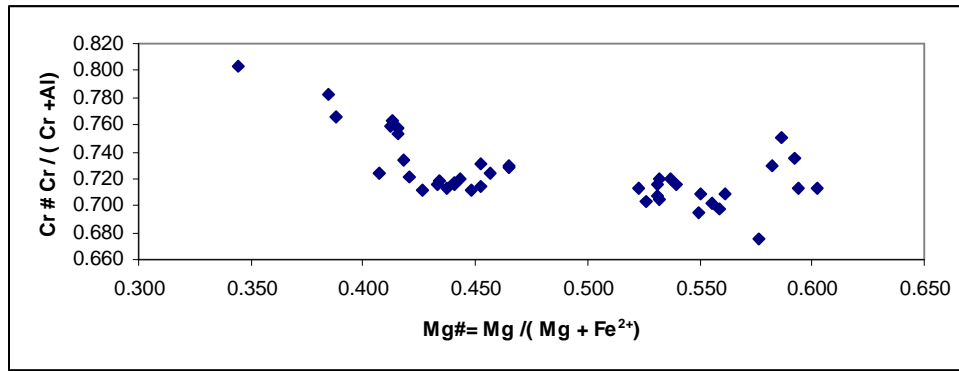


Fig. 3-11 The relationship between Mg# vs. Cr# in chromian spinel of chromitite rocks in MOC.

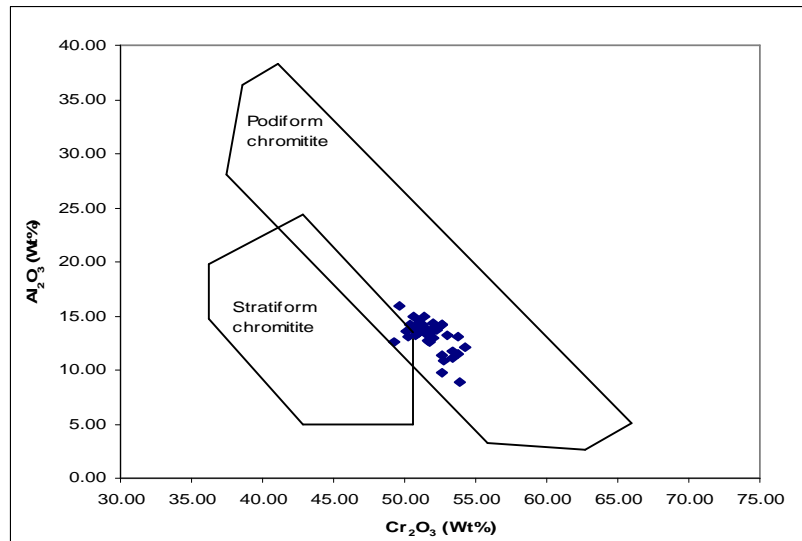


Fig. 3-12 Variation of Cr₂O₃ vs. Al₂O₃ of chrome spinel in the Mawat podiform chromitite. Compositional field of podiform & stratiform chromitite (Bonavia et al., 1993).

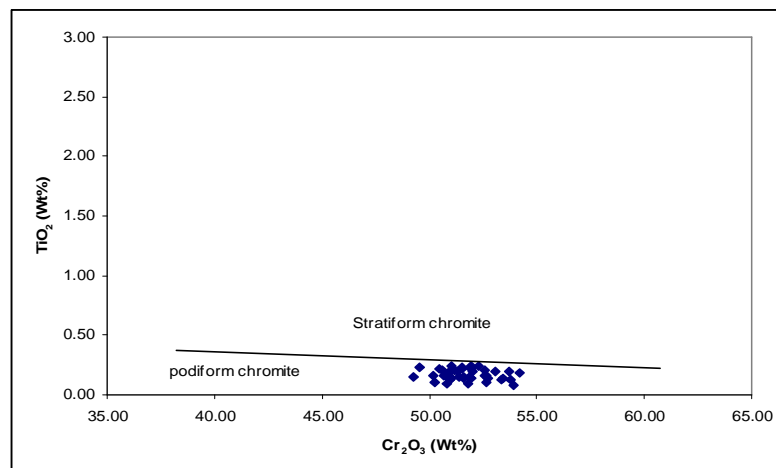


Fig. 3-13 Variation of TiO₂ Wt % vs. Cr₂O₃ of chromitite from MOC the boundary between stratiform and podiform (Bonavia et al. 1993).

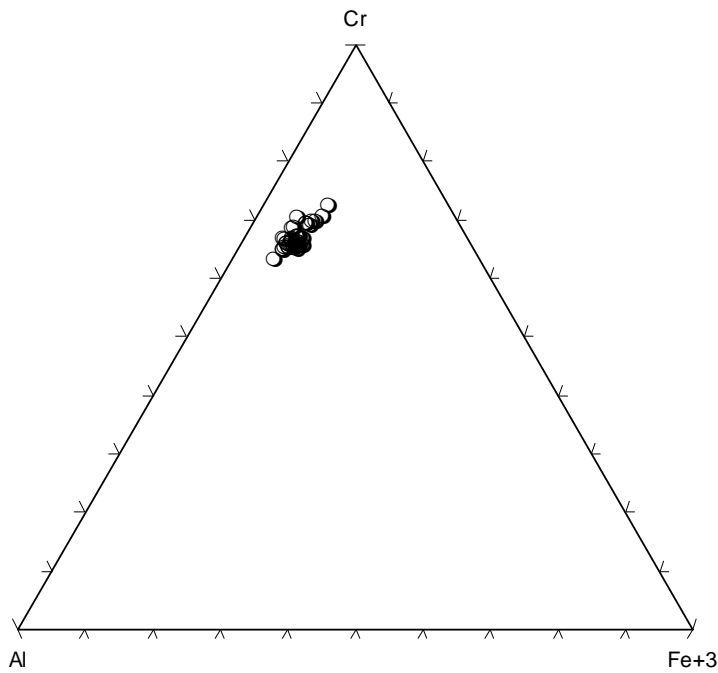


Fig. 3-14 Cr-Al-Fe⁺³ atomic ratio of chromian spinel in chromitite rocks of MOC.

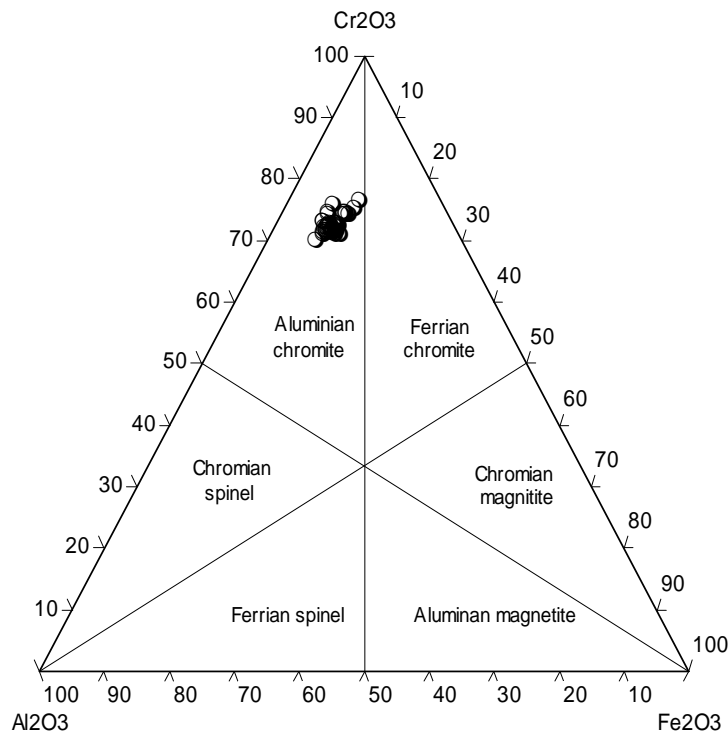


Fig. 3-15 Cr₂O₃-Al₂O₃-Fe₂O₃ diagram for podiform chromitite rocks in MOC. (Steven, 1944)

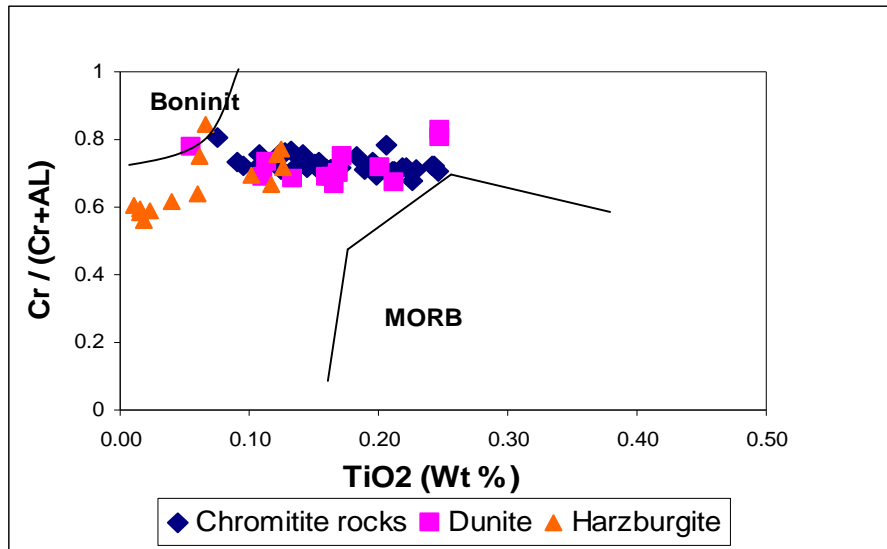


Fig. 3-16 Cr # versus TiO₂ content for chromite in MOC chromitite and their hosting dunite and harzburgite. Boninitic and MORB fields were defined by Arai (1992).

3.5.2 Chemistry of matrix

Olivine, amphibole, chlorite and serpentine are found as a matrix of chromitite rocks of MOC which fill the cracks and spaces between chromite grains. The matrix of massive chromitite are amphibole, chlorite and serpentine, the matrix of brecciated chromitite represented by chlorite, amphibole and olivine; while in the case of disseminated type the matrix is olivine. Buda and Al-Hashimi (1977) described the matrix of massive ore as probably being clinopyroxene (diopside) and the matrix of brecciated ore as serpentine and chlorite.

The present study based on microprobe analyses of the matrix in massive, and brecciated ore reveals that they are mainly chlorite and amphibole, the chemistry of chlorite and amphibole are shown in (Table 3-3). According to Leak et al. (1997) amphiboles of MOC are classified as tremolite (Fig. 2-29).

The average chemical formula of amphiboles in chromitite rocks can be summarized as $\text{Ca}_{1.97} \text{Mg}_{4.92} \text{Si}_{7.9} \text{O}_{22} (\text{OH})_2$ with uniform Mg # ranges between 0.977 - 0.98. The TiO₂ content is less than 0.06 Wt %. The origin of tremolite matrix may be related to clinopyroxene which apparently became altered to tremolite due to tectonic activities (Buda and Al-Hashimi, 1977).

Chlorite from the matrix of massive and brecciated chromitites shows SiO_2 contents between 36.101-38.68 Wt % and low FeO content (< 3.5 Wt %). The $\text{Fe}\# = (\text{Fe}/\text{Fe}+\text{Mg})$ atomic ratio is normally below 0.049. According to Hey, (1954) the chlorite of analyzed samples are classified as pennite and clinochlor (Fig. 3-17 a, b). In this case however the clinochlore and penninite are moderately Cr-rich (chromian clinochlore -chromian penninite) and contain up to 3.0 Wt% Cr_2O_3 (Table 3-3) (Fig.3-17c). The olivine is characterized by rich Fo. ₉₅₋₉₃. Content and the Fe # is normally around zero (Table 3-3).

3.5.3 Chemistry of inclusions

Two groups of silicate inclusions in chromitite rocks of MOC are distinguished which are chlorite and serpentine (Table 3-4). From the results of PGE (Table 3-5) analyses one can conclude the presence of platinum mineral inclusion. In this study the platinum minerals inclusion could not be distinguished due to unclear image of scanning electron microscope and very small size of this type of inclusion.

The chlorite is frequent as inclusions in massive and disseminated chromitite rocks and is similar to the chlorite matrix and according to the classification of (Hey, 1954) represents clinochlore and penninite (Fig. 3-17). The chlorite inclusion did not show any significant differences in chemistry with that of chlorite matrix (Table 3-4). The SiO_2 content range between 35.98 - 39.63 Wt % and MgO ranges from 37.28 to 40.29 Wt %. Their Cr_2O_3 is (1.56 - 6.79 Wt %) and it is somewhat richer in Cr_2O_3 than chlorite matrix. The Cr_2O_3 content of chlorite may be supplied from expulsion of Cr_2O_3 from chromite grain during alteration and metamorphism (Al-Chalabi, 2004). Serpentine is frequent as inclusion in massive and disseminated chromitite rocks. The serpentine inclusions contain elevated MgO ranges between 35.72- 45.64 Wt % the Mg# values are 0.92-0.96 (Table 3-4). The plots of SiO_2 - Al_2O_3 -MgO triangle by (Wickes and Plant, 1979 in Muhammad, 2004) reveal that the serpentine are lizardite and chrysotile in all types of chromitite rocks (Fig. 3-18).

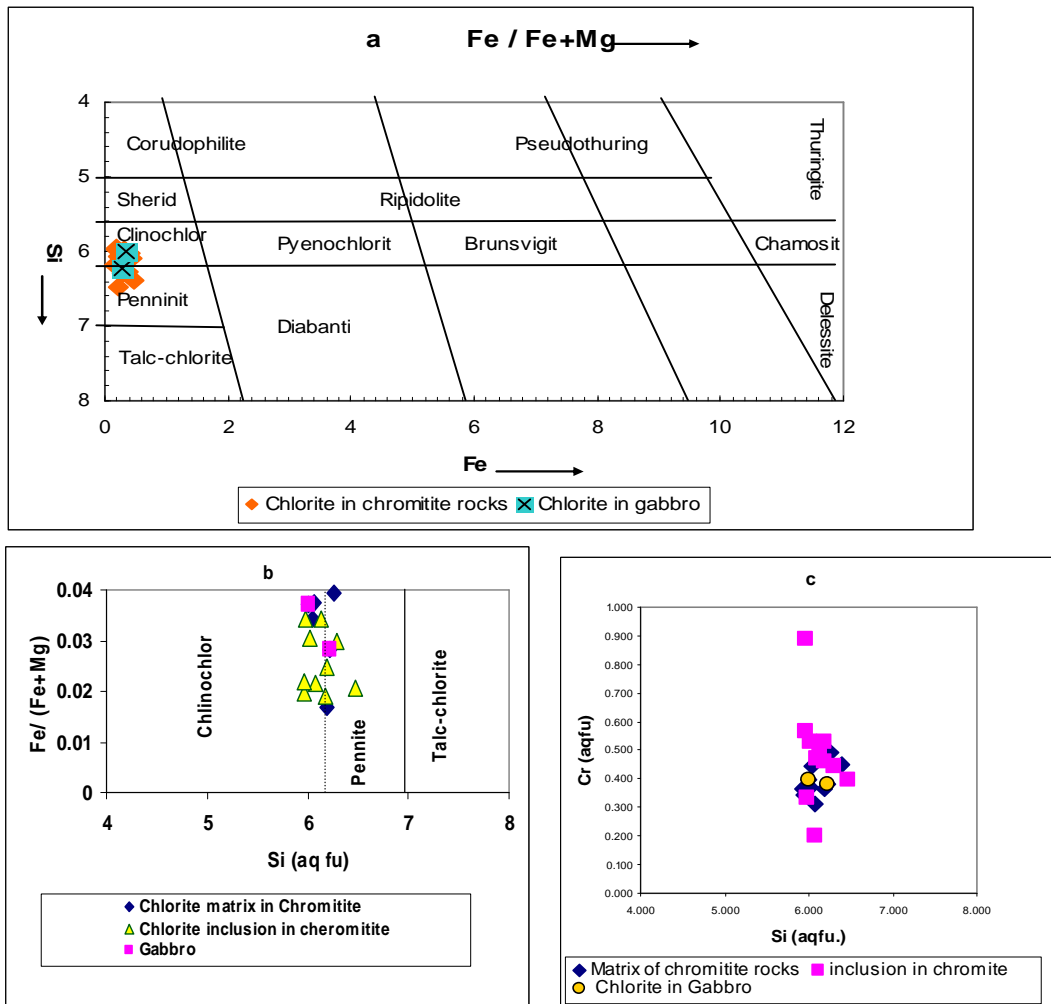


Fig. 3-17 Chemical composition of matrix and inclusion of chlorite in MOC chromitite and Gabbro rocks, (a: Fe vs. Si; b: Si vs. Fe/Fe+Mg c; Si vs. Cr.), (Hey 1954).

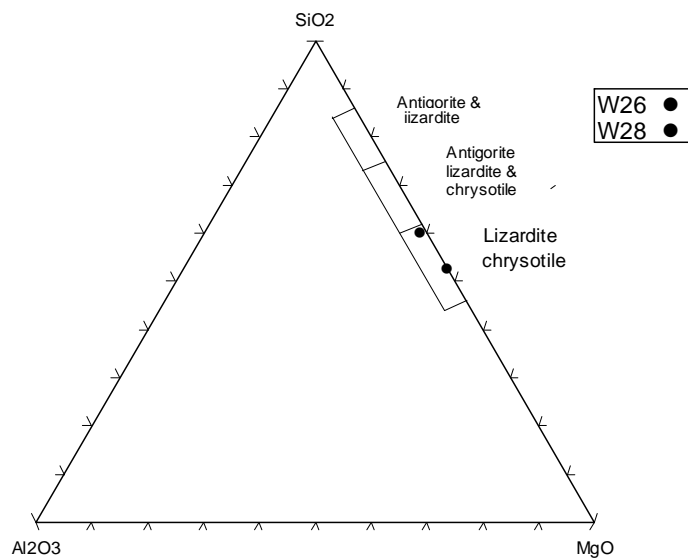


Fig. 3-18 SiO₂ - Al₂O₃ - MgO triangle, shows the field of serpentine mineral group of analyzed samples (Wickes and Plant, 1979 in Muhammad, 2004).

3.6 Chromite alteration

Chemical modification of chromian spinel through alteration or metamorphism is related to the alteration of silicate minerals (Barnes, 2000).

The high Cr#, low Fe⁺³ # spinel can be achieved by subtraction of substantial amount of Al without addition of appreciable amount of Fe (Barnes, 2000). These processes applied to chromitite where the silicate matrix is very low in Fe (Arai, 1980). Detailed compositional profiles were obtained by electron probe microanalyses (EPMA), in chromite grain from different types of chromitite grain in the studied area. The profiles are from core to the rim many points on chromite grains were analyzed between cores to rim.

The chromite grains in massive and disseminated chromitite display enrichment of Cr₂O₃, FeO, SiO₂ and depletion in MgO, Al₂O₃ (Figs. 3-19 and 3-20) from core to rim. The alteration of chromite grains in massive and disseminated types can be described by alteration to ferritchromite or (ferrian chromite) in chromitite which is characterized by progressive enrichment in Cr, total iron content (Fe⁺² and Fe⁺³) and depletion in Al and Mg (Figs. 3-19 and 3-20) and (Table 3-2). Chromites tend to lose Al during alteration and react with silicate to form chlorite and the easiest element to be diffused via alteration is Mg and Al which will form chlorite in cracks of chromian spinel. The decrease of Al and Mg will result in apparent increase in Cr and Fe because in the chromian spinel there are five elements: two divalent (Fe⁺² and Mg) and three trivalent cations (Cr, Al, Fe⁺³). In the massive chromitite, the diffusion of element between chromite and olivine is very limited because olivine is very much lack in massive chromite, so Al and Mg of chromite will contribute to the formation of chlorite resulting in apparent increase in Cr and Fe. While in the disseminated chromite, exchange ions between chromite and widely abundant olivine is high; so the expected alteration trend of chromian spinel is increasing the ferric iron, decreasing Mg and Al. The increase of Cr, total iron content and depletion of Mg and Al in altered chromite grain has been interpreted by many researchers like (Qasimjan et al., 1985, Ulmer, 1974, Kimball, 1990, Angeli and Vlach, 2004, and Arai, et al., 2006) and most of the interpretations related

such a trend of alteration in chromite grain to the diffusion of Al and Mg out of chromite grain during metamorphism and / or hydrothermal event which re-equilibrate chromite composition.

The origin of ferritchromite is related to metamorphic and/or hydrothermal processes (Kimball, 1990, Mellini, et al., 2005 and Anna, M., et al., 2007)). According to (Bliss and Maclean 1975 in Proenza et al., 2004) ferritchromite represents a product of prograde metamorphic reaction between Cr-spinel core and magnetite rim. Similarly (Abzalov, 1998) demonstrated, (in the Kola Peninsula, Russia) intrusions that the alteration induced by prograde metamorphism has a major control on the composition of Cr-spinel in the amphibolite metamorphic facies. Evans and Frost (1975) likewise concluded that the Cr content of spinels increase with increasing grade of metamorphism in the amphibolites facies. On the other hand, (Roder, 1994) showed ferritchromite to be the product of reaction between Cr-spinel and chlorite from the host rocks. Hence, the origin of ferritchromite remains an unsolved problem.

The chemical compositions of all analyzed spinels from MOC chromitites plotted on the triangular Fe^{+3} -Al-Cr diagram in (Fig. 3-14), together with the spinel compositional fields from different metamorphic facies where compositional changes in spinel have been recorded with increasing metamorphic grade (Evan and Frost, 1975, Frost, 1991, Suita and Streider 1996, and Barner and Roder, 2001). The chrome spinel of MOC in chromitites show slight alteration characterized by low Al contents with the resulting spinel (ferritchromite) plotting along the Cr-Al join in the field of greenschist-facies (Fig. 3-21). On the other hand, the compositions of Cr-spinel of accessory chromite are plots in the field of upper and lower amphibolite facies (Fig. 2-37).

The profile of chromite grain in the brecciated chromitite is characterized by enrichment in Mg and Al with depletion in Cr and total iron content from core to rim (Fig. 3-22). The common general trend of altered chromite grain from core to rim is an increase in Cr; total iron content and decrease Al and Mg in brecciated chromitite is in contrast with general trend. There are only two

possibilities for interpretation of this uncommon trend which are: first, due to the lack of point analyses, only one profile was obtained, and the second is the possibility that the point analyses in the rim are too close to the chlorite matrix. This will cause the Mg and Al contents to increase, while Cr and Fe will apparently decrease due to increasing Al and Mg, therefore the researcher is better to do the microprobe analyses personally to avoid such confusion.

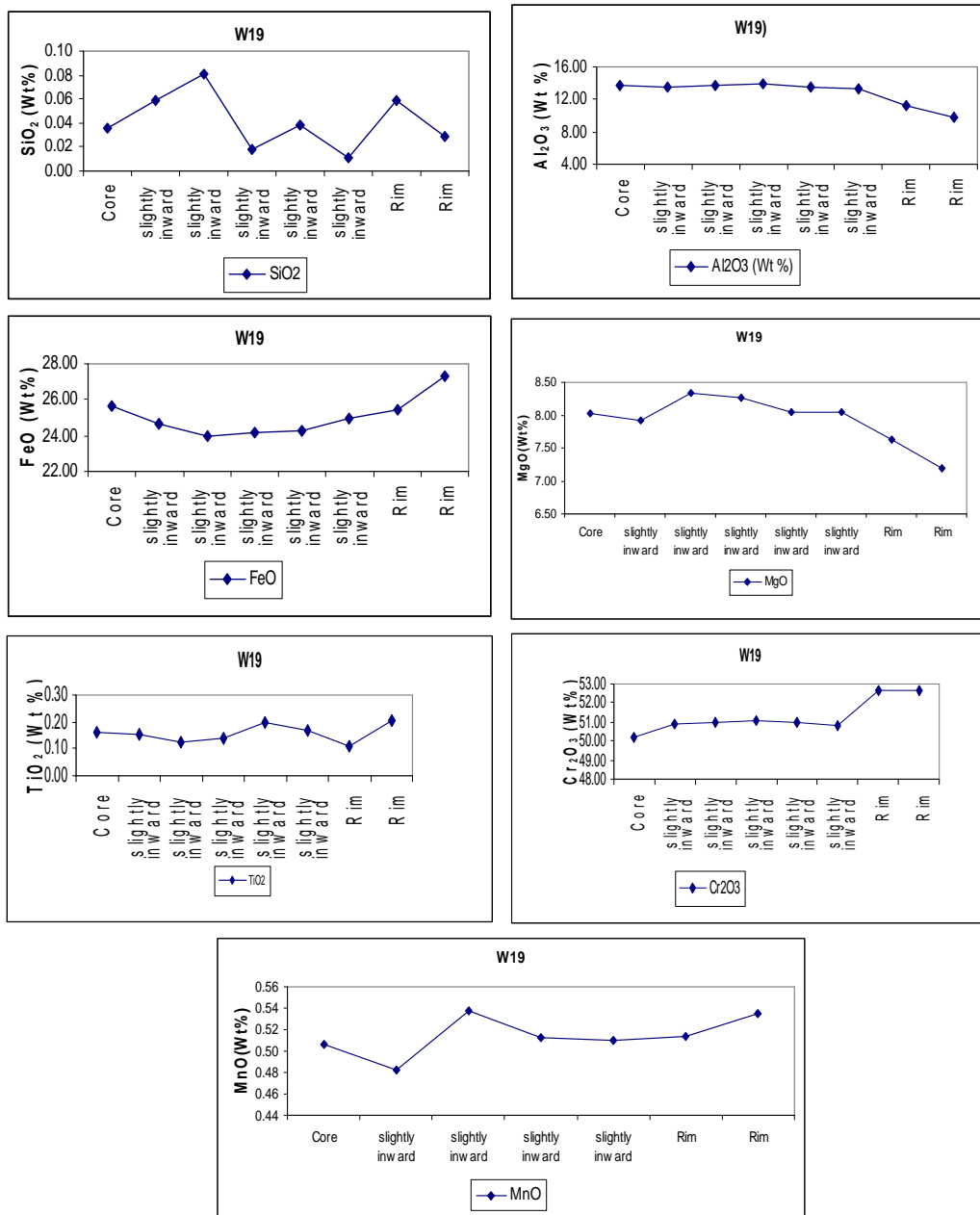


Fig. 3-19 Variation of major oxide from core to rim across grain in massive chromitite rocks (Sample W19).

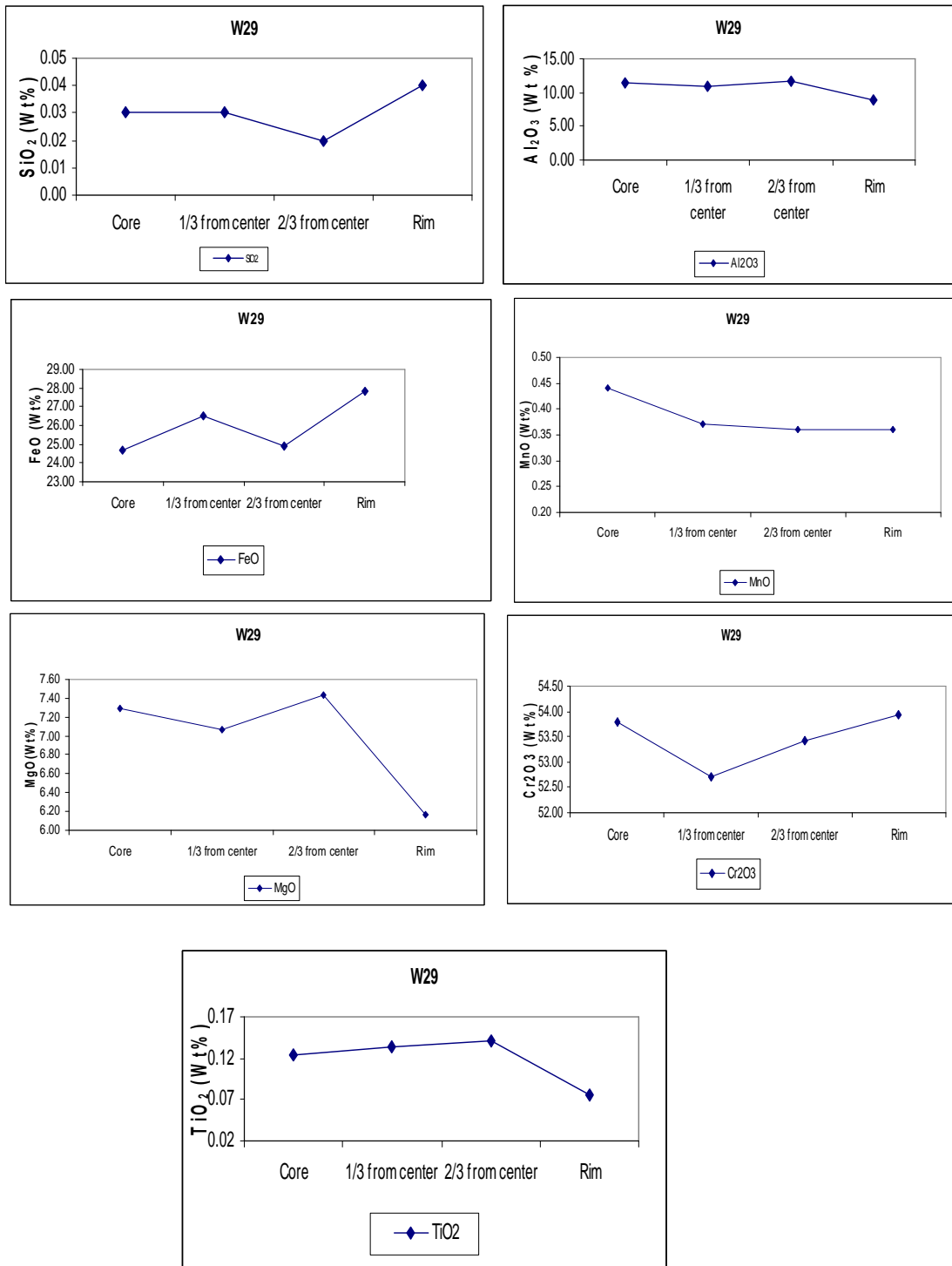


Fig. 3-20 Variation of major oxide from core to rim across grain in disseminated chromitite rocks (sample W29).

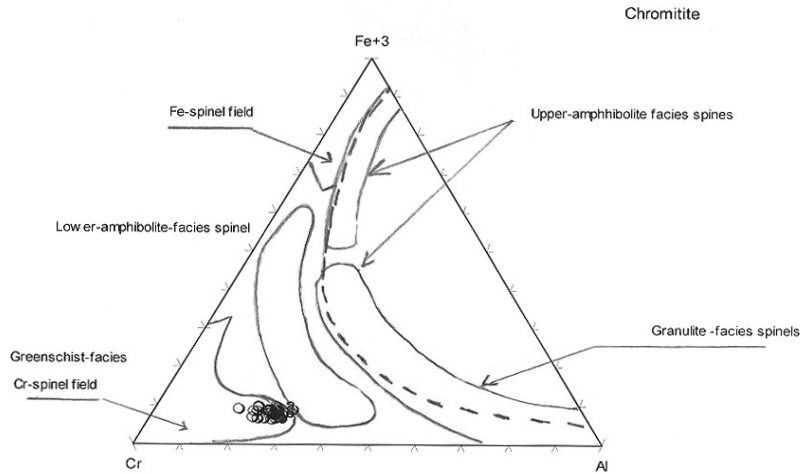


Fig. 3-21 The plots of Fe³⁺-Cr-Al of chromitite samples and fields for different metamorphic C-spinel phases after (Purvis et al., 1972, Evans & Frost, 1975; Suita and Strider, 1996)

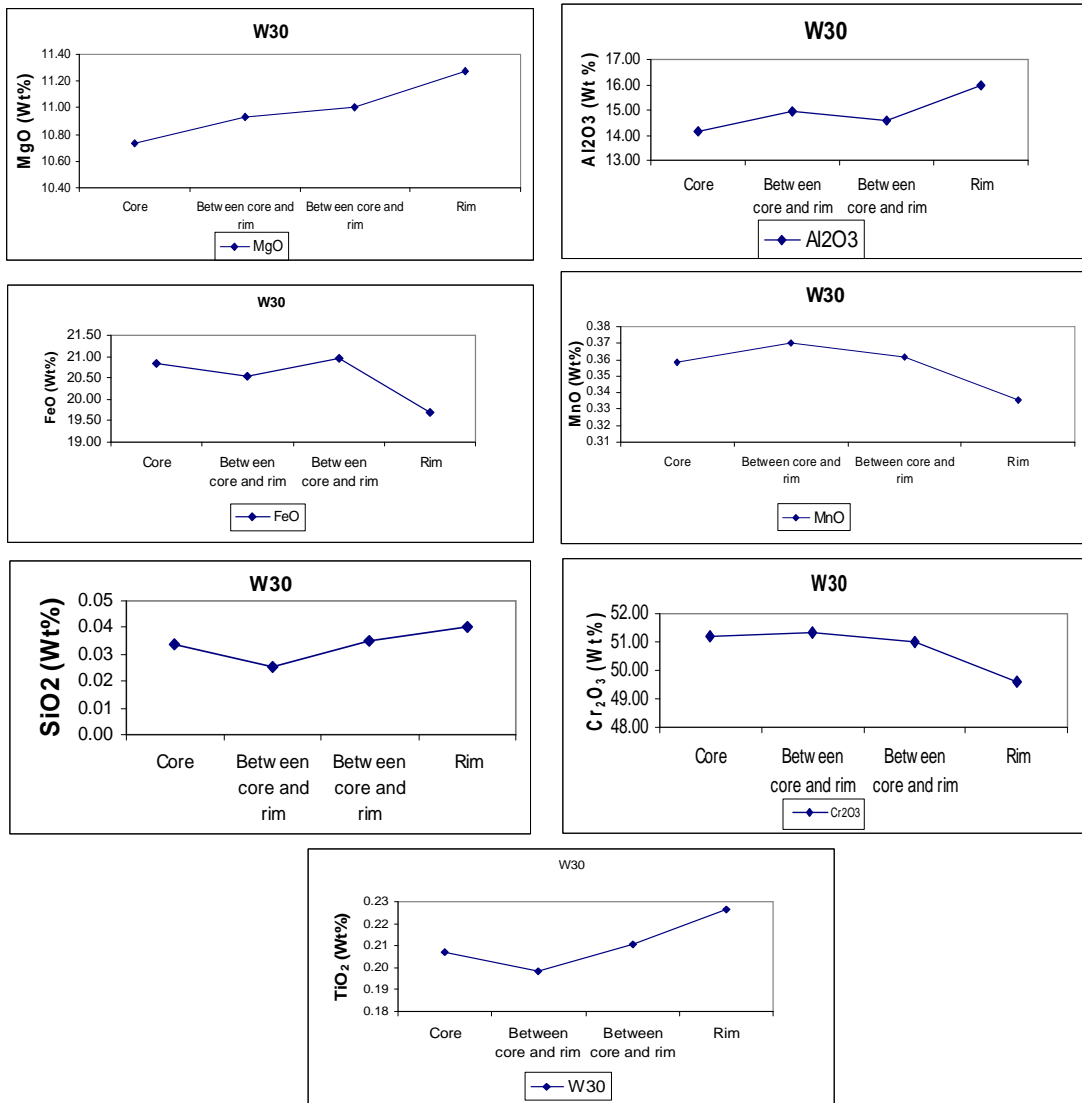


Fig.3-22 Variation of major oxide from core to rim across grain in brecciated chromitite rocks (Sample W30)

3.7 Platinum group elements in chromitite rocks of MOC

Platinum group elements (PGEs) represent a coherent group of siderophile elements. They include poorly soluble elements (Ir, Os, and Ru) and more soluble elements (Rh, Pt, and Pd) in basaltic melts (Amosse et al., 1990). Due to their siderophile nature, PGEs have been concentrated mainly in the earth's core and mantle during the early stages of planet's history (Jagoutz et al., 1979, Arculus and Delano, 1981, and O'Neill, 1991). The PGEs concentrations within ophiolitic chromitite are now well known (Legendre, 1982 and Ahmed et al., 2002) and PGE are considered as one of targets for mining exploration in ophiolites (Leblance, 1991). The PGE abundance is systematic, gives us information about the petrological nature and evolution of mantle source from which they were derived and to lesser extent can reflect the post magmatic events that have affected their host rocks.

The Mawat Ophiolite Complex (MOC) is one of the well exposed fragments of oceanic lithosphere in NE Iraq. It contains significant number of podiform – type chromitite bodies. The chromitite concentrations are mainly located in the central parts of the Ser-Shiw valley, 2km north of Kuradawi village as small lens and irregular bodies within slightly serpentinized dunite and harzburgite.

There are no studies dealing with PGE in chromitite rocks in IZTZ except one study concerned with platinum group mineral (PGM) from chromitite rocks of Rayat that is presented by Ismail (2007). This is the first comprehensive study of PGE in chromitite and associated peridotites of MOC.

In this study we present new data about PGE concentrations and distribution patterns in podiform chromitite and associated peridotite in MOC. The PGE enrichment origin is also discussed as well as making a comparison with PGE from other ophiolite in the world.

3.8 Geochemistry of PGE and Au

The results of bulk-rock PGE content are summarized in the (Table 3-5) and these data were normalized using PGE values published by O'Neill and Palme (1998) (Table 3-5). The chondrite-normalized PGE and Au patterns for

chromitite rocks and dunite envelopes with harzburgite host rocks from MOC are presented in (Fig. 3-23) and (Fig. 3-24). Leblance (1991) classified the PGE concentration in ophiolitic complex into rich PGE (> 750 ppb) and poor PGE (< 750 ppb). In chromitite rocks of MOC the PGE content ranges between (31-450ppb) (Table 3-5) and classified as poor-PGE with exception of one sample (W19) which gives anomalous PGE values rich in PGE (Σ PGE=1094 ppb). Chromitite rocks which belong to mantle transition zone (MTZ 1-2 Km below Moho) are depleted in PGEs (Frequently < 500 ppb and their Cr# is up to 0.6), while those locating in a deeper part of the mantle section are rich-PGE (> 750 ppb) and has Cr# > 0.7 (Legendre, 1982, Page et al., 1982a, 1982b, and Auge 1986). Accordingly, the PGE content of chromitite rocks in MOC can be classified into two types: (1) the high-PGE content (1094 ppb) which has Cr# ranges between 0.712-0.783 average 0.728 and their modal abundance of chromian spinel 85 % belongs to the deeper mantle section (2) all the other types of chromitite in (MTZ) which have (Cr# ranges between 0.67-0.75 average 0.659) and have less than 76 modal % of chromian spinel.

The PGE concentrations are highly variable in the chromitite of MOC; the PGE – poor chromitites have less than 500 ppb of total PGE and the PGE- rich one has unusually high PGE concentrations =1094 ppb (Table 3-5), more than two orders of magnitude higher than those in ordinary ophiolitic chromitite (Leblanc 1991). The chondrite – normalized PGE patterns of chromitite samples from MOC (Fig. 3-23) are characterized by enrichment in Ir-subgroup elements (IPGE=Os, Ir, Ru) relative to those of Pd-subgroup elements (PPGE= Rh, Pt, Pd). In addition all chromitite samples (PGE-poor) show slightly negative slopes from Ru to Pt, with positive Au anomaly (Ru/Pt range between 1.8-19). The IPGE / P PGE ratio ranges between 0.8 to 12.44 for the former one and is 6.758 for the latter. These patterns and the low PGE abundances are typical of ophiolitic chromitites elsewhere (Page and Talkington 1984, Proenza et al., 1999, Ahmed and Arai, 2002, and Mellini et

al., 2005). The Pd /Ir ratio is an indicator of PGE fractionation (Naldrett et al., 1979) and varies from 0.055 to 3.333 in chromitite of MOC, the PGE content of chromitite seems to increase with decreasing Pd / Ir ratios (Fig. 3-25) that is to say the high PGE contents result mainly from a concentration of Ir relatively to Pd. Inclusion of platinum group minerals were probable in massive and brecciated chromitite of MOC from the results of PGE analysis and using the plots of Os-Ir-Ru from (Harris and Cabri, 1991) (Fig. 3-26) and indicate that all chromitite samples from MOC which are poor PGE plot in the field of laurite and those which is rich-PGE plot in the field of iridium disulfide.

Table 3-5 Whole-rock platinum-group element contents (ppb) of representative samples from MOC.

Samples	Chondrite	W19	W25	W28	W30	W31	W33	W26	W29	W21	W36	Q20
Descriptions		Massive	Massive	Massive	Brecciated	Brecciated	Brecciated	Dessiminated	Dessiminated	Dunite	Harzburgite	Harzburgite
Os	514	54	61	68	67	25	26	2	10	5	6	12
Ir	540	557	110	91	75	43	46	3	12	6	6	10
Ru	690	342	190	172	172	106	104	9	38	11	12	23
Rh	200	17	13	19	13	9	10	2	4	2	4	5
Pt	1025	89	10	54	20	6	8	5	5	12	16	40
Pd	545	35	6	46	21	6	17	10	9	14	17	21
Au	152	<5	<5	<5	<5	<5	<5	<5	<5	<5	6	15
Σ PGE		1094	390	450	368	195	211	31	78	50	61	111
Σ IPGE/ Σ PPGE		6.758	12.448	2.7815	5.8148	8.2857	5.028	0.823	3.333	0.785	0.648	0.6818
Pd/Ir		0.063	0.055	0.505	0.28	0.14	0.37	3.333	0.75	2.333	2.833	2.1
Ru/Pt		3.843	19	3.185	8.6	17.667	13	1.8	7.6	0.917	0.75	0.575
Σ PPGE/ Σ IPGE		0.1479	0.0803	0.395	0.1719	0.1206	0.1988	1.2142	0.3	1.2727	1.5416	1.4666

Table 3-6 Chemical compositions of base metals (BM) in chromitite rocks from MOC.

Elements	Description	Ag	As	Co	Cr	Cu	Fe	Ni	Pb	S	Zn	Ni/Cu
Units		ppm	ppm	ppm	ppm	ppm	%	ppm	ppm	ppm	ppm	
Detection limit		1	5	1	2	1	0.01	1	5	10	1	
Samples												
W19	Massive	2	<5	375	338004	<1	15.92	829	<5	<10	1007	829
W25	Massive	2	45	219	380493	1	12.25	946	<5	<10	437	946
W28	Massive	2	<5	225	319828	<1	12.77	904	<5	<10	492	904
W30	Brecciated	2	<5	223	344428	1	13.1	917	<5	<10	402	917
W31	Brecciated	2	<5	363	309419	4	14.69	1012	<5	<10	1629	253
W33	Brecciated	2	<5	391	279339	<1	14.82	878	<5	<10	1348	878
W26	Dessiminated	<1	<5	123	22599	<1	5.86	2812	<5	<10	94	2812
W29	Dessiminated	<1	<5	234	141118	<1	10.3	1770	<5	<10	700	1770
W21	Dunite	<1	<5	126	3088	<1	6.1	2463	<5	13	21	2463
W36	Harzburgite	<1	<5	135	5961	<1	5.94	2235	<5	157	52	2235
Q20	Harzburgite	<1	<5	73	27685	53	4.59	569	<5	60	88	10.7358

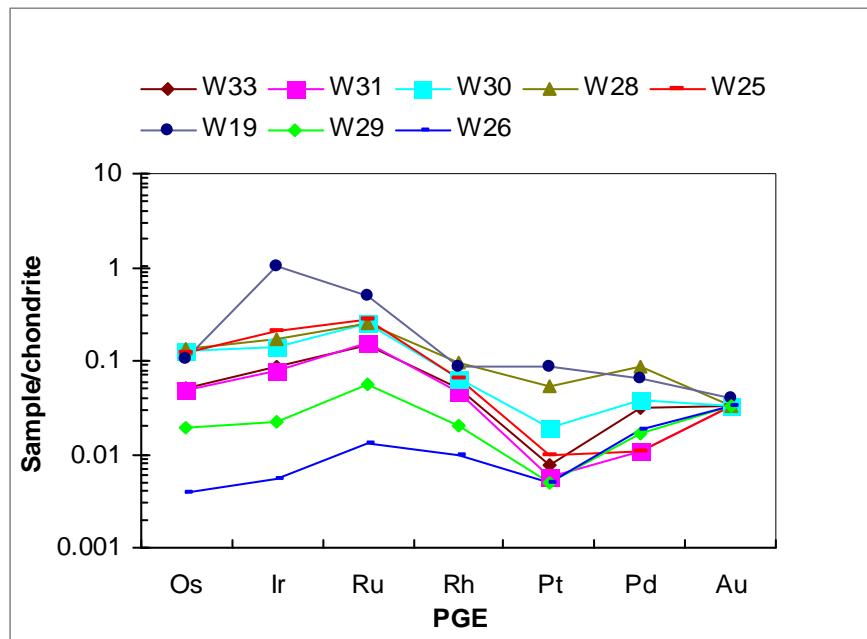


Fig. 3-23 Chondrite-normalized PGE content for podiform of chromitite from MOC.

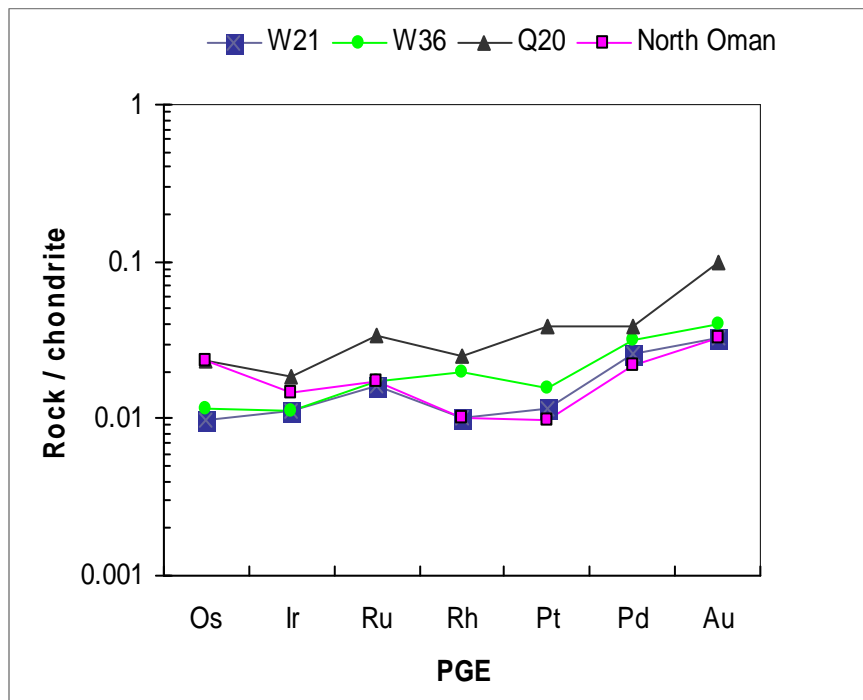


Fig. 3-24 Chondrite-normalized PGE patterns of dunite and harzburgite of the MOC.

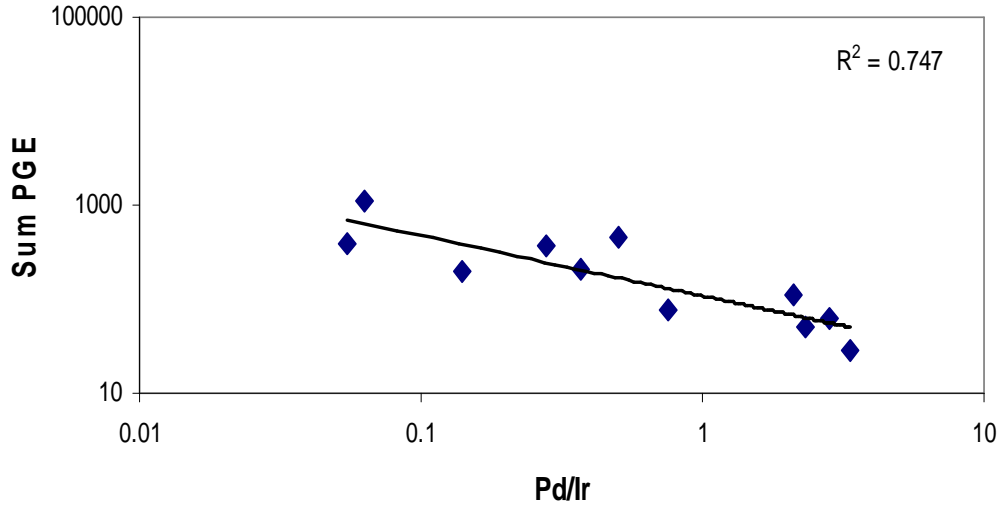


Fig. 3-25 PGE content versus Pd / Ir ratio diagram for podiform chromitite from MOC.

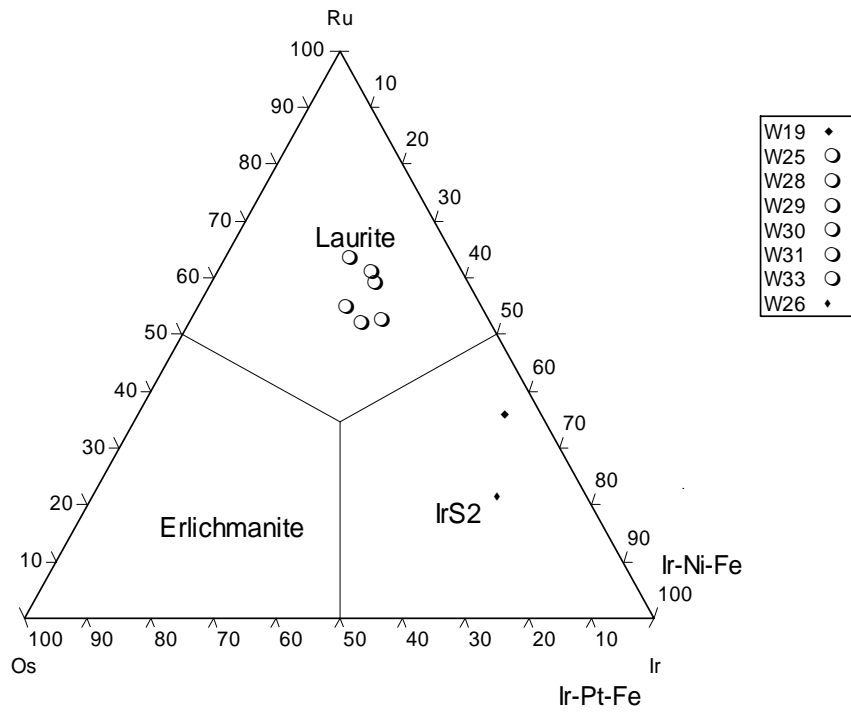


Fig. 3-26 Triangular diagram (Harris and Cabri, 1991) illustrating compositions of Platinum group minerals of MOC chromitites.

3.9 Comparison of PGE distribution

The PGE distributions in various types of chromian spinel were plotted and compared to other well-known podiform and Alaskan-type chromitites on the Σ PGE versus $PPGE_N / IPGE_N$ [chondrite –normalized platinum-group PGE (PPGE: Rh+Pt+Pd) versus iridium-group PGE (IPGE: Os+Ir+Ru)] diagram (Fig. 3-27 A and B), which was used as a fractionation indicator by Melcher (1999). All samples from the MOC chromitite plot into the upper part of the left hand side of the diagram, within the Main Ore Field chromitite field of Kempirsai. They show a negative slope following the ophiolitic chromitite trend (Fig. 3-27 B). In the cases shown in (Fig. 3-28B), the negative correlation may be used to discriminate ophiolitic from stratiform chromitites, which generally followed more horizontal trends (Fig. 3-27 A). Values of $PPGE_N / IPGE_N$ are usually below one (0.144-0.427), which is the characteristic of many mantle hosted podiform chromitites. While the analyzed samples for PGE contents from the dunite and harzburgite around the podiform chromitite show lower total PGE content and higher values of $PPGE_N / IPGE_N$ (1.28-1.66).

Application of the PGE data of ultrabasic and basic rocks from Alaskan-type complexes of the Urals to the plots of $[Pt/Pt^* = (Pt_N / (Rh_N * Pd_N))]$ versus Pd/Ir generated by Garuti et al. (1997) (Fig. 3-28) show that these rocks defined a fractionation trend. On the same diagram the MOC chromitite clearly follows a partial melting trend to high degree of partial melting similar to the Main Ore Field chromitites (Fig. 3-28), and are distinguished from the Batamshinsk-type chromitites of Kempirsai, which show both partial melting and fractionation trend (Melcher et al., 1999).

3.10 Distribution and fractionation of PGE in chromitite rocks of MOC

Three processes; that is, partial melting, crystal fractionation and alteration, possibly control the PGE in igneous rocks (Barnes et al. 1985). Gold and Pt are more easily mobile than the other PGEs during alteration process, and Pt may be mobilized by hydrothermal fluids (McCallum et al. 1976, Barnes 1985, and Stumpfl 1986). Os, Ir, and Ru have higher melting points than Pt and Pd, and tend to be concentrated in refractory residue and in early cumulate relative to Pt and Pd which are more incompatible and tend to be retained in the melt (Barnes et al., 1988, Edwards 1990, and Piichard et al., 1996 a, 1996 b). The strong variation of Pd/Ir ratios of chromitite rocks of MOC 3.333 to 0.055 (Table 3-5) was basically dependent on the variation of PGE contents in magmas responsible for chromitite genesis. The PGEs, which are very refractory, require high degree of partial melting for extraction from highly depleted mantle source and for concentration in appreciable amounts in resultant igneous rocks. A high-degree partial melt is, therefore, expected to be enriched in PPGEs and its residuum enriched in IPGEs (Sun 1982, Barnes et al., 1985 and Leblance, 1991). All chromitite samples of studied area are characterized by enrichment in IPGE and depletion in PPGE therefore a high degree of partial melt of mantle source is expected which causes the concentration of IPGE in chromitite rocks. In addition to this, all chromitite samples follow a partial melting trend to high degree of partial melting (Fig. 3-28).

At relatively low sulphur fugacity and high temperatures (1260-1380 C°) (Table 5-1), Os, Ir, and Ru will be concentrated into laurite and to a lesser extent PGE alloys (Leblanc 1991) and according to (Ahmad and Arai, 2002) chromian spinels, the early fractionate of the melt may include minerals Os-Ir-Ru crystal alloys or sulphide during the early stages of their growth.

Accordingly the chromian spinel of chromitites in MOC and their common abundance of Iridium disulphide in PGE-rich and Laurite in PGE-poor spinels (Fig. 3-26) suggest a possibly sulphur saturated melt involved in the formation

of laurite and iridium disulphide at relatively low sulphur fugacity and high temperatures (estimated temperature are 1260-1380C) (Table 5-1).

Two possible melt mantle interaction processes may control the differences in PGE contents between the PGE-rich chromitites in the deeper mantle section and PGE-poor chromitite around the MTZ in MOC: (1) fractionation of a single PGE-rich magma, which precipitated PGE-rich chromitite in the deeper section and a PGE-poor one around the MTZ; (2) two different magma involved in chromitite formation in the deeper mantle section and MTZ, depending on the tectonic setting in which these chromitite types are formed (Ahmad and Arai, 2002). Petrological, field characteristic (irregular and lens shape) and geochemistry of chromian spinel in chromitite rocks of MOC support the first possibility, because the second possibility assumes the Cr# must be ≤ 0.6 in the former and ($\text{Cr\#} > 0.7$) in the latter. In studied samples, the average Cr# of PGE-poor 0.659 and for the PGE rich is 0.728 and the inclusions are chlorite and serpentine (Tables 3-2 and 3-4).

3.11 Distribution and fractionation of PGEs in dunite and harzburgite of MOC

The dunite that envelopes the chromitite ores and the host rocks harzburgite in MOC display a slightly flat patterns with slightly negative slopes from Ru to Pt ($\text{Ru} / \text{Pt} = 0.917$, Fig. 3-24) and positive trend from Pt to Au which means slightly fractionated nature. The IPGE / PPGE is 0.785 and Pd / Ir is 2.33 (Table 3-5). According to Ahmad (2002) the unfractionated or undepleted peridotites, with respect to PGE, show Pd/Ir ratio around 1. The associated dunite in MOC is clearly depleted from Ru to Pt, and enrichment in Pd and the PGE content is 50 ppb. The harzburgite hosts which separate the chromitite pods from each other have low PGE contents (61-111 ppb). They exhibit slightly negative trend from Ru to Pt and positive trend from Pt to Au (Fig. 3-24), the Pd / Ir ranges from 2.1 to 2.833. The positive trend of dunite and to lesser extent harzburgite may be due to the partial concentration of PGE in the early formed chromitite which collect the IPGE relative to the PPGE.

The slightly negative slope of Ru to Pt distribution patterns of dunite is also best explained by the nature of early precipitates where PGE-bearing phases

have relatively high IPGE / PPGE PGE-rich magma which has lost its IPGEs by forming IPGE- rich chromitite at the depth of the mantle. The subsequent magma precipitated dunite higher in (PPGE/IPGE) ratios (Pd/Ir is 2.3). The slightly flat PGE distribution patterns of dunite and harzburgite (Fig. 3-24) coincided with CN pattern of the depleted upper mantle peridotite compiled by Ahmad and Arai (2002). This may indicate its slightly fractionated nature (Pd/Ir = 2.1-2.8). By contrast, highly depleted mantle peridotites usually have low total PGE contents and fractionated CN patterns with negative slopes from Ir to Pd and have Pd/Ir < 1 (Hertogen et al. 1980, Mitchell and Keays 1981 and Edward, 1990).

3.12 Base metal

Nickel concentrations in chromitite rocks range from 829 to 2812 ppm and in associated dunite and harzburgite ranges between 569 to 2463 ppm (Table 3-6). The bulk of nickel is incorporated into the chromite structure. According to (Melcher et al., 1997) varying amount of nickel may be present as interstitial sulfide and arsenide, but in most samples of studied area arsenic and lead were not detectable (< 5 ppm) except in one sample (W25) where the arsenic measured was about 45 ppm, so the bulk of nickel is incorporated into chromite structure. Only a few concentrations of trace metals (Co, Ag) in chromitite and associated peridotite are presented.

The Zn content of chromitite rocks ranges from 402 to 1629 ppm. Usually chromian spinels crystallized from sulfide melt have distinctly higher ZnO contents, i.e. > 0.5 wt % (Peltonen, 1995). The MOC chromitite contains much more chromite than sulfide; it is unlikely that the chromite crystallized from sulfide liquid which could only dissolve trace amounts of Cr. Therefore the Zn enrichment in chromitite rocks is related to metamorphic effect and introduction of Zn during hydrothermal alteration and subsequent crystallization. The high Zn contents of chromian spinel were related to crustal contamination (Wang et al., 2005). Individual high-Zn in chromitite rocks of MOC are thus not primary, but rather the result of introduction of Zn during low-temperature serpentinizations.

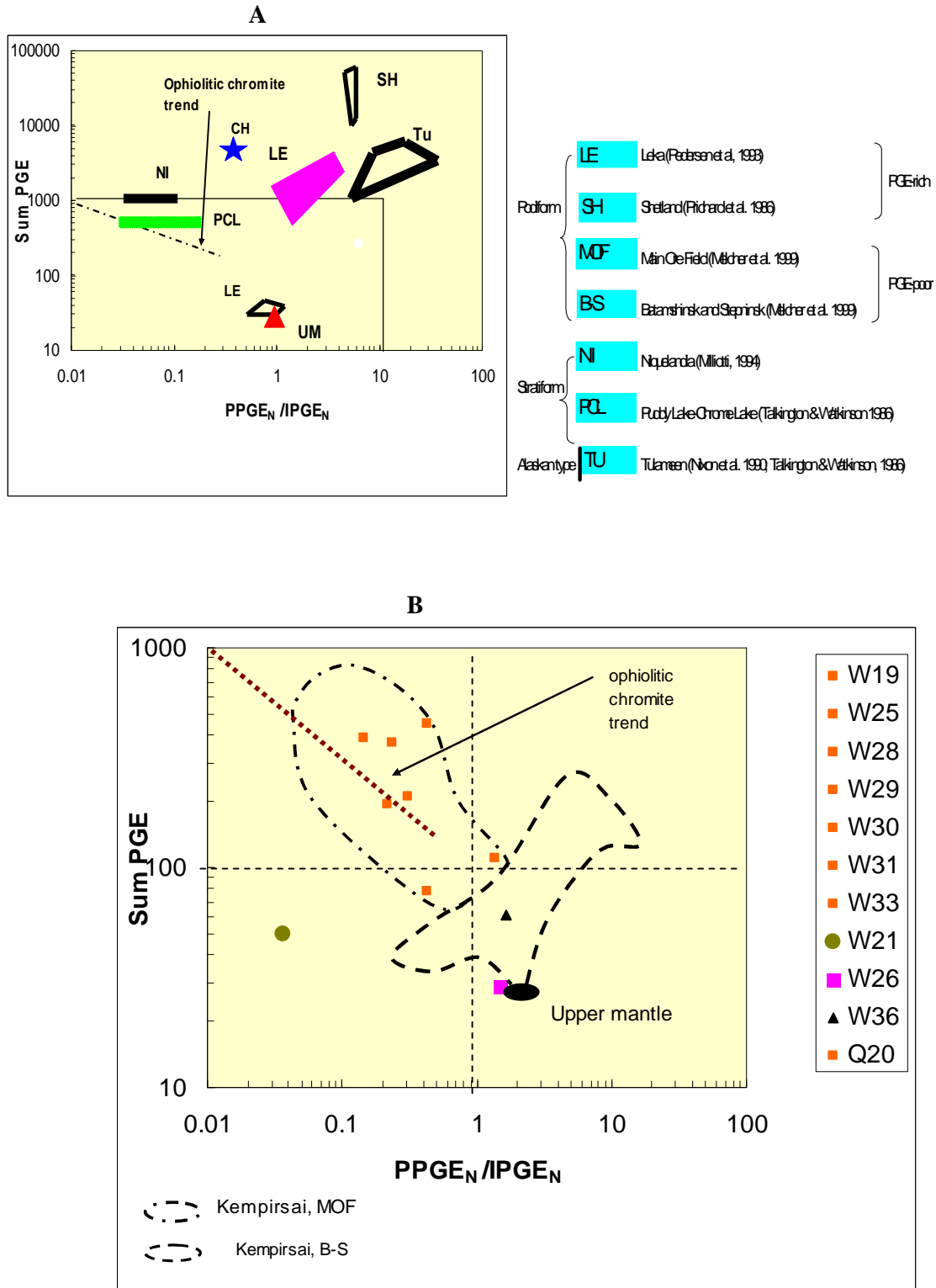


Fig. 3-27 (A and B) Chondrite-normalized PPGE / IPGE diagrams versus Σ PGE for the MOC chromitite and related ultrabasic rocks **A**-the upper inset plot shows trends and fields for important types of chromite deposits (CH: chondrite, UM: upper mantle) **B**- plottes of studied samples on this diagram which is following ophiolitic trend.

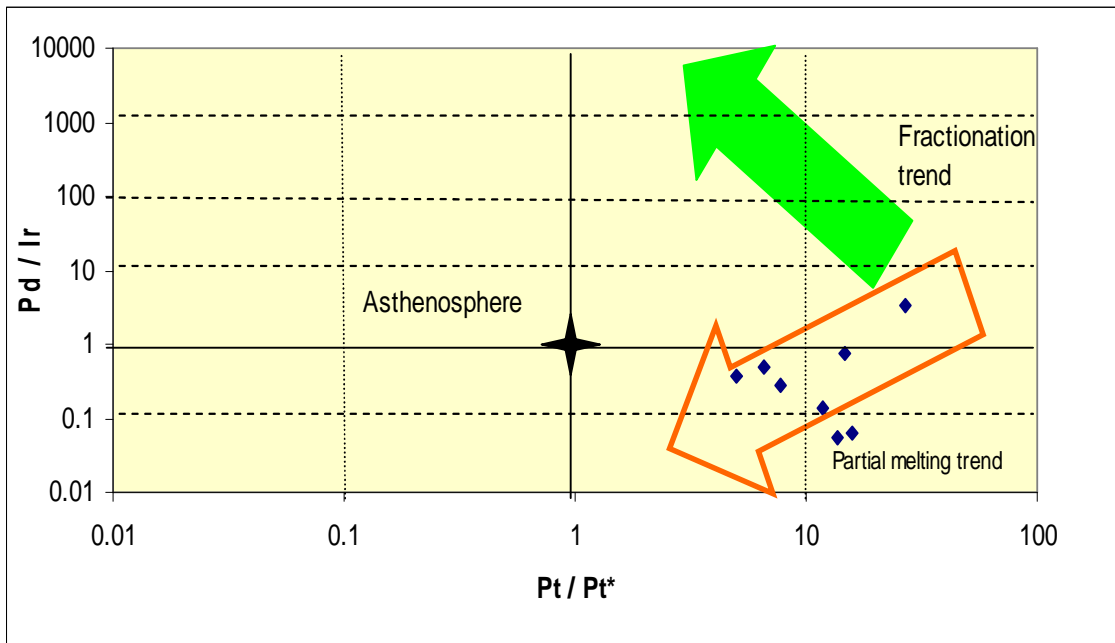


Fig. 3-28 Plots of Pt/Pt^* ($Pt_N / (Rh_N * Pd_N)$) versus Pd/Ir for the MOC chromitite shows that partial melting process which has influence on PGE concentration in chromitite rocks. Fractionation and partial melting trends from (Garuti et al. 1997).

Chapter Four

The Basic Rocks

4.1 Petrography of gabbroic rocks

The gabbro mass covers the major part of the MOC for about 170 Km² (Jassim and Al-Hassan, 1977). Based on field work and previous study by Jassim (1972, 1973) three petrographical differing gabbroic bodies are recognized which are:

- 1- Banded gabbro
- 2- The coarse gabbro
- 3- The sheared gabbro

Gabbroic samples are collected along three main traverses which are:

- 1- Amaden – Mirawa – Saraw.
- 2- Goranga- Kanaka Rash – Shakha Root traverses.
- 3- Rashakani – Daraban.

Forty-one samples are collected from these different traverses, the samples including banded gabbro (18 samples) and sheared gabbros (6 samples) which are collected along traverse 1 & 2, while the coarse gabbro (17 samples) collected from traverse 2 and 3. These samples are examined using polarized microscope. Modal proportions of minerals were determined and the results were listed in (Tables 4-1). The classification adapted for the basic rocks of MOC are based on Streckeisen (1973) modified by Bose (1997) and Best (2001) according to this classification all samples of gabbroic rocks plot in the field of hornblende gabbro and pyroxene hornblende gabbro / norite (Fig. 4-1).

4.1.1 Banded gabbro

The banded gabbro covers the main part of MOC; this body has intrusive contacts with the green schist in the west, southwest, and south (Fig. 1-2). This contact has been obscured by minor intrusions in the western part and in the east the banded gabbro has sharp contacts with coarser pyroxenite gabbro.

The banded gabbro is grey to grayish green on the weathered surface (Fig. 4-2), and it is medium to coarse grained. It consists of alternating thin light color band with darker bands. These alternating colors are due to crystal

settling mechanisms (Jassim, 1972, 1973, Jassim and Al-Hassan 1977 and Shawan et al., 2003). The banded gabbro shows crushed texture, the major components are made up of amphibole and plagioclase. Petrographic analyses of banded gabbro based on the method of Michel-Levy chart revealed that the plagioclase is Labradorite and bytownite ($An_{50} - An_{70}$). In addition to this major constituent chlorite, pyroxene, quartz, epidote and magnetite can also be observed which have developed around plagioclase and amphiboles minerals in some rock samples. The average modal % abundance is given in (Table 4-1).

The plagioclases are anhedral to subhedral, mostly lath like crystals up to 3 mm in size and enclose amphiboles within their intergranular spaces, they were subjected to crushing under the influence of tectonic deformation. The degrees of crushing vary from completely crushed plagioclase (Fig. 4-3) in rocks situated along or near shear zone (Amadine- Mirawa) to slightly and unaffected one in Mirawa-Saraw and Goranga –Shakha-Root area (Fig. 4-4).

The main observed effect of tectonic deformations on these plagioclases are indicated by crushed texture, (Fig. 4-5) and secondary twin lamellae on some coarse plagioclase grains (Fig. 4-6). In few samples the plagioclase revealed that moderately sursitized crystal is partially or completely transformed to a cloudy mesh of fine aggregate of epidote and secondary sodic plagioclase (Fig. 4-3)

Amphiboles identified in banded gabbro are mainly hornblende that occurs as anhedral to subhedral crystal ranging in size between 0.2 mm to more than 2 mm showing slight to strong pleochroism. They are brown to brownish green under transmitted microscope, which show two set of cleavages forming a rhombohedra angle (Fig. 4-7). Some of crystals appear as dark green to greenish black color, which is formed on expense of pyroxene (Buztug et al.,

1998). Some of amphiboles are slightly frayed in their outline and are non fibrous. Some grains also show penetrating amphibole chlorite boundary relation. Other amphibole grains show the alteration product of clinopyroxene indicated by small relict clinopyroxene grain within amphibole (Fig. 4-8). Two types of hornblende in a banded gabbro of MOC were distinguished; they are primary and secondary hornblendes the latter resulted from uralitization of original pyroxene content (Al- Etabi, 1974). Actinolite amphibole occurs as pale green acicular crystal fraction of 0.3 -0.6 mm in size, and show pleochroism (Fig. 4-8).

In addition to these major constituents, some pyroxene is observed. Pyroxene (diopsitic and augite variety) is present as fine anhedral crystal and as relict within amphibole crystals indicating the hornblendization of original pyroxene content of gabbro.

The alteration minerals in banded gabbro are represented by chlorite and sericite. Chlorite replaces hornblende and actinolite in some samples and closely associated with tremolite along fractures and around the margins, comprising less than 14 % of gabbro samples, while sericite represents the alteration of plagioclase. Accessory minerals in banded gabbro include magnetite, apatite and quartz (Fig. 4-9). Magnetite is disseminated anhedral and mostly intergranular to plagioclase, except where it occurs as very fine exsolved grain along the cleavage surface and grain boundaries of hornblende and it ranges in modal volume percent between (0.0 to 19 %). Quartz was observed from sheared gabbro reaching up to 15 % of the mode (Table 4-1), (Fig. 4-9). This mineral is interstitial and has been related to later magmatic activity that produced the plagiogranite (Jassim, 1973, Rao et al., 2004 and Mirza and Ismail, 2007). The quartz grains have undulated extinction indicating later deformation.

Table 4-1 Modal % of minerals composition of gabbroic rocks in MOC.

S.NO.	Minerals	Plagioclase	Amphibole	Clinopyroxene	Chlorite	Quartz	Magnetite
Banded gabbro							
W1		47	50	0	0	0	3
W4		42	54	2	2	0	0
W5		41	51	2	5	0	1
W6		44	51	0	4	0	1
W10		42	45	3	5	0	5
W11		42	46	2	3	3	4
W39		44	52	3	0	0	1
W41		44	47	2	3	0	4
W42		39	46	0	8	2	5
D3		34	48	2	8	0	8
D5		36	46	4	8	0	6
D13		49	40	0	9	0	2
D14		40	42	2	11	0	5
A4-1		37	44	0	5	6	8
A4-3		38	39	6	5	6	6
K1-1		38	48	2	2	0	10
K1-2		38	49	4	4	0	5
K1-3		36	47	5	7	0	5
Coarse gabbro							
R9		41	36	4	9	0	10
D17		41	48	4	3	0	4
D22		43	50	2	3	0	2
D26		44	46	4	4	0	2
D27		46	45	2	4	2	1
D31		42	48	4	4	0	2
A2-1		42	44	5	9	0	0
A2-2		39	45	10	6	0	0
A2-3		40	41	15	4	0	0
A2-4		32	52	10	4	0	2
A3-1		33	44	11	7	0	5
A9-1		41	37	4	7	0	11
A12-1		44	49	7	0	0	0
K2-4		37	52	8	3	0	0
K3-4		43	48	7	0	0	2
K3-5		44	46	8	0	0	0
K7		37	46	10	5	0	2
Gabbroic rocks near shear zone							
A4-2		38	53	0	3	5	1
A5-1		38	48	0	0	11	3
A5-2		32	42	0	4	3	19
A6-2		39	47	0	13	0	1
A7-1		46	37	0	2	15	0
A7-2		42	40	0	10	2	5

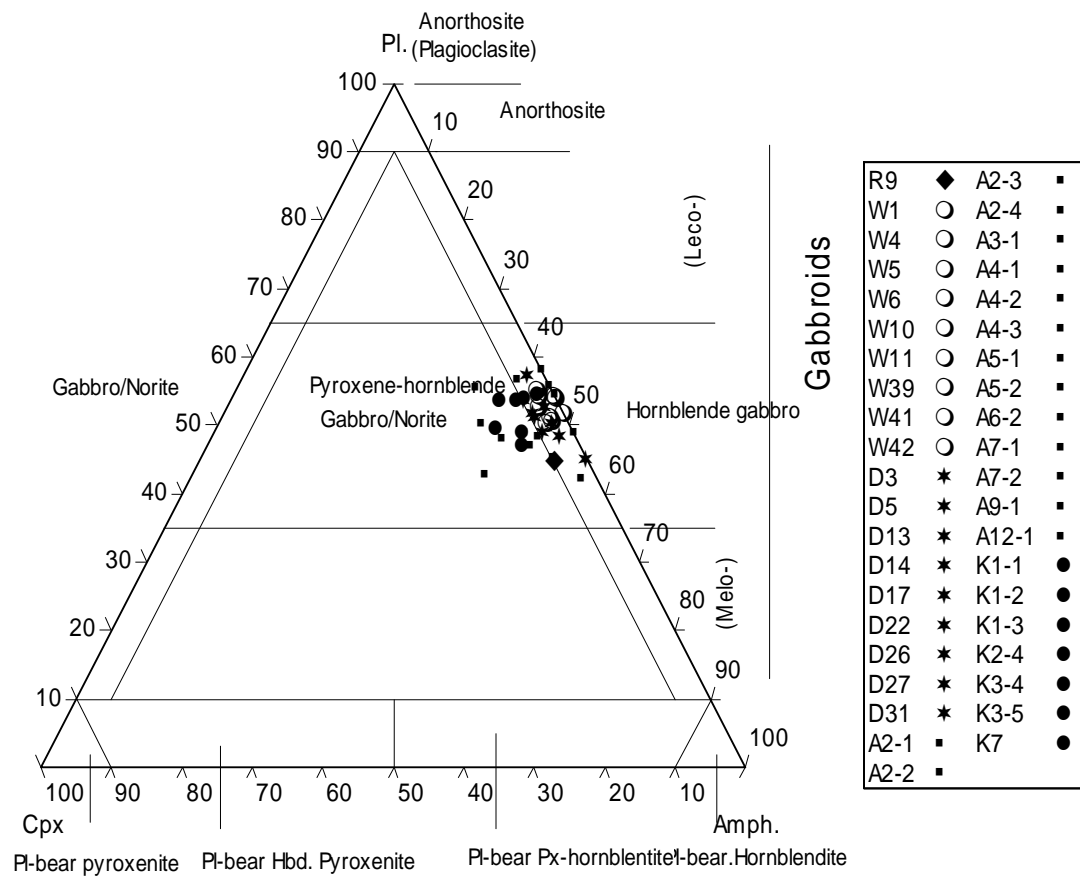


Fig. 4-1 Classification and nomenclature of gabbroic rocks in MOC (Diagram from Streckeisen 1973) modified by Bose, (1997) and Best (2001).

4.1.2 Coarse gabbro

This intrusion was first identified by Jassim (1973) as a separate body having characteristic petrography and mineralogy. The coarse gabbro body is bordered by the banded gabbro from the north, west and south, and by the ultrabasic mass of Daraban from the east.

The texture of this rock is variable, but the most abundant were of a pegmatitic texture, the grain size varies from 0.7 cm to more than 2 cm and it is dark green to greenish grey in color on weathered surface with white spots of plagioclase.

The coarse gabbro is composed of various amounts of amphibole, plagioclase, and pyroxene with small amounts of chlorite, magnetite and actinolite. The most abundant mafic minerals of coarse gabbro are

clinopyroxene which had been uralitized and ranges in modal abundant between (36 to 52 %), plagioclase is found ranging between (32 to 46 %) in the mode and slightly affected by granulation. The plagioclase is unihedral, with polysynthetic twinning, some of crystals are slightly granulated and on the bases of the method of Michel-Levy represent labradorite-bytownite in composition. Pyroxene in the coarse gabbro is relatively abundant and comprises 2-15 % and it is affected by deformation. Clinopyroxene is medium to coarse grained and in some of the grains the cores are partly replaced by amphibole grains (Fig. 4-10). The most abundant accessory minerals represented by magnetite (0.0 to 11 %) and alteration minerals represent by chlorite (0-9 Vol. %) (Table 4-1).

4.1.3 Sheared gabbro

The sheared gabbro is common in the western part of the Mawat Complex between Merawa and Amadin. It forms in roughly N-S zones mapped by Jassim (1972). The gabbroic rocks in the zone are traversed by small veins (Fig. 4-11). Within these shear belts; the gabbroic rocks are included within many minor acidic intrusions, which are classified by Jassim (1973), into coarse diorite, very fine-grained quartz dolerite and aplite granite. The geochemistry of aplite granite is studied by Mirza and Ismail (2007), and they showed that are trondhjemite in composition. The gabbroic rocks in the sheared zone contain very fine grains of plagioclase and amphibole. Quartz is present and according to (Jassim and Al-Hassan, 1977) this quartz is related to the plagiogranite that is restricted to this area. The accessory mineral represented by quartz and magnetite (Fig. 4-12).



Fig. 4-2 Green to greenish grey banded gabbro in Ser Shiw valley.

A

B

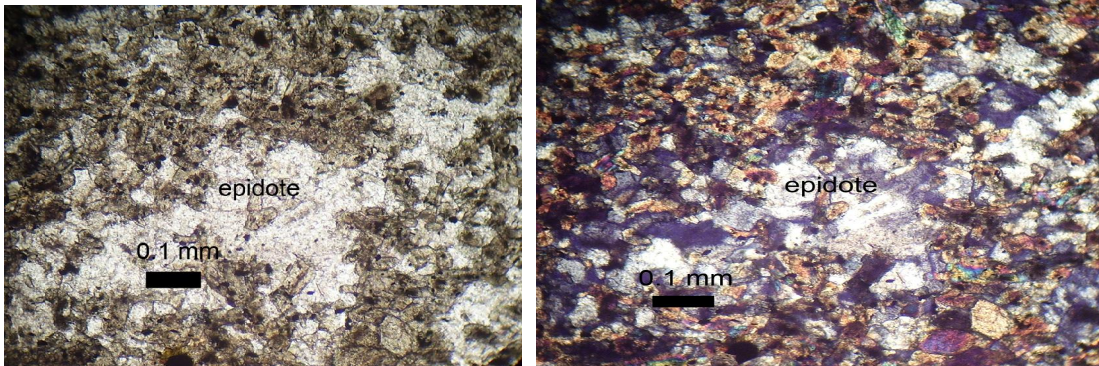


Fig. 4-3 Completely crushed plagioclase revealed that transformed to a cloudy mesh of fine aggregate of epidote under the effect of tectonic. (A: under PPL, B: XP)

A

B

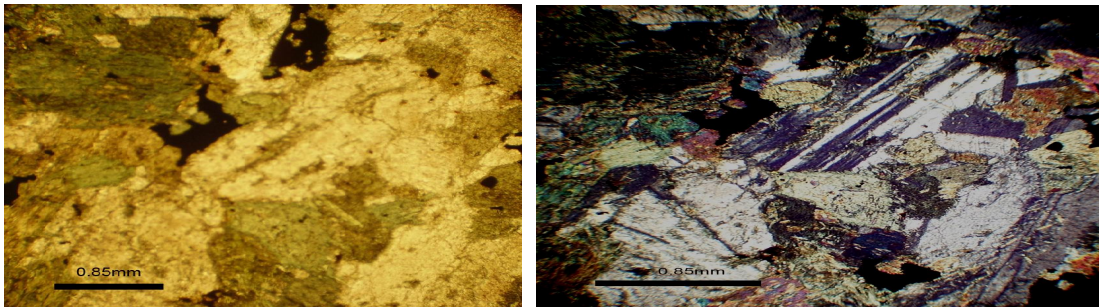


Fig. 4-4 Slightly affected plagioclase and amphibole by crushing, (A: under PPL, 4X, B: under XP).

A

B

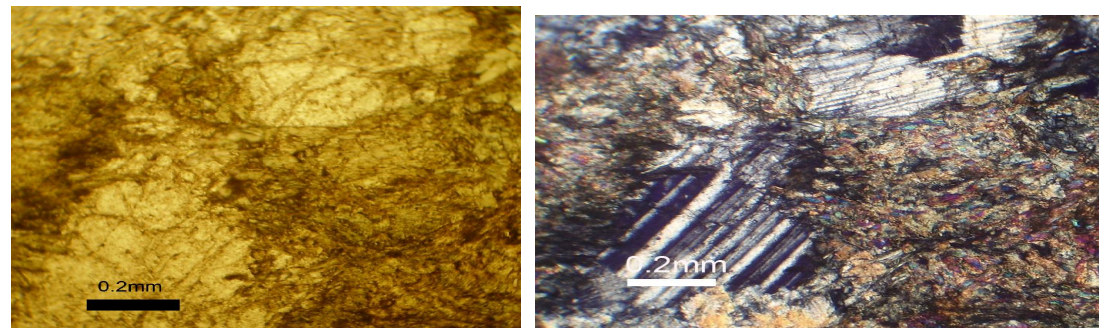


Fig. 4-5 porphyroclastic texture in banded gabbro (A: under PPL, B: under XP).

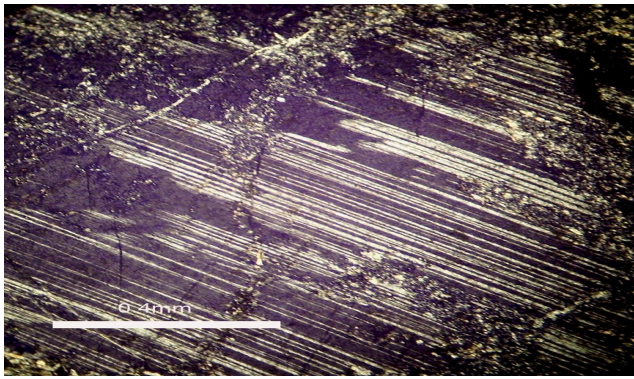


Fig. 4-6 Secondary twin lamellae in plagioclase (under XP).

A

B

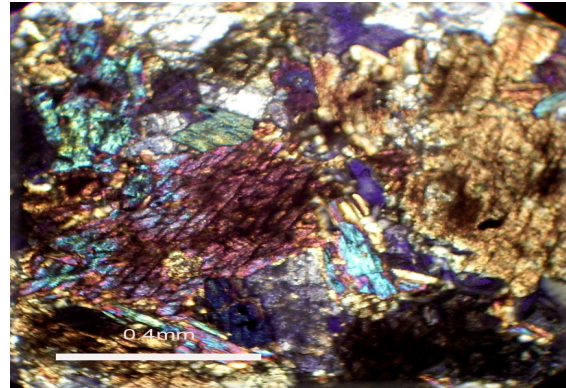
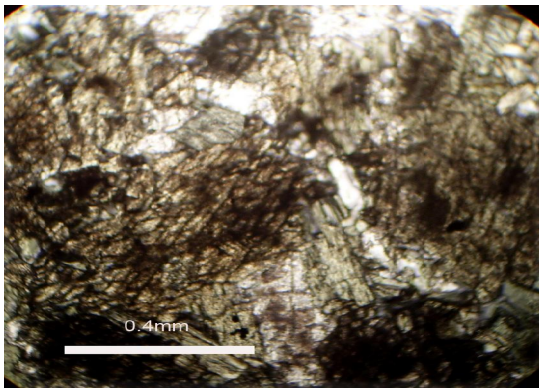


Fig. 4-7 Subhedral hornblende crystal in banded gabbro (A: under PPL, B: under XP).

A

B

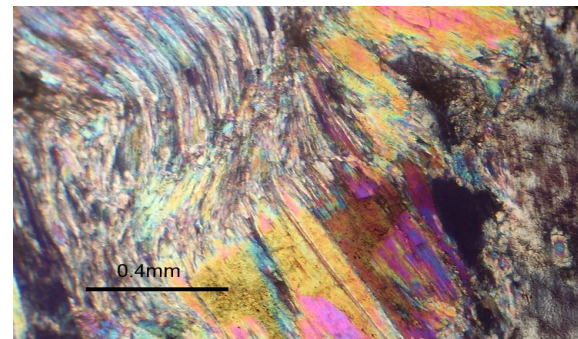
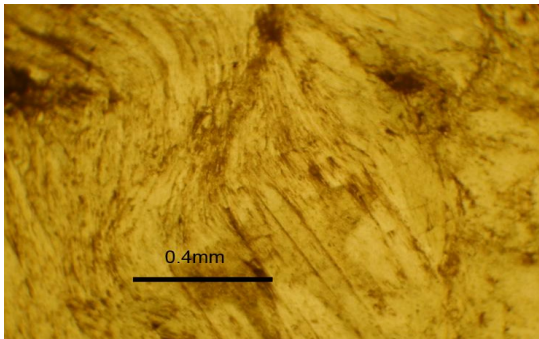


Fig. 4-8 Acicular crystal of actinolite resulted from the alteration of clinopyroxene (uralite).(A: under PPL, B: XP)

A

B

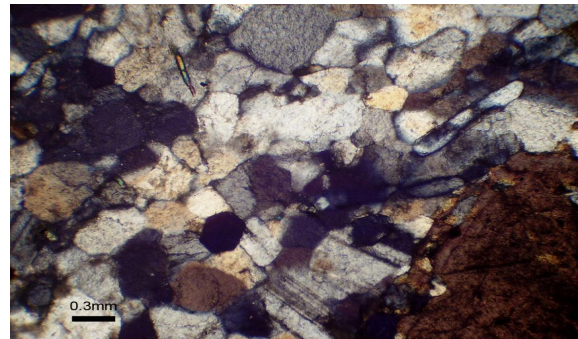
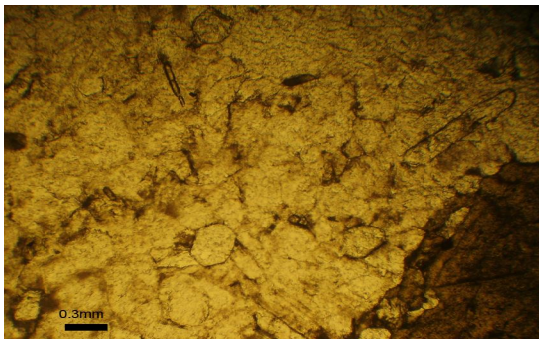


Fig. 4-9 Granulated plagioclase, apatite and quartz in banded gabbro near the shear zone. (A: under PPL, 4X, B: under XP).

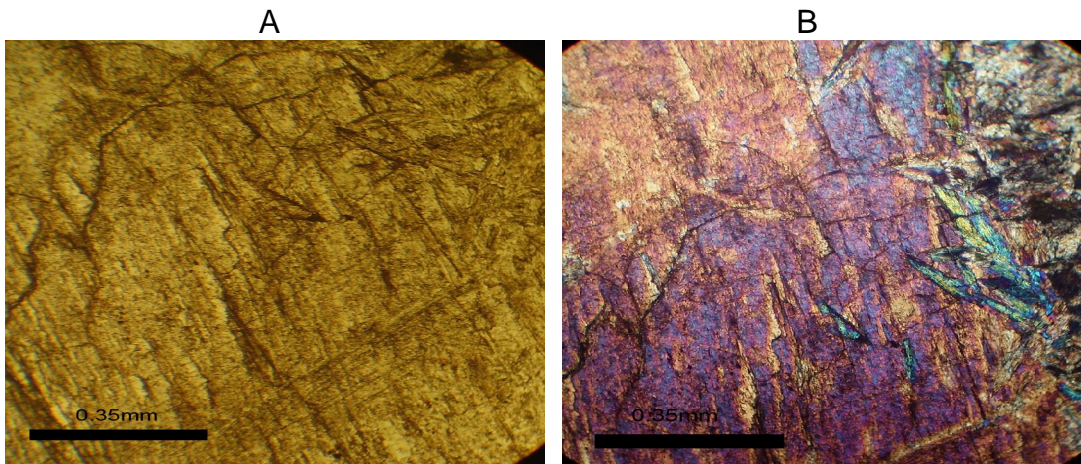


Fig. 4-10 Coarse clinopyroxene crystal contains small patches of amphibole. (A: under PPL,10X, B: under XP).



Fig. 4-11 Sheared gabbro between Amadin and Mirawa village traversed by tectonic cracks.

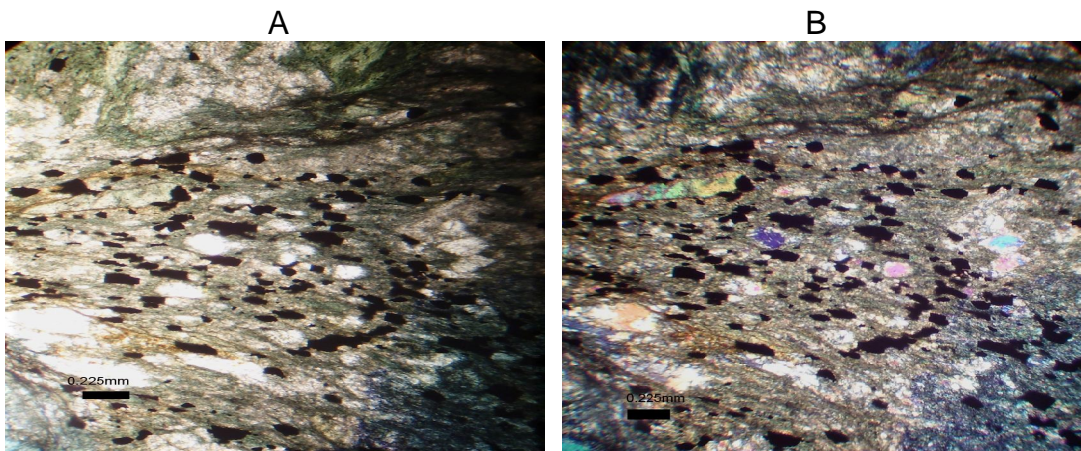


Fig. 4-12 Sheared gabbro with fine grain of plagioclase, secondary uraninite and accessory minerals quartz and magnetite. (A: under PPL, B: under XP, 40X)

4.2 Geochemistry of gabbroic rocks

4.2.1 Behavior of Major and trace elements in gabbroic rocks

Whole-rock geochemical data were obtained (using XRF) for eleven samples from gabbroic rocks of MOC (Table 4-2). Analyses of rare earth and selected trace elements (ICP-MS) of ten samples of gabbroic rocks are given in (Table 4-3). The whole rock major, trace, and REE compositions of the Mawat gabbroic rocks have been used to determine the main characteristics of the initial magma source and the process which modifies the initial magma composition.

The gabbroic rocks in the studied area have a moderate range of loss-on-ignition (LOI) values ranging from 0.88 to 2.88 (Table 4-2). The moderate variation in LOI is a crude measure of the degree of rock alteration (Parlak et al., 2006). Accordingly all types of the gabbro rocks have been affected by moderate degree of alteration.

The SiO₂ content of gabbroic rocks in MOC range from 45.57 Wt % to 55.14 Wt %. The average SiO₂ content in banded and coarse gabbro is 48.14, 49.15 % respectively while in sheared gabbro is 51.64 %. The high SiO₂ content in sheared gabbro related to the modal abundance of additional quartz content. FeO_{total} shows enrichment with differentiation and ranges from 5.9 to 22.34 Wt %. The gabbroic rocks also display rather low Al₂O₃ (\leq 17 Wt %) and high CaO (6.65–15.81 Wt %). The low Al₂O₃ content is related to the increase of clinopyroxene at the expense of plagioclase. Intermediate to low (0.08 to 1.15 Wt %) TiO₂ values suggest early precipitation of Fe-Ti oxides (Duclaux et al., 2006). P₂O₅ (0.008 to 0.53 Wt %), Zr (5 to 32 ppm), Nb (0.0 to 1.1 ppm) and Nb/Y (0.0 to 0.1) are the characteristics of the gabbroic rocks in the studied area which exhibit tholeiitic geochemical feature (Table 4-2).

The basic rocks of MOC have comparable compositions; enriched in FeO relative to Na₂O, K₂O and MgO (Fig. 4-13) hence based on Jenson diagram, (1976) it is classified as tholeiitic. Plots YTC (Y+Zr, TiO₂, Cr) diagrams (Fig. 4-14) and P₂O₅–Zr variation (Fig.4-15) demonstrate the tholeiitic character of all

the rocks. All the rock samples taken from the gabbroic rocks determine a good sub-alkaline tholeiitic trend in the total alkalis-silica and AFM diagrams (Figs. 4-15 A and B). This tholeiitic composition is also characterized by the low-K tholeiitic (Fig. 4-16 C).

Chemical behavior of major and trace elements is described using MgO as differentiation index. On variation diagrams of elements plotted against MgO (Fig. 4-17), TiO_2 , Al_2O_3 , FeO and P_2O_5 , show negative correlation with MgO.

The negative correlation between MgO and CaO indicates depletion of Mg in clinopyroxene with stability of Ca content (Sofy, 2003). The inverse relationship between MgO and TiO_2 may be related to the early precipitation of Fe-Ti oxides. $\text{Na}_2\text{O}+\text{K}_2\text{O}$ show slight negative correlation due to the presence of Ca-rich plagioclase, while SiO_2 and MnO for all samples show scattered correlations. The wide variation in P_2O_5 content (0.006 to 0.053 Wt %) and the inverse correlation with MgO is related to the presence of apatite which is crystallized at a late stage, from the magma differentiation process.

The MgO versus Ni and Cr variation diagrams (Fig 4-18 a,b) indicate positively correlated distribution, whereas elements such as Zr, Y, Sr, Ga and V show negative correlation. The positive correlation of Cr with MgO is related to the presence of clinopyroxene, because and most of chromium enters into the clinopyroxene structure. The positive relationship between Ni-MgO may be related to the Ni substituted for Mg due to their similarity in ionic radii.

Plots of major elements against MgO reveal how much of original chemistry of gabbros rocks is affected by alteration and / or metamorphism. This is because MgO is an important component of solid phases in equilibrium with mafic melts and shows a great deal of variation, either as a consequence of breakdown of magnesia phases during partial melting, or because of their removal during fractional crystallization (Yibas et al., 2003).

The remobilization of major and trace elements was tested using binary plots (Fig. 4-19) to determine the degree of correlation with Zr, which is assumed to be immobile (Cann, 1970). P_2O_5 and to lesser extent, SiO_2 and TiO_2 show positive correlation with Zr, whereas MgO shows negative correlation (Fig. 4-

19). The negative correlation of MgO with Zr is consistent with early crystallizing minerals such as olivine, pyroxene and Ca-plagioclase formed during magma differentiation. Both Na₂O and CaO exhibit slightly positive correlation when plotted against Zr, and such trends of CaO and Na₂O with Zr are results of primary fractionation processes. The remaining oxides show a wide scatter and poorly defined trends that suggest possible secondary effects. Among the trace elements Sr, Ba and all of HFSE, (Y, Hf, and Nb) show positive correlation (Fig. 4-20) which suggests that these elements have remained relatively immobile during alteration, and thus are suitable for geochemical interpretation. Whereas Cr and Ni show negative correlation with Zr and this supports crystallization of olivine, clinopyroxene and plagioclase phase during magma differentiation (Parlak et al., 2006).

The chemical characteristic observed for the gabbroic rocks of MOC can be summarized as an increase in TiO₂, Zr, P₂O₅, Y, Ga, and Sr with decreasing MgO, and increasing Ni, Cr with increasing MgO (Fig. 4-17) and (Fig. 4-18).

Fractional crystallization of mineral phases such as clinopyroxene, plagioclase and olivine could explain these chemical characteristics (Rollinson, 1993).

In the light of geochemical data mentioned above, the MgO-Zr variation of the gabbroic rocks in MOC can be considered to be formed from a single basic-mafic magma source by fractional crystallization (FC) process (Fig. 4-21a) (Wilson, 1989). A part from the Harker variograms in the interpretation of major element, geochemistry can be used to explain the genesis of basic rocks of MOC (Boztng et al., 1998). Two of them e.g. the variation of Al₂O₃ and CaO contents versus MgO content, undoubtedly show that the olivine and plagioclase accumulation/ fractionation is dominant in the genesis of gabbroic rocks in the MOC (Fig. 18 c, f). Similarly, the variation trend of Zr content versus SiO₂, Ga, La, Ce and Y contents are proposed to examine the FC process in basic-ultrabasic rocks by Wilson (1989). As apparently seen in (Fig. 4-21), the FC process has occurred during the solidification of tholeiitic-basic magma source and modified its initial composition to yield the gabbroic main body in the genesis of the MOC pluton.

Table 4-2 The results of XRF analysis of gabbroic rocks in MOC.

Types Oxide	Banded gabbro				Coarse gabbro					Sheared gabbro	
	W1	W11	A4-1	K1-1	D17	D26	A2-2	K3-5	K7	A5-1	A7-2
SiO ₂	53.97	47.27	45.57	45.76	49.32	49.71	52.85	46.23	47.65	55.13	48.16
TiO ₂	0.261	0.184	1.130	1.155	0.082	0.073	0.256	0.890	0.911	0.809	0.520
Al ₂ O ₃	12.32	16.86	15.28	14.68	14.22	10.87	15.75	13.68	14.23	13.98	16.58
FeO*	7.73	8.72	22.34	15.15	7.66	5.90	6.14	14.23	13.98	12.12	9.69
MnO	0.163	0.168	0.177	0.165	0.145	0.133	0.104	0.13	0.162	0.108	0.188
MgO	10.79	10.13	7.66	7.81	10.32	15.77	8.31	7.87	7.56	3.79	6.00
CaO	8.84	14.04	6.65	12.24	13.98	14.09	13.81	12.56	11.32	10.46	15.81
Na ₂ O	3.55	0.49	0.14	0.84	0.4	0.33	0.99	0.77	0.8	1.40	0.31
K ₂ O	0.18	0.02	0.01	0.06	0.09	0.17	0.06	0.06	0.07	0.03	0.03
P ₂ O ₅	0.021	0.006	0.016	0.012	0.008	0.008	0.020	0.02	0.018	0.053	0.028
LOI %	1.29	0.88	1.47	0.94	2.88	2.14	1.32	2.23	2.1	1.14	2.11
Total	99.13	98.76	100.44	98.81	99.11	99.21	99.61	98.67	98.80	99.02	99.43
Traces (ppm)											
Ni	200	105	47	40	200	309	72	44	50	20	77
Cr	715	275	23	386	351	832	93	29	32	9	12
Sc	43	50	58	52	45	51	48	55	62	38	64
V	243	281	756	1059	201	192	221	758	721	318	315
Ba	27	2	18	14	11	16	16	12	16	3	0
Rb	3	0	0	0	2	2	0	0	1	1	1
Sr	115	48	125	135	48	50	117	100	140	139	206
Zr	12	5	8	9	6	5	20	14	13	32	19
Y	8	11	9	8	7	3	9	7	6	20	16
Nb	0.3	0.5	0.0	0.2	0	0.0	0.5	0	0.6	1.1	0.6
Ga	8	13	18	13	7	6	14	14	11	17	16
Cu	39	63	12248	80	145	259	1	11	20	7	3
Zn	65	47	95	52	25	30	19	60	75	13	39
Pb	2	2	2	4	1	0	0	1	1	0	2
La	1	1	2	0	1	0	1	1	0	2	1
Ce	1	0	1	2	0	0	1	1	1	5	1
Th	0	0	2	5	0	0	0	1	1	0	0
Nd	0	0	0	0	0	0	3	0	1	4	2
sum tr.	1482	894	13412	1486	1047	1755	634	1108	1167	630	1147
in %	0.15	0.09	1.34	0.15	0.1	0.18	0.06	0	0.12	0.06	0.11

* Total iron content

Table 4-3 The results of REE analysis (ICP-MS) of gabbroic rocks in MOC.

S.No. Element (ppm)	Banded gabbro				Coarse gabbro				Sheared gabbro	
	W1	W11	A4-1	K1-1	D17	D26	A2-2	K3-5	A5-1	A7-2
La	0.51	0.17	0.45	0.42	0.14	0.12	0.46	0.68	1.11	1.11
Ce	1.29	0.29	1.31	1.19	0.33	0.22	1.45	1.65	3.41	2.89
Pr	0.19	0.05	0.21	0.21	0.06	0.04	0.25	0.26	0.6	0.44
Nd	0.99	0.28	1.23	1.25	0.21	0.17	1.47	1.59	3.53	2.32
Sm	0.45	0.19	0.54	0.61	0.15	0.1	0.65	0.9	1.59	1.01
Eu	0.19	0.13	0.34	0.3	0.07	0.05	0.26	0.5	0.57	0.48
Gd	0.77	0.36	1.03	1.03	0.25	0.19	1.06	1.25	2.49	1.71
Tb	0.17	0.08	0.22	0.22	0.09	0.05	0.22	0.32	0.52	0.38
Dy	1.32	0.64	1.55	1.57	0.5	0.37	1.61	1.8	3.68	2.7
Ho	0.31	0.15	0.37	0.35	0.12	0.08	0.36	0.38	0.83	0.63
Er	0.89	0.43	1.07	0.98	0.35	0.25	1.06	1.22	2.42	1.87
Tm	0.14	0.06	0.16	0.15	0.06	0.04	0.17	0.16	0.37	0.29
Yb	0.94	0.4	1	0.94	0.23	0.25	1.06	1	2.33	1.9
Lu	0.16	0.07	0.16	0.15	0.07	0.06	0.17	0.17	0.37	0.32
(La/Sm) _N	0.708	0.559	0.716	0.430	0.583	0.751	0.613	0.472	0.616	0.937
(Tb/Yb) _N	0.769	0.850	0.834	0.995	1.663	1.530	0.810	1.360	0.865	0.594
Other Elements (ppm)										
Ba	27	3	3	9	11	19	18	12	6	6
Th	0.13	0.05	0.05	0.06	<0.009	0.02	0.12	0.15	0.18	0.28
Nb	0.48	0.03	0.3	0.21	<0.018	0.03	0.24	0.11	0.71	0.61
Y	7.71	3.34	9.07	8.44	4	2.07	9.19	7	20.9	16.18
Hf	0.3	0.05	0.31	0.33	0.03	0.03	0.63	0.5	1.07	0.62
Ta	0.04	<0.014	0.02	0.01	0.02	<0.014	0.02	0.141	0.06	0.04
U	0.07	0.02	0.22	0.14	<0.014	0.01	0.06	0.168	0.12	0.14
Pb	1.91	0.14	0.31	0.35	1	0.28	0.16	1	0.39	0.67
Rb	3.9	0.4	0.1	0.6	2	2.4	1.1	0.11	0.6	1.7
Cs	0.15	0.07	0.26	0.08	0.15	0.24	0.24	0.31	0.13	0.46
Sr	115	49	143	143	48	50	120	89	141	215
Sc	46.9	55.1	62.2	69	45	56	52.9	55	41.7	71.9
Zr	8	1	7	8	1	1	16	14	19	16

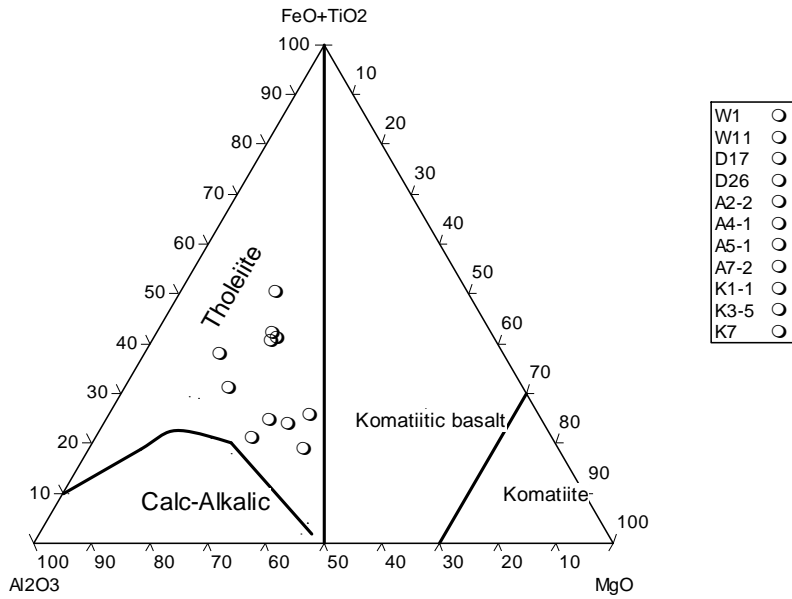


Fig. 4-13 Jenson (1976) plots of gabbroic rocks in MOC showing its tholeiitic character.

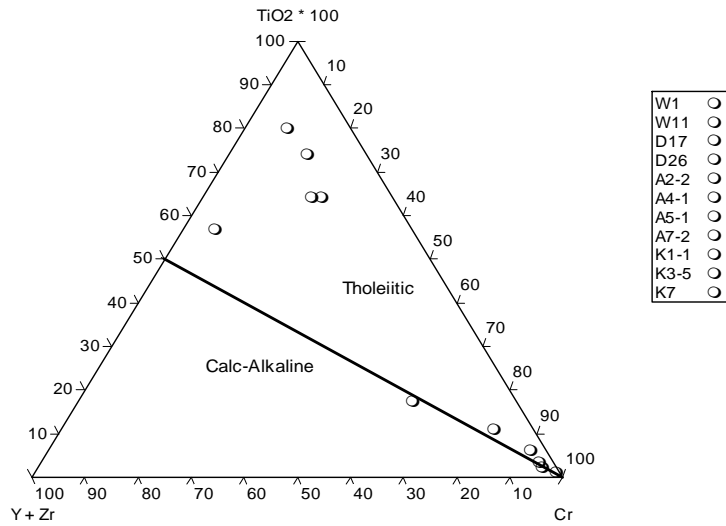


Fig. 4-14 YTC diagrams (Davies et al., 1979 in Shamim Khan, et al., 2005) for gabbroic rocks of MOC indicating their tholeiitic affinity.

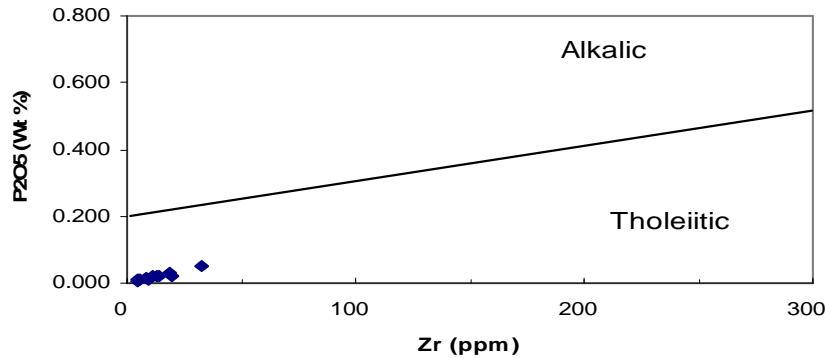


Fig. 4-15 Zr- P₂O₅ suggesting the tholeiitic affinity of gabbroic rocks of MOC.

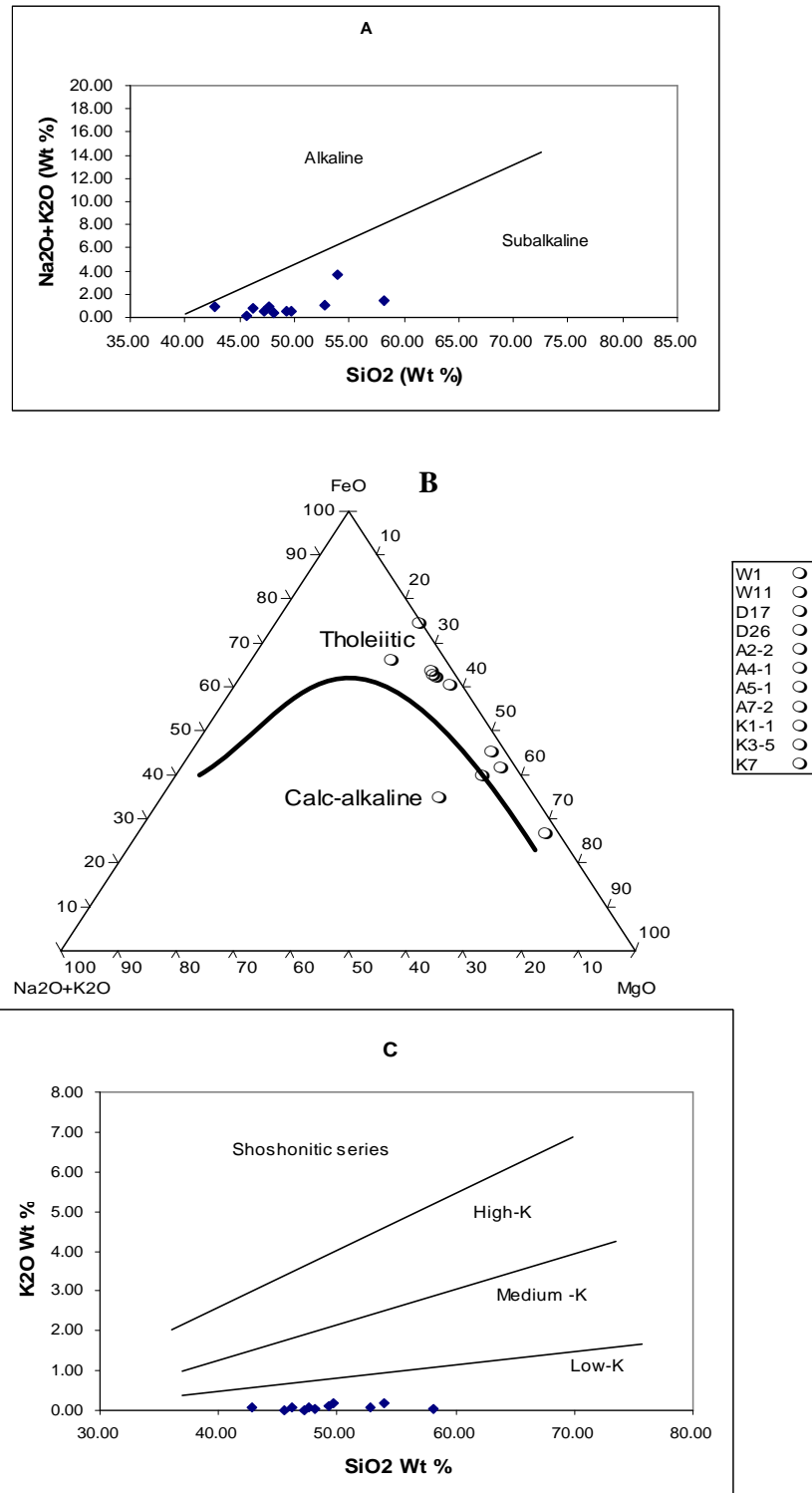


Fig. 4-16 **A**: Total alkali versus silica (Irvan and Baragar, 1971)
B: AFM (Irvan and Baragar, 1971)
C: K₂O versus silica (Le Maitre et al., 1989) diagrams of the gabbroic rock samples from MOC.

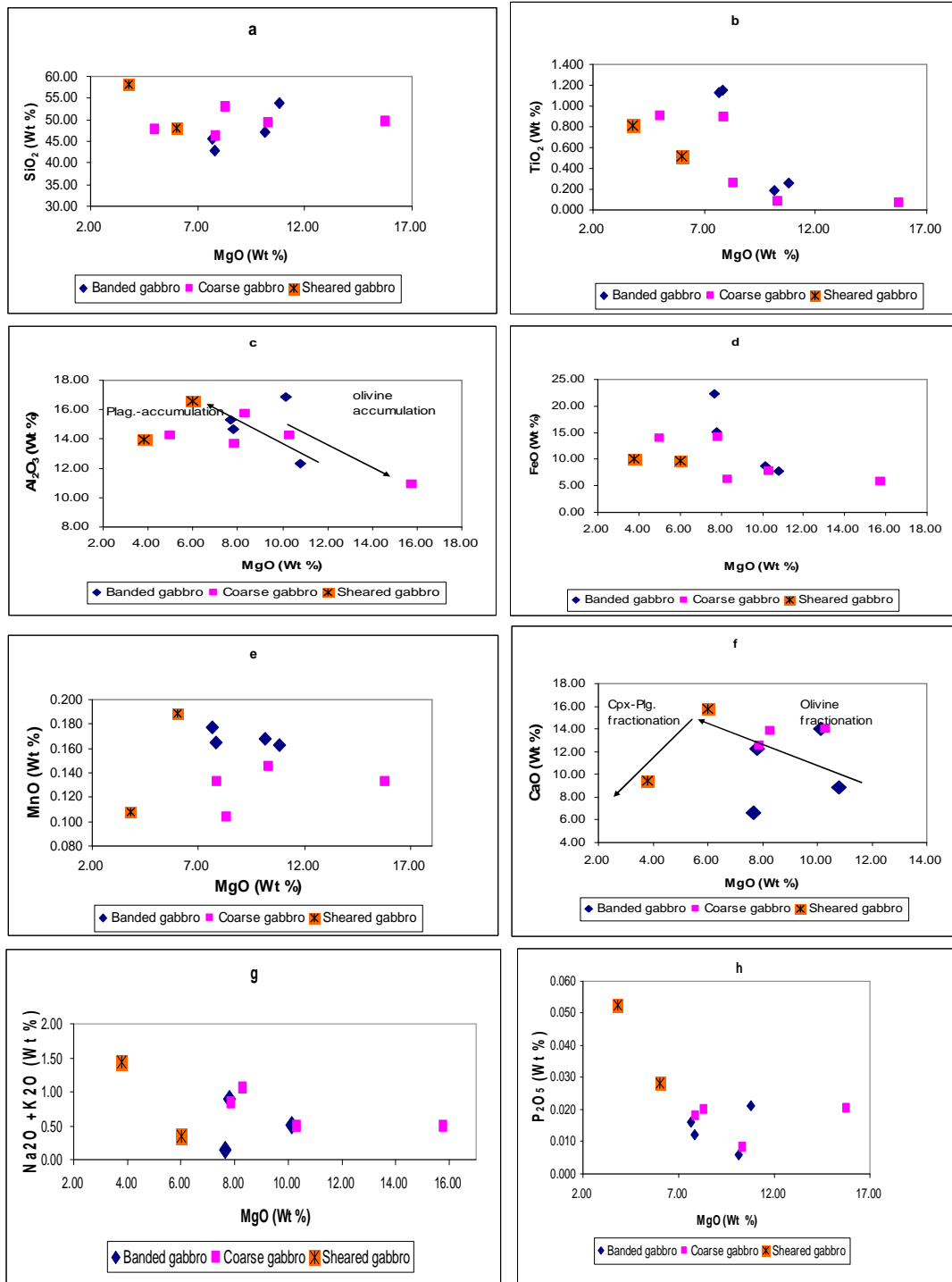


Fig. 4-17 The plots of MgO vs major oxides of gabbro rocks in MOC [Fig.4-17c, and f the trends are from (Boztng et al. 1998)]

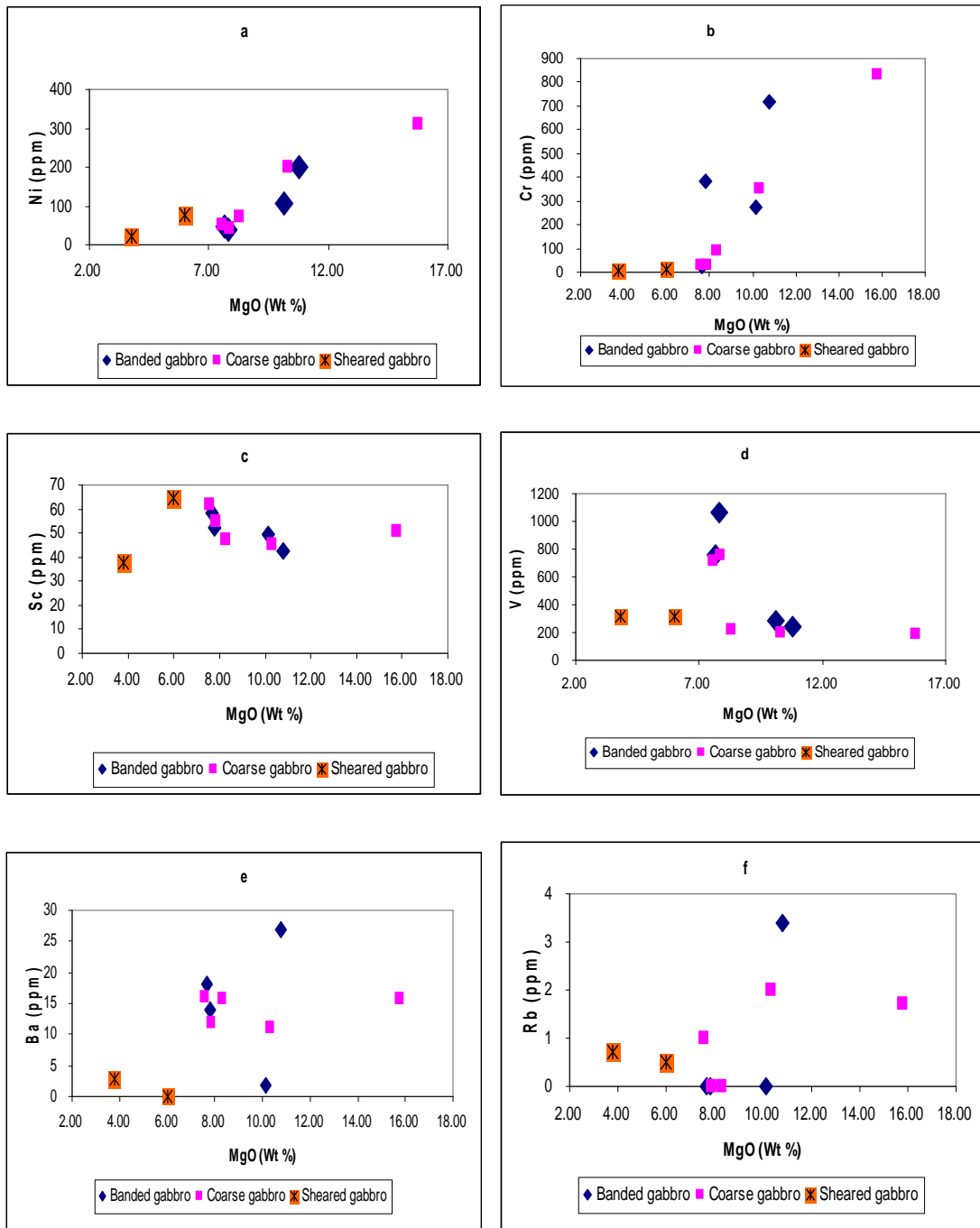


Fig. 4-18 The plots of MgO vs. trace elements of gabbro rocks in MOC.

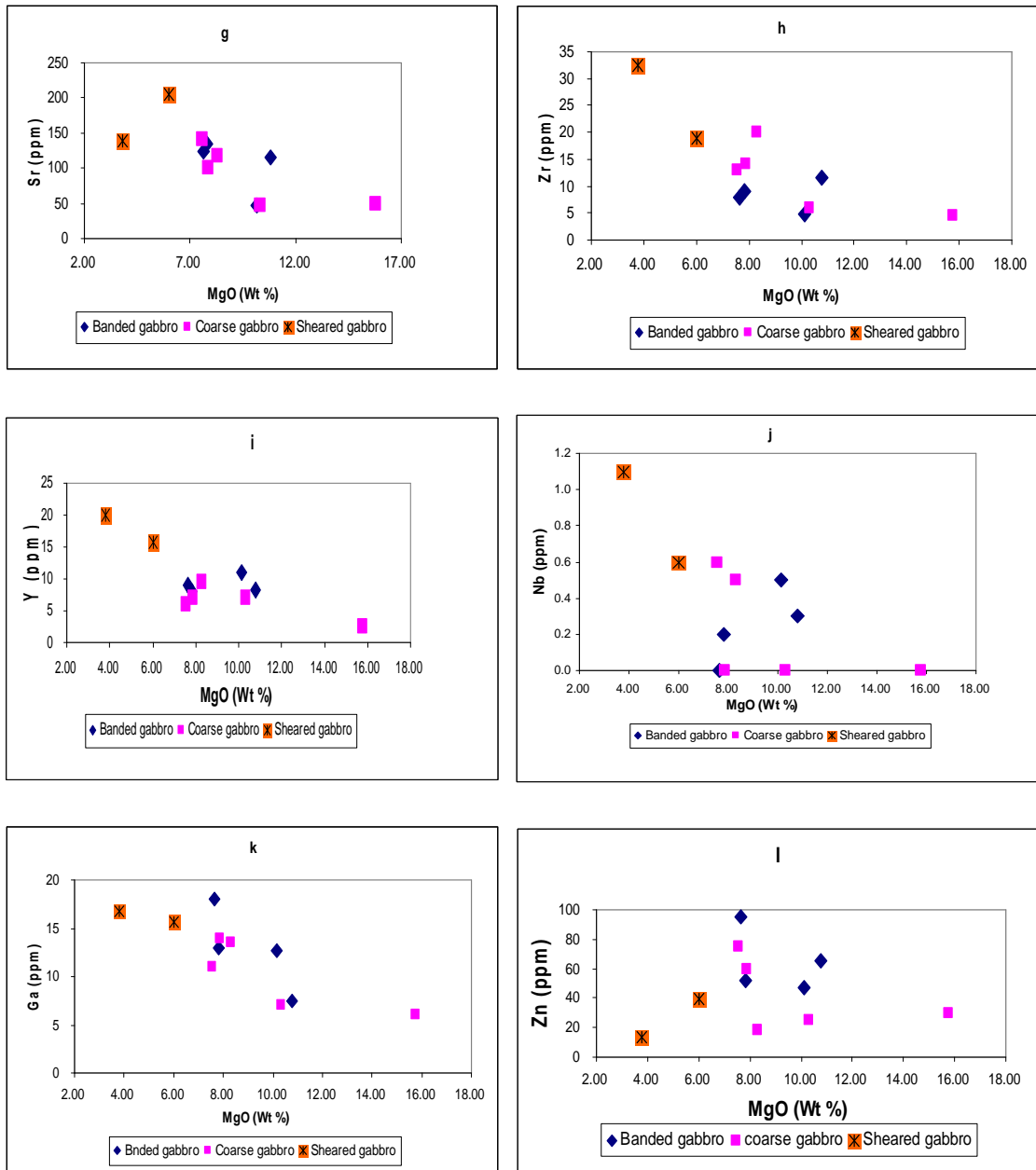


Fig. 4-18 Continued.

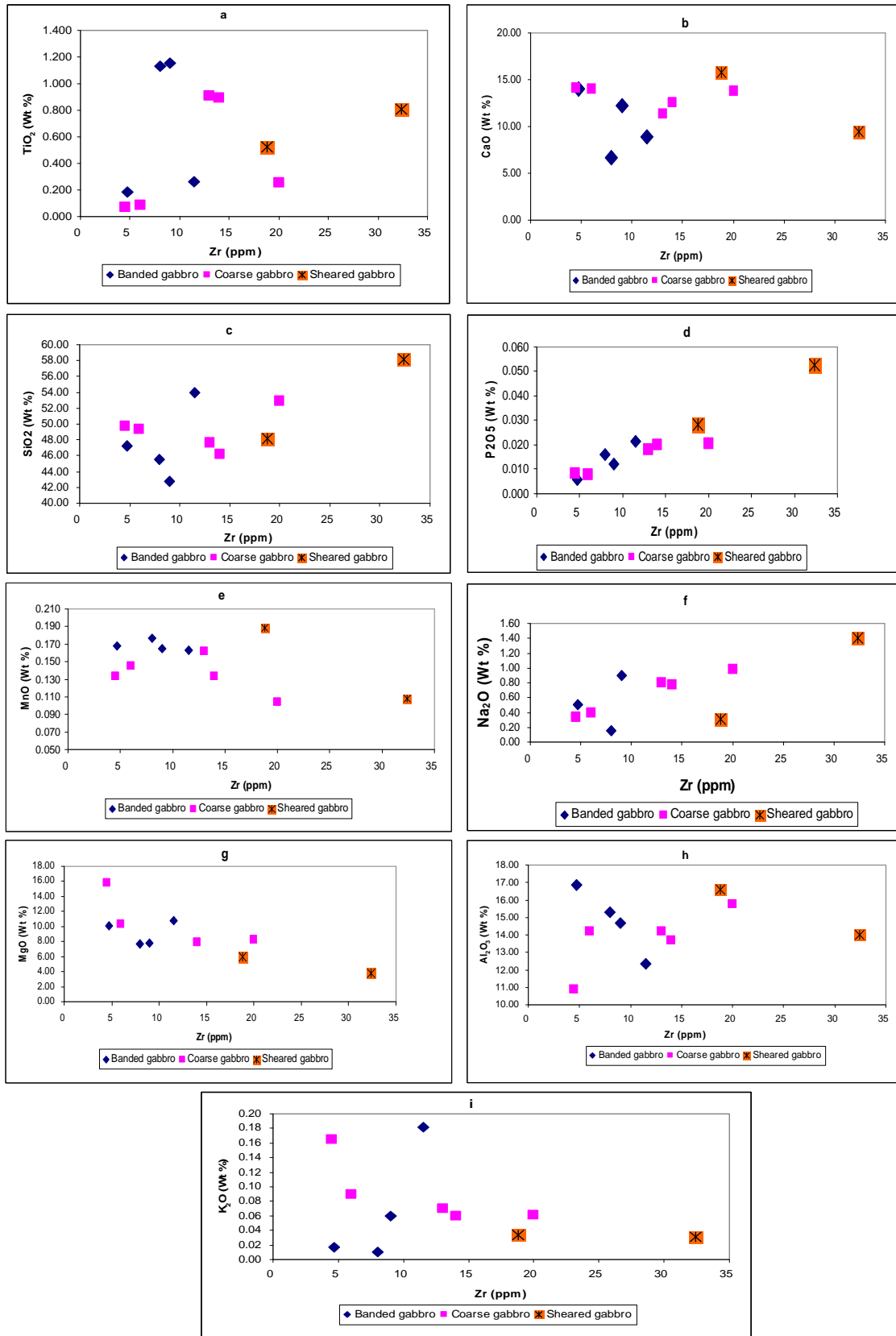


Fig. 4-19 Zr versus major elements plots for basic rocks of MOC.

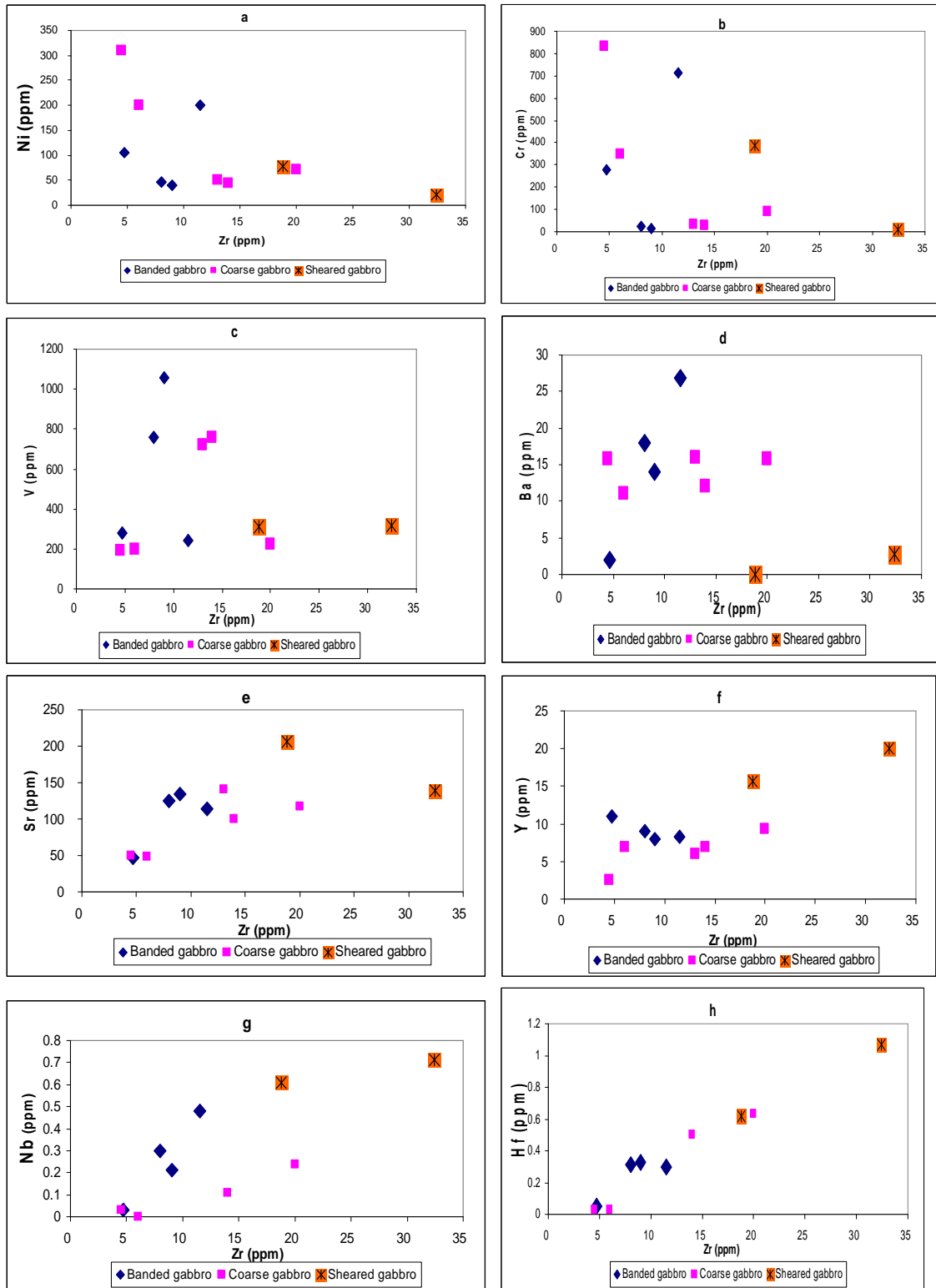


Fig. 4-20 Zr versus trace elements plots for basic rocks in MOC.

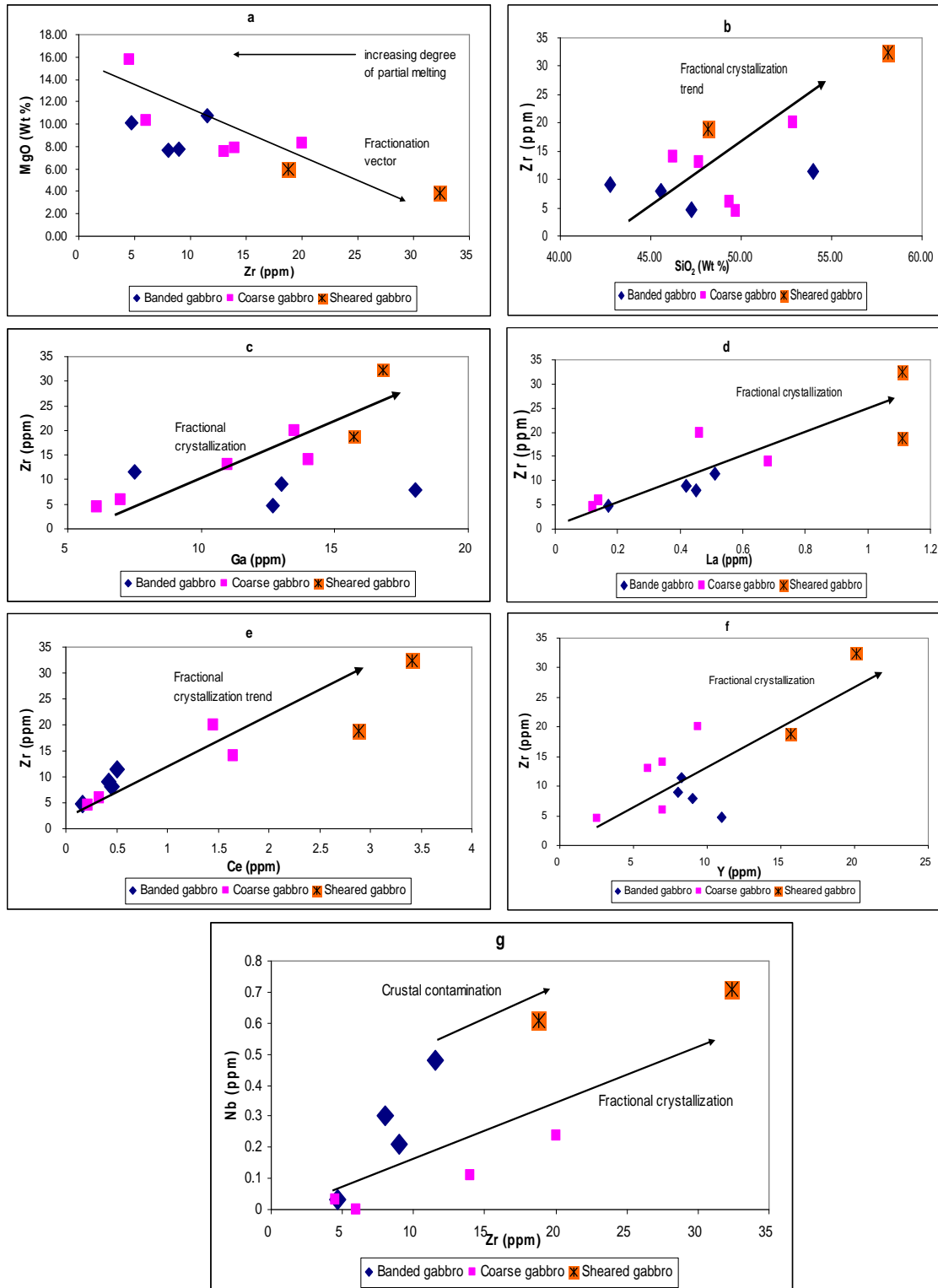


Fig. 4-21 Some selected geochemical diagrams representing fractional crystallization process in the MOC gabbroic rocks (the trends and field are from Wilson (1989)).

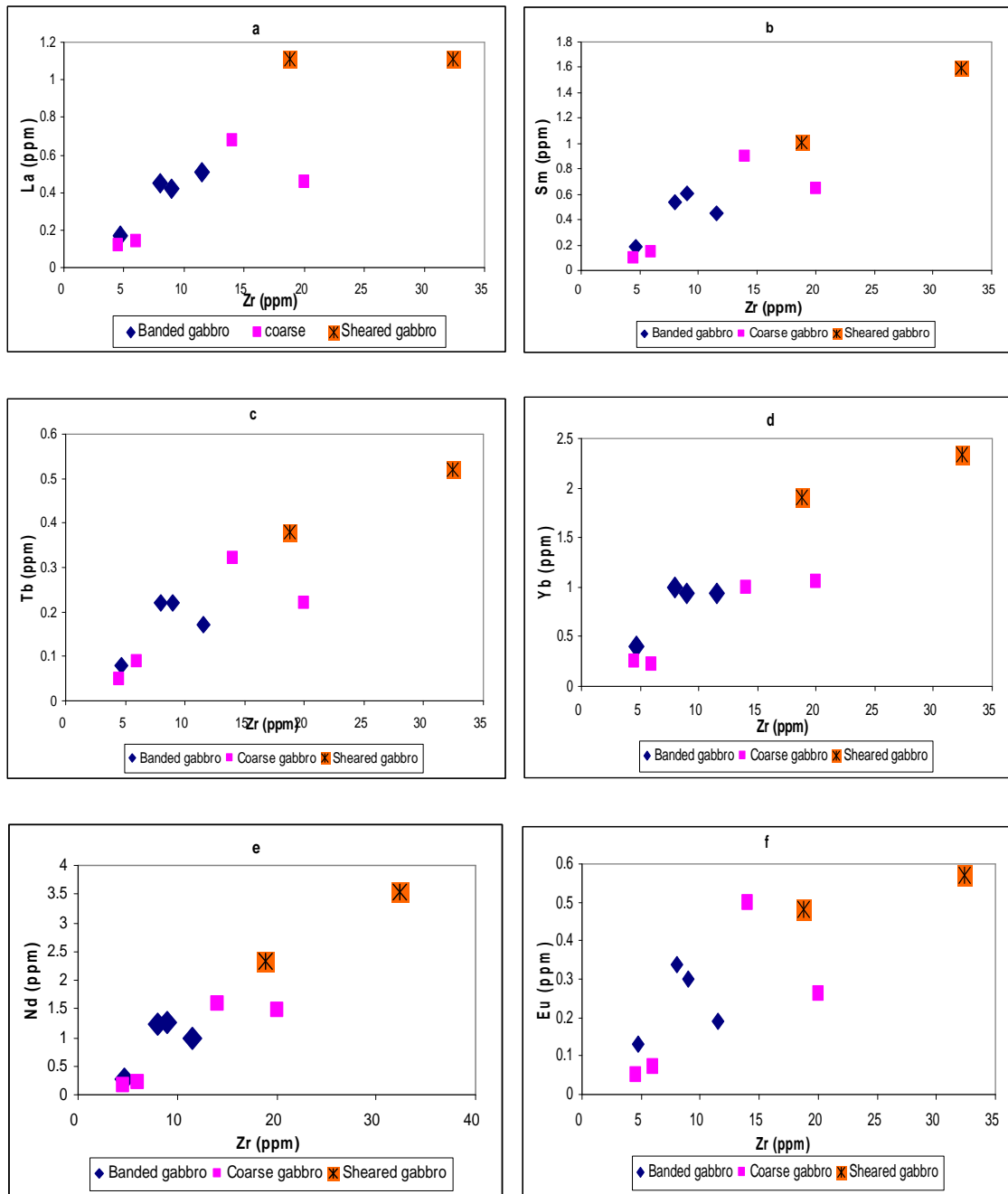


Fig. 4-22 Zr vs. rare earth elements plots in the MOC basic rocks.

4.2.2 REE geochemistry and trace elements of the gabbroic rocks in MOC

The most reliable tests to detect possible alteration and effect of metamorphism on the REE geochemistry of gabbroic rocks from MOC are the plots of REE against Zr (Fig. 4-22). These plots show that the REE abundances for gabbroic rocks in MOC have a systematic increase with increase of Zr concentrations, which suggest that the overall REE patterns have not changed significantly by alteration and / or metamorphism.

The chondrite-normalized REE patterns for basic rocks from MOC are presented in (Fig. 4-23) using normalizing values published by O'Neill and Palme (1998). The patterns show light rare element LREE (La to Sm) depletion [$(La / Sm)_N = 0.43-0.93$] and flat middle and heavy REE (MREE, HREE) patterns with [$(Tb/Yb)_N = 0.59-1.66$]. The very minor positive Eu-anomaly relative to neighboring elements reflects the substitution of Eu for Ca in the Ca-rich plagioclase (Rollinson, 1993). The overall patterns of gabbroic rocks are akin to flat lying REE patterns. Such flat lying patterns resemble the rocks formed in island arc tholeiitic (IAT) and subduction-related setting (Shamim, et al., 2005).

The multielement patterns (spider diagram) normalized to chondrite composition using normalizing values published by O'Neill and Palme (1998) are presented in (Fig. 4-24). The similar trace element patterns of all samples are indicative of their evolution from a single magmatic source.

The spider diagram shows the positive anomalies of Ba, Sr and U relative to neighboring elements and exhibit variable degrees in all samples. A positive Sr-anomaly can be explained by its substitution for Ca in plagioclase. Moreover the U enrichment in all samples indicates that the source was probably not a material enriched in highly incompatible elements such as the upper crust. The relative depletion in LREE and Nb also suggests a lower crustal source origin (Taylor and McLennan, 1985) and is typical for magmas generated in the suprasubduction mantle wedge (Duclaux et al., 2006). The selective enrichment of Sr, Ba and lack of enrichment of others (Zr, Ti, Y)

exhibited by the tholeiitic rocks are characteristic of a suprasubduction zone setting where boninitic and tholeiitic magma mixing occurs (Pearce et al., 1984).

The negative anomalies of high field strength elements (HFSEs)- (Th, Nb, Zr, and Hf), and Pb relative to neighboring elements are shown by all studied samples. The depletion of these conservative elements is a characteristic of decoupling of large ion lithophile elements LILEs (Cs,Rb, Ba, and Sr) and HFSEs during dehydration of subducting slab (Shawna et al., 2003).

Another possible explanation for depletion of HFSEs by Harmar and Von, (1991), involves crustal contamination during emplacement with an arc signature. On the other hand (John et al., 2004) explained that the processes such as fractional crystallization, metamorphism and crustal contamination can be the source of the HFSEs depletion in the gabbroic rocks.

The HFSEs depletion of the gabbroic rocks in the MOC can be evidenced in some diagrams based on the variation of Zr versus Nb (Fig. 4-21g) which indicates that the fractional crystallization and the nature of magmatic melt from which the MOC was crystallized.

In general the most distinctive features exhibited by the spider diagrams of gabbroic rocks in MOC are selective enrichments of certain elements (Sr, Ba and U) and the relative lack of enrichment of others (Zr, Y and Hf). These patterns and the HFSEs variations exhibited by tholeiitic rocks are characteristic of a supra-subduction zone (SSZ) setting (Pearce et al. 1984, and Resimic-Saric et al., 2004).

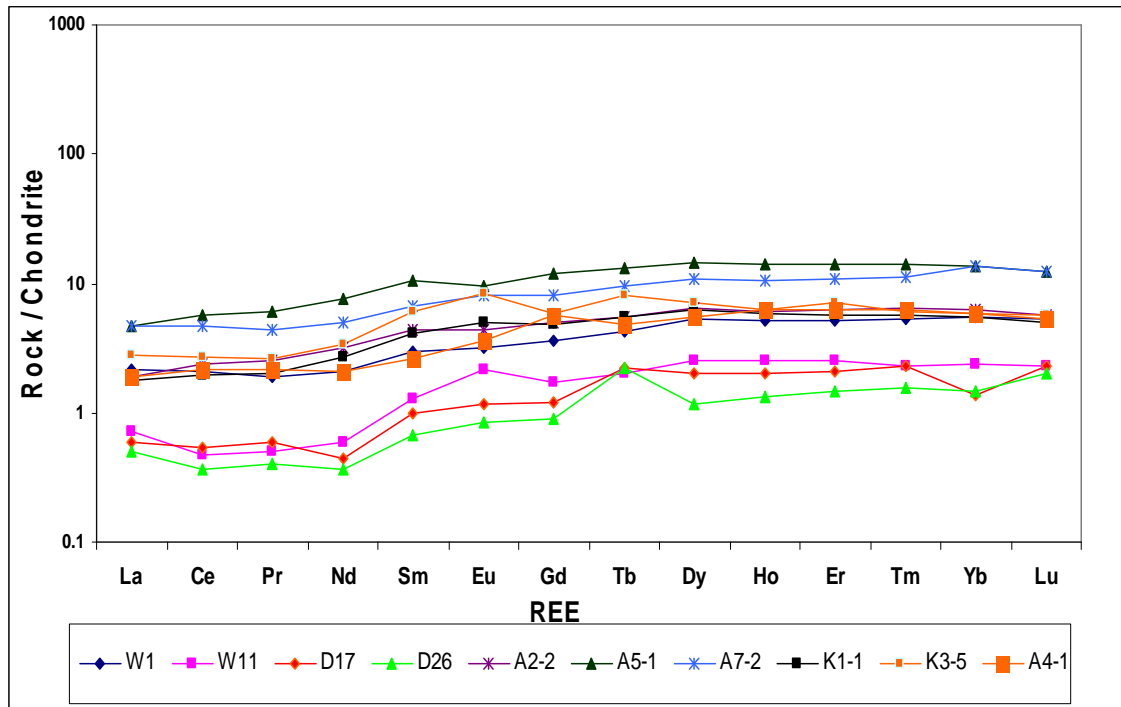


Fig. 4-23 Chondrite-normalized REE patterns of gabbroic rocks in MOC.

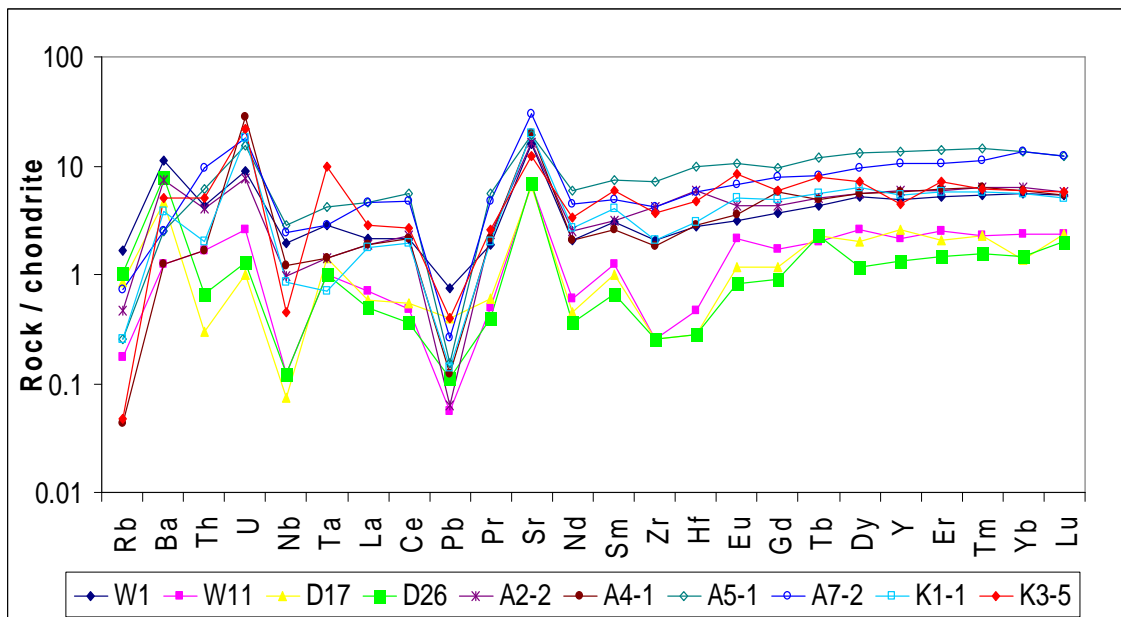


Fig. 4-24 Chondrite-normalized spider diagrams of gabbroic rocks in MOC.

4.3 Mineral chemistry

Plagioclase, amphiboles, pyroxene, chlorite and opaque minerals were analyzed in three samples of gabbroic rocks from MOC by electron probe microanalyses at Washington State University. These samples represented coarse, banded and sheared gabbro and the results of analyses were summarized in (Table 4-4).

The plagioclases from banded and coarse gabbro are Ca rich and classify as anorthite ($An_{91} - An_{96}$). Plagioclase from sheared gabbro is relatively more sodic (An_{50}) and represents labradorite (Fig. 4-25). The variation in plagioclase compositions from different types of gabbroic rocks in the studied area may be related to fractional crystallization process, which became more sodic plagioclase with progressive magma differentiation (Shawna et al., 2003).

The amphiboles compositions were determined based on the classification of Leak, et al., (1997). These data show that the composition of the amphibole ranges from actinolite to tschermarkite in banded and coarse gabbro and is represented by actinolite in sheared gabbros (Fig. 2-29).

The clinopyroxene of gabbroic rocks in MOC are classified as low Ti diopside according to Yalinzi and Goncuoglu (1999), (Fig. 4-26). Ti in clinopyroxene reflects the degree of depletion of the mantle source and Ti activity of parent magma that generated the cumulate pile (Pearce et al., 1984). The low Ti content of clinopyroxene in the MOC gabbros is 2-3 times lower than those from MORB, this is indicative of crystallization of clinopyroxene from Ti-poor magma. The clinopyroxenes composition is in the range of $Wo_{48.1} En_{44.27} Fs_{4.38}$ to $Wo_{48.6} En_{47.5} Fs_{7.3}$.

SiO_2 contained ranges from 52.22 to 54.03 Wt % and Mg # ranges between 0.8 to 0.9. Ti/Al ratios are less than 0.43. On the bases of the Ti content, clinopyroxenes from MOC gabbroic rocks are similar to samples from other ophiolitic suprasubduction zone such as Troodos, Oman (Beccaluva, 1998 in Yaliniz and Goncuoglu, 1999).

The chlorite in the gabbroic rocks of MOC appears as an alteration product and replaces some of amphiboles and account for up to 11 modal % .The SiO_2 content ranges between 31.2 to 32.01 wt% and FeO content (< 3 Wt %).

The $Fe\# = (Fe/Fe+Mg)$ atomic ratio is normally below 0.1. Based on Hey (1954) the chlorites were classified as clinocllore and pennite (Fig 3-18 a, b). Opaque minerals in three samples were analyzed to determine the oxide mineral compositions (Table 4-4). The three oxide analyses are plotted on the ternary diagram of Cr_2O_3 - Al_2O_3 - Fe_2O_3 by Steven (1944) (Fig. 4-27). The composition of opaque minerals is chromite if ($Cr_2O_3 > Al_2O_3 + Fe_2O_3$) and it is spinel if ($Fe_2O_3 < Al_2O_3 + FeO$), where as it is magnetite if it ($Fe_2O_3 > Al_2O_3 + FeO$) (Steven 1944). Accordingly all analyzed opaque minerals in gabbroic rocks of the studied area represent chromian magnetite and secondary magnetite (Fig. 4-27).

Table 4-4 Microprobe analyses for mineral composition of different types of gabbroic rocks in MOC. Mgf#: $Mg/(Mg+Fe^{2+})$, Fe²⁺#: $Fe^{2+}/(Fe^{2+}+Mg)$ atomic ratio

Oxide	S.M.O																				
	Mineral		D26 Pl (C.G)	W10 Pl (B.G)	A6-2 Pl (S.G)	D26 CPX (C.G)	W10 CPX (B.G)	W10 CPX (B.G)	D26 Magn (C.G)	W10 Magn (B.G)	A6-2 Magn (S.G)	D26 Amph (C.G)	W10 Amph (B.G)	W10 Amph (C.G)	A6-2 Amph (S.G)	D26 Amph (B.G)	W10 Amph (B.G)	D26 Chlo (C.G)	W10 Chlo (B.G)		
SiO ₂			44.102	46.040	53.610	53.500	53.220	54.030	0.021	0.200	0.138	54.384	54.932	54.538	54.980	55.074	39.680	42.868	32.012	31.202	
Al ₂ O ₃			36.352	36.050	30.030	1.265	1.403	1.830	0.550	0.030	0.049	2.528	2.459	2.491	2.292	2.224	14.500	14.762	15.061	16.481	
TiO ₂			0.009	0.000	0.000	0.065	0.370	0.000	0.005	0.540	0.765	0.091	0.074	0.114	0.064	0.074	1.960	1.000	0.021	0.033	
FeO			0.200	0.196	0.150	3.146	2.867	4.800	4.300	0.000	0.000	6.089	5.990	6.940	6.828	6.263	15.980	12.414	1.703	2.243	
Fe ₂ O ₃			0.000	0.000	0.000	0.000	0.000	0.000	100.038	95.450	93.832	0.000	0.000	0.000	0.000	0.000	0.000	0.000	0.000	0.000	
MnO			0.009	0.027	0.000	0.112	0.118	0.000	0.200	0.006	0.120	0.161	0.099	0.260	0.150	0.245	0.080	0.140	0.006	0.008	
MgO			0.404	0.000	0.170	16.825	17.412	15.280	16.600	0.650	0.440	0.488	19.672	19.905	19.285	19.581	19.553	9.610	10.657	32.706	32.757
CaO			18.553	18.073	12.070	24.488	24.131	24.010	24.350	0.005	0.030	0.024	12.870	13.044	12.925	13.008	12.640	12.748	0.020	0.006	
Na ₂ O			0.384	0.763	4.040	0.075	0.081	0.260	0.000	0.007	0.020	0.036	0.208	0.098	0.175	0.088	1.870	1.082	0.002	0.045	
K ₂ O			0.010	0.020	0.080	0.012	0.008	0.000	0.000	0.001	0.020	0.006	0.028	0.008	0.017	0.003	0.008	1.490	1.020	0.027	0.041
NiO			0.008	0.000	0.000	0.057	0.062	0.000	0.000	0.085	0.240	0.216	0.039	0.030	0.030	0.064	0.026	0.000	0.022	0.152	0.180
Cr ₂ O ₃			0.015	0.100	0.000	0.461	0.446	0.230	0.000	0.023	3.300	3.905	0.303	0.145	0.132	0.158	0.147	0.050	0.018	2.493	2.605
Totals			100.009	100.269	100.160	98.726	100.085	100.000	100.030	100.263	100.380	99.567	96.311	96.945	96.947	97.006	96.620	97.920	97.891	84.203	85.585
O=			8.000	8.000	8.000	6.000	6.000	6.000	4.000	4.000	4.000	4.000	23.000	23.000	23.000	23.000	23.000	23.000	23.000	28.000	28.000
Si			2.001	2.118	2.401	1.940	1.946	1.938	1.973	0.003	0.008	0.005	7.708	7.728	7.705	7.742	7.774	5.990	5.637	6.225	6.001
Al			1.997	1.883	1.603	0.055	0.060	0.079	0.024	0.001	0.001	0.002	0.422	0.408	0.440	0.381	0.370	2.580	2.234	3.452	3.736
Ti			0.000	0.000	0.000	0.002	0.002	0.010	0.000	0.000	0.017	0.023	0.010	0.008	0.012	0.006	0.008	0.220	0.112	0.003	0.005
Cr			0.001	0.003	0.000	0.014	0.013	0.007	0.000	0.001	0.109	0.118	0.034	0.016	0.015	0.018	0.016	0.010	0.002	0.383	0.396
Fe			0.008	0.007	0.006	0.098	0.087	0.144	0.128	2.990	3.320	2.793	0.722	0.705	0.820	0.805	0.739	2.020	1.890	0.277	0.361
Mn			0.000	0.001	0.000	0.004	0.004	0.000	0.006	0.000	0.004	0.005	0.012	0.031	0.018	0.029	0.010	0.020	0.016	0.001	0.001
Mg			0.027	0.000	0.012	0.932	0.944	0.867	0.904	0.003	0.027	0.028	4.157	4.174	4.061	4.117	4.115	2.160	2.334	9.461	9.392
Ca			0.952	0.883	0.579	0.975	0.956	0.937	0.955	0.000	0.001	1.954	1.966	1.966	1.934	1.967	2.040	1.951	0.004	0.001	
Na			0.034	0.085	0.388	0.005	0.006	0.010	0.000	0.001	0.002	0.033	0.027	0.048	0.027	0.045	0.530	0.300	0.001	0.017	
K			0.001	0.001	0.005	0.001	0.000	0.000	0.000	0.001	0.000	0.005	0.001	0.003	0.000	0.001	0.290	0.252	0.007	0.010	
Ni			0.000	0.000	0.000	0.002	0.002	0.000	0.000	0.008	0.007	0.004	0.003	0.003	0.007	0.003	0.000	0.002	0.024	0.028	
Mgf#			0.771	0.000	0.667	0.905	0.915	0.858	0.876	0.001	0.008	0.010	0.852	0.856	0.822	0.836	0.848	0.517	0.553	0.972	0.963
Fe #			0.229	1.000	0.333	0.095	0.065	0.142	0.124	0.999	0.992	0.148	0.144	0.168	0.164	0.152	0.483	0.447	0.028	0.037	

amph. Amphibole, Chlo. Chlorite, CPX, Clinopyroxene, Mag. Magnetite, C.G: coarse gabbro, B.G. Banded gabbro, S.G.: Sheared gabbro.

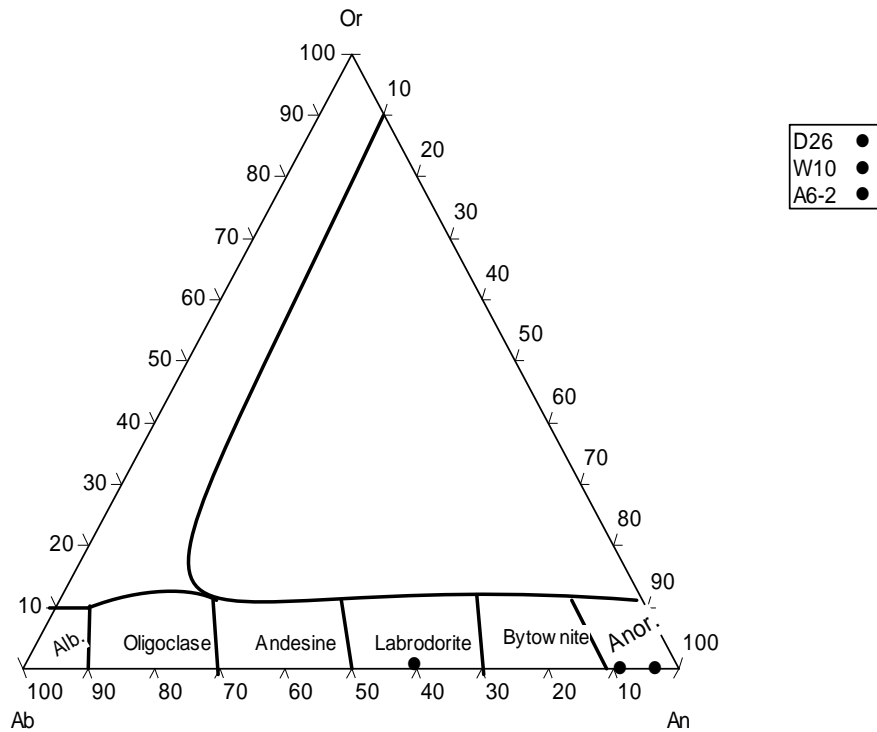


Fig. 4-25 Composition variation of plagioclase in gabbroic rocks of MOC. Field are from Klein et al. (1993).

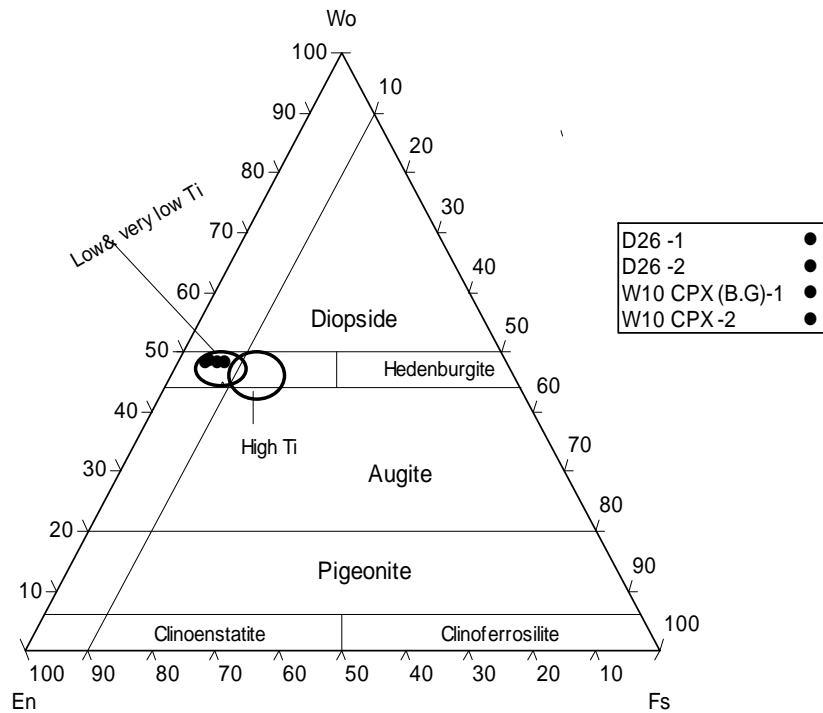


Fig. 4-26 Pyroxene compositions in the system Wo-En-Fs general compositional field are from Beccaluva et al., (1989).

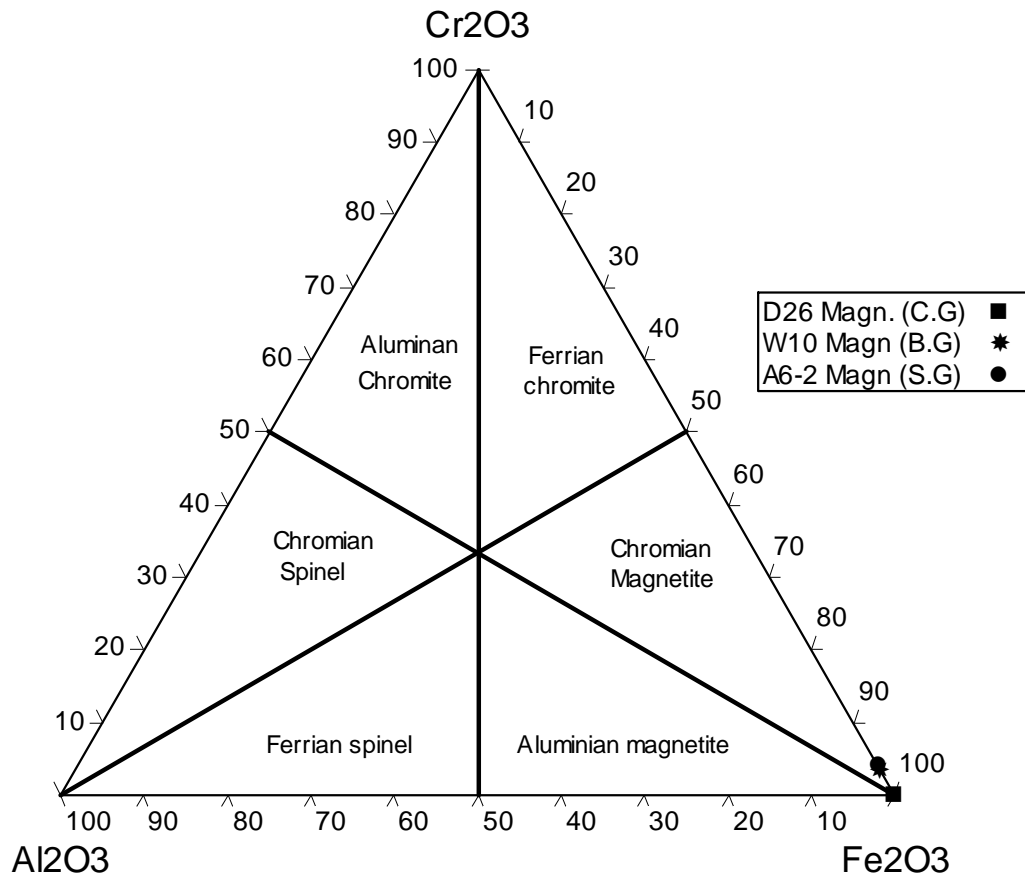


Fig. 4-27 Cr₂O₃-Al₂O₃-Fe₂O₃ diagram opaque minerals in gabbroic rocks of MOC. (Steven, 1944).

Chapter Five Genesis of Ultrabasic and Chromitite Rocks

In order to clarify the genesis of ultrabasic and chromitite rocks of MOC, the calculated geothermometry, partial melting and a comparison between studied ophiolite with local and regional ophiolites were used.

5.1 Geothermometry

Many methods can be applied to determine the geothermometry of metasomatized and unmetasomatized peridotite. These methods are (1) the two pyroxene (orthopyroxene and clinopyroxene) equilibrium temperature by Wells (1977), and Bohlen, et al. (1979). In this method the temperature dependence of solution of enstatite in diopside provides the original calibration of two pyroxene thermometer for end-member compositions. (2) Olivine-spinel geothermometer (Roder et al., 1979). This method was first treated by Irvan, (1965, 1967) and formulated by Jackson (1969). This method yields magmatic temperature when applied to plutonic rocks. Evan and Wright (1972) have demonstrated that the olivine-spinel geothermometer give temperatures in excess of 2000°C, therefore (Roder et al. 1979) made re-evaluation of this geothermometer as:

$$K_d = [X_{Mg} / X_{Fe^{2+}}]_{\text{olivine}} [X_{Fe^{2+}} / X_{Mg}]_{\text{spinel}}$$

Where

K_d = equilibrium constant.

X = mole fraction in solid solution ($Mg / (Mg + Fe^{2+})$) and $Fe^{2+} / (Mg + Fe^{2+})$.

For the present study the olivine-spinel geothermometer of Roder et al. (1979) was applied for calculating the temperature of formation in dunite, harzburgite, and chromitite rocks.

The temperature of formation obtained from this equation varies from (1260-1380°C average is 1336°C) in chromitite and ranges between (1200-1250°C, the average is 1209°C), (1180 -1410°C the average 1278°C), in dunite, and

harzburgite respectively (Table 5-1). These values correspond to the temperature of formation of Alpine-type peridotite, as reported in Burro Mountain in California (Loney et al. 1971) and (Massif due Sud, New Caledonia) (Rodgers, 1973) and (Buda, 1988). The determined temperature shows variation ranges which is related to the alteration and the wide ranges of variation in temperatures of studied samples are related to the subsolidus re-equilibration between spinel and olivine during the post-magmatic process (Ahmad Hassan, personal communication, 2007).

The estimated temperatures of formation of chromites in MOC by Buda (1988) and Buda and Al-Hashimi (1972) was 1350 °C in dunite and harzburgite and (1200-1250 °C) in chromitites. These values also show variation range and they are close to variation of the calculated temperature in this study.

Table 5-1 Calculated temperatures of formation for studied samples according to Roeder (1979).

Samples	Olivine		chromite		lnK _d	Temperature C°
	X Mg	X Fe	X Mg	X Fe ²⁺		
Chromitite						
W26	0.930	0.070	0.443	0.557	2.809	1320
W26	0.933	0.067	0.465	0.535	2.769	1330
W26	0.931	0.069	0.465	0.535	2.749	1355
W29	0.914	0.086	0.413	0.587	2.712	1370
W29	0.912	0.088	0.344	0.656	2.986	1260
W30	0.953	0.047	0.576	0.424	2.699	1380
Dunite						
R10-2	0.920	0.080	0.350	0.647	3.060	1200
R10-2	0.920	0.080	0.330	0.669	3.140	1205
W20	0.895	0.105	0.209	0.791	3.470	1100
W21	0.909	0.091	0.399	0.601	2.713	1250
W21	0.912	0.088	0.402	0.598	2.730	1250
W21	0.914	0.086	0.410	0.590	2.730	1250
Harzburgite						
R7	0.912	0.088	0.520	0.480	2.269	1410
W36	0.896	0.104	0.300	0.700	2.990	1250
W36	0.893	0.107	0.350	0.650	2.768	1310
K7-5	0.902	0.098	0.320	0.680	3.010	1250
K7-5	0.905	0.095	0.460	0.540	2.420	1180
A1-5	0.910	0.090	0.360	0.640	2.800	1270

5.2 Oxygen fugacity of chromian spinel in MOC chromitite

The Fe^{3+} content of spinel is the function of oxygen fugacity and the low Fe^{3+} content of chromian spinel $\text{Fe}^{3+\#}$ [$\text{Fe}^{3+} / \text{Cr} + \text{Al} + \text{Fe}^{3+}$] ~ 0.1] in chromitite is the key to the origin of chromitite (Hill and Roeder, 1974, Arculus, 1994, Klingenberg and Kushiro, 1996). In mantle-derived spinel peridotites the oxygen fugacity is relatively constant [$\Delta \log f\text{O}_2$ (FMQ) (relative to the fayalite-magnetite-quartz buffer) = -1.5 - +1.5; Wood 1991]. Even though some arc-related mantle peridotites indicate more oxidized conditions [$\Delta \log f\text{O}_2$ (FMQ) < +2], the Fe^{3+} contents of their spinels are very low ($\text{Fe}\# < 0.2$) (Parkinson and Arculus 1999, Parkinson and Pearce, 1998). In the mantle – melt reaction, therefore, the melt should strongly control the conditions under which Fe^{3+} - rich / or Fe^{3+} -poor spinel will crystallize. On the other hand, the high $f\text{O}_2$ in peridotites reflects the interaction of peridotites with percolating hydrous melt. This melt possibly formed in SSZ (Uysal et al., 2007).

In the MOC chromitite rocks, the chromian spinels which have Cr# range between (0.67-0.8) and Fe^{3+} are around zero values which have slightly high oxygen fugacity (0.07- 0.08) and in dunite and harzburgite have (0.06 -1.0) above the FMQ buffer (Fig. 5-1). Parkinson and Arculus, (1999), Uysal et al. (2007) reveal a positive correlation between $f\text{O}_2$ and spinel Cr# they suggest that partial melting process influences the redox state. Accordingly, it could be suspected that a high oxidized melt generated within deeper mantle has the potential to crystallize the high Cr# spinel. The MOC chromian spinel is characterized by oxygen fugacity $f\text{O}_2 \Delta \log^{\text{FMQ}}$ between (0.06-1.0), slightly above the fayalite-magnetite-quartz buffer.

The temperature calculation and oxygen fugacity suggest that the investigated chromitite and peridotite were subsequently affected by interaction with boninitic melt in which the high-Cr# chromitites were formed within the mantle wedge in a suprasubduction zone.

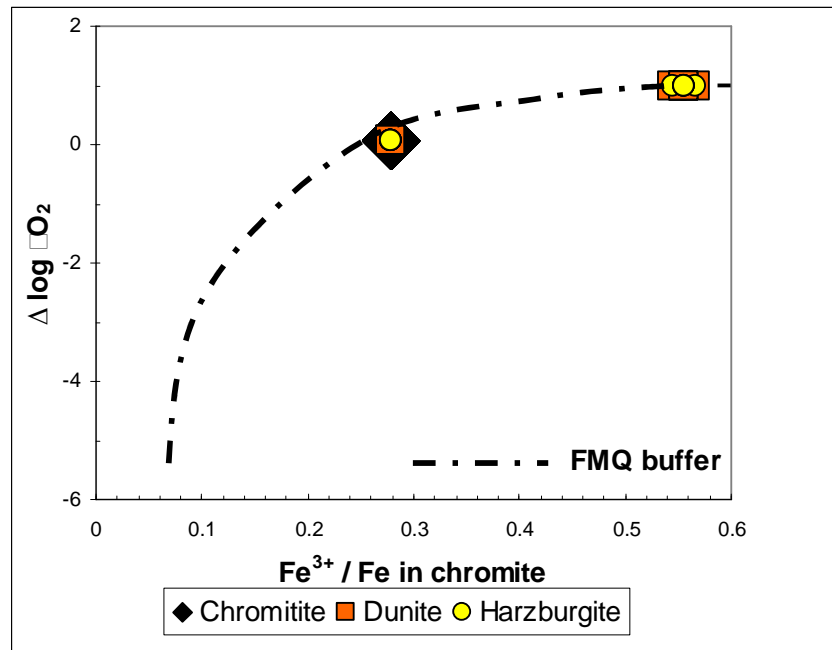


Fig. 5-1 Plots of $\Delta \log fO_2$ vs. $Fe^{3+} / \Sigma Fe$ of chromite in chromitite, dunite, and harzburgite of MOC. showing the range of FMQ buffer (Parkinson & Richard, 1999).

5.3 Partial melting

It is well known that clinopyroxene is the phase consumed most rapidly during partial melting in the spinel facies. Therefore, modal mineralogy of peridotite is a useful tool to formulate the partial melting model. However, Dick and Fisher, (1984) suggest that the clinopyroxene content of peridotites reflects only the degree of depletion, whereas the forsterite content of the olivine is a measure of total degree of melting as olivine-melt equilibria are not changed substantially by H_2O (Gaetani and Grove 1998). Based on these criteria, the Mawat peridotites with very low modal clinopyroxene and high forsterite olivine are highly depleted and have undergone high degrees of partial melting. Aluminum contents in pyroxene and spinels are known to be sensitive to the degree of mantle melting, decreasing systematically with increasing depletion of peridotites (Dick and Nattland 1996, and Zhou et al., 2005).

The Al_2O_3 contents of orthopyroxene and clinopyroxene in Mawat peridotites are correlated with Cr# of coexisting spinel (Fig. 5-2a and b). The depleted harzburgite and dunite have low Al_2O_3 contents in orthopyroxene and clinopyroxene for a given Cr# of spinel and plot within the fore-arc fields, clearly following a depletion trend. The systematic increase in Cr# of spinel

from harzburgite towards dunite is considered to have resulted from partial melting and melt extraction process. Therefore, chromian spinel is regarded as one of the best indicators of partial melting process in mantle peridotites (Matsukage and Kubo 2003, Tamura and Arai 2006).

The Cr# vs. Mg# of spinels is inversely correlated, consistent with increasing degree of partial melting (Fig. 5-3). According to this trend, the Mawat peridotite shows a narrow variation of spinel melting, which is regarded as the main reason for near homogeneity within the upper mantle (Takazawa et al. 2000). Compared with modern oceanic setting, most of spinels in clinopyroxene harzburgite fall in the field of abyssal peridotites whereas those of spinels in depleted harzburgite and dunite are plotted within overlapping field of abyssal and fore-arc peridotite. Some of the samples containing high-Cr chromian spinel plotted within the overlapping field of fore-arc peridotite and boninite. The increasing Cr# up to 0.77 and low TiO₂ content of spinel suggest a linkage to boninite melt. For the relationship between the Fo content of olivine and Cr# of spinel, all rock types fall into the olivine-spinel mantle array (OSMA) of Arai (1994a), which is regarded as evidence for their residual origin, showing a trend caused by partial melting (Fig. 2-26).

In order to explain the melting process better, we used the bivariate plot subduction conservative elements such as V vs. Yb shown in (Fig. 5-4). The plot of V vs. Yb is useful as depletion trends are strongly dependent on oxygen fugacity (Parkinson and Pearce, 1998, Pearce et al., 2000). In the low oxygen fugacity conditions, vanadium has high mineral-melt partition coefficients and thus less rapidly depleted during mantle melting whereas partition coefficient is low when oxygen fugacity is high. Melt formed in suprasubduction zone, have high oxygen fugacities, therefore, it should have high V contents and their mantle residues should have correspondingly a low ratio (Pearce et al. 2000). For the Mawat rocks, V vs. Yb values follow the FMQ-1 to FMQ+1 trends and indicate that these rocks are oxidized relative to reduce mantle. The lherzolite is located mainly between FMQ-1 and FMQ+1 line with approximately 7-17 partial melting, the harzburgite and dunite follow the oxidation trend with up to 25 melting (Fig. 5-4).

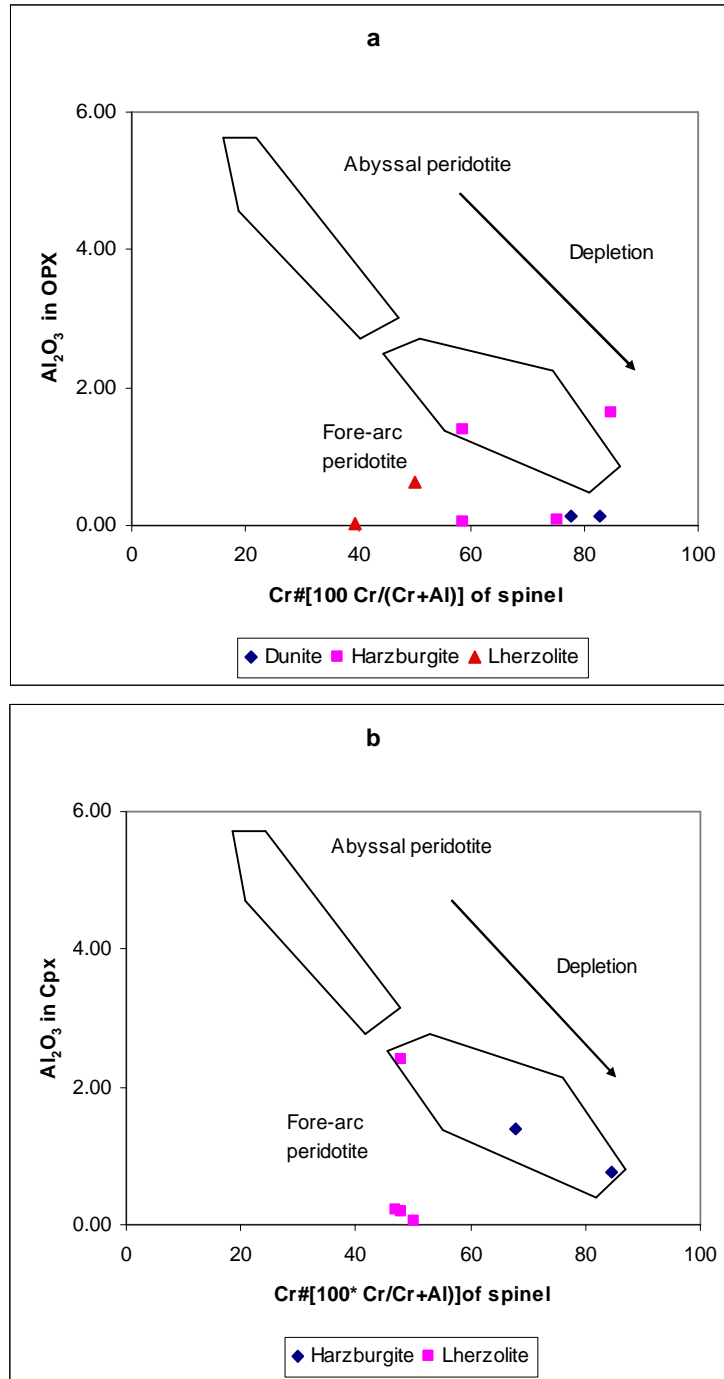


Fig. 5-2 Al_2O_3 Wt % in orthopyroxene (a) and clinopyroxene (b) versus Cr# in Spinel diagrams for Mawat peridotites. Abyssal and fore-arc peridotite fields for orthopyroxene compositions from Bonatti and Michael (1989) and Parkinson et al. (2003), Abyssal and fore-arc peridotites field compositions from Usyal et al., (2007)

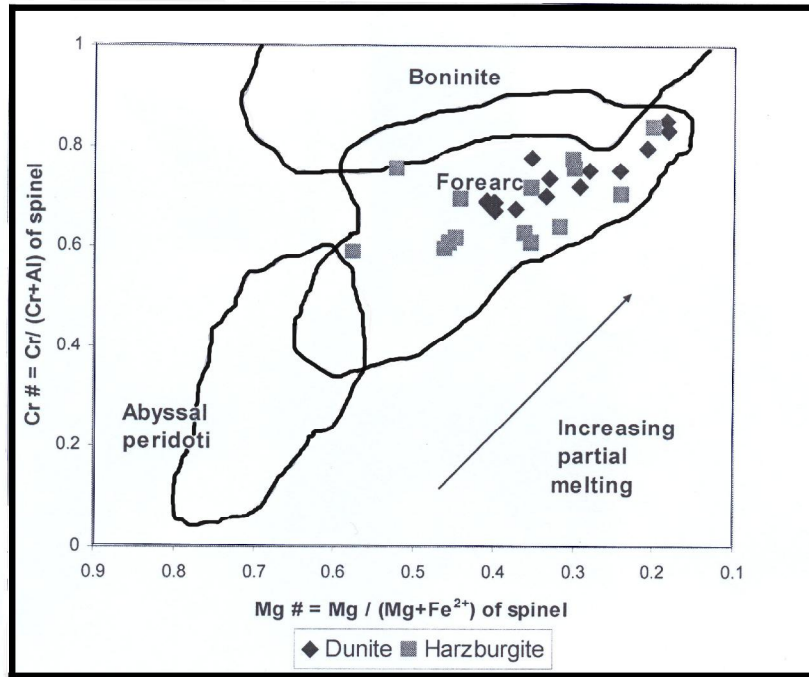


Fig. 5-3 Cr# vs. Mg# Compositional variation of chrome spinel from the peridotite of MOC. Abyssal peridotite field is from Dick and Bullen (1984) and Arai, (1994a), fore-arc peridotite is from Ishii, et al. (1992), Parkinson and Pearce (1998) and boninite field is from Van der Laan et al., (1992) and Sobolov and Danyushevsky (1994)

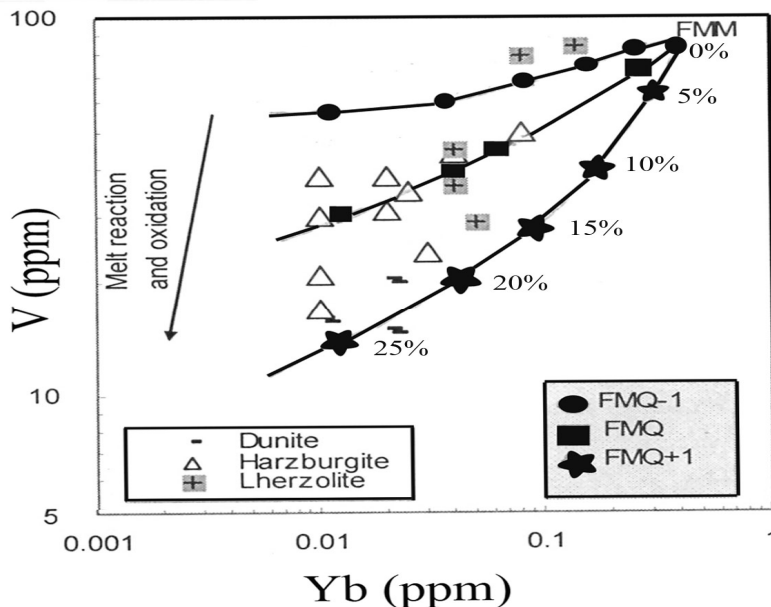


Fig. 5-4 V vs. Yb abundance (Pearce et al. 2000) for whole rock data shown with fractional melting trends for the oxygen fugacities of FMQ-1, FMQ, and FMQ+1 imply that the primary composition of peridotite samples suite from Mawat are similar to fertile MORB mantle (FMM) and modified by interacting hydrous melt generated in a suprasubduction environment as a result of increasing degree of partial melting.

5.4 Comparison of chromite from MOC with chromite elsewhere

Most of the well known ophiolite complexes are mainly Late Paleozoic to Mesozoic in age; however, there have been few studies on the older ophiolites of Archean and Neoproterozoic ages (Leblanc, 1981; Quick 1990; Vuollo et al. 1995, Ahmad, 2001 and Hussein et al., 2004).

The MOC belong to the Phanerozoic ophiolites (Cretaceous Tethyan ophiolite) (Buday 1980 and Jassim &Goff 2006).

The chromitite-dunite-harzburgite association from the MOC is very similar to that in Cretaceous ophiolites in the term of spinel chemistry (Fig. 5-5). The Cr# of spinel in chromitite is almost similar to that in dunite which is an essential feature of podiform chromitite and dunite envelope in Phanerozoic ophiolites [(Fig. 5-5); (Arai and Abe, 1995, Arai, 1997)]. The Cr# of spinel in chromitite pods ranges between 0.67 to 0.803 average 0.73 and in dunite the Cr# ranges between 0.67 to 0.85 average 0.73, due to the similarities in Cr# of spinel in chromitite and dunite envelopes they are grouped as podiform chromitites. In the term of Cr# of spinel in chromitite pods in the studied area they belong to Cr-rich chromitite and are distributed along the harzburgite-dunite transitional zone and deeper mantle section. This situation is similar to New Caledonia, Troodos, Albania, N.Oman and Loubusa Tibet ophiolites (Fig. 5-5). In the term of spinel, harzburgite of the studied area (Cr# average is 0.679) show a highly depleted nature and are more refractory than abyssal peridotites which have (Cr#< 0.6). The chrome spinels of harzburgite in MOC are also similar to the composition of the mantle harzburgite, dunite and chromitite of Neoproterozoic ophiolite in southern to central Eastern Desert of Egypt, and the Wadi Onib Neoproterozoic ophiolite, northern Red Sea hills of Sudan (Cr#s ranging from 0.5-0.85), which also show the highly depleted nature of the mantle (Ahmad et al. 2001, Ahmad & Arai 2005, Hussein et al. 2004).

The presence of hydrous minerals inclusion in spinel in some chromitite indicates involvement of melt enriched in incompatible components during chromite genesis in both the Proterozoic ophiolitic mantle and Phanerozoic one (Ahmad, 2001). The secondary inclusions as chlorite and serpentine

which is probably result of serpentinizations process of olivine grains within chromites are also observed in spinel of chromitite pods in MOC. This means that origin of podiform chromitite might be the same, both for the Proterozoic ophiolite and Phanerozoic Mawat ophiolite. Reaction between an exotic melt and refractory harzburgite and subsequent melt mixing possibly produced the podiform chromitite in the both Proterozoic lithospheric mantle and in the Phanerozoic one (Arai and Yurimoto 1992 and 1994). So, the Mawat chromitite may have been produced by the same mechanism as the Proterozoic and Phanerozoic chromitite. This suggests that the thermal state of the Earth that controlled formation of the crust-mantle system has not considerably changed since the Proterozoic.

On the other hand, the comparison of Cr# of chromian spinel in chromitite and ultrabasic rocks in MOC with those in other localities in Iraq (Fig. 5-6) reveals that the chromitite rocks of the studied area are similar to other localities in Iraq. While the comparison of Cr# in chromite of ultrabasic rocks show similarity with Qalander and Bulfat area. This also indicates that the ultrabasic rocks of MOC are related to the depleted mantle rocks and closely resemble alpine-type peridotites probably produced from medium spreading center and having genetic linkage with fore- arc setting of suprasubduction zone.

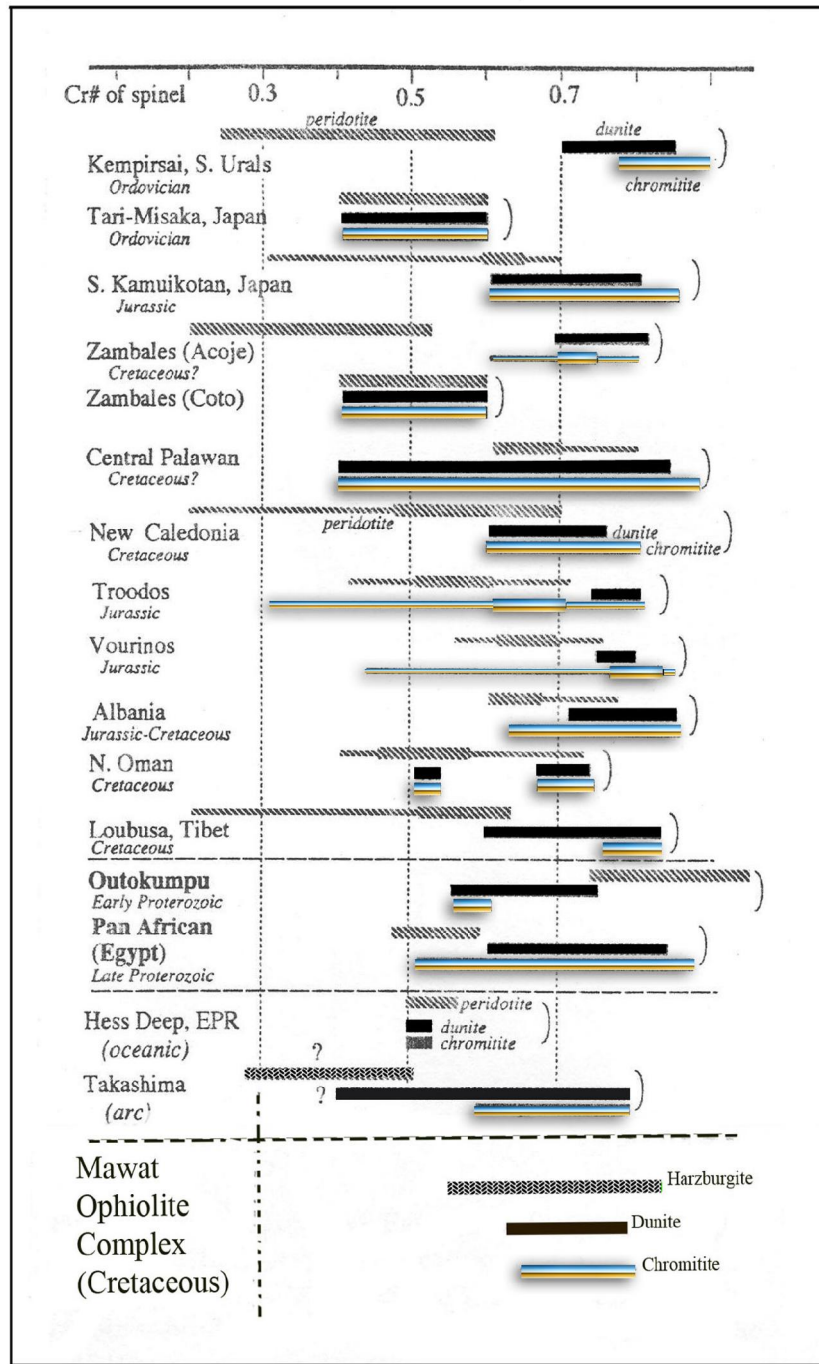


Fig.5-5 Comparison of Cr# of spinel in chromitite and associated dunite and peridotite of Proterozoic and Phanerozoic ophiolites (Arai, 1997). Note that the Cr# of spinel in chromitite and dunite is quite similar, while it is not correlated with that of enclosing peridotite.

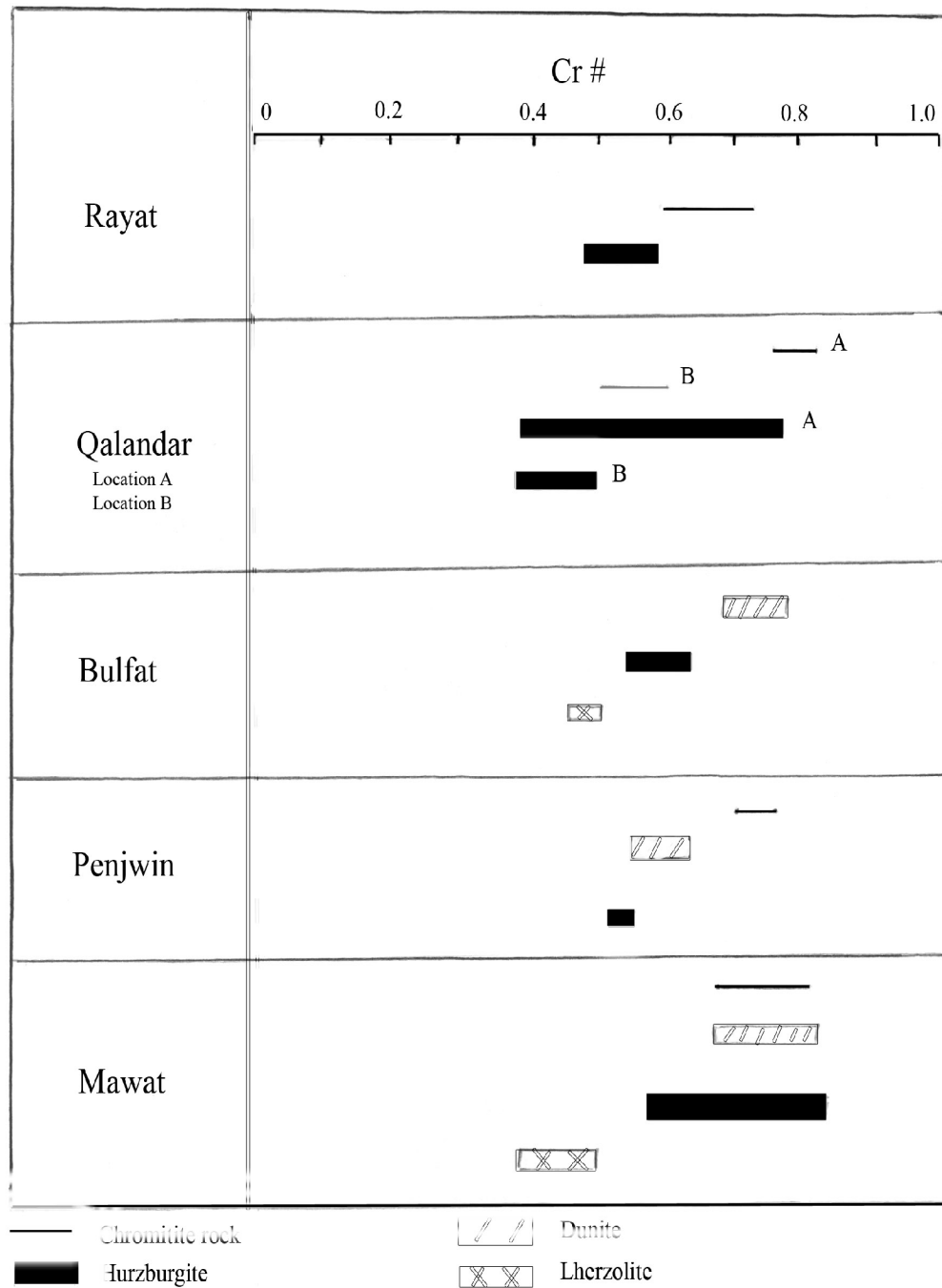


Fig. 5-6 Comparison of Cr# of chromian spinel in chromitite and ultrabasic rocks of MOC with other localities in Iraq. Source data from (Ismail et al., 2007, Hamasalh, 2004, Buda, 1988, and Al-Chalabi, 2004 and the present study).

5.5 Origin of Podiform Chromitites

The model for the formation of podiform chromitites is extensively described elsewhere such as; Arai and Yurimoto (1994), Zhou et al., (1994), Arai (1997a and b), Tamura and Arai, (2005).

Recently the podiform chromitites have been interpreted to be conduit-filling cumulates initially penetrating mantle peridotites especially harzburgite (Lago et al. 1982 and Arai et al., 2004). Arai and Yurimoto (1992 and 1995) interpreted that the podiform chromitites may have been produced by interaction between harzburgite and melt at low pressures. Arai (1992) and Arai Yurimoto, (1994) proposed that the alpine-type or (podiform) chromitites are formed by a combined process, that is, an interaction between melt of deeper origin and harzburgite wall rock with associated magma mixing.

Due to a partial melting in the upper mantle exotic melt will be produce at higher pressure and will move upward, inevitably will interacted with wall peridotite of mantle to produce dunite and SiO₂ -rich secondary melt by selective consumption of orthopyroxene (or pyroxene) of peridotite wall (Arai and Yurimoto 1994). By releasing its latent heat the melt may necessarily have precipitated olivine (+ chromite), thus promoting the melt –peridotite interaction; the dunite produced by this melt-peridotite interaction should be a mixture of two kinds of olivine: the cumulus phase from the melt and residue phase from the peridotite wall. The secondary melt formed could be blended with the next inflow of relatively primitive melt and enter primary spinel field (Irvine, 1977). The hybrid melt (secondary Si enriched melt+ primitive melt) can precipitate only chromite to make chromite rich cumulates (Arai and Yurimoto, 1994) (Fig. 5-7).

The MOC chromitites have high Cr# [Cr/ (Cr+Al) atomic ratio] (>0.7) compared with the majority of podiform chromitites and they are identical to those between chromitite, dunite envelops and harzburgite host. It can be suggesting the process by which the chromitites of MOC formed by high degree of partial melting and consumption of Mg-rich and Al-poor orthopyroxene in wall peridotite by this melt. The relatively high Cr# of

podiform chromitite in studied samples may be due to a possibly high Cr# of the Si-enriched hybrid melt inherited from high-Cr# orthopyroxene in harzburgite. In conclusion, the podiform chromitites of MOC can be concentrated by mantle-melt interaction (1) if the wall-rock peridotite, especially the orthopyroxene is sufficiently high in Cr# and (2) if secondary Si- and Cr-enriched melt are formed by decomposition of orthopyroxene are well mixed with more primitive melts.

The geological, petrographical and geochemical diversity of podiform chromitite suggest that two stages of magma generation were involved in their formation in the MOC. Poor-PGE chromitites were produced around the MTZ and to lesser extent, in the deeper part of the mantle section in the first stage.

The PGE-rich chromitite in the deeper part of mantle section, were formed during the second stage of magma generation possibly linked to arc-type magmatism by higher degree of partial melting of peridotite in a supra-subduction zone setting. A part of chromitite rocks in studied area is characterized by unusual high PGE concentrations it has a high-Cr# (0.78) spinel and a very low PPGE/IPGE ratio ($Pd/Ir=0.062$). This strongly implies that the PGE-rich chromitite was formed either from a high-degree partial melt or from melting of already depleted peridotite.

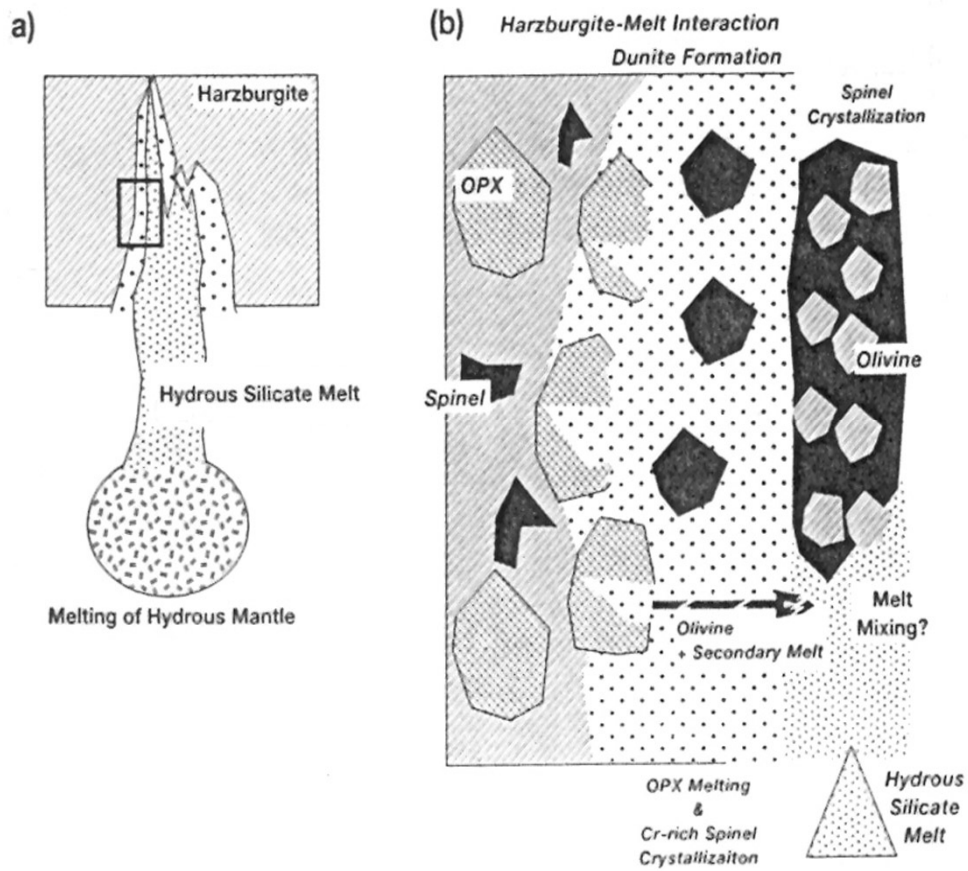


Fig. 5-7 Schematic illustration of genesis of podiform chromitite (a) oxidized hydrous melt generated by melting of hydrous mantle was supplied to harzburgite. (b) Close-up of the reaction zone (square in a). The reaction between harzburgite and the melt caused decomposition of orthopyroxene (OPX) and give rise to dunite. The reaction produced the high-Cr spinel in dunite and the secondary melt rich in SiO_2 . The mixing with primary melt may have promoted spinel crystallization. Phase diagrams from Tamura and Arai, (2005).

Chapter Six

Tectonic Setting of MOC

6-1 Introduction

The subduction of the Neo- Tethyan ocean floor beneath Iran, sutured Iran to Arabia and the subsequent continental convergence built the Zagros orogenic belt (Jassim and Goff, 2006 & Ghasemi and Talbot, 2006). The late Cretaceous Ophiolite of Iraq defines the Neo Tethyan suture that resulted from the closure of oceanic basin between Iranian and Afro- Arabian plate during the Late Triassic to Late Cretaceous period (Parlak et al., 2006).

Various studies of geochemistry, mineral chemistry and petrogenesis of part of the MOC (NE Iraq) show their affinity to MORB. The recent study used different rock types in MOC to define the tectonic setting of this complex. The geological, petrographical and geochemical diversity of ultrabasic rocks, chromitite, and gabbroic rocks of MOC were used for possible interpretation of tectonic setting of the studied area. The variety of mineral chemistry and the refractoriness of the upper mantle peridotite also associated with large amount of rocks (dunite, harzburgite, lherzolite and pyroxenite) are the characteristics of mantle rocks of MOC that are used as indicators for their tectonic setting interpretations.

In recent years the geochemistry of the immobile trace elements has been employed extensively to define the tectonic affinity of ophiolite complexes throughout numerous studies made by Pearce et al., (1983 and 1985), (Ohara et al., 1996 and 2002), and others. This study has mainly focused on using different significant discrimination diagrams for interpreting the tectonic settings.

6-2 Tectonic setting indication from the ultrabasic rocks of MOC

Major, trace and REE elements of ultrabasic rocks were used for indicating the tectonic setting of the studied area. On using the TiO_2 (wt %) versus Cr (ppm) diagram (Fig. 6-1) (Pearce et al., 1985) all samples of ultrabasic rocks in

MOC also plot in the field of supra subduction zone (SSZ). This is related to the nature of magma as generated of depleted upper mantle slab.

The chemical composition of chromian spinel can be used for discrimination of different tectonic setting as indicated in (Fig. 6-2). It can be observed that Mawat ultrabasic represents alpine-peridotites, probably trapped from leading mantle wedge of moderately to fast spreading mid-oceanic ridge within fore-arc setting of suprasubduction zone. In the term of Cr# of chromian spinel in ultrabasic rocks of MOC, it is observed that Mawat ultrabasic rocks overlaps fore-arc fields (Fig. 6-2).

Based on Niu and Hekinian (1997), in the moderately spreading ridges chromian spinel have Mg# value (< 0.65), Cr# values (> 0.4) and Al_2O_3 content of orthopyroxene and clinopyroxene of (< 4.0 Wt %), whereas slow spreading ridge has Mg# values (> 0.7) and Cr# (values ≤ 0.3) with Al_2O_3 content of two pyroxene (> 4.0 Wt%). Accordingly the Mawat ultrabasic rocks have trapped from leading mantle wedge of moderately spreading mid-oceanic ridge (Appendixes 11, 12, 13 and 14). Additionally the Cr# of accessory chromite in peridotites has been extensively used as an indicator of the degree of melting in the upper mantle, high Cr# chromites correlate with the highest degree of melting and, hence, the greater degree of depletion of peridotites (Dick and Bullen, 1984, Arai, 1992). Accessory chromite in the Mawat ultrabasic rocks plot in Cr-rich part of compositional range of fore-arc basin peridotite from the Mariana Trench (Fig. 6-3).

According to Ohara and Ishii, (1998), fore-arc basin peridotites contain accessory chromite with high Cr# (up to 0.7). In contrast, according to Ohara et al. (1996 and 2002) accessory chromites in back-arc basins have Cr# ≤ 0.55 . Accessory chromite in dunite and harzburgite from MOC has Cr# range between 0.67-0.85 and 0.56-0.838, close to those described in fore-arc basin peridotites. Accordingly, it can be suggested that the MOC peridotite and the associated chromite can be fragments of oceanic lithosphere formed or modified in fore-arc environment, and represent the mantle sequence of a suprasubduction zone ophiolite in the sense of Pearce et al., (1984) and (Fig. 6-4).

TiO₂ content of spinel in magma varies depending on the tectonic setting of generation: it is lowest for the arc magma, intermediate for MORB and the highest for intraplate magma (Arai 1992). The Cr# of residual peridotites from MORB have Cr# 0.2-0.5 and usually 0.2-0.6 (Dick and Bullen 1984) and some island-arc magma have Al-rich spinels 0.2-0.6 Cr#; while peridotite with Cr# of 0.7-0.9 may be residues after extraction of high-Mg silica over saturated basalts (Johnson et al., 1985). The depleted harzburgite with high Cr# and low TiO₂ chromite from MOC suggest an origin from mantle wedge or sub-arc mantle. According to Cr# and TiO₂ content the suite of depleted ultrabasic i.e., dunite, harzburgite, and chromitite from the MOC may have a genetic linkage with boninitic magma or high Mg arc tholeiite. The MOC may possibly be a fragment of arc lithosphere that formed or has been modified from a precursor (e.g. oceanic lithosphere) at a supra subduction zone environment (Figs. 6-3 and 6-4). The high Cr# of spinel of the mantle tectonite may indicate high degrees of melting of peridotite or alternatively re-melting of a previously depleted peridotite (Ahmad et al. 2005), such as spinel composition of mantle harzburgite, dunite and chromitite of Neoproterozoic ophiolite in the southern to central Eastern Desert of Egypt and the Wadi Onib Neoproterozoic ophiolite, northern Red Sea hills of Sudan (Cr# ranging from 0.5 to 0.85).

Therefore, according to these examples and according to the Cr# (0.7-0.8) and low TiO₂ content (< 0.3) characters of spinel in ultrabasic rocks and chromitite rocks, we conclude that the formation of MOC may have been linked with some high-Mg, high-Cr supra-subduction zone magma (Fig. 6-5) such as high-Mg andesite, boninite or high-Mg tholeiite where partial melting is quite high.

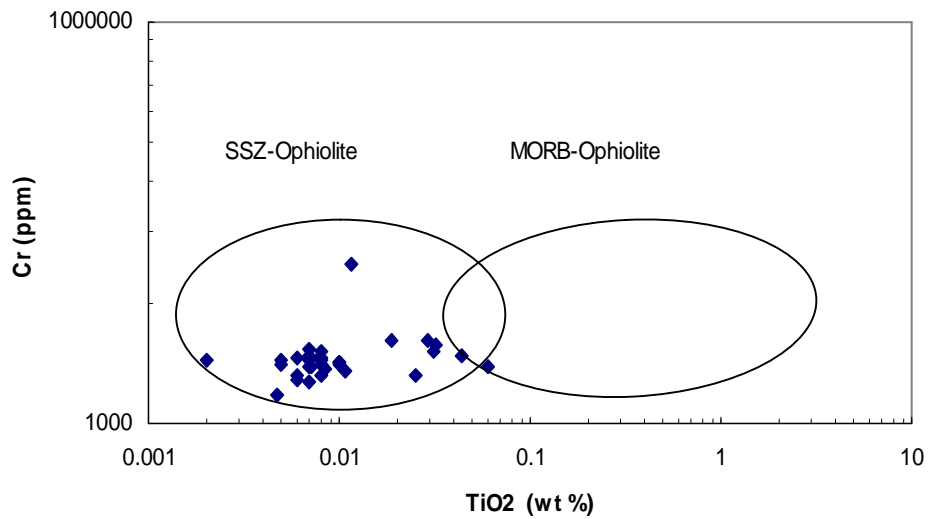


Fig. 6-1 Tectonic discrimination diagram (Pearce, 1985) showing the plots of ultrabasic rocks from MOC in the field supra subduction zone, (SSZ).

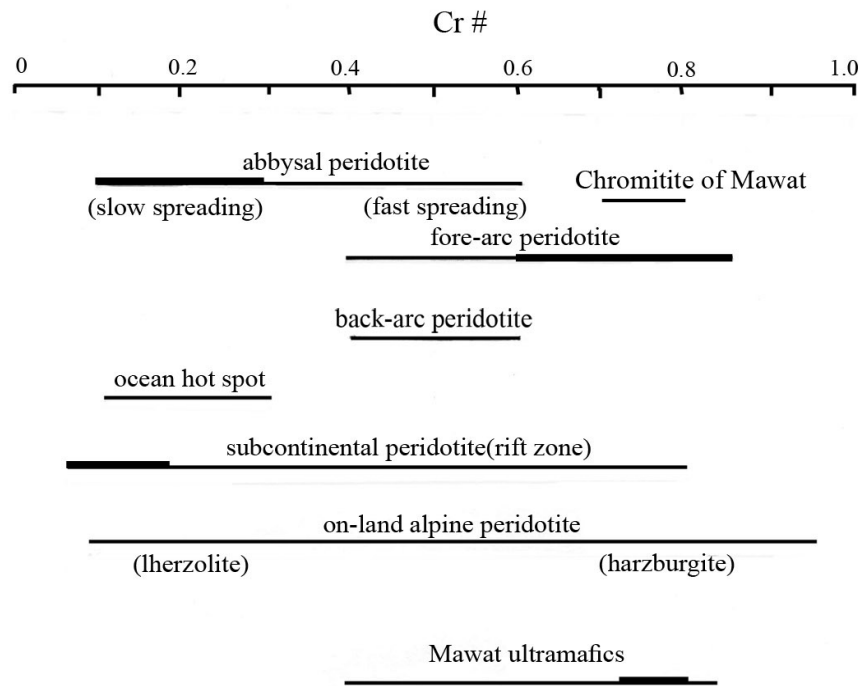


Fig. 6-2 Diagram showing ranges of Cr# of spinels in peridotites from Different tectonic settings (Lee, 1999). The heavy-line part represents the majority of data plots. The ranges of Cr# in peridotites and chromitite rocks of MOC are indicated.

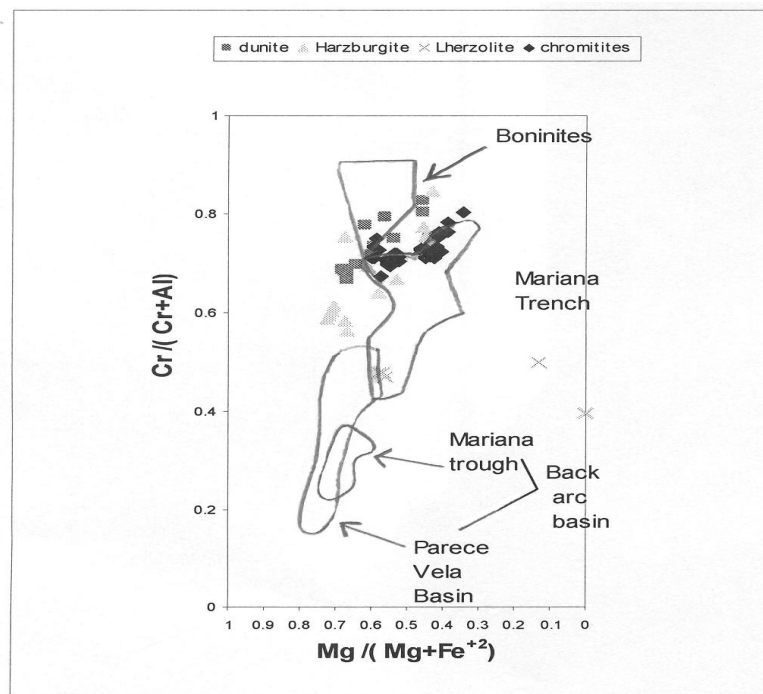


Fig. 6-3 Comparative Cr# vs. Mg# plot chromian spinel of chromitites ultrabasic, and pyroxenite of MOC and those in peridotites from (1) Mariana Trench (fore-arc basin; Ohara and Ishii, 1998), (2) Vela Basin and Mariana Trough (back-arc basins; Ohara et al., 1996 and 2002).

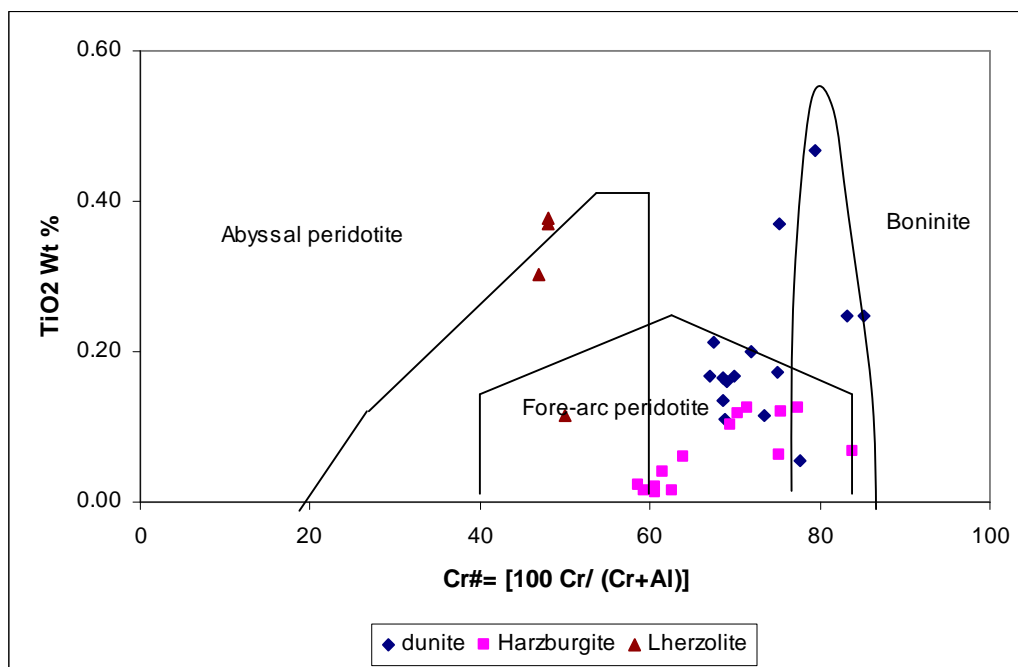


Fig. 6-4 Compositional variation of Cr# versus TiO_2 of chrome spinel from the peridotite of MOC. Abyssal peridotite field is from Dick and Bullen (1984) and Arai, (1994a), fore-arc peridotite is from Ishii et al., (1992), Parkinson and Pearce (1998) and boninite field is from Van der Laan et al., (1992) and Sobolov and Danyushevsky (1994)

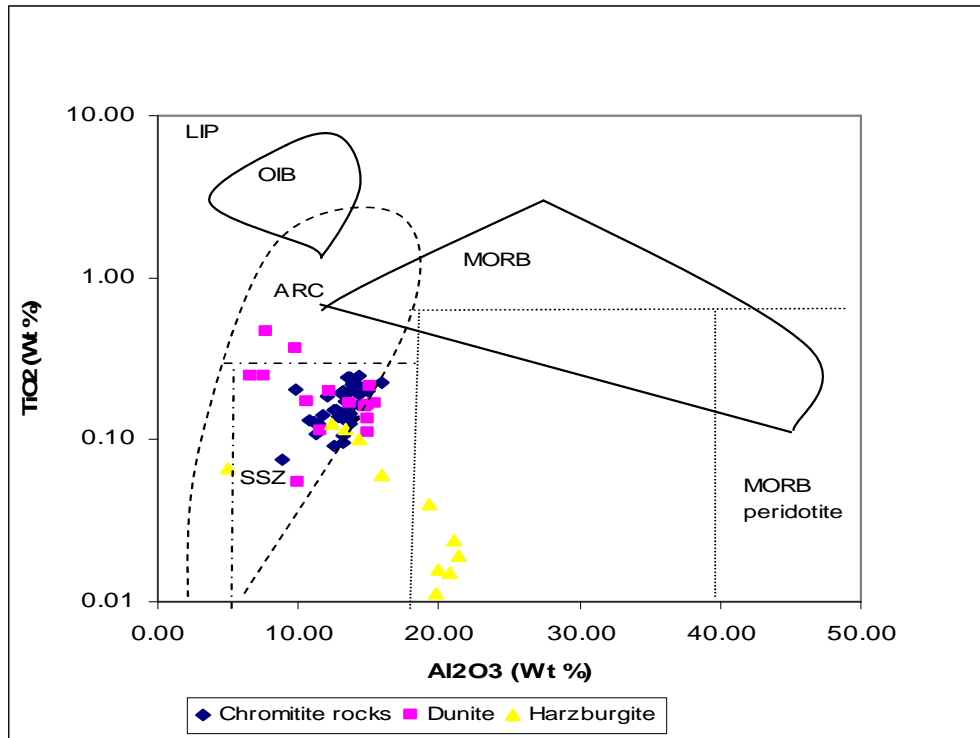


Fig. 6-5 Relation between TiO_2 vs. Al_2O_3 of chromite in the studied area. Fields are after (Kamensky et al., 2001). SSZ; Supra-subduction zone; LIP, large igneous province; MORB, mid ocean ridge basalt; OIB, ocean island basalt

6.3 Tectonic implications from chromitite rocks

Low pressure, high water-vapor pressure, high temperature and compositional stress may be necessary for favorable upper mantle conditions for the formation of podiform chromitites. Low pressure (Boyd et al., 1964 in Arai, 1995) and/or high $P_{\text{H}_2\text{O}}$ (Kushiro et al., 1968 in Arai, 1995) conditions may be favorable for the selective dissolution of orthopyroxene in peridotites to produce the dunite and the silica - and Cr- rich melt which is mixed with a primitive melt to precipitate chromian spinel (Arai, and Yurimoto, 1994).

Ambient high temperature conditions are great advantage to promote the melt-peridotite interaction. Lithospheric compression may make an uprising melt stagnant, which should also promote interaction with peridotite wall. All these conditions are likely to be simultaneously available only within the arc setting.

Chromian composition, especially the Cr# [(Cr / (Cr+Al) atomic ratio] of chromian spinel may create strong constraint on the setting of chromitite

genesis. Chromian spinel from podiform chromitite has a relatively high Cr#, from 0.4 to 0.9, mostly around 0.7-0.8 (Arai, 1995). The chromian spinel of chromitite rocks in MOC plots in this range (0.7-0.8), (Fig. 6-3). This range of Cr# for chromitite spinel is almost identical to that for chromian spinel coexisting with Mg-rich olivine in arc and related (fore-arc, arc proper and back-arc) magmas (Figs. 6-6 and 6-7) indicating that the magma in equilibrium with the podiform chromitite could be primitive arc magma in term of Fo of olivine – Cr# of spinel relationship (Arai, 1990 and 1994). This conclusion is further confirmed with petrological and geochemical data from MOC which are taken into consideration. Origin of the main podiform chromitite bodies beneath mid oceanic ridge can be excluded because neither ocean floor peridotite nor MORB has high Cr# (>0.6) spinel (Dick and Bullen, 1984).

The Cr# of chromian spinel coexisting with Mg-rich olivine (Fo. content range between 90-92) in the dunite of the studied area ranges from 0.68-0.85 (mean > 0.7) which is again similar to the Cr# range of chromian spinel coexisting with Mg-rich olivine in arc magma (Fig. 6-6).

The dunite as well as the chromitites from the studied area can thus be in equilibrium with primitive arc magma (Fig. 2-26)

According to the tectonic discrimination diagram (Fig. 6-7 Arai, 1992a) and the low Ti contents at a given $Fe^{+3\#}$ ratio one might suggest that the chromitite rocks of Mawat have an arc magma origin. The high Cr# (0.7-0.8) is most easily available at supra-subduction zone which possibly has genetic linkage with some boninite or high-Mg arc tholeiite (Fig. 6-2, and Fig. 6-3) (Arai, 1992 and 1994b, Ahmad et al., 2001). On the other, hand in the term of $Cr_2O_3-Al_2O_3$ relationship all samples of chromitite and ultrabasic rocks are plots in the field of supra-subduction zone (Fig. 6-5).

The Cr# > 0.7 is considerably enriched in IPGE over PPGE and has been interpreted by (Melcher et al., 1997) as a multistage process, in which high-Al chromite has formed from MORB-type tholeiitic melts, and high Cr-chromite has formed by interaction of hydrous melts and fluids with depletion mantle in

a supra subduction zone setting. Both types of chromite are invariably surrounded by dunite that are generally LREE enriched (Melcher et al., 1999).

All these phenomena: enrichments in IPGE (Figs. 3-24 and 3-25) and LREE enrichment in dunite (Fig. 2-18) and $Cr\# > 0.7$ (Table 3-2) in chromitite rocks are observed in the studied chromitite and associated rocks. Therefore, it can be concluded that the formation of MOC may have been linked with high-Mg, high-Cr such as high Mg-andesite, boninite or high Mg-arc tholeiitic that have been modified at a supra subduction zone magma (Fig. 6-3), (Fig. 6-5) and that the depleted harzburgite is common to MOC, suggesting that a high degree of partial melting was prevalent in the source magma.

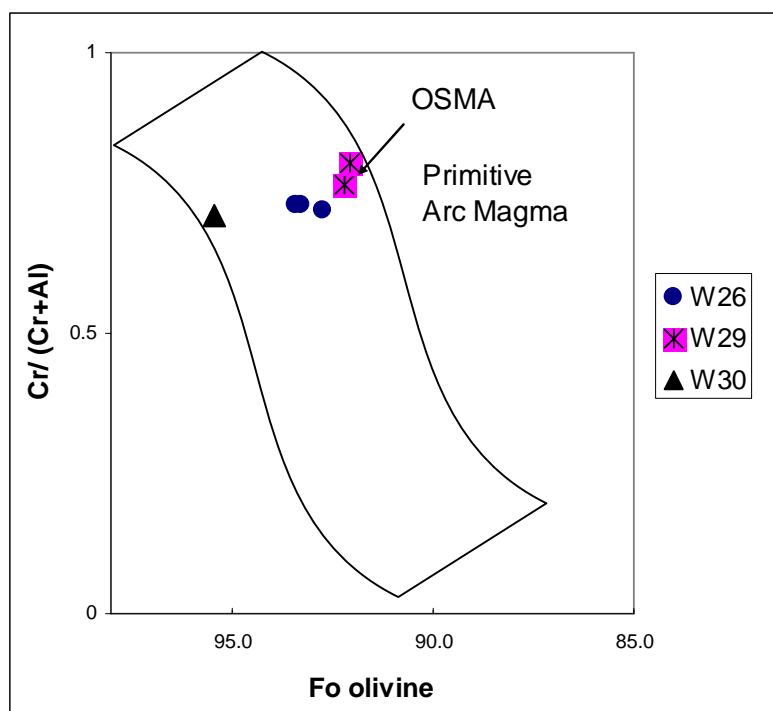


Fig. 6-6 Relation between Fo olivine and Cr# of spinel in chromitite rocks of MOC follow the spinel mantle array and plots in the field of relatively primitive arc magmas (basalt and high-Mg andesite). The field of (OSMA, and primitive arc magma Arai, 1987, = the region of mantle peridotites).

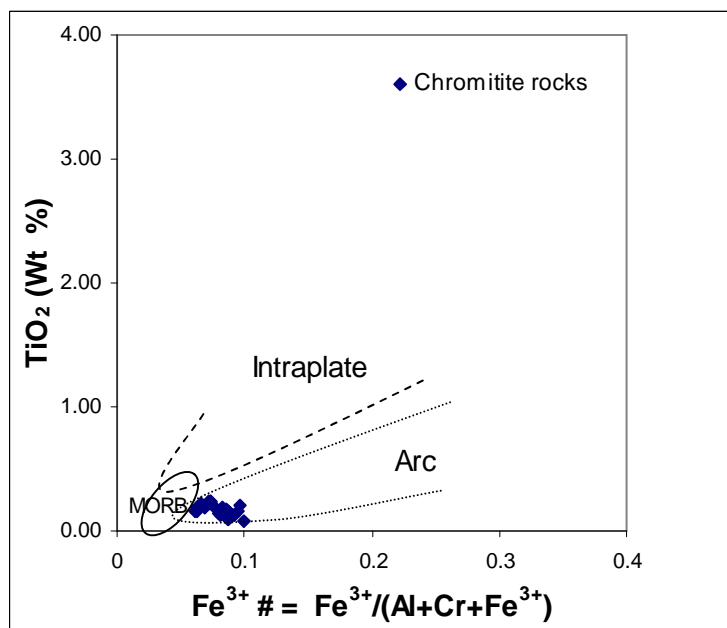


Fig. 6-7 Relationship between $(\text{Fe}^{3+} / (\text{Fe}^{3+} + \text{Al} + \text{Cr}))$ atomic ratio and TiO_2 Wt% of chromitite rocks in MOC. The discrimination boundaries of spinel compositions of MORB, Arc magma and intraplate magma are Arai (1992a).

6.4 Tectonic implication from gabbroic rocks

The supra-subduction zone signature of gabbroic rocks in MOC is expressed as a relative Nb anomaly and enriched large ion lithophile element abundances (Fig 4-24). Whattam et al. (2004) and Duclaux et al. (2006) argued that the strong negative Nb anomaly and enrichment in LILEs with depletion in HFSEs spider diagram patterns are characteristic of a magmas generated in the supra-subduction zone.

The multi-element distribution patterns of gabbroic rocks in MOC (Fig. 4-24) follow the same characteristic spider diagram of magma generated in a SSZ. It is also noted that the Th -Hf-Ta discrimination diagram of (Wood, 1980, in Whattam, 2004) (Fig. 6-8) shows that most of the samples are plotted in the field of SSZ. Therefore, it may be suggested that the gabbroic rocks in MOC source are related to the magma generated from SSZ. The plots Y against fractionation index Cr in most of the samples are fall in IAT (island arc tholeiite) fields, and to the left side of it (Fig. 6-9). It is a side of the fore-arc and boninitic rocks that has a linkage with suprasubduction zone similar to those of Mariana fore-arc basin (Pearce et al. 1984) and boninitic rocks in Oman ophiolite (Pearce 1982). Finally, all of the above evidences may lead to the conclusion that the studied gabbro rocks from MOC have possibly been formed by fore-arc spreading in a basin close to subduction zone where the source magma of the basic rocks. Beccaluva et al., (1989) in Yaliniz and Goncuoglu, (1999) reported that Ti differences in ophiolites correspond well to distinct magma types of the modern oceanic setting, and are grouped as high-Ti, low-Ti and very low-Ti ophiolites. They reported that high -Ti ophiolites compare favorably with the magmatic association occurring at mid-ocean ridges and well developed marginal basins, whereas low-Ti and very low-Ti ophiolites are best equated with magmatic series of island-arc and boninitic types respectively, generated in the supra-subduction zone settings. Accordingly, the low Ti content of clinopyroxene in the MOC gabbros is 2-3 times lower than those from MORB, this is indicative of crystallization of clinopyroxene from Ti-poor magma. In addition to that, the clinopyroxene chemistry of the gabbroic rocks supports the assertion that gabbroic rocks of MOC related to island arc and boninitic rocks which have a linkage with SSZ (Figs 6-10 a, b and c).

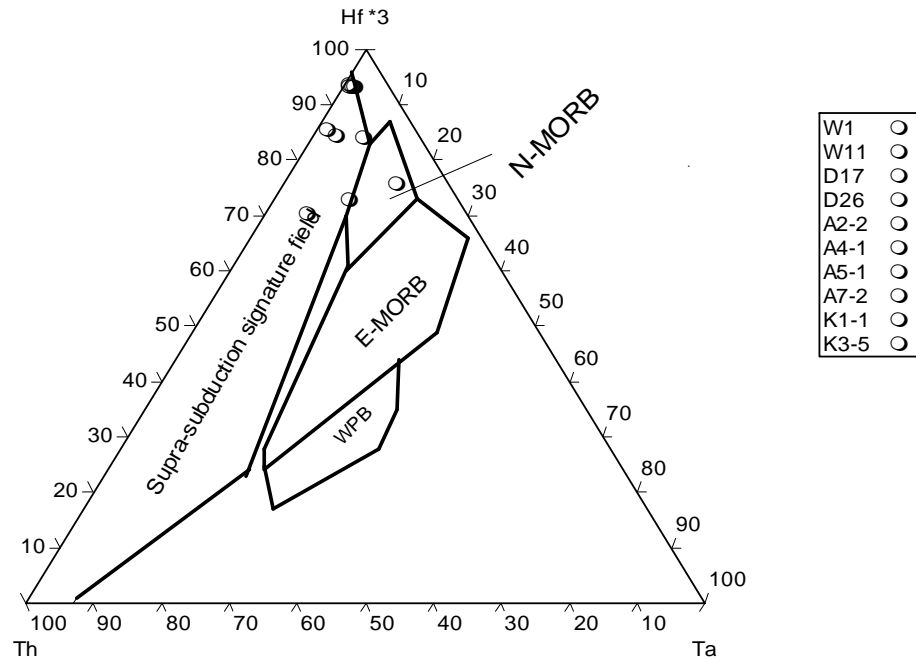


Fig. 6-8 TH-Hf-Ta tectonic discrimination diagrams according to (Wood, 1980 in Whattam, 2004) of rocks from MOC gabbroic rocks, N-MORB: is normal mid-ocean basalt, E-MORB: is enriched mid-ocean ridge basalt, WPB: within plate basalt.

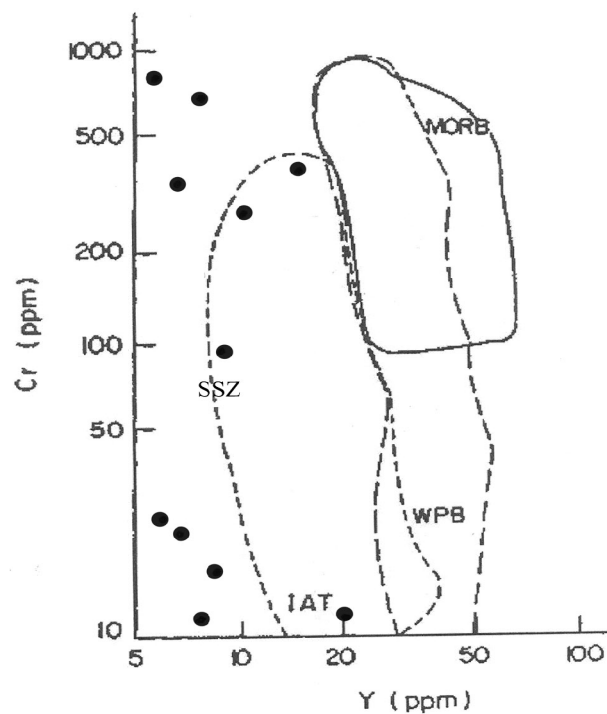


Fig. 6-9 Cr-Y variation of gabbroic rocks from the MOC (the discrimination fields Pearce, 1980). IAT, Island arc tholeiitic, MORB, mid oceanic ridge basalt, WPB, within plate basalt, SSZ, supra subduction zone.

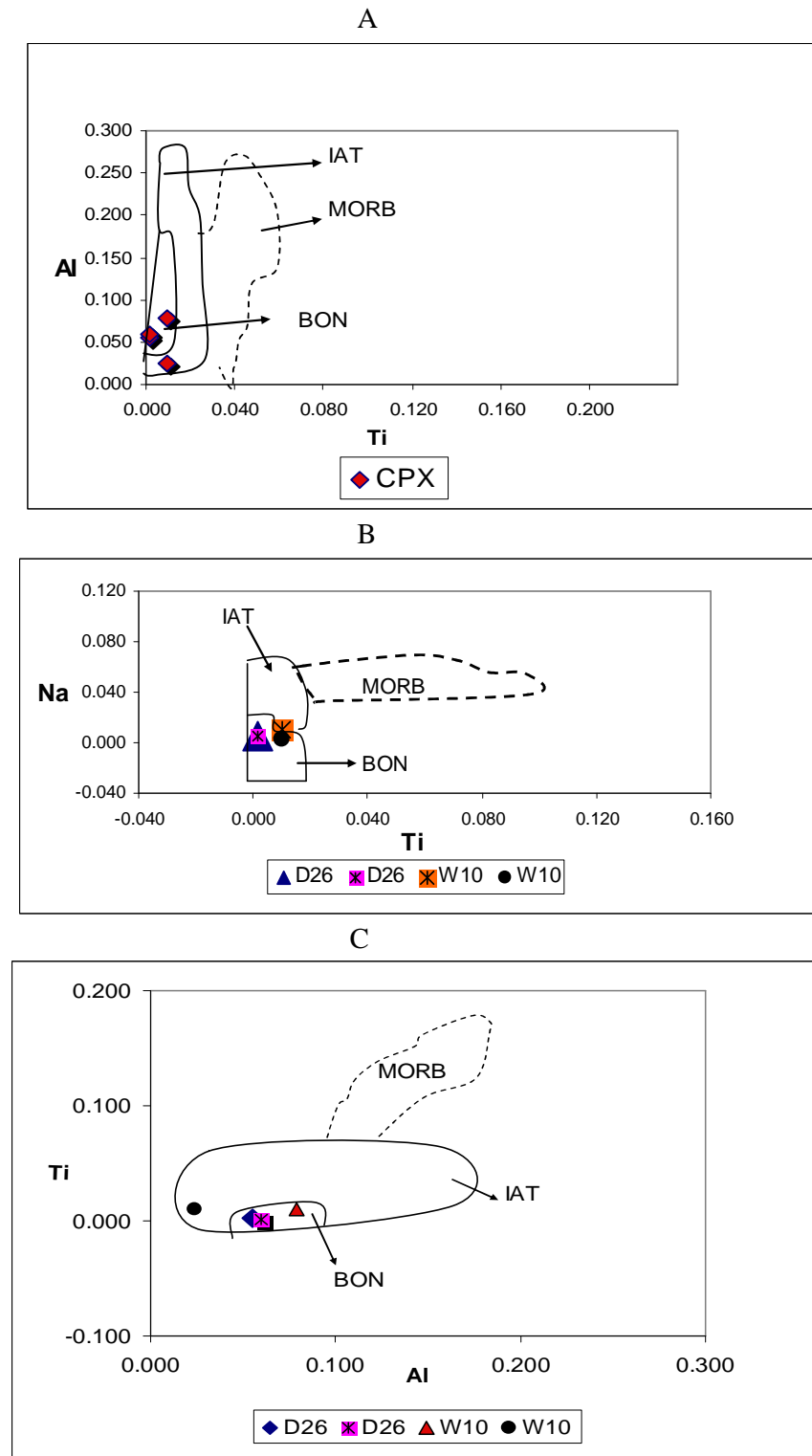


Fig. 6-10 Co-variation diagrams of studied pyroxene indicating their tectonic settings (IAT: Island Arc Tholeiite, BON: Boninite, MORB: Mid-ocean-ridge basalt, (after Beccaluva, 1989 in Yaliniz and Goncuoglu, 1999). **A-** Al vs. Ti (atomic ratios), **B-** Na vs. Ti (atomic ratios), **C-** Ti- vs. Al (atomic ratios).

Chapter Seven

Conclusions and Recommendations

7.1 Conclusions

The following points can be concluded at the end of this study:

- 1- The Mawat peridotites consist mainly of the refractory harzburgite and dunite, and less abundant lherzolite which are characterized by tectonic textures. The depleted harzburgite and dunite are of residual origin with varying degree of partial melting (up to 25 %) and extraction of arc-related magma. The pyroxenite rocks occur as a narrow belt at the contact of dunite-peridotite mass and small dykes with small isolated bosses cutting the harzburgite and gabbro.
- 2- The chondrite normalized REE patterns of dunite and harzburgite have a pronounced slightly U-shape, depletion in middle REE relative to light REE and heavy REE. Such patterns were typical of ophiolitic ultrabasic rocks and compatible with the supra- subduction zone (fore-arc setting).
- 3- The chondrite-normalized REE patterns of pyroxenite reveal two patterns. The first show enrichments in LREE and MREE relative to HREE with convex –upward REE patterns and the second show a slight depletion in LREE relative to MREE and HREE. Both two patterns are typically of ophiolitic characteristics (supra-subduction zone setting).
- 4- The genesis of pyroxenite rocks, can be concluded from the low Al_2O_3 content (< 10 %) and enrichments in LREE and MREE relative to HREE as well as the LREE depletion pyroxenite dykes cross-cutting peridotite as segregation and transporting boninitic melt in a supra subduction zone.
- 5- Systematic increase in Cr# of spinel from lherzolite to dunite is in consistent with partial melting and melt extraction process.
- 6- The olivine in dunite is mostly Fo_{92-90} and those in harzburgite and lherzolite were Fo_{92-89} and Fo_{90-84} respectively. They plot within olivine spinel mantle array (OSMA) which is a spinel peridotite restite trend in the term of olivine-

spinel composition relation and characterized by rich-Fo content at a given Cr#, and are indicative of fore-arc setting environments.

7-The chromite in ultrabasic rocks of MOC is of two main types, the Cr-rich chromite in dunite and harzburgite which is the $Cr\# > 0.65$ and the Al-rich chromite in harzburgite and lherzolite. The Cr-rich chromite is mostly associated with olivine rich tectonites (i.e. dunite). This is related to the earliest precipitating olivine and chrome spinel in primary magma and almost identical in chemistry to those of residual phase, if physical conditions were not largely different.

8- The alteration products of primary chromite grain in the ultrabasic rocks of the studied tectonite exhibit two contrasting compositional zones from core to rim. The core which has retained the primary composition in comparison with rims which display high Fe^{3+} ferritchromite. Based on Cr-Al- Fe^{3+} diagram, the rim composition plots with the field of lower amphibolite's facies.

9- From the chemical composition of chromian spinel of ultrabasic rocks in MOC it can be concluded that they are of alpine-type peridotite, probably trapped from the leading mantle wedge of moderately spreading mid ocean ridge within fore-arc setting of suprasubduction zone.

10- The low TiO_2 content < 0.3 Wt % and high Cr# of dunite and harzburgite > 0.7 suggest an origin of these rocks from mantle wedge of sub-arc mantle and may have a genetic linkage with boninitic magma or high Mg-tholeiite, and the high Cr# of spinel may indicate high degree of melting of peridotite.

11- The oxygen fugacity values of peridotites and chromitites, record fO_2 values of (0.06-1.0) slightly above FMQ suggesting that the mantle wedge is oxidized to oceanic mantle and source of oxygen that oxidizes the mantle wedge is thought to result from hydrated subducting slab.

12- Nine podiform chromitite were investigated from 2 Km north of Kuradawi village. The pods in these locations were heterogeneous in physical properties and mode of occurrence. They have relatively sharp contact with surrounding mantle transition zone dunite, which in turn enclosed lenses from the mantle harzburgite.

13- The common alteration in chromite of chromitite rocks were described as alteration to ferritchromite from core to rim or progressive enrichment in Cr, total iron content and depletion in Al and Mg. Such a trend of alteration in chromite grain is related to metamorphic and hydrothermal event which re-equilibrated chromite composition. The plots of Cr-Al-Fe⁺³ shows that all chromite are plots in the field of green schist facies.

14- The chondrite normalized PGE patterns for chromitite rocks display a negative PGE slope from Ru to Pt, more or less a characteristic of ophiolite PGE patterns. The slightly flat PGE distribution patterns of dunite and harzburgite coincide with chondrite normalized patterns of depleted upper mantle peridotite and this indicates its different degree of partial melting.

15- The PGE concentration in chromitite rocks of the studied area was highly variable. They varied between PGE-poor it belongs to the (MTZ) to PGE-rich chromitite belongs to the deeper mantle section.

16- The strong variation of Pd/Ir ratios of chromitite rocks in the studied area (3.33 to 0.055) and its characteristic chondrite-normalized patterns expected a high degree of partial melt of mantle source cause the concentration of PGE in chromitite rocks at relatively low sulphur fugacity and high temperature.

17- The estimated temperature of formation for chromitite rocks was 1336 °C and those for dunite was 1209°C and for harzburgite and lherzolite were 1278 and 1358 °C respectively. These values correspond to the temperature of formation for Alpine-type peridotite.

18- The strong variation of Pd/Ir ratios of chromitite rocks and its characteristic CN- patterns expected a high degree of partial melt of mantle source cause the concentration of PGE in chromitite rocks at relatively low sulphur fugacity and high temperature.

19- The Mawat chromitite pods are probably formed by high degrees of partial melting of upper mantle and produced the exotic melt which interact with peridotites of mantle wall to produce dunite and SiO₂ and Al-poor orthopyroxene in wall peridotites by this melt.

20- Geochemical study of the gabbro rocks in MOC demonstrate the tholeiitic character and the plots of MgO against major elements show much of original chemistry of gabbro rocks were affected by metamorphism. In the light of geochemical data, it could be concluded that the gabbroic rocks formed from single basic mafic magma by fractional crystallization process. The chondrite-normalized REE patterns of gabbroic rocks in the studied area show light REE depletion and flat middle and heavy REE patterns with the overall patterns akin to flat lying REE patterns and such flat patterns resemble the rocks formed in island arc tholeiitic and subduction related setting.

21-The clinopyroxene chemistry of the gabbroic rocks also support the assertion that gabbroic rocks of MOC are related to island arc and boninitic rocks which have a linkage with SSZ.

7.2 Recommendations

At the end of this study these points can be recommended:

- 1- Determine the economic importance of chromitite rocks.
- 2- Determine the economic importance of the high-PGE concentration in chromitite of MOC, therefore further investigations are urgently needed to estimate to which extent the PGE-rich chromitite is distributed in the deeper mantle section.
- 3- Study the distribution composition of platinum group minerals in chromitite rocks.
- 4- Study the placer deposits of MOC with respect to the PGE source.

REFERENCES

- Abe, N., Arai, S., and Yutimoto, H., 1998.** Geochemical characteristics of the uppermost mantle beneath the Japan island arcs: implications for upper mantle evolution, *Physics of the Earth and Planetary Interiors*, Vol.107, pp.233-248.
- Abzalov, M.Z. 1998;** Chrome-spinel in gabbro-wehrlite intrusions of the Pechenga area, Kola Peninsula, Russia emphasis on alteration features, *Jour. Lithos.* Vol. 43, pp.109-134.
- Ahmed, A. H. and Arai, S., 2002.** Unexpectedly high-PGE chromitite from the deeper mantle section of the northern Oman ophiolite and its tectonic implications, *Contrib. Mineral Petrol*, Vol.143, pp.263-278.
- Ahmed, A.H., Arai, S., Abdel-Aziz, Y.M., and Rahimi, A., 2005.** Spinel composition as a petrogenetic indicator of the mantle section in the Neoproterozoic Bou Azzer ophiolite, Anti-Atlas, Morocco, *Precambrian Research*, Vol.138, pp.225-234.
- Ahmed, A.H., Arai, S., and Attia, A.K., 2001.** Petrological characteristics of podiform chromitites and associated peridotites of the PanAfrican Proterozoic ophiolite complexes of Egypt. *Jour. Mineral Deposita*, Vol. 36, pp. 72-84.
- Akif, A., Satran, V., and Al – Kaabi, A. 1972.** Preliminary report on geology and mineralization of Sershiw ultrabasic body, unpublished report, SOM. Library No.565.
- Akira Ishiwatari, 2003** Ophiolite succession and seismic layers of oceanic crust (Dr. Assoc. Prof., Fac. Sci., Kanazawa University) [Ishiwatari's Home Page] [Ishiwatari Labo Page] [Earth... earth.s.kanazawa-u.ac.jp/ishiwata/ophiol_e.htm - 13k
- Alavi, M. and Mahdavi, M.A., 1994,** Stratiography and structure of the Nahavand region in western Iran, and their implications for the Zagros tectonics, *Geological Magazine*, V.131, pp.43-47.
- Alavi, M., 2004.** Regional stratigraphy of the Zagros Fold-Thrust belt of Iran and its proforeland evolution, *American journal of science*, vol. 304, pp.1-20.
- Al-Chalabi, S.N.A., 2004.** Mineralogy and origin of chromitite in Qalander area Iraqi Kurdistan region, MSc, thesis, Salahaddin University-Erbil, 102p.

- Al - Etabi, W., 1972.** Petrography of Mawat Igneous Complex, unpublished report, petrological lab. NIMCO, No.560
- Al – Hassan, M.I., 1975.** Comparative petrologic study between Mawat and Penjwin Igneous Complexs, Northeastern Iraq, unpublished M.Sc.Thesis, Baghdad University.114pp.
- Al – Hashimi, A.R., and Al – Mehaidi, H., 1975.** Cu, Ni, Cr distribution in Mawat Ophiolite Complex, NE Iraq, Jour.Geol.Soc.Iraq, special issue.
- Al – Hassan, M.I., 1982.** Petrology, mineralogy and geochemistry of the Penjwin igneous complex, northeast Iraq, Ph. D Thesis, University of Dundee.
- Allan, J.F., Sack, R.O., and Batiza, R., 1988.** Cr-rich spinels as petrogenetic indicators:MORB-type lavas from the Lamont seamount chain, eastern Pacific, Am. Mineral.Vol.73, pp.741-753.
- Al- Mehiadi, H., 1975.** Geological investigation of Mawat – Chwarta area, NE Iraq, unpublished report, SOM Library, No. 609.
- Al-Saadi, A., J., H., 1990.** Petrology and geochemistry of volcanic rocks in Northeastern Thrust Zone, NE-Iraq, Unpublished MSc. Thesis, University of Baghdad, 136p. (In Arabic).
- Al-Samman, A.H., Zekaria, M. B., Younis, J. S., 1996.** Geochemical variation of Mawat Ophiolite Volcanics, Waraz, NE Iraq, Raf. Jour. Sci., Vol. 7, No. 2, pp. 55-67.
- Amosse, J., Allibert, M. Fischer, W., and Piboule, M., 1990.** Experimental study of the solubility of platinum and iridium in basic silicate melts- implication for differentiation of platinum- group elements during magmatic processes, Jour. Chem.Geol. Vol. 81, pp. 45-53.
- Angeli, N., 2005.** Platinum Group Minerals in Eastern Brazil Geology and occurrences in Chromitite and Placers, Platinum Metals Review, Vol.49 Issue 1, pp.41-53.
- Angeli, N., and Vlach, S. R. F., 2004.** Chromite Composition, Metamorphism, and PGM Distribution in Chromitites from the Espinhaco Ridge, Brazil, Applied Mineralogy, pp.849-852.

- Anna, M., Giovanni, G. and Valeria, D., 2007.** Chromitite alteration in serpentinite mélanges of Nurali and Kalan Massifs, Russia, Goldschmidt Conference (Abstract).
- Aqrawi, A., M., M., 1990.** Petrochemistry and petrogenesis of ultramafic and gabbroic rock around Mawat ophiolite complex, northeastern Iraq. Unpublished Msc Thesis, Mosul University, 155p. (in Arabic).
- Aqrawi, A., M., M., 2000.** Assessment of Iraqi serpentinites for utilization in ceramics Unpublished PhD Thesis, Baghdad University, 220p. (in Arabic).
- Auge, T. 1987.** Chromite deposits in the northern Oman ophiolite; mineralogical constraints. *Miner. Deposita*, Vol. 22, pp.1-10.
- Arai, S., 1980.** Dunite-Hurzburgite-chromitite complexes as refractory residue in the Sangun-Yamaguchi zone, western Japan, *Journal of Petrology*, 21, 141-165.
- Arai, S., 1987.** An estimation of least depleted spinel peridotite on the basis of olivine-spinel mantle array. *Necues Jahrb., Mineral., Monatsh.* Vol. 8, pp. 347-354.
- Arai, S., 1990.** What kind of magmas could be equilibrated with ophiolitic peridotite? In: J. Malpas, E. M. Moores, A. Pnyiotou and C. Xenophontos (eds.), *Ophiolites, Oceanic Crustal Analogues*, The geological survey Department, Ministry of Agriculture and Natural Resources, Nicosia, Cyprus, pp.557-565.
- Arai, S., 1991.** The circum-Izu Massif Peridotite, Central Japan, as Back-Arc Mantle Fragments of the Izu-Bonin Arc System. In: T. J. Peters (ed.), *Ophiolite genesis and Evolution of the Oceanic Lithosphere*, pp.801-816.
- Arai, S., 1992,** Chemistry of chromian spinel in volcanic rocks as a potential guide to magma chemistry. *Mineral Mag.* 56; pp.173-184.
- Arai, S., 1992a.** Chemistry of chromian spinel in volcanic rocks as a potential guide to magma chemistry, *Mineralogical Magazine*, Vol.56, pp.173-184.
- Arai, S., 1992b.** Petrological and geological significance of detrital chromian spinel and detrital serpentinite, *Memoirs of the Geological society of Japan*, Vol.38, pp.329-344. (in Japanese with English abstract).

- Arai, S, and Yurimoto, H., 1992.** Origin of Podiform chromitites from southwest Japan as a melt-mantle interaction, 29th Int. Geol. Congr., Kyoto, 1:176 (Abstract).
- Arai, S., 1994 (a).** Characterization of spinel peridotite by olivine-spinel compositional relationships; review and interpretation. *Chem. Geol.* 113, 191-204.
- Arai, S, and Yurimoto, H., 1994.** Podiform chromitites of the Tari-Misaka ultramafic complex, southwest Japan, as mantle-melt interaction products, *Econ. Geol.* Vol.89, pp.1279-1288.
- Arai, S., 1994 (a).** Compositional variation of olivine-chromian spinel in Mg-rich magma as guide of residual spinel peridotite *Jour. Volcanol Geoth. Res.* 59, 279-293.
- Arai, S., and Abe, N., 1995.** Reaction of orthopyroxene in peridotite xenoliths with alkali-basalt melt and its implication for genesis of alpine-type chromitite, *American Mineralogist*, Vol.80, pp.1041-1047.
- Arai, S., and Yurimoto, H., 1995.** Possible sub-arc origin of podiform chromitites, *The Island Arc*, Vol. 4, pp.104-111.
- Arai, S., 1997.** Control of wall-rock composition on the formation of podiform chromitites as a result of magma/peridotite interaction, *Resource Geology*, Vol.47, pp.177-187.
- Arai, S., and Matsukage, K., 1998.** Petrology of a chromitite micropod from Hess Deep, equatorial Pacific: a comparison between abyssal and alpine-type podiform chromitites, *LITHOS*, Vol.43, pp.1-14.
- Arai, S, Prichard, H.M., Matsumoto, I., Fishsher, P.C. 1999.** Platinum group minerals in podiform chromitite from the the Kammuikkotan Zone, Hokkaido, northern Japan. *Res. Geol*, Vol. 49, pp. 39-47.
- Arai, S., Hirai, H., and Uro, K., 2000.** Mantle peridotite xenoliths from the Southwest Japan arc: a model for the sub-arc upper mantle structure and composition of the Western Pacific rim, *Journal of Mineralogical and Petrological Sciences*, Vol.95, pp.9-23.
- Arai, S., Ishimaru, S., and Okrugin, V. M., 2003.** Metasomatized harzburgite xenoliths from Avacha volcano as fragments of mantle wedge of the

Kamchatka arc: Implication for the metasomatic agent, *The Island Arc*, Vol.12, pp.233-246.

Arai, S., Uesugi, J., and Ahmed, A. H., 2004. Upper crustal podiform chromitite from the northern Oman ophiolite as the stratigraphically shallowest chromitite in ophiolite and its implication for Cr concentration, *Contrib. Mineral Petrol*, Vol.147, pp.145-154.

Arai, S., Shimzu, Y., Ismail, S. A., and Ahmed, 2006. Low-T formation of high-Cr spinel with apparently primary chemical characteristics within podiform chromitite from Rayat, northeastern Iraq, *Mineralogical magazine*, Vol.70., No.5, pp.499-508.

Arculus, R.J. 1994. Aspect of magma genesis in arcs. *Lithos*, 33, 189-208.

Arculus, R.J. and Delano, J.W., 1981. Siderophile element abundances in the upper mantle :Evidence for sulfide signature and equilibrium with the core, *Jour.Geochim. Cosmochim. Acta*. Vol. 55, pp.1159-1172.

Aswad, K.J., and Ojha, D.N., 1984. The geochemistry and petrology of the spilitic diabasic rocks of the Mawat Ophiolite Complex, North East Iraq, *Iraqi Jour.Sci.*, Vol.25,Nos. 1-2, pp..57-74.

Aswad, K.J., and Elias, E.M., 1988. Petrogenesis, Geochemistry, and Metamorphism of spilitized subvolcanic rocks of the Mawat Ophiolite Complex, NE Iraq., *Ophiolite*, Vol.13 No.2/3, pp.95-109.

Aswad, K.J., Alsamman, A.H., and Aqrawi, A.M. 1993. Petrogenesis of ultramafic tectonite Root Mountain of Mawat Ophiolite Complex, NE Iraq. *Mu'tah Jour. for Research and Studies*, Vol. 8, No. 4. pp. 49-75.

Aswad, K.J., 1999. Arc- continent collision in Northeastern Iraq as evidenced by Mawat and Penjain Ophiolite Complexes, *Raf. , Jour. Sci*, Vol. 10, No.1 pp.51-61.

Barkov, A.Y., Martin, R.F., Halkoaho, T.A.A., and Poirier, G., 2000. The mechanism of charge compensation in Cu-Fe-PGE thiospinels from the Penikat layered intrusion, Finland, *American Mineralogist*, Vol.85, pp.694-697.

Barnes, S. J., Naldrett, A. J., and Gorton, M.P., 1985. The origin of the fractionation of platinum-group elements in terrestrial magmas, *Jour. Chem.Geol.* Vol. 53, pp 303-323.

- Barnes, S.J., Boyd R., Korneliussen, A., Nilsson L-P, Often, M., Pedersen, R.B., and Robins, B., 1988.** The use of mantle normalization and metal ratios in discriminating between effects of partial melting, crystal fractionation and sulfide segregation in platinum-group elements, gold, nickel and copper: example from Norway. In Prichard HM, Potts, Bowles JFW, CribbSJ(eds), Jour. Geo-Platinum, Vol. 87, Essex. Elsevier, Amsterdam, pp. 113-144.
- Barnes, S.J., 2000.** Chromite in komatites, II.Modification during greenschist to mid-amphibolite facies metamorphism,Journal of Petrology,41, 387-409
- Barnes, S.J., and Roeder, P.L., 2001, The range of spinel compositions in terrestrial mafic and ultramafic rocks, Journal of Petrology, Vol.42, pp.2279-2302.
- Berger, S., Cochrane, D., Simons, K., Savov, I., Ryan, J. G. and Peterson, V.L., 2001.** Insights from rare earth elements into the genesis of the bulk Creek Complex, Clay County,NC, Jour. of Southeastern Geology, Vol. 40, No.3, pp.201-212.
- Best, M. G., 2001.** Igneous petrology, Blackwell Science, Inc., 443p.
- Bodinier, J., L., 1988.** Geochemistry and petrogenesis of the Lanzo peridotite body. Western Alps. Jour of Tectonophysics, Vol. 149, pp. 67-88.
- Bodinier, J., L., and Godard, M.; 2004.** Orogenic, Ophiolitic, and Abyssal peridotites. In Holland, H. D. and Turekian, K. K. (Eds.), Treatise on Geochemistry, Elsevier Pergamon, Amsterdam – Boston, Vol. 2, pp. 103-170.
- Bohlen, S. R., and Essene, E. J., 1979.** A critical evaluation of two-pyroxene thermometry in Adirondack granulites, LITHOS, Vol.12, pp.335-345.
- Bolten, C.M.G. 1957.** Explanation of the geological map – Kurdistan series (1: 100,000) sheet K5 Choarta. Unpublished report, SOM.Library No. 27.
- Bolten, C.M.G. 1958.** The geology of the Rania area. Site Inv.Co. Unpubl.Report, G.S.M.Lib., No.271, Baghdad, Iraq
- Bolten, C.M.G., 1957 a.** Explanation of the geological map Kurdistan series (1: 100,000), sheet K5 Choarta site Inv.Co. unpubl.report, G.S.M.Lib., Baghdad, Iraq

- Bonatti, E., and Michael, P.J., 1989.** Mantle peridotites from continental rifts to ocean basins to subduction zones, *Earth planet Sci. Lett.*, Vol.91, pp.297-311.
- Bose, M.K., 1997.** Igneous petrology, first edition, the world Press Private Limited, Calcutta,567p.
- Buda, G. and Al-Hashimi, W.S. 1977A.** Alpine type chromite from Mawat, Northeastren Iraq, *Jour.Geol.Soc.Iraq*, special issue, pp.61-77.
- Buda, G, 1988.** Chromite occurrences in Iraq Zagros, *Jour. Acta. Mineralogica-Petrographica*, Szeged, Vol. XXIX, pp. 69-79.
- Buda,G. and Al Hashimi, W.S. 1977B.** Petrology of Mawat Ophiolite Complex.Northeastren Iraq .*Jour. Geol. Soc. Iraq* Vol. X, P.69-98
- Buday, T. 1980.** The regional geology of Iraq , Stratigraphy and paleogeography, edited by Kassab, I.M. and Jassim S.Z., Dar Al- Kutib publishing house ,Mosel, Iraq, 445p.
- Buday, T. and Jassim, S.Z. 1987.** The regional geology of Iraq, Tectonism, Magmatism, and Metamorphisim, edt. By Kassab, I.M. and Abass, M.J., Geological Survey and Mineral Investigation, Baghdad, Iraq, 352p.
- Buztug, D., Yagmur, ., Otlu, N., Tatar, S, and Yesiltas, A.; 1998,** Petrography of the post-collisional, within-plate, Yildizdag Gabbroic pluton, Yildize- Sivas Region, central Anatolia, Turkey. *Jour. Earth Science, Turkish Jour.*Vol. 7, pp. 37-51.
- Cann, J. R., 1970.** Rb, Sr, Y, Zr, and Nb in some ocean floor basaltic rocks, *Earth Planet,Sci.Lett.*, Vol.10, pp.7-11.
- Cassard, D., Nicolas. A., Pabinoritch, M., Moutte, J., Leblance, M., and Prinzhofer, A., 1981;**Structural classification of chromite pods in southern New Caledonia, *Econ. Geol.*Vol. 76, pp.805-831.
- Carmichael, I.S.E., 1967.** The iron-titanium oxide of saic volcanic rocks and their associated ferromagnesian silicates. *Jour. Contrib Mineral Petrol.* Vol. 14, pp. 36-64.
- Cina, A., Neziraj, A., Karaj, N., Johan, Z., and Ohnenstetter,M.** PGE mineralization related to Albanian Ophiolitic Complex,
- Coleman, R.G. 1977.** Ophiolites, Springer- Verlag , New York, 229p.

- Crocket, J. H. 1979.** Platinum-group elements in mafic and ultramafic rocks, a survey. *Jour. Can. Mineral* Vol. 17, pp. 391-402.
- Davis, J. F., Grant, R.W.E., and Whitehead, R.E.S., 1979.** Immobile trace elements and Archian volcanic stratigraphy in the Timmins mining area, Ontario, *Can.J. Earth. Sci.* Vol.16, pp.305-311.
- Dickey, J. S., JR, 1975.** A hypothesis of origin for podiform chromite deposits, *Geochemica et Cosmochimica Acta*, Vol.39, pp.1061-1074.
- Dick, H.J. B. and Fisher, R.L 1984.** Mineralogical studies of mantel residues of abyssal and alpine- type peridotite in Kimberlites II. The mantle and crust relationships (J. Kornprobst, Ed.) Amsterdam Elsevier, pp 295-308.
- Dick, H.J. B. and Bullen, T. 1984.** Chromian spinel as petrogenetic indicator in abyssal and Alpine-type peridotite and specially associated lavas, *Contrib. Mineral. Petrol.* 86, pp 54-76.
- Dick, H.J. B 1989.** Abyssal peridotites, very slow spreating ridge and ocean ridge magmatism. In *magmatism ocean basins* (S.D Sunder, M.J Norry, Eds). *Geol. Soc,London. Special publication 42*, pp.71-105.
- Dick, H.J. B. and Natland, J. H. 1996.** Late stage evolution and transport in the shallow mantle beneath the east Pacific Rice: Deep sea drilling project, *Initial reports 147*, pp. 103-134.
- Duclaux, G., Menot, R.P., Guillot, S., Agbossoumonde, Y. and Hilairet, N. 2006.** The mafic layered complex of the Kabye' massif (north Togo and north Benin): Evidence of a Pan-African granulitic continental arc root, *Jou. Of Precambrian Research*, No. 2720, pp. 1-18.
- Dunnington, H.V., 1858.** Generation migration accumulation and dissipation of oil in Northern Iraq, *Habitat of oil, symposium. A. A.P.G. Wecks* (Ediitor), pp.1194-1251.
- Economou, M.I., 1986.** Platinum-group elements (PGE) in chromite and sulfide ores within the ultramafic zone of some Greek ophiolite complexes. In: Gallagher MJ, Ixer, RA, Neary CR, Prichard HM (eds), *Jour. Metallogeny of basic and ultrabasic rocks Inst. Mining and Metallurgy Publ., London*, pp. 441-454.

- Edwards, S. J., 1990.** Harzburgites and refractory melts in the Lewis Hills massif, Bay of Island ophiolite complex: the base metals and precious-metals stony. *Jour. Can. Mineral*, Vol. 28, pp. 537-552.
- Edwards, S. J. and Malpas, J.,1995.** Multiple origins for mantle harzburgite; examples from the Lewis Hills, Bay of Islands ophiolite, Newfoundland. *Can., Jour. Earth Sci.* Vol. 32, pp. 1046-1057.
- Engler, A., Koller, F., Meisel, T. and Quemeneur, J., 2002.** Evolution of the Archean/Proterozoic crust in the southern Sao Francisco craton near Perdoes, Minas Gerais, Brazil: Petrological and geochemical constraints. *Jour. of South American Earth Science*, Vol. 15, pp. 709-723.
- Evans, B.W., and Frost, B. R., 1975.** Chrome-spinel in progressive metamorphism- a preliminary analysis, *Geochemica et Cosmochimica Acta*, Vol.39, pp.959-972.
- Frost, B. R., 1991.** Stability of oxide minerals in metamorphic rocks. In: Lindsley, D.H.(Ed.), *Oxide minerals, Petrologic and Magnetic Significance*, *Review Mineral.*, Vol,25, pp.469-487.
- Falcon N.L., 1969.** Problems of the relationship between surface structure and deep displacements illustrated by the Zagros rang .In:Kent, P.E., Satterthwaite, G.H. and Spencer, A.M. (eds) *Time and place in Orogeny*.Geological Society, London, pp.9-22.
- Falcon N.L., 1974.** Southern Iran:Zagros Mountain.In: Sphencer, A.(ed.) *Mesozoic-Cenozoic Orogenic Belt*. Geological Society, London,special publications, 4, pp. 199-211.
- Farjo, S., F., 2006.** Geochemistry and petrogenesis of the volcanic rocks of Mawat ophiolite complex, NE-Iraq, Unpublished MSc. Thesis, Unieversity of Mosul, 176p. (in Arabic).
- Frey, F. A., Suen, C. J. and Stockman, H. W., 1985.** The Ronda high temperature peridotite: geochemistry and petrogenesis. *Geochem. Cosmochim. Acta*, Vol. 49, pp. 2469 – 2491.
- Gaetani, G. A. and Grove, T. L., 1998.** the influence of water on melting of mantle peridotite. *Contrib. Mineral, Petrol.* 131, pp223-246.

- Garuti, G., Zaccran, F., Cabella R., and Fershatater, G., 1997.** Occurrence of unknown Ru-Os-Ir-Fe oxides in chromitite of Nurali-ultramafic complex south of Urals, Russia, *Can. Mineral*, Vol 35, pp. 1431-1439.
- Gervilla, F. and Remaidi, M., 1993.** Field trip to the Ronda ultramafic massif: an example of asthenosphere-lithosphere interaction? *Ofioliti*, vol. 18, pp. 21-35.
- Ghasemi, A., and Talbot, C.J., 2006.** A new tectonic scenario for the Sanandaj-Sirjan Zone (Iran), *Asian Earth Science Jour.*, Vol. 26, pp. 683-693.
- Hamasalh, F. R.; 2004.** Petrochemistry, Petrogenesis and tectonic setting of the Pauza ultramafic rocks-Bulfat complex north-east Iraq, Kurdistan region, MSc. Thesis, University of Sulaimani, 115p.
- Hamilton, W. and Mountjoy, W., 1965, Alkali content of Alpine ultramafic rocks, *Geochim. Cosmochim. Acta* Vol. 29, pp. 661-671.
- Harmer, R. E. and Von Gruenewaldt, 1991.** A review of magmatism associated with the Tranvaal basin-implication for its tectonic setting; *Jour. Geol. S. Africa*, Vol. 93, pp.104-122.
- Harris, D. C. and Cabri, I. J., 1991.** Nomenclature of Platinum-group alloys: review and revision, *Jour. Canadian Mineralogist*, Vol., 54, pp. 231-237.
- Hebert, R. Admason, A.C. and Komoro, S.C. 1990.** Metamorphic petrology of ODP 190, Hole 670 A, serpentinized peridotite: serpentinization process at slow spreading ridge environment. In proceeding of ODL, *Sci. result*, 106/109. (R Detrik, J. Honneriz, W.B. Bryan, T. Juteau, Eds). College Station, Texas, pp. 103-115.
- Hertogen, J., Janssen, M.J., and Palme, M., 1980.** Trace elements in ocean ridge basalt glasses: implication for fractionation during mantle evolution and petrogenesis., *Geochim Cosmochim., Acta*, Vol. 44, pp. 2125-2143.
- Hessami, K., Koyi, H., Talbot, C.J., Tabasi, H. and Shabanian, E. 2001** Progressive unconformities within an evolving foreland fold-thrust belt, Zagros mountains, *Jour. Of the geological society* vol. 158, pp969-981.
- Hey, M. H., 1954,** A new revision of the Chlorite, *Mineralogical Magazine*, Vol. 30, pp. 277-292.

- Hill, R., and Roeder, P. 1974.** The crystallization of spinel from basaltic liquid as function of oxygen fugacity. *Jour. of Geology*, 82, 709-729.
- Hisada, K-I., Sugiyama, M., Ueno, K., Charusiri, P., and Arai, S., 2004.** Missing ophiolitic rocks along the Mae Yuam Fault as the Gondwana-Tethys divide in north-west Thailand, *The Island Arc*, Vol.13, pp.119-127.
- Hofmann, A.W., 2004.** Sampling mantle heterogeneity through oceanic basalts: Isotopes and trace elements, In Holland, H. D. and Turekian, K. K. (Eds.), *Treatise on Geochemistry*, Elsevier Pergamon, Amsterdam – Boston, Vol. 2, pp. 61-101.
- Holloway, M.I., and Bussy, F., 2006.** Trace element partitioning during partial melting of basic igneous rocks in a contact aureole (Fuerteventura, Canary Islands), *Jour. of Geophysical Research Abstracts*, Vol. 8, No. 09116.
- Horn, A. M., and Less, G., M., 1943.** The zone of nappes in Iraq Kurdistan, Min. of development, unpublished report, SOM.Library, No. 133.
- Hussein, I.M., Kroner, A., and Reischmann, T., 2004.** The Wadi Onib mafic –ultramafic complex: a Neoproterozoic supra-subduction zone ophiolite in the northern Red Sea hills of the Sudan. In : Kusky, T. M.(Ed.), *Precambrian Ophiolite and Related Rocks*, Elsevier, pp.163-206.
- Irvine, T. N., 1965.** Chromian spinel as a petrogenetic indicator, Part 1, theory, *Canadian Journal of Earth Sciences*, Vol.2, pp.648-672.
- Irvine, T. N., 1965.** Chromian spinel as a petrogenetic indicator, Part 1, theory, *Canadian Jour. of Earth Sciences*, Vol. 2, pp. 648-672.
- Irvine, T. N., 1967.** Chromian spinel as a petrogenetic indicator, Part 2, petrologic applications, *Canadian Journal of Earth Sciences*, Vol.4, pp.71-103.
- Irvine, T.N., and Baragar, W.R.A., 1972.** Muskox Intrusion and Coppermine River Lavas, Northwestern Territories, Canada: 24th Internat. Geol.Congr., Montreal, Excursion A29, Gudebook, 70p.
- Irvine, T.N., 1977.** origin of chromite layers in the Muskox intrusion and other intrusions: a new interpretation, *Geology* 5, pp.273-277.
- Ishii, T. Robinson P.T. Maekawa, H. Fiske R. 1992.** Petrological studies of peridotites from diapiric serpentine seamounts in the Izu Ogasawara- Mariana

forearc, LEG 125, In proceedings of the ODP, Sci. Results, Vol. 125. (P. Fryer, J.A., Pearce, L.B. Stokking Eds). College Station, Texas, pp. 445-485.

Ismail S. A. and Al-Chalabi S. A. 2006. Genesis of Chromitite in Qalander Area, Northern Iraq, Employing Cr-rich spinel, Jour. Kirkuk University – Scientific Study, Vol.1No. 2

Ismail, S.A, Arai, S., Ahmed. A. H., Shimizu, Y., 2007. Chromitite and peridotite from Rayat, northeastern Iraq, as a fragment of Tethyan ophiolite, Jour. Island arc, in press.

Ismail, S.A, 2007. The occurrence of platinum group minerals Laurite in ophiolitic-chromitite rocks Zagros Thrust Zone, Rayat area, NE Iraq, in press.

Jackson, E.D., 1969. Chemical variation in co-existing chromite and olivine in chromite zones of the Stillwater complex, In: Wilson, H.D.B.,(Ed.), Magmatic Ore Deposits, Econ. Geol. Monogr., Vol.6, pp.265-296.

Jacobson, C.E., 1989. Estimation of Fe³⁺ from electron microprobe analyses: observations on calcic amphibole and chlorite, Journal Metamor. Geol., Vol.7, pp.507-513.

Jagoutz, E., Palme, H., Baddenhausen, H., Blum, K., Cendales, M., Dreibus, G., Spettel, B, Lorenz, V., and Wanke, H., 1979. The abundance of major, minor and trace elements in earth's mantle as derived from primitive ultramafic nodules. In: Proc 10th Lunar Planet Science Conf., pp. 2031-2050.

Johnson, R. W., Jaques, A.L., Hickey, R.L., Mckee, C.O., and Chappell, B.W., 1985. Manam Island, Papua New Guinea: Petrology and geochemistry of low TiO₂ basaltic island-arc volcano: Jour. of Petrology. Vol. 26, pp. 283-323.

Johnson, K.T., Dick, H.J. B., and Shimizu, N., 1990. Melting in the oceanic upper mantle: ion microprobe study of diopsides in abyssal peridotites, Journal Geophysics Research, Vol.95, pp.2661-2678.

Jassim, S., Z., 1972. Geology of the central sector of the Mawat Igneous Complex, Northeastern Iraq, Jour. Of Geo. Soc. Iraq, Vol.VI, pp.83-92.

Jassim, S.Z., and Al – Hassan M. I. 1977. Petrography and origin of the Mawat and Penjwin Igneous Complex: a comparison, Jour.Geol.Soc.Iraq, special issue, pp.169- 210.

- Jassim, S.Z. and Goff, C. ed.), 2006.** Geology of Iraq, Published by Dolin, Prague and Moravian Museum, Brno, 341p.
- Jensen, L.S., 1976.** A new caption plot for classifying subalkaline volcanic rocks; Ontario Division of Mines, Geological Report 66, pp. 1-20.
- John, T., Schherer, E. E., Haase, K., and Schenk, V. 2004.** Trace elements fractionation during fluid –included eclogitization in a subducting slab: trace element and Lu-Hf-Sm-Nd isotope systematics, Jour. of Earth and Planetary Science Letters, Vol. 227, pp.441-456.
- Karim, K.H., 2005.** Some sedimentary structural evidence of possible graben in Mawat-Chuarta area, NE-Iraq, Iraqi Jour. Earth Sci., Vol. 5, No. 2, pp. 9-18.
- Kimball, K. L, 1990.** Effect of hydrothermal alteration on the compositions of chromia spinels, Jour. Contrib. Mineral Petrol., Vol. 105, pp. 337-346.
- Kamenetsky, V. S., Crawford, A.J. and Meffre, S. 2001.** Factor controlling chemistry of magmatic spinel: an empirical study of associated olivine, Cr-spinel and melt inclusions from primitive rocks, Jour. Petrol. Vol. 42, pp. 655-671.
- Katzir, Y., Avigad, A., Matthews, A., Garfunkel, Z., and Evans, B., W. 1999.**Origin and metamorphism of ultrabasic rocks with subducted continental margin, Naxos (Cycladaes, Greece), Jour, of Metamorphic Geol., Vol. 17, No. 3, pp. 301-318.
- Kim, J., Coish, R., Evans, M., and Dick, 2003.** Supra-subduction zone extensional magmatism in Vermont and adjacent Quebec: Implication for early Paleozoic Appalachian tectonics, Jour. Geological Society of America, Vol. 115, No. 12, pp. 1552-1569.
- Klein, C. and Harlbut, Jr. C.S., 1993.** Manual of Mineralogy, JohnWiley & Sons, New York, 681p.
- Klingenberg, M.N.E.T. and Kushiro, I. 1996.** Melting of chromite-bearing harzburgite and generation of boninitic melts at low pressure under controlled oxygen fugacity. Lithos, 37, 1-13.
- Kocks, H., Meisel, T., Melcher, F., and Burgath, K-P., 2006.** PGE- and Os-isotope data of chromites in the Shebeniku ophiolitic complex, Albania:

evidence for two stage melting in a supra subduction zone environment, Geophysical Research Abstracts, Vol. 8, No. 07237.

Kohler, T. and Brey, G.P., 1990. Calcium exchange between olivine and clinopyroxene calibrated as geothermobarometer for natural peridotites from 2-60 kb with applications. Jour. Geochim, Cosmochim. Acta, Vol. 54, pp. 2375-2388.

Kopylova, M.G., Russel, J.K, and Kookenboo, H. 1999. Petrology of peridotite and pyroxenite xenolith from the Jericho Kimberlite: implication for the thermal state of the mantle beneath the Slave craton, northern Canada, Jour. Petrol. Vol. 40, pp. 79-104.

Koyi, A., M.A.2006. Petrochemistry, petrogenesis and Isotope dating of Walash volcanic rocks at Mawat-Chowarta area, NE Iraq, Unpublished MSc. Thesis, Universty of Mosul 230p. (In Arabic).

Lago, B. L., Rabinowicz, M., and Nicolas, A., 1981. Podiform Chromite Ore Bodies: A genetic Model, Journal of Petrology, Vol.23, part 1, pp.103-125.

Lago, B.L., Rabinowicz, M., and Nicolas, A., 1982. Podiform chromite ore bodies: a genetic model, Journal Petrology, Vol.23, pp.103-125.

Leake, B.E., Wooley, A. R., Arps, C. E. S., Gilbert, M. C., Grice, J. D., Hawthorne, F. C., Kato, A., Kisch, H. J., Krivovichev, V. G., Linthout, K., Laird, J., Mandarino, J. A., Maresch, W. V., Nickel, E. H., Rock, N. M. S., Schumacher, J. C., Smith, D. C., Stephenson, N. C. N., Ungaretti, L., Whittaker, E. J. W., and Youzhi, G., 1997 Nomenclature of amphiboles: Report of the subcommittee on amphiboles of the international mineralogical association, commission on new minerals and mineral names, The Canadian Mineralogist, Vol.35, pp.219-246.

Leblanc, M., 1981. The Proterozoic ophiolites of Bou Azzer (Morocco): evidence for Pan African plate tectonics, Elsevier, Amsterdam, pp.436-451.

Leblance, M. , 1991. Platinum Elements and Gold in Ophiolitic Complexes: Distribution and Fractionation from Mantle to Oceanic Floor, In: Peters T et al. (eds) Ophiolite Genesis and Evolution of the Oceanic Lithosphere, Ministry of Petroleum and Minerals, Sultanate of Oman, 231- 260p.

- Leblance, M., 1995.** Chromite and ultramafic rock compositional zoning through a paleotransform fault, Poum, New Caledonia, *Jour. Economic Geology*, Vol. 90, pp. 2028-2039.
- Lee, Y., 1999.** Geotectonic significance of detrital chromian spinel A review, *Geosci. Jour.* Vol. 3, pp. 23-29.
- Lehner, H.P.E., 1954.** Report on geological survey of the area north of Choarta, Site Inv. Co. report, unpublished report, SOM. Library.
- Li, J., Kusky, T. M., and Huang, X., 2002.** Archian Podiform Chromitites and Mantle Tectonites in Ophiolitic Melange, North China Craton, *GSA Today*, pp.1-11.
- Legendre, O., 1982.** Mineralogie et geochimi des platinoides dans les chromitites ophilitiques. These. Doct. 3eme Cycle, Universit'e de Paris 6.
- Lehmann, J., 1983; Diffusion between olivine and spinel: application to geothermometry. *Earth and Planetary Science Letters* 64, pp. 123-138.
- Le Maitre, R.W., Bateman, P., Dudek, A., Keller, J., Lameyre, J., LeBas, M.J., Sabine, P.A., Schmid, R., Sorenson, H., Streckeisen, A., Woolley, A.R., and Zenettin, B., 1989.** A Classification of Igneous rocks and Glossary of Terms, Recommendations of the International Union of Geological Sciences, Subcommittee on the Systematics of Igneous Rocks, Blackwell, Oxford, 193p.
- Lonley, R. A., Himmelberg, G. R. and Coleman, R. G. 1971.** Structure and petrology of the Alpine-type peridotite at Burro Mountain, California, U.S.A. *Jour. of Petrol.* Vol. 12, pp.245-309.
- Maier, W. D., 2005.** Platinum-group element (PGE) deposits and occurrences: Mineralization styles, genetic concepts, and exploration criteria, *Journal of African Earth Sciences*, Vol.41, pp.165-191.
- Malich, K. N., Knauf, V. V., Meisel, T., Paliulionyte, V., Efimov, A. A., and Kostoyanov, A. 2003.** Contracting platinum-group mineral assemblages from chromitites of clinopyroxinite-dunitite massifs (Russia): new compositional and osmium isotope data, This is contribution for IGCP project 479p.
- Mashek, J., and Etabi, W., 1973.** Petrology of the Mawat Igneous-metamorphic complex. NIMCO Lib. Unpublished report.

- Matsukage, K. and Kubo, K. 2003.** Chromian spinel during melting experiments of dry peridotite (KLB-1) at 1.0-2.5 GPa. *American Mineral*, 88, pp.1271-1278.
- McCallum, M.E., 1996; Loucks, R. R., Carlson, R. R., Cooley, E.F...., Doerge, T. A., 1967.** Platinum metals associated with hydrothermal Cu ores of New Rambler Mine, Medicine Bow Mountains, Wyoming. *Jour. Eco. Geol.* Vol. 71, pp. 1429-1450.
- McDonough, W.F., and Frey, F. A. 1989.** Rare earth elements in upper mantle rocks, In Lipin, B. R., and Mckay , G. A. (Eds.), *Geochemistry and mineralogy of rare earth elements.* *Rev. Mineral.*, 21, pp. 99-145.
- Melcher, F., Grum, W., Simon, G., Thalhammer, T.V., and Stumpel, E., 1997.** Petrogenesis of the Ophiolitic giant Chromite Deposits of Kempirsai, Kazakhstan: a Study of Solid and Fluid Inclusions in Chromite, *Journal of Petrology*, Vol.38, No.10, pp.1419-1458.
- Melcher, F., Grum, W., Thalhammer, T. V., and Thalhammer, O. A. R., 1999.** The giant chromite deposits at Kemirisai, Urals: constraints from trace elements (PGE, REE) and isotope data, *Mineralium Deposita*, Vol.34, pp.250-272.
- Melcher, F., 2000.** Base metal-platinum- group element sulfides from the Urals and the Eastern Alps: characterization and significance for mineral systematics, *Mineralogy and Petrology*, Vol.68, pp.177-211.
- Mellini, M., Rumori, C., and Viti, C., 2005.** Hydrothermally reset magmatic spinels in retrograde serpentinites: formation of " ferritchromit" rims and chlorite aureoles, *Contrib. Mineral Petrol*, Vol.149, pp.266-275.
- Mirza, T.A, and Ismail, S.A. 2007.** Origin of plagiogranite in the Mawat ophiolite complex, Kurdistan Region, NE Iraq. *Jour. of Kirkuk University-Scientific Studies*, Vol. 2, No. 1, pp 1-25.
- Mitcheel, R.H., Heays, R.R., 1981.** Abundance and distribution of gold, palladium and iridium in some spinel and garnet lherzolite: Implications for the nature and origin of precious metal rich intergranular components in the upper mantle. *Geochim.Cosmocheim Acta*, 45, pp.2425-2442.

- Miyake, K., Arai, S., and Okuno, M., 1997.** Petrology of Peridotite and Chromitite in Wakamatsu Mine of the Tari-Misaka Ultramafic Complex, Western Japan, *Resource Geology*, Vol.47, pp.211-221.
- Muhammad, Y.O, 2004.** Petrology and geochemistry of serpentinite and associated rocks in Mawat and Penjwin area, Kurdistan Region, northeastern Iraq, MSc. Thesis, University of Sulaimani, 152p.
- Naldrett, A.j, Hoffiman E.L., Green, A.H., Chou Chin-Lin, Naldrett, S.R., and Alcock R.A. 1979.** The composition of Ni-sulfidated ores, with particular reference to their content of PGE and Au. *Jour. Can. Mineral*, Vol.17, pp. 403-415.
- Nayak, P. K., 2004.** Complementary PIXE and EDXRF studies on Chromites, Proceedings of the 10th International Conference on Particle Induced X-ray Emission and its Analytical Applications, Portoroz, Slovenia, June 4-8.
- Nickel, K. G., 1986.** Phase equilibria in the system $\text{SiO}_2\text{-MgO-Al}_2\text{O}_3\text{-Cr}_2\text{O}_3$ (SMACCR) and their bearing on spinel/garnet lherzolite relationships. *Neues Jahrbuch Mineralogic Abhandlungen*, Vol. 155, pp. 259-287.
- Niu, Y.; Langmuir, C. H., and Kinzler, R.J. 1997.** The origin of abyssal peridotites: a new perspective. *Earth and Planetary Science Letters*, Vol. 152, pp. 251-265.
- Niu, Y., Hekinian, R. 1997.** Spreading –rate dependence of the extent of mantle melting beneath ocean ridges. *Nature* 385, pp. 326-329.
- Niu, Y., Regelous, M. Wendt, J. Batiza, R. and O'Hara, M.J. 2002a;** Geochemistry of near EP R seamounts; importance of source vs. process and origin of enriched mantle component. *Earth and Planetary Science Letters* 199, pp. 329-348.
- Niu, Y., O'Hara, M.J. and Pearce, J.A., 2003.** Initiation of subduction zones as consequence of lateral compositional buoyancy contrast within the lithosphere: a petrologic perspective, *Jour. of Petrology*, Vol. 44, pp. 851-866.
- Niu, Y.; 2004.** Bulk – rock major and trace element composition of abyssal peridotite: Implication for mantle melting, melt extraction and post – melting processes beneath mid – ocean ridges, *Jour. of Petrology*, vol. 45, No. 12, pp. 2423-2458.

- Numan, N.M.S., 1997.** A plate tectonic scenario for the Phanerozoic succession in Iraq, *Geol.Jour.*, Vol. 30, pp. 2-28.
- Numan, N.M.S., 2000.** Major Cretaceous Tectonic Events in Iraq, *Raf. Jour. Sci.* Vol. 11, No. 3, pp. 32-52.
- O'Neill HStC, 1991.** The origin of the moon and the early history of the earth, A chemical model, part 2, *Jour. The Earth .Geochim Cosmochim Acta*, Vol. 55, pp. 1159-1172.
- O'Neill H.St.C. and Palme H. 1998.** Composition of the silicate Earth: implications for accretion and core formation. In *The Earth's Mantle: Structure, Composition, and Evolution- the Ringwood*, volume (ed I, Jackson) Cambridge University Press Cambridge, pp 3-126.
- Ohara, Y., and Ishii, T., 1998.** Peridotites from the southern Mariana forearc: Hetrogenous fluids supply in mantle wedge, *The Island Arc*, Vol.7, pp.541-558.
- Ohara,Y., Kasuga,S. and Ishii, T., 1996,Peridotites from the Parece Vela Rift in the Philippine Sea upper mantle material exposed in an extinct back-arc basin, *Proceeding Japan Acad.*,72, pp.118-123.
- Ohara, Y., Stern, S., Ishii,T., Yurimoto, H, and Yamazaki,T,2002.** Peridotites from the Mariana Trough : first look at the mantle beneath an active back-arc basin, *Contribution to Mineralogy and Petrology*,Vol.143,pp.1-18.
- Ortega, L., Lunar, R., Garica-Palomero,F., Moreno, T., Martin-Estevez, J. R., Prichard, H. M., and Fish, P.C., 2004.** The Aguablanca Ni-Cu-PGE deposit, Southwestern Iberia: Magmatic ore-forming processes and retrograde evolution, *The Canadian Mineralogist*, Vol.42, pp.325-350.
- Page, NJ, Cassard, D., and Haffity J., 1982a.** Palladium, Platinum, rhodium, ruthenium, and iridium in chromitite from du Sud and Tiebaghi Massif, New Caledonia. *Jour. Econ.G eol.*, Vol. 77, pp.1571-1577.
- Page, NJ, and Talkington, R.W., 1984.** Palladium, Platinum, rhodium, ruthenium, and iridium in peridotites and chromitite from ophiolite complexes in Newfoundland. *Jour. Can Mineral* Vol. 22, pp137-149.
- Palme, H., and O'Neill, H. S.; 2004.** Cosmochemical estimate of mantle composition. In Holland, H. D. and Turekian, K. K. (Editors), *Treatise on Geochemistry*, Elsevier Pergamon, Amsterdam – Boston, Vol. 2, pp. 1-38.

Parkinson, I.J. and Arculus, R. J. 1999. The redox state of subduction zones: Insight from arc-peridotites. *Chemical Geology*, 160, 409-423.

Parkinson, I. J., Pearce, J.A., Thirlwall, M.F., Johnson , K.T.M., and Ingram, G., 1992; Trace element geochemistry of peridotites from the Izu-Bonin-Mariana, Forearc, LEG 125, Proceeding of the Ocean Drilling Program, Scientific Results Vol. 125, pp. 487-506.

Parkinson, I.J. and Pearce, J.A. 1998. Peridotites from the Izu-Bonin-Mariana forarc (ODP Leg 125): Evidence for mantle melting and melt-mantle interaction in a suprasubduction zone setting. *Jour. of Petrology* , 39, 1577-1618.

Parlak, O., Yilmaz, H., Boztug, D., 2006. Origin and tectonic significance of the metamorphic Sole and isolated dykes of divirgi ophiolite (Sivas, Turkey): Evidence for break-off prior to ophiolite emplacement, *Jour. of Earth Science (Turkish J. Earth Sci.)*, Vol. 15, pp. 25-45.

Pearce, T.H., Gorman, B.E and Birket, T.C., 1977. Tectonic setting of basic volcanic rocks determined using trace element analyses. *Jour. Earth Planet. Sci. Lett.* Vol. 19, pp. 290-300.

Pearce, J.A., 1983. Role of sub-continental lithosphere in magma genesis at active continental margins, in Hawkesworth, C. J., et al. Eds., *Continental basalts and mantle xenoliths*; Ceshire, UK, Shiva publishing, pp. 230-249.

Pearce, J.A., Lippard, S. J., and Robert, S., 1984. Characteristics and tectonic significance of Supra-subduction zone ophiolite. In: Kokellar, B. P. and Howells, M. F. (eds), *Marginal Basin Geology*, *Jour. Geological Society*, London, Special Publications 16, pp. 77-94.

Pearce, J.A., Lippard, S.J. and Robert, S.S., 1985. Characteristic tectonic significance of supra-subduction zone ophiolite, reproduced from marginal basin, geology publ. for the geological society by Blackwell Scientific publication, pp. 77-94.

Pearce, J.A., Barker P. F., Edwards S.J., Parkinson .I.J. Leat P.T. 2000; Geochemistry and tectonic significance peridotite from south Sandwich arc-basin system, south Atlantic, *Contrib. Mineral, Petrol.*, 139, pp. 36-53.

- Pearson, D.G., Canil, D., Shiery, S.B., 2004.** Mantle samples in volcanic rocks: Xenoliths and Diamonds. (Eds.), Treatise on Geochemistry, Elsevier Pergamon, Amsterdam – Boston, Vol. 2, pp. 171-275.
- Pedersen, P.B., Johannesen G.M., Boyd R. 1993.** Stratiform platinum-group element mineralization in the ultramafic cumulates of Leka ophiolite complex, Central Norway. *Jour. Econ Geol.* Vol. 88; pp. 782-803.
- Peltonen, P., 1995.** Petrogenesis of ultramafic rocks in the Vammala Nickel Belt: implications for crustal evolution of the early Proterozoic Svecofennian arc Terrane, *Jour. Lithos*, Vol. 34, pp. 253-274.
- Pfeiler, H.R., 1990.** Major and trace element discrimination diagrams to determine possible protoliths of orogenic ultramafic rocks, Universite' de Lausanne.
- Pretorius,W., Helmstaedt, H., and Kyser, K., 2007.** Whole rock platinum Group element geochemistry of Kimberlitic Rocks- A window into the nature of the diamondiferous mantle, 8th International Kimberlite Conference Long Abstract.
- Prichard, H., M., Neary C. R., Plotys, P.J. 1986.** Platinum group minerals in the Shetland ophiolite, In: Gallagher, M.P. et al. (eds.) *Metalogeny*, pp. 395-414.
- Prichard, H., M., Lord, R. A., Neary, C. R. 1996a.** A method to explain the occurrence of platinum- and palladium-rich ophiolite complex. *Jour. Geol. Soc. Lond.* Vol. 153, pp. 323-328.
- Prichard, H., M., Puchelt, H., Eckhardt, J. D., Fisher, P.C. 1996b.** Platinum-group element concentrations in mafic and ultramafic lithologies drilling from Hess Deep. In Mevel C., Gillis K.M. Allan J.F. Meyer, P.S. (eds) *Proc Ocean Drilling Program, Sci. Results*, Vol.147, pp. 77-90.
- Proenza J., Sole J, and Melgarejo, JC, 1999.** Uvarovite in podiform chromitite; the Moa-Baracoa ophiolitic massif, Cuba, *Jour. Can Mineral* Vol. 37 pp. 679-690.

- Proenza J., Gervila, F., Melgarejo, J.C., Vera, O., Alfonso, P., and Fallick, A., 2001.** Genesis of sulfide-rich chromite ores by the interaction between chromitite and olivine-norite dikes in Potasi Mine (Mao-Baracoa ophiolitic massif, eastern Cuba). *Jour. Mineralium Deposita*, Vol. 36, pp. 658-669.
- Proenza J., Ortega-Gutierrez, F. Camprubi, A., Tritlla, J., Elias-Herrera, M. and Reyes-Salas, M., 2004.** Paleozoic serpentinite- enclosed chromitites from Tehuizingo (Acatlan Complex, southern Mexico): a petrological and mineralogical study, *Jour. South American Sciences*, Vol. 16, pp. 649- 666.
- Purvis, A.C., Nesbitt, R. W., and Hallberg, J. A., 1972.** The geology of part of the Carr Boyd Complex and its associated nickel mineralization, Western Australia, *Economic Geology*, Vol.67, pp.1093-1113.
- Quick, J.E., 1990.** Geology and origin of Late Proterozoic Darb Zubadah ophiolites kingdom of Saudi Arabia, *Geol.Soc. Am. Bull.*, Vol.102, pp.1007-1020.
- Quintiliani, M., Andreozzi, G.B., and Graziani, G., 2006.** Fe²⁺ and Fe³⁺ quantification by different approaches and f_{O2} estimation for Albanian Cr-spinels, *American Mineralogist*, Vol.91, pp.907-916.
- Rao, A., Sarkar, A. Jeyakumar, S., Aggrawal, S.K., Ebihara, M. and Satoh, H., 2004.** Late Archaean mantle metasomatism below eastern Indian craton: Evidence from trace elements, REE geochemistry and Sr-Nd-O isotope systematic of ultramafic dykes. *Earth Planet, Sci.*, Vol. 113, No. 4, pp. 649-665.
- Resimic-Saric, K., Koroneos, A., Cvetkovic, V. and Balogh, K., 2004.** Origin and evolution of the ophiolitic complex of Zdraljica (Central Serbia), *Jou. of Bulletin of Geological Society of Greece*, Vol. XXXVI, pp. 597-606.
- Rivalenti, G. Mazzuccheli, M., Vannucci, R., Hofmann, A.W., Ottolini, L. Bottazi, P., and Obermiller, W., 1995.** The relationship between websterite and peridotite in the Balmuccia peridotite massif (NE Italy) as revealed by trace element variation in clinopyroxene. *Contrib. Mineral Petrol.* Vol. 121, pp. 275-288.
- Rodgers, K. A., 1973.** Chrome-spinels from the Massif du Sud, southern New Caledonia, *Min. Mag.*, Vol. 39, pp.326-339.

- Roeder, P. L., Campbell, I. H., and Jamieson, H. E., 1979.** A Re-Evaluation of the Olivine - Spinel Geothermometer, *Contrib. Mineral Petrol*, Vol.68, pp.325-334.
- Roeder, P.L., and Reynolds, I., 1991.** Crystallization of chromite and chromium solubility in basaltic melts , *Journal of Petrology*, Vol.32, pp.909-934.
- Roeder, p.L., 1994.** Chromite: from the fiery rain of chondrolues to Kilauea lave lake, *The Canadian Mineralogist*, Vol.32, pp.729-746.
- Rollinson, H. 1993.** Using geochemical data evolution, presentation, and interpretation; Wiley, New York, 351p.
- Shamim Khan, M., Smith, T.E. Raza, M., and Huang, J., 2005.** Geology, geochemistry and tectonic significance of mafic-ultramafic rocks of Mesoproterozoic Phulad ophiolite suite of south Delhi fold belt, NW Indian Shield. *Jour. of Gondwana Research*, Vol. 8, No., 4, pp.553-566.
- Shawna, M., Leatherdale, Maxeiner, R.O. and Ansdell, K. M., 2003.** Petrography and geochemistry of Love Lake leucogabbro, Swan River complex, Peter lake domain, northern *Jour. Saskatchewan*, Saskatchewan Geological Survey, Vol. 2, pp. 1-17.
- Shen, P. Hwang, S.L., Chu, H.T., Jeng R.C. 1988.** STEM study of ferritchromite from the "Heng-Chun chromitite. *Jour. Am Mineral* Vol. 73, pp. 383-388.
- Shervais, J. W., 1982.** Ti-V plots and the petrogenesis of modern and ophiolitic lavas; *Earth and Planetary Science letters*, Vol. 59, pp. 101-118.
- Smirnov, V. A., and Nelidove, 1961.** Report on 1:200000 prospecting correlation of Sulaimaniya-Choarta and Penjween areas, Report No.290, NIMCO Library.
- Smith, D. S., Basson, I. J., and Reid, D. L., 2003.** Normal reef subfacies of the Merensky reef at Northam Platinum mine, Zwartklip facies, Western Bushveld Complex, South Africa, *The Canadian Mineralogist*, Vol. 42, pp.243-260.

- Sobol, A.V., and Dunyushevsky, L.V.1994.** Petrology and geochemistry of boninites from the north of termination of Tonga trench: constrains on generation condition of primary high Ca boninite mgmas, Jour. Petrol. 35 pp. 1183-1211.
- Sofy, M.M.,2003.** Petrochemistry and petrogenesis of Bulfat mafic layered igneous intrusion around Herro (Qaladizeh)-Iraq Kurdistan, Msc, thesis, Salahaddin University-Erbil, 123p.
- Stockllin, J., 1968a.** Structural history and tectonics of Iran: a review; American Association of Petroleum Geologists Bulletin, vol. 52 pp. 1229-1258.
- Stockllin, J.,1977.** Structural correlation of the Alpine rangees between Iran and central Asia; Societe Geologique de France Memoire Hors- Serie, vol. 8, pp. 333-353.
- Steven, R.E., 1944.** Composition of some chromites of western Hemisphere Am. Mineral,Jour. Vol. 26, pp. 1-34.
- Stumpfl, E.F., 1986.** Distribution, transport and concentration of platinumiumgroup elements .In: Metallogeny of basic and ultrabasic rocks, Gallagher,M.J., Ixer, R. A., Neary, C.R.,and Prichard, H.M.,(Eds.), The Institution of Mining and Metallurgy Publ.,London, U.K.,pp.379-394.
- Suita, M. T., and Streider, A. J., 1996.** Cr-spinels from Brazilian mafic-ultramafic complexes: metamorphic modifications, International Geology Review, Vol.38, pp. 245-267.
- Sun, Shen-Su., 1982.** Chemical composition and origin of the earths primitive mantle,Geochim. Cosmochim. Acta, 46, pp. 179-192.
- Takazawa, E., Frey, F.A., Shimizu, N. and Obata, M. 2000.** Whole rock compositional variation in upper mantle peridotite, (Horoman, Hokaido, Japan): Are they consisting with partial melting process, Geochim. Cosmochim. Acta, 64, 695-716.

- Talkington, R.W., Watkinson, D.H., Whittaker, P.J., and Jones, P.C., 1986.** Platinum group element-bearing minerals and other solid inclusions in chromite of mafic and ultramafic complexes: chemical compositions and comparisons. In: Carter, B., et al. (Eds.), *Metallogeny of Basic and Ultrabasic Rocks (regional presentations)*. Theophrastus Publications, Athens, pp.223-249.
- Tamura, A., and Arai, S., 2005.** Unmixed spinel in chromitite from the Iwanai-dake peridotite complex, Hokkaido, Japan: A reaction between peridotite and highly oxidized magma in the mantle wedge, *American Mineralogist*, Vol.90, pp.473-480.
- Tamura, A., and Arai, S., 2006.** Harzburgite-dunite-orthopyroxenite suite as a record of suprasubduction zone setting for Oman ophiolite mantle, *Lithos*. 90, 43-56.
- Taylor, S.R., McLennan, S.M., 1985.** *The continental Crust: Its composition and Evolution*. Blackwell, Oxford, 321 p.
- Trung, N. M., Tsujimori, T., and Itaya, T., 2006.** Honvang serpentinite body of the Song Ma fault zone, Northern Vietnam: A remnant of Oceanic lithosphere within the Indochina-South China suture, *Gondwana Research*, Vol.9, pp.225-230.
- Ulmer, G.C. 1974.** Alteration of chromite during serpentizations in Pennsylvania Maryland District, *Jour. Am. Min*, Vol. 59, pp. 1236-2342.
- Uysal, I., Kaliwoda, M. Karsli, O., Tarkian, M. and Sadiklar, M. B. 2007.** Compositional variation of whole-rock and coexistings phase with partial melting and melt-rock interaction of peridotite in an upper mantle section from Ortaca area, SW Turkey. *Geophysical Research, Abstracts*, Vol. 9, pp.1-55
- Uysal, I., Tarkian, M., Sadiklar, B. M., and Sen, C., 2007.** Platinum-group – element geochemistry and mineralogy of ophiolitic chromitites from the Cop Mountains northeastern Turkey, *The Canadian Mineralogist*, Vol. 45, pp. 355-377.

- Van der Lann, S.R., Arculus, R.L. Pearce, J.A. and Murton, B. J. 1992.** 10 Petrography, mineral chemistry and phase relations of the basement boninite series of site 786, Iz-Bonin forarc. Proc. Ocean Drill, Program Sci. Res. Vol. 25, pp. 171-201.
- Ven Seckendorff, V. and ÓNeill, H.S.C., 1993.** An experimental study of Fe-Mg partitioning between olivine and orthopyroxene at 1173, 1273 and 1423 K and 1.6 GPa. Contrib. Min. Petrol. 113. pp.196-207
- Vuello, J., Liipo, J., Nykanen, V., Piirainen, T., Pekkarinen, L., Tuokko, I., and Ekdahl, E., 1995,** An early Proterozoic podiform chromitites in the Outokumpu ophiolites complex, Finland. Econ. Geol., Vol.90, pp.445-452.
- Wang, C. Y., Zhou, M.-F., and Zhao, D., 2005.** Mineral Chemistry of chromite from the Permian Jinbaoshan Pt-Pd-sulphide-bearing ultramafic intrusion in SW China with petrogenetic implications, LITHOS, Vol.83, pp.47-66.
- Wells, P. R. A., 1977.** Pyroxene Thermometry in Simple and Complex Systems, Contrib. Mineral Petrol, Vol.62, pp.129-139.
- Whattam, S., Malpas, J., Ali, J., Smith, I. E. M., and Hualo, C., 2004.** Origin of the Northland Ophiolite, northern New Zealand: discussion of new data and reassessment of the model. Jour. of Geology and geophysics, Vol. 47; pp. 383-389.
- Wilson, M., 1989.** Igneous Petrogenesis, A Global Tectonic Approach. Unwin Hyman, London, 400 p.
- Wood, B.J. 1991.** Oxygen barometry of spinel peridotite. In D. H. Lindsley, Ed., Oxide minerals: Petrologic and magnetic significance, Mineralogical Society of America, Washington, D.C. pp. 417-431.
- Yaliniz, M. K. and Goncuoglu, M. C., 1999.** Clinopyroxene compositions of the isotropic gabbros from the Sarikaraman ophiolite: New evidence on supra-subduction zone type magmagenesis in central Anatolia. Jour. of Turk J. Earth Sci., Vol. 8, pp. 103-111.
- Yang, J-J., and Enami, M., 2003.** Chromian disakisite –(Ce) in a garnet lherzolite from the Chinese Su-Lu UHF metamorphic terrane: Implications for Cr incorporation in epidote-group minerals and recycling of REE into the Earth's mantle, American Mineralogist, Vol.88, pp.604-610.

- Yibas, B., Reimold, W. U., Anhaeusser, C. R., Koeberl, C., 2003.** Geochemistry of the mafic rocks of the ophiolitic fold and thrust belts southern Ethiopia: constraints on the tectonic regime during the Neoproterozoic (900-700 Ma). *Jour. Precambrian Research*, Vol. 121, pp. 157-183.
- Zekaria, M., B., M., 1992.** Petrology and geochemistry of the southern part of Mawat ophiolite complex, Northeastern Iraq, Unpublished Msc.Thesis, Mosul University,84p. (in Arabic)
- Zhou, M-F., and Bai,W-J., 1992.** Chromite deposits in China and their origin, *Mineralium Deposita*, Vol.27, pp. 192-199.
- Zhou, M.-F., Robinson, P.T., and Bai, W.-J., 1994.** Formation of podiform chromitites by melt/rock interaction in the upper mantle, *Miner. Deposita*, Vol.29, pp.98-101.
- Zhou, M.F., Robinson P.T., and Malpas, J. Li. Z., 1996.** Podiform chromitites in the Luobusa ophiolite (southern Tibet): Implications for melt-rock interaction and chromite segregation in the upper mantle, *Jour. Petrol.* Vol. 37, pp. 3-21.
- Zhou, M.F., Sun, M., Keays, R.R., and Kerrich, R.W., 1998.** Controls on platinum-group elemental distributions of podiform chromitites: A case study of high -Cr and high-Al chromitite from Chinese orogenic belts, *Jour. Geochimica et Cosmochimica Acta*, Vol. 62, pp. 677-688.
- Zhou, M.F., Robinson, P. T. Malpas, J. Edwards, S. J. and Ol, L. 2005.** REE and PGE geochemical constraints on the formation of dunites of Luobusa ophiolite southern Tibet. *Jour. Petrol.* .46, pp.615-639.

Appendix 1

WSU XRF precision, limit of determination (2-sigma)

Unnormalized Major Elements (Weight %):		
Oxide	Precision	Limit of detection (2-Sigma)
SiO2	0.99929	0.58
TiO2	0.99992	0.017
Al2O3	0.99949	0.16
FeO*	0.99948	0.20
MnO	0.99983	0.002
MgO	0.99994	0.076
CaO	0.99976	0.064
Na2O	0.99981	0.045
K2O	0.99992	0.031
P2O5	0.99990	0.005
Estimated LOD	0.966	1.00
SO3	0.989	0.07
Cl	0.992	0.002
Normalized Major Elements (Weight %):		
SiO2	0.99992	0.19
TiO2	0.99996	0.012
Al2O3	0.99987	0.082
FeO*	0.99956	0.18
MnO	0.99988	0.002
MgO	0.99994	0.073
CaO	0.99998	0.043
Na2O	0.99989	0.036
K2O	0.99998	0.015
P2O5	0.99996	0.003
Trace Elements (ppm):		
Ni	0.9992	3.5
Cr	0.9998	3.0
Sc	0.997	1.6
V	0.9996	5.0
Ba	0.9997	11.7
Rb	0.9998	1.7
Sr	0.99992	4.6
Zr	0.99994	3.9
Y	0.9987	1.2
Nb	0.99987	1.2
Ga	0.955	2.7
Cu	0.994	7.4
Zn	0.9991	3.3
Pb	0.9966	2.6
La	0.9941	5.7
Ce	0.996	7.9
Th	0.997	1.6
Nd	0.992	4.3
U	0.983	2.7
Bi	0.758	2.0
Cs	0.365	5.1

Appendix 2

Detection limits of REE and trace elements using ICP-MS.

Elements (ppm)	Detection Limits
La	0.007
Ce	0.012
Pr	0.009
Nd	0.045
Sm	0.014
Eu	0.010
Gd	0.026
Tb	0.007
Dy	0.024
Ho	0.006
Er	0.021
Tm	0.006
Yb	0.023
Lu	0.007
Ba	0.258
Th	0.009
Nb	0.018
Y	0.015
Hf	0.032
Ta	0.014
U	0.014
Pb	0.204
Rb	0.057
Cs	0.014
Sr	0.115

Appendix 3

The results of XRF analyses of Dunite rocks in MOC

Oxide S.No.	W15	W17	W20	W21	W23	W26	W37	W38	R10-1	R10-2
SiO ₂	38.3	39.21	39.5	39.27	39.62	38.34	39.33	39.02	37.01	36.47
TiO ₂	0.007	0.007	0.002	0.008	0.005	0.011	0.008	0.0071	0.01	0.01
Al ₂ O ₃	0.3	0.4	0.31	0.28	0.12	0.64	0.23	0.38	0.25	0.27
FeO*	6.98	8.09	6.9	7.97	7.71	7.28	6.89	6.68	7.21	7.1
MnO	0.13	0.141	0.13	0.125	0.123	0.125	0.11	0.11	0.12	0.11
MgO	44.6	45.34	45.4	44.99	45.32	44.68	45.88	45.33	42.69	43.68
CaO	0.2	0.54	0.47	2.30	2.06	1.07	0.14	0.5	0.15	0.17
Na ₂ O	0.14	0.09	0.05	0.08	0.08	0.08	0.12	0.08	0.1	0.1
K ₂ O	0.02	0	0.001	0.00	0.00	0.00	0.01	0.003	0.001	0
P ₂ O ₅	0.007	0.012	0.002	0.003	0.002	0.003	0.006	0.018	0.008	0.01
LOI (%)	9.87	5.33	6.46	4.43	4.12	5.58	6.011	7.11	11.55	11.49
Sum	100.554	99.16	99.225	99.46	99.16	97.80	98.735	99.2381	99.099	99.41
Traces(ppm)										
Ni	2900	3002	2798	2575	2750	2844	2882	2784	2795	2786
Cr	2686	3211	3005	3053	1636	15562	2741	2697	2881	2737
Sc	4	11	7	6	5	4	4	8	8	4
V	15	35	26	20	15	45	14	18	20	16
Ba	7	4	4	4	5	8	6	8	9	7
Rb	1	0	1	1	0	0	1	1	0	1
Sr	9	30	43	64	70	33	5	9	7	6
Zr	2	2	1	2	1	2	1	4	1	2
Y	0	1	1	0	1	2	1	0	1	2
Nb	1	0.5	0	0.0	0.0	0.0	1	0	1	1
Ga	2	0.8	1	1	0	1	0	1	1	1
Cu	4	17	16	4	6	8	6	7	7	5
Zn	39	47	46	30	22	82	42	41	48	44
Pb	2	1	1	0	0	0	1	1	2	1
La	1	1	1	0	4	0	1	0	0	0
Ce	0	1	1	1	0	0	1	0	0	0
Th	0	1	1	0	0	0	0	0	1	0
Nd	1	0	1	6	2	3	0	0	2	0
sum tr.	5674	6365.3	5954	5765.843	4516.348	18594	5707	5579	5784	5613
in %	0.57	0.63	0.59	0.57	0.45	2	0.57	0.56	0.57	0.56
sum major+trace	101.124	99.79	99.815	100.0289	99.60719	99.65288	99.305	99.7981	99.669	99.97

Appendix 4

The results of XRF analyses of harzburgite rocks in MOC

S.No. Oxide	R6	R7	R8	W12	W14	W16	W19	W35	W36	D23	D34	K7-5	K9-2	K9-4	A1-5
SiO ₂	38.87	40.6	41.725	41.35	41.48	51.07	41.34	42.32	45.92	42.93	45.12	40.64	42.27	41.89	40.53
TiO ₂	0.007	0.007	0.006	0.008	0.008	0.025	0.007	0.008	0.011	0.005	0.008	0.01	0.006	0.008	0.01
Al ₂ O ₃	0.1	0.39	0.43	0.66	0.56	0.71	0.57	0.36	0.44	0.61	0.7	0.56	0.41	0.42	0.45
FeO	8.31	7.58	8.01	7.34	8.11	4.71	6.89	7.77	6.81	8.84	7.89	8.84	6.88	7.08	7.22
MnO	0.124	0.123	0.133	0.118	0.132	0.097	0.111	0.122	0.097	0.133	0.122	0.13	0.114	0.12	0.12
MgO	38	40.11	41.01	41.34	43.54	33.02	43.22	41.39	38.24	40.59	39.83	41.38	43.72	45.66	38.17
CaO	0.09	1.17	1.32	0.81	0.58	3.89	1.58	1.12	2.69	1.3	1.37	0.34	0.85	0.69	1.66
Na ₂ O	0.06	0.07	0.08	0.08	0.08	0.12	0.08	0.06	0.08	0.06	0.1	0.11	0.07	0.09	0.1
K ₂ O	0	0	0	0.00	0.00	0	0	0	0.00	0	0	0	0	0.05	0
P ₂ O ₅	0.007	0.008	0.004	0.003	0.003	0.008	0.009	0.007	0.003	0.004	0.004	0.01	0.011	0.021	0
LOI (%)	13.64	8.95	6.32	7.54	4.87	5.85	5.38	5.95	5.10	5.51	4.87	6.99	4.78	3.56	10.93
Sum	99.208	99.008	99.038	99.24559	99.3649	99.5	99.187	99.107	99.39927	99.982	100.014	99.01	99.111	99.589	99.19
100*MgO/MgO+FeO	82.05	84.11	83.65	84.92	84.30	87.52	86.25	84.19	84.88	82.12	83.46	84.07	86.4	86.57	84.09
Trace (ppm)															
Ni	2986	2362	2594	2335	2526	670	2576	2911	2031	2511	2610	2493	2594	2365	2369
Cr	3600	2965	3110	2768	2556	2253	2068	3510	2439	3003	3011	2833	2153	2276	2867
Sc	4	7	9	10	8	15	8	8	9	15	10	9	8	6	10
V	17	31	41	40	27	50	24	32	35	30	44	38	21	24	38
Ba	7	3	2	9	7	6	7	4	8	1	4	8	5	3	9
Rb	0	0	1	1	0	0	0	1	0	1	1	1	1	0	0
Sr	2	23	26	3	0	4	37	23	30	52	4	2	10	12	55
Zr	3	4	3	2	2	3	5	3	2	2	1	2	5	4	1
Y	1	1	0	0	1	1	1	0	1	1	1	1	1	1	1
Nb	0	0	0.1	0.0	0.0	0	0	0.3	0.0	0.1	0.1	1	0	1	0
Ga	1	1	0	0	1	2	3	1	0	0	1	0	2	1	0
Cu	3	3	5	4	4	0	6	32	5	18	17	8	4	5	10
Zn	53	46	50	45	44	25	38	51	32	48	60	47	40	45	43
Pb	1	1	2	0	0	0	1	4	0	1	3	0	0	0	0
La	3	0	0	1	0	0	3	1	0	1	2	0	0	0	2
Ce	0	0	1	0	3	0	0	1	0	1	0	0	0	0	0
Th	0	0	0	0	1	0	0	1	0	0	1	0	0	0	0
Nd	1	1	1	3	1	0	0	1	2	1	1	4	2	1	0
Sum.tr.	6682	5448	5845.1	5222.095	5182	3029	4777	6584.3	4594	5686.1	5771.1	5447	4846	4744	5405
in%	0.66	0.54	0.58	0.52	0.51	0.3	0.48	0.66	0.46	0.57	0.55	0.55	0.48	0.47	0.54
Sum trace & major	99.868	99.548	99.618	99.76559	99.8749	99.8	99.667	99.767	99.85927	100.552	100.564	99.56	99.591	100.059	99.73

Appendix 5

The results of XRF analyses of Iherzolite rocks in MOC.

S.No.									
Oxide	K3-1	K4-1	K4-2	K4-5	K5-1	K5-2	K7-6	D32	D33
SiO ₂	43.59	40.53	41.6	46.02	42.88	43.59	42.01	41.55	43.11
TiO ₂	0.060	0.019	0.029	0.044	0.032	0.008	0.031	0.006	0.005
Al ₂ O ₃	1.03	0.91	1.5	2.00	1.2	1.1	2.2	1.55	1.67
FeO	11.34	12.01	11.78	6.55	11.52	7.78	10.11	8.21	7.32
MnO	0.204	0.156	0.188	0.108	0.159	0.123	0.11	0.125	0.111
MgO	31.84	36.87	35.87	36.66	34.92	40.28	36.69	39.59	40.83
CaO	7.98	3.96	3.46	6.11	3.33	2.31	3.21	2.46	2.41
Na ₂ O	0.11	0.1	0.1	0.14	0.07	0.08	0.06	0.07	0.06
K ₂ O	0.00	0	0	0.00	0.004	0	0.001	0	0
P ₂ O ₅	0.004	0.012	0.011	0.004	0.013	0.006	0.02	0.006	0.007
LOI (%)	2.96	4.52	4.55	2.19	5.55	4.73	4.56	6.55	4.39
Sum	99.12	99.09	99.09	99.83	99.68	100.01	99.00	100.12	99.91
100*MgO/MgO+FeO	73.73	75.42	75.27	84.84	75.19	83.81	78.39	82.82	84.79
Trace Elements (ppm)									
Ni	1019	1701	1516	1780	1666	2531	1973	2330	2560
Cr	2694	4231	4127	3187	3883	3056	3495	2316	2790
Sc	33	18	20	30	35	11	30	10	15
V	112	75	79	84	90	45	85	36	29
Ba	7	9	7	5	5	6	10	1	4
Rb	0	1	0	0	1	0	0	1	1
Sr	2	4	3	15	5	3	4	46	15
Zr	2	1	3	2	1	4	2	3	2
Y	2	1	2	3	0	0	1	0	1
Nb	0.0	0	0.1	0	0.2	0	0.3	0	0.1
Ga	2	2	1	2	0	2	0.9	0	1
Cu	14	8	4	38	9	9	3	39	50
Zn	64	72	57	29	62	45	63	38	44
Pb	0	4	0	0	1	0	1	1	1
La	1	1	0	0	1	2	0	1	0
Ce	0	0	0	3	1	0	1	2	2
Th	0	1	0	0	0	0	0	0	1
Nd	0	1	1	4	0	0	1	1	1
Sum.tr.	3950.92522	6130	5820.1	5182	5760.2	5714	5670.2	4825	5517.1

Appendix 6

The results of XRF analyses of pyroxenite rocks in MOC.

S.No. Oxide	R12	D15	D35	K2-1	K2-2	K3-2	K4-3	K4-4	K9-5	A12-4
SiO ₂	49.03	50.02	50.91	48.05	46.05	47.5	48.1	47.01	50.06	48.79
TiO ₂	0.03	0.04	0.04	0.1	0.1	0.06	0.077	0.087	0.044	0.142
Al ₂ O ₃	2.04	2.09	2.77	1.76	1.76	1.82	2.13	2.06	1.13	2.32
FeO*	4.41	6.35	6.75	8.2	8.2	7.82	8.01	7.3	3.16	4
MnO	0.181	0.105	0.14	0.169	0.169	0.111	0.12	0.143	0.079	0.079
MgO	26.86	25.47	26.33	25.54	25.54	22.81	24.01	26.12	26.44	24.26
CaO	14.17	10.89	11.11	13.21	13.21	15.16	14.62	13.83	16.71	16.86
Na ₂ O	0.33	0.54	0.14	0.1	0.1	0.091	0.156	0.17	0.13	0.09
K ₂ O	0.022	0.02	0.01	0	0	0.02	0.02	0	0.01	0
P ₂ O ₅	0.006	0.007	0.005	0.004	0.004	0.003	0.003	0.005	0.004	0.004
LiO %	2.55	3.74	1.56	1.92	3.72	3.61	2.31	2.81	1.24	2.92
Total	99.629	98.872	99.765	99.053	98.853	99.005	99.556	99.535	99.007	99.465
100*MgO/MgO+FeO	85.89	85.21	79.59	74.95	74.95	74.47	74.98	77.48	87.98	84.77
Traces(ppm)										
Ni	687	2119	710	673	673	592	600	646	558	498
Cr	2115	2191	2611	2364	2364	2872	3473	3691	2576	2785
Sc	16	19	28	56	56	41	50	48	40	60
V	51	61	110	181	181	101	139	166	138	123
Ba	3	1	0	0	0	1	0	0	0	1
Rb	0	0	0	0	0	0	0	0	0	0
Sr	2	25	5	5	5	7	3	5	10	9
Zr	2	5	3	2	2	2	1	2	2	3
Y	3	6	2	4	4	2	2	3	2	4
Nb	0.4	0.3	0.4	0	0	0.1	0	0	0	0
Ga	2	4	1	4	4	1	1	2	1	2
Cu	72	110	115	302	302	82	10	9	121	13
Zn	30	26	29	35	35	30	44	39	14	16
Pb	1	2	1	2	2	0	0	0	0	1
La	1	5	0	0	0	1	0	0	0	1
Ce	1	5	1	1	1	2	1	2	2	4
Th	1	0	1	0	0	1	0	0	0	2
Nd	1	5	1	1	1	1	0	1	1	3
sum tr.	2988.4	4634.3	3618.4	3630	3630	3736.1	4324	4614	3465	3525
in %	0.3	0.5	0.4	0.36	0.4	0.4	0.4	0.5	0.3	0.4

Appendix 7

The results of REE analyses (ICP-MS) for dunite rocks in MOC and the chondrite REE values from O'Neill and Palme, (1998).

REE elements (ppm)	Chondrite	W21	W23	R10-2
La	0.24	0.09	0.05	0.19
Ce	0.61	0.19	0.09	0.34
Pr	0.1	0.02	0.01	0.04
Nd	0.47	0.07	0.05	0.13
Sm	0.15	0.02	0.01	0.02
Eu	0.06	0.01	0.01	0.01
Gd	0.21	0.01	0.01	0.02
Tb	0.04	<0.007	<0.007	<0.007
Dy	0.25	0.02	0.02	0.02
Ho	0.06	<0.006	<0.006	<0.006
Er	0.17	0.02	0.01	0.01
Tm	0.026	<0.006	<0.006	<0.006
Yb	0.17	0.02	0.02	0.01
Lu	0.03	0.01	0.007	<0.007
Other Elements (ppm)				
Ba	2.4	1	2	3
Th	0.0298	0.04	0.03	0.06
Nb	0.247	0.06	0.02	0.14
Y	1.56	0.13	0.12	0.13
Hf	0.107	0.02	0.01	0.03
Ta	0.0142	<0.014	<0.014	0.01
U	0.0078	0.01	0.01	0.02
Pb	2.53	0.1	0.14	0.2
Rb	2.32	0.1	0.1	0.3
Cs	0.188	0.05	0.01	0.07
Sr	7.26	4	69	8
Sc	5.9	10.2	5.3	3.7
Zr	3.86	1	3	1

Appendix 9

The results of REE analyses (ICP-MS) of Iherzolite in MOC.

S.No. Elements(ppm)	K3-1	K4-2	K4-5	K5-2	D32	D33
La	0.06	0.08	0.05	0.04	0.07	0.05
Ce	0.18	0.16	0.13	0.08	0.15	0.16
Pr	0.03	0.02	0.02	0.01	0.02	0.02
Nd	0.2	0.09	0.13	0.04	0.07	0.05
Sm	0.11	0.03	0.07	0.01	0.01	0.02
Eu	0.04	0.03	0.03	<0.01	0.01	0.01
Gd	0.19	0.08	0.15	0.01	0.02	0.01
Tb	0.04	0.02	0.04	<0.007	<0.007	<0.007
Dy	0.33	0.11	0.26	0.02	0.03	0.04
Ho	0.07	0.03	0.06	0.01	0.01	0.015
Er	0.21	0.09	0.16	0.02	0.03	0.02
Tm	0.03	0.01	0.02	<.006	<.006	<.006
Yb	0.18	0.08	0.14	0.04	0.04	0.05
Lu	0.03	0.01	0.02	0.01	0.01	0.02
Other Elements						
Ba	3	6	2.00	3	4	4
Th	0.03	0.02	0.03	0.02	0.04	0.06
Nb	0.03	0.02	0.03	0.02	0.03	0.02
Y	1.71	0.67	1.34	0.13	0.17	0.2
Hf	0.03	0.02	0.09	0.01	0.01	0.01
Ta	<0.014	<0.014	0.00	<0.014	<0.014	0.01
U	0.19	0.51	0.01	0.15	0.01	0.02
pb	0.1	0.14	0.14	0.08	0.16	0.14
Rb	0.1	0.1	0.10	0.1	0.3	0.2
Cs	0.01	0	0.01	0.01	0.02	0.01
Sr	4	3	16.00	4	47	40
Sc	34.2	21.2	30.10	11.5	10.2	11
Zr	0.5	<0.059	0.45	<0.059	<0.059	<0.059

Appendix 10

The results of REE analyses (ICP-MS) of pyroxenite rocks in MOC.

S.No. Elements (ppm)	D15	D35	K2-1	K2-2	K4-4	K9-5	A12-4	R12
La	2.43	2.32	0.05	0.04	0.07	0.03	0.11	2.33
Ce	6.79	7.1	0.17	0.2	0.17	0.07	0.39	6.71
Pr	1.02	0.95	0.04	0.06	0.04	0.01	0.08	1.05
Nd	4.49	5.02	0.29	0.23	0.25	0.06	0.56	4.19
Sm	1.17	1.13	0.18	0.19	0.15	0.05	0.28	1.09
Eu	0.67	0.71	0.07	0.05	0.06	0.02	0.13	0.8
Gd	1.04	1.03	0.34	0.4	0.27	0.1	0.46	0.98
Tb	0.18	0.21	0.08	0.08	0.06	0.03	0.09	0.21
Dy	1.09	1.06	0.57	0.61	0.46	0.22	0.6	1.15
Ho	0.21	0.23	0.12	0.19	0.1	0.05	0.13	0.2
Er	0.54	0.53	0.36	0.33	0.31	0.16	0.33	0.61
Tm	0.09	0.07	0.05	0.03	0.04	0.02	0.05	0.09
Yb	0.53	0.51	0.33	0.3	0.27	0.16	0.26	0.61
Lu	0.08	0.05	0.05	0.05	0.04	0.02	0.04	0.07
Other Elements								
Ba	4	2	1	0.6	3	3	2	2
Th	0.17	0.3	0.01	<0.009	0.01	0.01	0.02	0.03
Nb	0.5	0.2	0.02	<.018	0.02	0.02	0.02	0.2
Y	5.63	7	3.02	4	2.48	1.24	2.96	3
Hf	0.07	0.9	0.06	0.04	0.05	0.01	0.1	0.06
Ta	0.02	0	<0.014	0.02	<0.014	<0.014	<0.014	0.01
U	0.09	0.05	<0.014	0.1	0.02	<0.014	0.01	0.051
pb	0.49	0.61	0.24	1.2	0.18	0.039	0.2	1
Rb	0.2	0.3	0.1	<0.057	0.1	0.1	0.1	0.1
Cs	0.03	0.01	<0.014	0.03	<0.014	0.02	0.02	0.016
Sr	75	82	5	5	5	11	9	7
Sc	20.8	19.2	60.4	56	54.9	45.6	69.4	36
Zr	2	1	1	2	1	<0.059	2	2

Appendix 11
The results of microprobe analyses of mineral composition in dunite of MOC.

Samples	Oxides																											
	SiO ₂	Al ₂ O ₃	TiO ₂	FeO	MnO	MgO	CaO	Na ₂ O	K ₂ O	NiO	Cr ₂ O ₃	Totals	Si	Al	Ti	Cr	Fe ²⁺	Fe ³⁺	Mn	Mg	Ca	Na	K	Ni	Mg#	Cr#	Fe ³⁺ #	Fe ²⁺ #
R10-2 OL	40.092	0.007	0.005	7.834	0.125	50.850	0.021	0.040	0.015	0.292	0.020	99.291	0.984	0.000	0.000	0.000	0.161	0.000	0.003	1.860	0.001	0.002	0.000	0.006	0.920	0.000	0.000	0.080
R10-2 OL	40.337	0.001	0.018	7.845	0.051	50.567	0.004	0.028	0.003	0.318	0.008	99.123	0.990	0.000	0.000	0.000	0.161	0.000	0.001	1.851	0.000	0.001	0.000	0.006	0.920	0.000	0.000	0.080
W20- OL	38.932	0.000	0.013	10.179	0.142	48.871	0.016	0.032	0.006	0.235	0.614	99.040	0.979	0.000	0.000	0.000	0.214	0.000	0.003	1.820	0.000	0.002	0.000	0.005	0.895	0.000	0.000	0.105
W21- OL	39.878	0.006	0.006	8.786	0.159	49.323	0.006	0.014	0.006	0.283	0.014	98.481	0.978	0.000	0.000	0.000	0.185	0.000	0.003	1.850	0.000	0.001	0.000	0.006	0.909	0.000	0.000	0.091
W21- OL	39.966	0.019	0.010	8.572	0.113	49.576	0.002	0.027	0.000	0.292	0.000	98.482	0.991	0.001	0.000	0.000	0.178	0.000	0.002	1.833	0.000	0.001	0.000	0.006	0.912	0.000	0.000	0.088
W21- OL	39.729	0.004	0.001	8.283	0.148	49.690	0.018	0.014	0.007	0.289	0.032	98.177	0.988	0.000	0.000	0.001	0.172	0.000	0.003	1.842	0.000	0.001	0.000	0.006	0.914	0.000	0.000	0.086
R10-2 OPX	49.188	0.1648	0.000	3.586	0.1018	46.22	0.4109	0.0216	0.034	0.2929	0.0161	100.032	1.7177	0.007	0.000	0.001	0.104	0.000	0.003	2.4209	0.0154	0.000	0.000	0.0082	0.956	0.000	0.000	0.044
R10-2 OPX	47.99	0.1673	0.015	2.309	0.03	49.26	0.1086	0.0163	0.016	0.0827	0.0054	100.000	1.6706	0.007	0.0004	0.000	0.060	0.000	0.000	2.5722	0.004	0.0011	0.000	0.0023	0.977	0.000	0.0254	0.023
W20 Amph.	57.163	0.601	0.066	1.633	0.047	23.603	13.081	0.062	0.001	0.066	0.413	96.736	7.887	0.098	0.007	0.045	0.180	0.010	0.006	4.855	1.934	0.016	0.000	0.007	0.964	0.000	0.065	0.036
W20 Amph.	57.826	0.161	0.033	1.668	0.080	23.967	13.145	0.006	0.007	0.083	0.118	97.081	7.942	0.026	0.003	0.013	0.190	0.000	0.009	4.907	1.934	0.002	0.001	0.009	0.963	0.000	0.000	0.037
W21 Amph.	57.370	0.160	0.021	1.484	0.060	23.813	13.292	0.052	0.012	0.061	0.114	96.439	7.933	0.026	0.002	0.012	0.170	0.000	0.007	4.909	1.969	0.014	0.002	0.007	0.967	0.000	0.000	0.033
R10-2 Serpentine	43.651	0.142	0.013	1.956	0.025	41.721	0.092	0.014	0.014	0.070	0.005	87.702	1.954	1.954	0.000	0.000	0.079	0.000	0.001	2.990	0.005	0.001	0.001	0.003	0.974	0.000	0.000	0.026
R10-2 Serpentine	43.222	0.135	0.001	2.933	0.083	39.787	0.336	0.018	0.028	0.239	0.013	86.795	2.010	2.010	0.000	0.001	0.123	0.000	0.004	2.814	0.018	0.002	0.002	0.010	0.958	0.000	0.000	0.042
R10-2 Spinel	0.025	10.040	0.055	29.144	0.436	6.680	0.003	0.092	0.015	0.027	52.777	99.292	0.001	0.403	0.001	1.402	0.62	0.21	0.013	0.339	0.000	0.006	0.001	0.001	0.353	0.777	0.1031	0.647
R10-2: Spinel rim	0.286	6.635	0.248	36.931	0.544	4.379	0.003	0.058	0.005	0.039	47.561	100.006	0.008	0.223	0.005	1.276	0.84	0.28	0.013	0.188	0.000	0.003	0.000	0.001	0.184	0.851	0.1567	0.816
R10-2: Spinel core	0.089	11.624	0.114	30.890	0.461	6.377	0.000	0.013	0.014	0.049	49.732	99.361	0.003	0.470	0.003	1.295	0.66	0.22	0.013	0.326	0.000	0.001	0.001	0.001	0.331	0.734	0.1106	0.669
R10-2: Spinel between core, rim	0.171	7.928	0.263	37.742	0.521	4.403	0.012	0.006	0.006	0.078	48.869	100.000	0.005	0.257	0.005	1.264	0.82	0.27	0.012	0.182	0.000	0.000	0.000	0.002	0.182	0.831	0.1525	0.818
R10-2: Spinel between core & rim	0.051	10.659	0.172	33.670	0.457	5.541	0.003	0.006	0.008	0.074	48.555	99.162	0.002	0.433	0.004	1.297	0.73	0.24	0.013	0.285	0.000	0.000	0.000	0.002	0.281	0.75	0.1231	0.719
W-20 Spinele rim	0.050	10.821	0.370	36.574	0.507	5.741	0.067	0.006	0.001	0.094	44.948	99.178	0.002	0.411	0.010	1.243	0.79	0.26	0.015	0.251	0.003	0.000	0.000	0.003	0.242	0.751	0.1369	0.758
W20 Spinel core	0.061	7.742	0.466	38.612	0.559	5.764	0.042	0.030	0.002	0.096	45.613	98.987	0.002	0.330	0.013	1.276	0.85	0.28	0.017	0.224	0.002	0.002	0.000	0.003	0.209	0.794	0.1498	0.791
W20 Spinel 1/3 from core	0.033	12.295	0.201	33.574	0.452	5.751	0.014	0.040	0.014	0.040	46.669	99.085	0.001	0.499	0.005	1.270	0.71	0.24	0.013	0.295	0.001	0.003	0.001	0.001	0.293	0.718	0.1185	0.707
W20 Spinel 1/3 from core toward rim Spinel	0.048	13.589	0.169	29.917	0.401	7.996	0.005	0.000	0.014	0.031	46.938	99.107	0.002	0.543	0.004	1.258	0.63	0.21	0.012	0.318	0.000	0.000	0.001	0.001	0.335	0.698	0.1046	0.665
W20 Spinel 2/3 from core toward rim	0.035	15.107	0.212	28.658	0.378	7.610	0.004	0.042	0.004	0.040	46.999	99.088	0.001	0.597	0.005	1.235	0.60	0.20	0.011	0.355	0.000	0.003	0.000	0.001	0.374	0.674	0.0978	0.626
W21 Spinel	0.027	14.997	0.110	26.851	0.417	7.474	0.012	0.025	0.003	0.025	48.963	98.905	0.001	0.581	0.003	1.282	0.55	0.19	0.012	0.369	0.000	0.002	0.000	0.001	0.399	0.688	0.0904	0.601
W21 Spinel rim	0.006	15.504	0.167	27.994	0.388	7.806	0.007	0.009	0.008	0.012	46.995	98.896	0.000	0.605	0.004	1.224	0.58	0.19	0.011	0.385	0.000	0.001	0.000	0.000	0.4	0.669	0.0953	0.6
W21 center of spinel	0.015	14.974	0.165	26.897	0.396	7.562	0.026	0.000	0.004	0.053	48.887	98.978	0.000	0.583	0.004	1.276	0.55	0.18	0.011	0.372	0.001	0.000	0.000	0.001	0.402	0.686	0.0905	0.598
W21 1/3 from center of Spinel	0.004	14.988	0.134	26.822	0.461	7.780	0.024	0.001	0.023	0.039	48.687	98.963	0.000	0.585	0.003	1.275	0.55	0.18	0.013	0.384	0.001	0.000	0.001	0.001	0.41	0.685	0.0902	0.59
W21 2/3 from center of Spinel	0.006	14.883	0.161	26.534	0.390	7.756	0.015	0.002	0.017	0.067	48.874	98.704	0.000	0.574	0.004	1.273	0.55	0.18	0.011	0.380	0.001	0.000	0.001	0.002	0.409	0.689	0.0904	0.591

The atoms per formula of minerals are calculated on the bases of these numbers of oxygen: Spinel O=4, Olivine=4, Pyroxene: O=6, amphibole O=23, talc O= 22, Serpentine, O= 14

Appendix 12

The results of microprobe analyses of mineral composition of harzburgite in MOC

Oxide	PROBE																				Fe ²⁺	Fe ³⁺	Mn	Mg	Ca	Na	K	Ni	Mg#	Cr#	Fe ³⁺ #	Fe ²⁺ #
	SiO ₂	Al ₂ O ₃	TiO ₂	FeO	MnO	MgO	CaO	Na ₂ O	K ₂ O	NiO	Cr ₂ O ₃	SUM	Si	Al	Ti	Cr																
R7- OI	40.011	0.010	0.010	8.589	0.105	50.126	0.004	0.020	0.001	0.314	0.010	99.098	0.987	0.000	0.000	0.000	0.177	0.000	0.002	1.843	0.000	0.001	0.000	0.006	0.912	0.000	0.000	0.088				
R7- OI	40.182	0.030	0.013	8.546	0.077	49.515	0.002	0.014	0.009	0.309	0.029	98.670	0.994	0.001	0.000	0.001	0.177	0.000	0.002	1.826	0.000	0.001	0.000	0.006	0.912	0.000	0.000	0.088				
W36 OI	39.937	0.025	0.001	10.093	0.136	48.606	0.010	0.020	0.012	0.226	0.016	99.037	0.991	0.001	0.000	0.000	0.210	0.000	0.003	1.799	0.000	0.001	0.000	0.005	0.896	0.000	0.000	0.104				
W36- OI	39.961	0.020	0.020	10.440	0.067	47.946	0.015	0.003	0.001	0.235	0.015	98.724	0.995	0.000	0.000	0.000	0.214	0.000	0.001	1.789	0.000	0.000	0.000	0.005	0.893	0.000	0.000	0.107				
K7-5 OI	40.095	0.013	0.015	9.459	0.148	48.968	0.005	0.037	0.017	0.283	0.011	99.051	0.993	0.000	0.000	0.000	0.196	0.000	0.003	1.807	0.000	0.002	0.001	0.006	0.902	0.000	0.000	0.098				
K7-5 OI	39.847	0.019	0.001	9.184	0.144	48.595	0.005	0.025	0.016	0.291	0.120	98.246	0.994	0.001	0.000	0.000	0.192	0.000	0.003	1.807	0.000	0.001	0.000	0.006	0.904	0.000	0.000	0.096				
K7-5 OI	39.944	0.004	0.000	9.184	0.173	49.325	0.009	0.035	0.011	0.257	0.012	98.948	0.989	0.000	0.000	0.000	0.190	0.000	0.004	1.821	0.000	0.002	0.000	0.005	0.905	0.000	0.000	0.095				
K7-5 OI	39.130	0.010	0.016	8.844	0.120	49.964	0.030	0.071	0.097	0.265	0.082	98.628	1.029	0.000	0.000	0.002	0.153	0.000	0.003	1.772	0.001	0.004	0.004	0.006	0.921	0.000	0.000	0.079				
K7-5 OI	38.991	0.038	0.004	8.961	0.099	49.873	0.047	0.089	0.035	0.350	0.187	98.674	1.091	0.001	0.000	0.004	0.145	0.000	0.002	1.649	0.001	0.005	0.001	0.008	0.919	0.000	0.000	0.081				
D24-OI	39.705	0.010	0.015	8.986	0.072	49.741	0.015	0.004	0.002	0.375	0.020	98.944	0.999	0.000	0.000	0.000	0.149	0.000	0.002	1.847	0.000	0.000	0.000	0.006	0.926	0.000	0.000	0.074				
D24- OI	40.011	0.010	0.010	8.589	0.105	50.526	0.004	0.020	0.001	0.314	0.010	99.598	0.987	0.000	0.000	0.000	0.177	0.000	0.002	1.843	0.000	0.001	0.000	0.006	0.912	0.000	0.000	0.088				
D24- OI	40.595	0.013	0.015	9.459	0.148	48.968	0.005	0.037	0.017	0.283	0.011	99.551	0.993	0.000	0.000	0.000	0.196	0.000	0.003	1.807	0.000	0.002	0.001	0.006	0.902	0.000	0.000	0.098				
A1-5 OI	39.705	0.009	0.010	8.723	0.075	49.228	0.000	0.012	0.013	0.336	0.023	98.109	0.990	0.000	0.000	0.000	0.182	0.000	0.002	1.829	0.000	0.001	0.000	0.007	0.910	0.000	0.000	0.090				
R7- OPX	49.981	0.986	0.010	7.576	0.048	40.016	0.087	0.023	0.034	0.152	0.437	99.350	1.804	0.004	0.000	0.001	0.190	-0.010	0.002	2.387	0.004	0.002	0.002	0.005	0.926	0.000	2.086	0.074				
R7- OPX	48.981	0.986	0.010	7.376	0.048	40.916	0.087	0.023	0.034	0.152	0.437	99.050	1.804	0.004	0.000	0.001	0.190	-0.010	0.002	2.387	0.004	0.002	0.002	0.005	0.926	0.000	2.086	0.074				
K7-5 OPX	49.696	0.052	0.010	6.144	0.120	39.913	2.961	0.012	0.041	0.183	0.021	99.153	1.804	0.003	0.000	0.001	0.210	0.000	0.004	2.032	0.131	0.001	0.002	0.006	0.906	0.000	0.000	0.094				
D24-OPX	57.938	1.636	0.002	6.168	0.199	33.290	0.351	0.059	0.027	0.066	0.204	99.941	2.057	0.062	0.000	0.005	0.160	0.000	0.005	1.597	0.012	0.004	0.001	0.002	0.909	0.000	0.000	0.091				
A1-5 OPX	56.934	1.4239	0.021	5.373	0.1588	33.17	2.283	0.0103	0.036	0.0661	0.5195	100.000	1.96	0.058	0.0005	0.017	0.150	0.000	0.005	1.713	0.0842	0.000	0.002	0.0018	0.917	0.000	0.111	0.081				
A1-5 OPX	56.499	1.595	0.002	5.797	0.1568	34.85	0.3891	0.0031	0.029	0.0874	0.6031	100.005	1.945	0.065	0.000	0.019	0.166	0.010	0.005	1.7955	0.0144	0.000	0.001	0.0024	0.916	0.000	0.111	0.082				
K7-5-CPX	53.500	1.403	0.056	2.867	0.118	17.412	24.531	0.081	0.008	0.062	0.446	100.485	1.946	0.060	0.002	0.013	0.090	0.000	0.004	0.944	0.956	0.006	0.000	0.002	0.913	0.000	0.000	0.087				
D24- CPX	54.280	0.769	0.076	2.794	0.132	17.323	24.882	0.045	0.004	0.015	0.193	100.506	1.971	0.033	0.002	0.006	0.090	0.000	0.004	0.938	0.968	0.003	0.000	0.000	0.912	0.000	0.000	0.088				
R7- Amph.	58.030	0.162	0.008	6.697	0.199	30.593	0.337	0.131	0.000	0.089	0.058	96.303	7.928	0.026	0.001	0.006	0.760	0.000	0.023	6.230	0.049	0.034	0.000	0.010	0.891	0.000	0.000	0.109				
R7- Amph	58.466	0.246	0.007	6.624	0.156	30.531	0.344	0.122	0.001	0.055	0.066	96.616	7.949	0.039	0.001	0.007	0.750	0.000	0.018	6.187	0.050	0.032	0.000	0.016	0.892	0.000	0.000	0.108				
R7- Amph	58.751	0.156	0.014	6.218	0.170	30.985	0.214	0.044	0.008	0.072	0.064	96.697	7.961	0.025	0.001	0.007	0.710	0.000	0.020	6.258	0.031	0.012	0.001	0.008	0.898	0.000	0.000	0.102				
W36- Amph	58.152	0.207	0.010	1.988	0.083	23.747	12.643	0.074	0.009	0.053	0.060	97.027	7.982	0.033	0.001	0.007	0.230	0.000	0.010	4.860	1.859	0.020	0.002	0.006	0.955	0.000	0.000	0.045				
W36-Amph	57.265	0.168	0.007	1.488	0.020	23.578	13.267	0.020	0.001	0.079	0.056	95.912	7.954	0.027	0.001	0.006	0.170	0.000	0.002	4.882	1.975	0.005	0.000	0.006	0.966	0.000	0.000	0.034				
W36- Amph	58.022	0.087	0.002	1.172	0.050	23.822	13.418	0.010	0.005	0.095	0.063	96.625	7.983	0.014	0.000	0.007	0.150	-0.020	0.005	4.886	1.978	0.003	0.001	0.006	0.97	0.000	0.000	0.03				
K7-5 Amph	56.465	0.078	0.000	7.184	0.260	28.899	0.504	0.093	0.024	0.113	0.045	93.667	7.959	0.013	0.000	0.005	0.850	0.000	0.031	6.073	0.076	0.026	0.004	0.013	0.877	0.000	0.000	0.123				
K7-5 Amph	58.003	0.349	0.010	6.986	0.282	29.588	0.949	0.176	0.021	0.103	0.092	96.542	7.932	0.056	0.001	0.010	0.810	-0.010	0.033	6.032	0.139	0.047	0.004	0.011	0.882	0.000	0.000	0.118				
K7-5 Amph	58.551	0.110	0.010	7.140	0.303	29.431	0.514	0.082	0.034	0.077	0.064	96.320	8.006	0.018	0.001	0.007	0.810	0.000	0.035	5.999	0.075	0.022	0.006	0.008	0.881	0.000	0.000	0.119				
K7-5 Amph	58.148	0.215	0.010	1.847	0.067	23.817	13.036	0.156	0.056	0.086	0.048	97.470	7.958	0.035	0.001	0.005	0.210	0.000	0.008	4.859	1.911	0.041	0.010	0.009	0.959	0.000	0.000	0.041				
K7-5 Talc	60.492	0.162	0.010	1.312	0.026	29.592	0.020	0.084	0.017	0.155	0.048	91.900	7.979	0.025	0.001	0.005	0.145	0.000	0.003	5.819	0.003	0.022	0.003	0.007	0.976	0.000	0.000	0.024				
W36-Chlorite inclusion in spinel	38.718	15.902	0.002	3.459	0.0237	38.32	0.0119	0.0258	0.016	0.1599	3.4397	100.075	6.2844	3.034	0.0003	0.021	0.468	0.000	0.003	9.3293	0.0021	0.0081	0.003	0.0209	0.952	0.000	0.000	0.048				
W36- serpentine inclusion in spinel	47.688	0.8988	0.003	12.4	0.7591	36.97	0.1005	0.0454	0.05	0.064	1.0312	100.006	2.0128	0.045	0.000	0.040	0.441	0.000	0.003	2.3405	0.0045	0.0037	0.003	0.0022	0.842	0.000	0.000	0.158				
R7 -serpentine	42.581	0.086	42.581	5.576	0.048	40.016	0.087	0.023	0.034	0.152	0.037	88.631	1.988	0.005	0.000	0.001	0.218	0.000	0.002	2.784	0.004	0.002	0.002	0.006	0.927	0.000	0.000	0.073				
R7 -serpentine	43.807	0.071	43.807	5.963	0.133	39.753	0.141	0.020	0.016	0.117	0.029	90.045	2.012	0.004	0.000	0.001	0.229	0.000	0.005	2.722	0.007	0.002	0.001	0.004	0.922	0.000	0.000	0.078				
K7-5 serpentine	50.67	0.0606	0.007	7.125	0.1386	38.28	3.4339	0.0141	0.047	0.2124	0.0247	100.015	2.1003	0.003	0.0002	0.001	0.248	0.000	0.005	2.3802	0.1525	0.0011	0.002	0.0071	0.906	0.000	0.000	0.094				
R7 - spinel	0.003	11.909	0.062	24.903	0.400	7.924	0.005	0.029	0.004	0.014	54.062	99.316	0.000	0.469	0.002	1.427	0.33	0.34	0.011	0.359	0.000	0.002	0.000	0.000	0.52	0.753	0.15	0.48				
W36- spinel, rim	0.019	9.148	0.125	36.225	0.449	5.852	0.010	0.016	0.006	0.055	46.593	98.498	0.001	0.383	0.003	1.310	0.52	0.50	0.014	0.225	0.000	0.001	0.000	0.002	0.30	0.774	0.23	0.70				
W36-spinel 1/3 from center	0.033	10.111	0.121	36.617	0.439	4.999	0.001	0.036	0.020	0.017	46.710	99.105	0.001	0.419	0.003	1.280	0.51	0.5														

Appendix 13
The results of microprobe analyses of mineral composition in Iherzolite of MOC.

Samples	Oxide												PROBE SUM	Si	Al	Ti	Cr	Fe ²⁺	Fe ³⁺	Mn	Mg	Ca	Na	K	Ni	Mg#	Cr#	Fe ⁺³ #	Fe ^{2+#}
	SiO ₂	Al ₂ O ₃	TiO ₂	FeO	MnO	MgO	CaO	Na ₂ O	K ₂ O	NiO	Cr ₂ O ₃																		
K3-1: Ol ₁	39.918	0.022	0.006	15.485	0.182	44.007	0.006	0.016	0.001	0.122	0.002	99.768	0.988	0.001	0.000	0.000	0.314	0.000	0.004	1.701	0.000	0.001	0.000	0.003	0.844	0.000	0.000	0.156	
K3-1: Ol	39.784	0.004	0.009	15.025	0.292	43.971	0.034	0.014	0.011	0.169	0.005	99.278	0.981	0.000	0.000	0.000	0.326	0.000	0.006	1.702	0.001	0.001	0.000	0.004	0.839	0.000	0.000	0.161	
K3-1:Ol	39.239	0.031	0.010	15.457	0.215	44.919	0.007	0.021	0.008	0.139	0.017	100.062	0.986	0.001	0.000	0.000	0.324	0.000	0.005	1.693	0.000	0.001	0.000	0.003	0.839	0.000	0.000	0.160	
K3-1: Ol	38.600	0.010	0.017	15.297	0.230	43.790	0.001	0.020	0.007	0.128	0.009	98.055	0.992	0.000	0.000	0.000	0.329	0.000	0.005	1.678	0.000	0.001	0.000	0.003	0.836	0.000	0.000	0.164	
K4-2 Ol	39.468	0.000	0.001	12.878	0.184	46.313	0.013	0.000	0.000	0.189	0.000	99.043	0.992	0.000	0.000	0.000	0.271	0.000	0.004	1.736	0.000	0.000	0.000	0.004	0.865	0.000	0.000	0.135	
D32: Ol	40.013	0.009	0.003	10.106	0.165	48.146	0.018	0.030	0.006	0.169	0.001	98.584	0.997	0.000	0.000	0.000	0.211	0.000	0.003	1.789	0.000	0.001	0.000	0.003	0.895	0.000	0.000	0.105	
D32: Ol	39.649	0.020	0.009	10.635	0.166	48.624	0.020	0.010	0.006	0.227	0.009	99.303	0.985	0.000	0.000	0.000	0.221	0.000	0.004	1.801	0.001	0.000	0.000	0.005	0.891	0.000	0.000	0.109	
D32: Ol	39.966	0.015	0.001	10.367	0.173	48.384	0.009	0.002	0.002	0.203	0.009	99.079	0.993	0.000	0.000	0.000	0.215	0.000	0.004	1.792	0.000	0.000	0.000	0.004	0.893	0.000	0.000	0.107	
D32: OPX	40.033	0.020	0.009	10.634	0.166	48.623	0.020	0.010	0.006	0.227	0.009	99.684	0.992	0.001	0.000	0.000	0.235	0.001	0.004	1.773	0.001	0.000	0.000	0.004	0.883	0.000	0.529	0.117	
D33 OPX	51.702	0.780	0.014	7.192	0.109	39.542	0.251	0.008	0.001	0.371	0.030	100.000	1.816	0.032	0.000	0.000	0.210	0.000	0.003	2.083	0.009	0.001	0.000	0.010	0.908	0.000	0.000	0.092	
K3-1 CPX	53.801	0.225	0.029	2.503	0.062	17.214	26.154	0.040	0.000	0.039	0.110	100.177	1.967	0.010	0.001	0.003	0.080	0.000	0.002	0.938	1.025	0.003	0.000	0.001	0.921	0.000	0.000	0.0786	
K3-1:CPX	54.137	0.181	0.026	2.479	0.100	17.534	25.603	0.024	0.009	0.010	0.103	100.208	1.974	0.008	0.001	0.003	0.070	0.000	0.003	0.953	1.000	0.002	0.000	0.000	0.932	0.000	0.000	0.0684	
K4-2: CPX	52.086	2.807	0.115	3.332	0.140	16.921	24.078	0.188	0.007	0.046	1.765	101.485	1.888	0.120	0.003	0.051	0.100	0.000	0.004	0.914	0.935	0.013	0.000	0.001	0.901	0.000	0.000	0.0986	
K4-2: CPX	54.613	0.044	0.002	1.209	0.058	18.165	26.086	0.010	0.028	0.028	0.029	100.250	1.980	0.002	0.000	0.001	0.040	0.000	0.002	0.982	1.014	0.000	0.001	0.001	0.961	0.000	0.000	0.0391	
D32: Amph.	56.593	0.173	0.011	2.037	0.058	23.039	12.924	0.042	0.008	0.057	0.130	95.073	7.951	0.029	0.001	0.014	0.230	0.010	0.007	4.825	1.946	0.011	0.001	0.006	0.955	0.000	0.188	0.0455	
D32: Amph.	57.670	0.158	0.007	2.116	0.082	23.822	13.017	0.016	0.012	0.069	0.114	97.084	7.936	0.026	0.001	0.012	0.250	0.000	0.010	4.887	1.919	0.004	0.002	0.008	0.951	0.000	0.000	0.0487	
D33Amph.	54.449	2.345	0.093	2.228	0.016	22.240	13.363	0.371	0.035	0.037	0.646	95.822	7.650	0.388	0.010	0.072	0.250	0.010	0.002	4.658	2.011	0.101	0.006	0.004	0.949	0.000	0.021	0.0509	
D33 Amph.	55.696	1.633	0.094	1.999	0.190	22.552	12.835	0.196	0.009	0.174	0.976	95.965	7.773	0.269	0.010	0.108	0.220	0.010	0.022	4.692	1.919	0.053	0.001	0.020	0.955	0.000	0.026	0.0448	
D33Amph.	56.121	1.362	0.051	2.006	0.026	22.386	13.249	0.175	0.009	0.071	0.584	96.041	7.827	0.224	0.005	0.064	0.230	0.010	0.003	4.654	1.980	0.047	0.002	0.008	0.953	0.000	0.034	0.0471	
D33 Serpentine	49.081	0.336	0.050	11.339	0.140	38.433	0.125	0.054	0.067	0.395	0.024	100.043	2.062	0.017	0.002	0.000	0.397	0.000	0.005	2.422	0.006	0.004	0.004	0.013	0.858	0.000	0.000	0.142	
D33 serpentine	52.861	0.842	0.054	2.763	0.056	25.658	9.932	0.201	0.069	0.076	0.246	92.756	2.325	0.044	0.002	0.009	0.102	0.000	0.002	1.683	0.468	0.017	0.004	0.003	0.943	0.000	0.000	0.057	
D33 serpentine	51.702	0.780	0.014	7.192	0.109	39.542	0.251	0.008	0.001	0.371	0.030	100.000	2.123	2.119	0.038	0.001	0.245	0.000	0.004	2.430	0.011	0.001	0.000	0.012	0.907	0.000	0.000	0.092	
D33 serpentine	49.081	0.336	0.050	11.339	0.140	38.433	0.125	0.054	0.067	0.395	0.024	100.043	2.062	0.017	0.002	0.000	0.396	0.000	0.005	2.422	0.006	0.004	0.004	0.013	0.858	0.000	0.000	0.142	
K3-1 Spinel travers	0.077	24.880	0.302	35.700	0.402	7.347	0.004	0.012	0.012	0.044	31.063	99.843	0.003	0.899	0.007	0.805	0.245	0.734	0.011	0.310	0.000	0.001	0.001	0.001	0.560	0.470	0.301	0.441	
K3-1 Spinel travers	0.030	23.154	0.370	35.124	0.413	6.479	0.008	0.013	0.023	0.085	31.910	98.609	0.001	0.773	0.008	0.850	0.460	0.470	0.010	0.276	0.000	0.001	0.001	0.002	0.370	0.523	0.244	0.620	
K3-1 Spinel core	0.010	23.932	0.390	35.722	0.484	6.817	0.004	0.009	0.013	0.040	32.605	100.026	0.000	0.659	0.007	0.715	0.710	0.240	0.010	0.239	0.000	0.000	0.000	0.001	0.252	0.480	0.293	0.748	
K2-4 Spinel	0.034	22.809	0.120	35.530	0.472	6.838	0.015	0.011	0.005	0.050	34.156	100.038	0.001	0.740	0.002	0.838	0.710	0.240	0.011	0.283	0.000	0.001	0.000	0.001	0.280	0.544	0.128	0.740	
D32:magnetite	0.071	0.024	0.005	101.19*	0.006	0.050	0.010	0.010	0.001	0.125	0.023	101.469	0.003	0.001	0.000	0.001	2.990	0.000	0.000	0.003	0.000	0.001	0.000	0.004	0.001	0.396	0.000	0.998	

Appendix 14

The results of microprobe analyses for mineral composition in pyroxenite rocks of MOC.

Samples	SiO ₂	Al ₂ O ₃	TiO ₂	FeO	MnO	MgO	CaO	Na ₂ O	K ₂ O	NiO	Cr ₂ O ₃	PROBE SUM	Si	Al	Ti	Cr	Fe ²⁺	Fe ³⁺	Mn	Mg	Ca	Na	K	Ni	Mg#	Cr#	Fe ³⁺ #	Fe ²⁺ #	
K2-2 OL	39.970	0.000	0.020	14.560	0.250	45.250	0.010	0.010	0.020	0.230	0.030	100.350	0.990	0.000	0.000	0.000	0.301	0.000	0.005	1.707	0.000	0.001	0.001	0.004	0.850	0.000	0.000	0.150	
K2-2 OL	39.980	0.000	0.030	14.270	0.240	45.340	0.020	0.000	0.010	0.210	0.030	100.130	0.990	0.000	0.001	0.001	0.296	0.000	0.005	1.712	0.001	0.000	0.000	0.004	0.853	0.000	0.000	0.147	
K3-2 OL	40.140	0.010	0.000	16.310	0.240	44.280	0.020	0.000	0.020	0.180	0.000	101.200	1.001	0.000	0.000	0.000	0.340	0.000	0.005	1.647	0.001	0.000	0.001	0.004	0.829	0.000	0.000	0.171	
K3-2 OL	39.340	0.000	0.020	16.730	0.250	43.760	0.000	0.000	0.000	0.160	0.010	100.270	0.994	0.000	0.000	0.000	0.354	0.000	0.005	1.649	0.001	0.000	0.000	0.003	0.823	0.000	0.000	0.177	
K3-2 OL	39.430	0.000	0.010	16.210	0.290	44.220	0.020	0.000	0.020	0.160	0.000	100.360	0.993	0.000	0.000	0.000	0.342	0.000	0.006	1.661	0.000	0.000	0.001	0.003	0.829	0.000	0.000	0.171	
K3-2 OL	39.480	0.010	0.000	16.270	0.290	44.280	0.000	0.000	0.010	0.160	0.020	100.520	0.993	0.000	0.000	0.000	0.342	0.000	0.006	1.661	0.000	0.000	0.001	0.003	0.829	0.000	0.000	0.171	
K3-2 OL	39.670	0.000	0.000	16.370	0.270	44.310	0.010	0.000	0.020	0.180	0.000	100.830	0.995	0.000	0.000	0.000	0.343	0.000	0.006	1.657	0.000	0.000	0.001	0.004	0.829	0.000	0.000	0.172	
K3-2 OL	39.470	0.000	0.000	16.460	0.320	44.040	0.020	0.010	0.010	0.170	0.000	100.500	0.990	0.000	0.000	0.000	0.345	0.000	0.007	1.665	0.001	0.000	0.001	0.003	0.828	0.000	0.000	0.172	
D35 OL	38.657	0.021	0.011	17.734	0.358	43.013	0.007	0.042	0.002	0.194	0.023	100.062	0.984	0.000	0.000	0.000	0.375	0.000	0.008	1.642	0.000	0.002	0.000	0.004	0.812	0.000	0.000	0.188	
O=	4.000	4.000	4.000	4.000	4.000	4.000	4.000	4.000	4.000	4.000	4.000	4.000	4.000	4.000	4.000	4.000	4.000	4.000	4.000	4.000	4.000	4.000	4.000	4.000	4.000	4.000	4.000	4.000	4.000
K9-1, CPX	53.500	1.403	0.056	2.867	0.118	17.412	24.531	0.081	0.008	0.062	0.446	100.485	1.946	0.060	0.002	0.013	0.090	0.000	0.004	0.944	0.956	0.006	0.000	0.002	0.913	0.000	0.000	0.087	
K9-1, CPX	54.280	0.769	0.076	2.794	0.132	17.323	24.882	0.045	0.004	0.015	0.193	100.506	1.971	0.033	0.002	0.006	0.090	0.000	0.004	0.938	0.968	0.003	0.000	0.000	0.912	0.000	0.000	0.088	
K9-1, CPX	52.712	1.510	0.070	3.586	0.154	17.079	23.793	0.086	0.025	0.027	0.425	99.468	1.941	0.066	0.002	0.012	0.110	0.000	0.005	0.938	0.939	0.006	0.001	0.001	0.895	0.000	0.000	0.105	
K9-1, CPX	53.298	1.320	0.063	3.217	0.117	17.250	23.949	0.070	0.001	0.046	0.346	99.679	1.953	0.057	0.002	0.010	0.100	0.000	0.004	0.943	0.940	0.005	0.000	0.001	0.904	0.000	0.000	0.096	
K9-1, CPX	51.943	2.080	0.134	3.535	0.101	16.994	24.542	0.168	0.010	0.021	0.472	100.000	1.905	0.090	0.004	0.016	0.108	0.000	0.003	0.935	0.964	0.012	0.000	0.001	0.894	0.000	0.000	0.103	
K9-1, CPX	53.267	1.334	0.049	3.076	0.125	17.759	23.805	0.091	0.006	0.048	0.440	100.000	1.940	0.057	0.001	0.015	0.093	0.000	0.004	0.970	0.929	0.006	0.000	0.001	0.915	0.000	0.000	0.085	
K9-5 cpx,	51.275	1.285	0.057	2.893	0.105	16.369	24.215	0.054	0.000	0.043	0.570	96.866	1.941	0.057	0.002	0.017	0.090	0.000	0.003	0.924	0.982	0.004	0.000	0.001	0.911	0.000	0.000	0.089	
K9-5 cpx	52.515	1.206	0.033	3.199	0.111	16.769	24.225	0.112	0.002	0.054	0.446	98.671	1.950	0.053	0.001	0.013	0.100	0.000	0.003	0.928	0.964	0.008	0.000	0.002	0.903	0.000	0.000	0.097	
K9-5 CPX	52.219	1.265	0.065	3.146	0.112	16.825	24.488	0.075	0.012	0.057	0.461	98.726	1.940	0.055	0.002	0.014	0.100	0.000	0.004	0.932	0.975	0.005	0.001	0.002	0.903	0.000	0.000	0.097	
K9-5 cpx,	51.712	1.404	0.050	3.071	0.109	16.349	24.590	0.089	0.020	0.019	0.595	98.009	1.937	0.062	0.001	0.018	0.090	0.000	0.003	0.913	0.987	0.006	0.001	0.001	0.91	0.000	0.000	0.09	
K9-5 CPX	52.537	1.295	0.034	3.090	0.103	16.628	24.620	0.036	0.001	0.058	0.454	98.852	1.947	0.057	0.001	0.013	0.100	0.000	0.003	0.919	0.978	0.003	0.000	0.002	0.902	0.000	0.000	0.098	
K9-5 CPX	52.158	1.134	0.042	2.927	0.095	16.896	24.671	0.049	0.002	0.043	0.454	98.470	1.942	0.050	0.001	0.013	0.090	0.000	0.003	0.938	0.984	0.004	0.000	0.001	0.912	0.000	0.000	0.081	
K9-5 cpx	53.327	1.267	0.052	2.659	0.117	16.621	24.969	0.031	0.015	0.024	0.500	99.582	1.957	0.055	0.001	0.015	0.080	0.000	0.004	0.909	0.982	0.002	0.001	0.001	0.919	0.000	0.000	0.081	
K2-1 CPX	53.070	2.030	0.210	4.690	0.160	16.220	22.760	0.220	0.000	0.040	0.460	99.860	1.948	0.088	0.006	0.013	0.140	0.010	0.005	0.888	0.895	0.015	0.000	0.001	0.864	0.000	0.090	0.136	
K2-1 CPX	52.890	2.380	0.160	4.250	0.120	16.500	21.550	0.240	0.010	0.030	0.360	98.490	1.956	0.104	0.005	0.010	0.130	0.000	0.004	0.910	0.854	0.017	0.001	0.001	0.875	0.000	0.000	0.125	
K2-1 CPX	53.870	1.560	0.150	3.560	0.160	16.360	23.820	0.100	0.000	0.040	0.360	99.980	1.967	0.067	0.004	0.010	0.100	0.010	0.005	0.891	0.932	0.007	0.000	0.001	0.899	0.000	0.115	0.101	
K2-2 CPX	53.330	2.110	0.040	3.090	0.110	17.010	23.350	0.110	0.020	0.010	0.680	99.860	1.946	0.091	0.001	0.020	0.090	0.000	0.003	0.925	0.913	0.007	0.000	0.001	0.911	0.000	0.000	0.089	
K2-2 CPX	53.480	2.090	0.070	3.290	0.120	17.010	23.460	0.120	0.010	0.030	0.760	100.440	1.943	0.089	0.002	0.022	0.100	0.000	0.004	0.921	0.913	0.009	0.000	0.001	0.902	0.000	0.000	0.098	
K2-2 CPX	53.900	1.560	0.010	3.160	0.100	17.190	23.710	0.080	0.010	0.030	0.420	100.170	1.961	0.088	0.000	0.012	0.160	-0.060	0.003	0.932	0.924	0.005	0.000	0.001	0.853	0.000	1.500	0.147	
K2-2 CPX	53.600	2.070	0.080	3.100	0.120	17.080	23.950	0.130	0.020	0.030	0.620	100.800	1.941	0.088	0.002	0.018	0.110	-0.020	0.004	0.932	0.929	0.009	0.001	0.001	0.894	0.000	0.233	0.106	
K2-2 CPX	54.110	1.990	0.050	3.000	0.100	17.150	23.750	0.090	0.010	0.020	0.590	100.860	1.953	0.085	0.001	0.017	0.090	0.000	0.003	0.922	0.919	0.007	0.000	0.001	0.911	0.000	0.000	0.089	
K2-2 CPX	53.180	2.300	0.050	3.380	0.100	16.650	23.240	0.120	0.020	0.020	0.760	99.820	1.943	0.099	0.001	0.022	0.130	-0.030	0.003	0.923	0.910	0.009	0.001	0.001	0.877	0.000	0.330	0.123	
K2-2 CPX	53.090	2.220	0.060	3.100	0.100	16.870	23.700	0.110	0.010	0.030	0.740	99.700	1.942	0.095	0.002	0.021	0.070	0.030	0.003	0.907	0.916	0.008	0.000	0.001	0.928	0.000	0.205	0.072	
K2-2 CPX	53.360	2.140	0.070	3.360	0.130	17.180	23.070	0.120	0.020	0.020	0.740	100.210	1.942	0.092	0.002	0.021	0.080	0.020	0.004	0.920	0.900	0.009	0.000	0.001	0.92	0.000	0.150	0.08	
K2-2 CPX	53.080	2.260	0.050	3.360	0.100	17.140	23.210	0.110	0.000	0.040	0.760	100.110	1.935	0.097	0.001	0.022	0.100	0.000	0.003	0.932	0.907	0.008	0.001	0.001	0.903	0.000	0.000	0.097	
K3-2 CPX	53.870	2.240	0.130	3.870	0.120	16.440	22.920	0.110	0.000	0.010	0.510	100.220	1.959	0.096	0.004	0.015	0.120	0.000	0.004	0.891	0.893	0.007	0.000	0.000	0.881	0.000	0.000	0.119	
K3-2 CPX	53.040	1.880	0.240	3.220	0.100	16.490	24.140	0.050	0.020	0.020	0.590	99.790	1.943	0.081	0.007	0.017	0.090	0.010	0.003	0.901	0.948	0.004	0.000	0.000	0.909	0.000	0.093	0.091	
K2-2 OPX	56.450	1.690	0.010	8.690	0.220	32.420	0.890	0.000	0.030	0.050	0.430	100.880	1.956	0.069	0.000	0.012	0.250	0.000	0.006	1.674	0.033	0.000	0.001	0.001	0.87	0.000	0.000	0.13	
K2-2 OPX	56.090	1.720	0.030	8.720	0.250	32.420	0.780	0.000	0.000	0.040	0.480	100.530	1.956	0.070	0.001	0.013	0.270	-0.020	0.007	1.680	0.029	0.000	0.001	0.001	0.862	0.000	0.317	0.138	
K3-2 OPX	55.250	2.200	0.090	11.160	0.290	30.540	0.540	0.020	0.010	0.040	0.360	100.500	1.942	0.091	0.002	0.010	0.320	0.010	0.008	1.600	0.020	0.001	0.000						